Universitat Autònoma de Barcelona

Targeting NRAS mutant melanomas through metabolic stress

Kimberley Anne Mc Grail Fernández

Universitat Autònoma de Barcelona

PhD Thesis

Targeting *NRAS* mutant melanomas through metabolic stress

Kimberley Anne Mc Grail Fernández

Thesis Director: Dr. Juan Ángel Recio Conde
Academic Tutor: Dr. José Miguel Lizcano de Vega

Biochemistry, Molecular Biology and Biomedicine PhD program
Biochemistry and Molecular Biology Department
Universidad Autónoma de Barcelona (UAB)
2021

Kimberley Anne Mc Grail Fernández | Juan Ángel Recio Conde, PhD | José Miguel Lizcano de Vega, PhD

"Nothing in life is to be feared,
it is only to be understood.
Now is the time to understand more,
so we may fear less".

Marie Curie

ACKNOWLEDGEMENTS

En primer lugar, me gustaría agradecer al Dr. Recio. Gracias Kelle por todo lo que me has enseñado, por el apoyo continuo y por confiar siempre en mí.

Millones de gracias a mi equipo VHIR: Sara, Yoelsis, Mª José, Natalia, Pedro J, Marta. Ha sido una suerte compartir momentos científicos y no científicos con vosotros. En especial gracias Pauli, no sé que hubiera hecho sin ti. Gracias también a las chicas que han pasado por el lab, sobre todo a Sara G., por atreverse a acompañarme en este proyecto.

Aunque no formen parte de esta tesis me gustaría agradecer a Isa y Marta, porque gracias a ellas empecé este camino, y me hicieron ver que era capaz. Han sido un referente y su apoyo ha sido fundamental.

Por supuesto, gracias a mi familia, sin ellos no habría llegado hasta aquí. Gracias por apoyarme siempre en todo.

Por último, pero no menos importante, gracias a la que considero mi otra familia, por hacerme sentir como en casa. Gracias Pedro, has sido la pieza clave de esta etapa. Eres el responsable de que haya llegado hasta el final. *T'estimo*.

LIST OF CONTENTS

SUMMARY/RESUMEN

BRAF and *NRAS* are the most commonly found mutated genes in cutaneous melanoma. Alterations in these genes result in the constitutive activation of the RAS-ERK1/2 pathway, contributing to tumor development and progression. Beside both genes are consecutive located in the same signaling cascade, *BRAF* and *NRAS* mutated tumors are considered two different entities at clinical and molecular levels, resulting in distinct signaling patterns and different biological behavior. Furthermore, while there is a first line of treatment using targeted therapy against *BRAF* mutant melanomas, *NRAS* mutant tumors remain without specific line of treatment, showing low response rates and high toxicity to the currently applied therapies. Thus, the understanding of the molecular differences between *BRAF* and *NRAS* mutant tumors is essential to improve therapeutic opportunities for the treatment of patients carrying *NRAS* mutations.

Previous results in our group, together with additional investigations, have highlighted the presence of different metabolic settings subjected to $BRAF^{V600E}$ oncogene regulation. However, little is known about the role of *NRAS* mutations in metabolic rewiring. Deciphering metabolic settings in *NRAS* mutant melanomas could provide new avenues for the establishment of specific therapeutic approaches against these, until now, untargetable tumors.

In this study, we have investigated the molecular implications of glucose starvation in $NRAS^{Q61}$ and $BRAF^{V600E}$ mutant cells in order to establish whether the presence of NRAS-dependent metabolic settings can be exploited for the development of targeted therapies against *NRAS* mutant melanomas. Overall, in this study we have demonstrated the presence of $NRAS^{Q61}$ oncogene-dependent metabolic settings. $NRAS^{Q61}$ mutant cells show a differential response to metabolic stress when compared to $BRAF^{V600E}$ mutant cells, which results in the hyperactivation of the RAS-ERK1/2 pathway and the sensitization to the multi-kinase inhibitor Sorafenib. PFKFB2, PFKFB3 and PFK-1 are key players in the regulation of this process. We also propose a novel approach for the specific targeting of $NRAS^{Q61}$ mutant melanomas based on the combination of 2-deoxy-D-glucose (2DG) and Sorafenib. We conclude that *NRAS* and *BRAF* mutant tumors are different entities at different levels, not only at molecular and clinical levels but

also at metabolic level and this fact provides a new therapeutic window for the targeting of *NRAS* mutant tumors.

Los genes *BRAF* y *NRAS* presentan una mayor incidencia mutacional en melanoma cutáneo. Alteraciones en estos genes resultan en la activación constitutiva de la vía de RAS-ERK1/2, lo que contribuye activamente al desarrollo y la progresión tumoral del melanoma. Aunque ambas mutaciones dan lugar a alteraciones de la misma vía de señalización, ha sido ampliamente descrito que los tumores que se generan de las mismas, constituyen dos entidades diferentes tanto a nivel molecular como desde el punto de vista clínico. Una cuestión relevante reside en el hecho de que mientras los melanomas mutados en *BRAF* disponen de terapias específicas dirigidas contra el oncogén, los melanomas que presentan mutaciones en *NRAS* carecen de tratamientos específicos. Como consecuencia, estos pacientes son tratados con tratamientos antitumorales más genéricos, que desembocan en tasas de respuesta mucho menores y en una elevada toxicidad. En este contexto, el desenmascaramiento de las diferencias moleculares existentes entre los tumores con mutaciones en *BRAF* y en *NRAS* es esencial para el establecimiento de nuevas estrategias terapéuticas dirigidas a pacientes que presentan mutaciones en *NRAS*.

Resultados obtenidos previamente en nuestro grupo de investigación, sumados a los de otras investigaciones, han confirmado la presencia de diferentes patrones metabólicos sujetos a la regulación por $BRAF^{V600E}$. Sin embargo, apenas existe evidencia sobre el papel de las mutaciones en *NRAS* en la regulación metabólica. El establecimiento de características metabólicas específicas de melanomas con mutaciones en *NRAS* podría contribuir al desarrollo de nuevos enfoques terapéuticos dirigidos contra este tipo de tumor.

Durante el desarrollo de este estudio hemos investigado las implicaciones moleculares derivadas de la falta de glucosa en células de melanoma mutadas en $NRAS^{Q61}$ y $BRAF^{V600E}$, con el fin de establecer si la presencia de características metabólicas dependientes de NRAS podría ser explotada para el desarrollo de nuevas terapias contra este tipo de tumor. En este estudio, hemos demostrado la presencia de patrones metabólicos bajo el control de $NRAS^{Q61}$. Las células que presentan mutaciones en $NRAS^{Q61}$ muestran una respuesta diferencial al estrés metabólico, en comparación con las células mutadas en $BRAF^{V600E}$, que desemboca en la hiperactivación de la vía de RAS-ERK1/2 y en la sensibilización de estas células al inhibidor multi-quinasa Sorafenib. PFKFB2, PFKFB3 y PFK-1 son

elementos clave en la regulación de este proceso. Adicionalmente, proponemos una nueva aproximación terapéutica para el tratamiento dirigido de los melanomas mutados en $NRAS^{Q61}$, basada en la combinación de 2-deoxi-D-glucosa (2DG) y Sorafenib. Tras los resultados obtenidos, podemos concluir que los tumores que presentan mutaciones en *NRAS* y *BRAF* son entidades diferentes a distintos niveles, no solo a nivel clínico y molecular, sino también a nivel metabólico, lo que implica la existencia de nuevas ventanas terapéuticas para el tratamiento de tumores que presentan mutaciones en *NRAS*.

INTRODUCTION

1. Skin cancer

1.1. Subtypes, incidence and mortality

Skin cancer is the most frequently diagnosed cancer worldwide, with millions of new diagnosed cases each year[1,2]. It can be generally divided in three subtypes depending on the cell type the tumor is originated from: Basal Cell Carcinoma (BCC), Squamous Cell Carcinoma (SCC) and Melanoma (Table I.1)[3,4]. While BCC and SCC are both derived from epithelial cells (keratinocytes), melanomas arise from melanocytes, specialized cells originated from neural crest progenitors that migrate to eye, meninges, mucosal epithelia, and the skin during embryonic development. These cells are essential for protection against environmental mutagenic agents as they are involved in the synthesis of melanin, a photo-protective pigment that avoid DNA damage upon UV radiation[5].

Skin cancer types	Origin	Incidence	Mortality
Basal Cell Carcinoma (BCC)	Basal cells (Deep epidermis)	75-80%	Low
Squamous Cell Carcinoma (SCC)	Squamous cells (Superficial epidermis)	15-20%	Low
Melanoma	Melanocytes	2-5 %	High

Table I.1. Skin cancer subtypes. Table includes information regarding tumor origin, incidence and mortality rate[3,4].

In terms of frequency, BCC and SCC are the most frequent types of skin cancer and accounts for more than 90% of all the cases, however both types of tumors present a good prognosis due to its low proliferation rate and minimum invasion capacity. Melanoma, even accounting for less than five percent of all skin cancers, is the most aggressive and treatment-resistant form. It is a very heterogeneous disease that can be subclassified at the same time according to the histological and molecular features of the tumor. All melanoma subtypes are characterized by an increased proliferation rate and a high metastatic capacity, so these tumors present a bad prognosis and are responsible of more than 80% of skin cancer-related deaths[6].

1.2. Risk factors

Several factors have been observed to influence the risk of suffering melanoma, including harboring multiple benign or atypical nevi, fair skin, previous melanoma, family history of melanoma, continued exposure to UV radiation and immunosuppression. These risk factors or environmental stressors involve a genetic predisposition to suffering skin cancer[6]. Particularly, repeated intense childhood sun damage influences potential risk of melanoma[7]. UV radiation has multiple effects in the skin including DNA damage, induction of oxidative stress, alteration of immune response and production of growth factors; and this is of particular relevance because it is responsible of the high mutational burden that characterize skin tumors and make of them a challenge as well as an opportunity in terms of treatment[8].

2. Melanoma

2.1. Classification

Melanoma is the most aggressive and treatment-resistant form of skin cancer. It can be subdivided according to its primary site of location into cutaneous, mucosal and uveal melanoma. Marked differences in the genomic landscape have been described depending on the origin of the tumor[9]. Cutaneous melanoma is the most frequent one and it is at the same time classified in four major subgroups: Superficial spreading, nodular, lentigo maligna and acral lentiginous (Table I.2)[10–12].

Melanoma subtypes	Incidence	Main phenotypic features
Superficial Spreading	70%	It is often flat and thin but can undergo vertical growth.
Nodular	5%	It grows into the skin and spread quickly.
Lentigo Maligna	5-15%	It often develops in older people. It usually grows outward across the surface of the skin for many years before it starts to grow down into the skin.
Acral	5%	It locates to the soles of the feet, the palms of the hands or under the nails. It usually grows outward across the surface of the skin for a long time before it starts to grow down into the skin.

Table I.2. Melanoma subtypes. Incidence values correspond to Caucasian populations[10–12].

2.2. Progression and prognosis

The Clark model of the progression of melanoma describes the transformation from normal to tumoral melanocytes. It starts from the development of a benign lesion or nevus resulting from the proliferation of normal melanocytes in the epidermis. Then, these cells undergo uncontrolled growth and acquire invasion capacities giving rise to metastasis. All these phenotypic changes are the reflection of genetic and epigenetic alterations taking place during the progression of the disease, which involve the acquisition of mutations in regulatory genes, the deregulation of growth factors secretion and the loss of adhesion receptors[6,10] (Figure I.1).

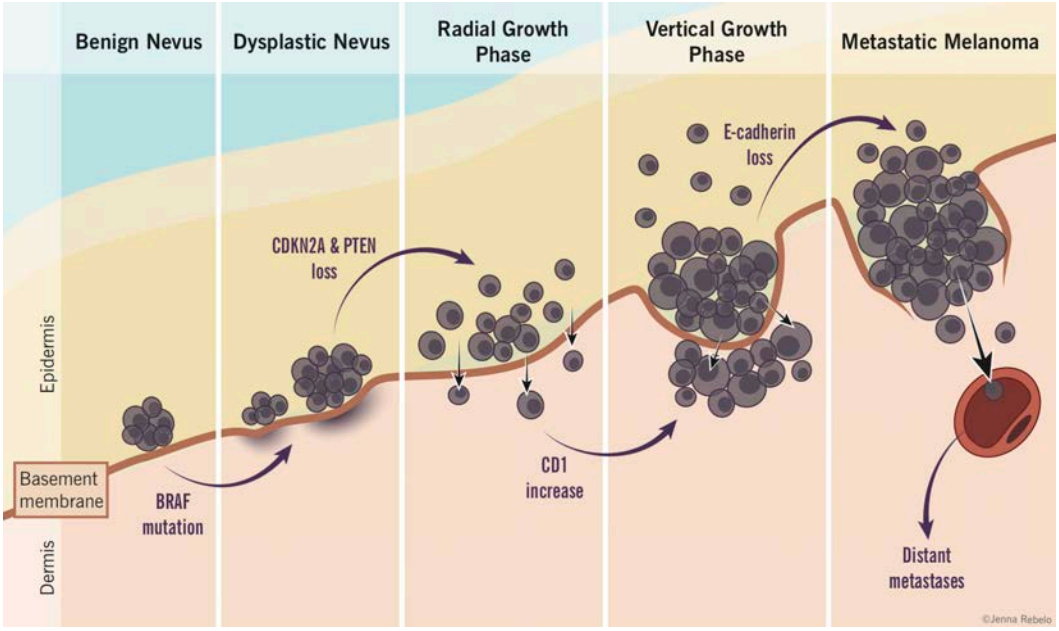

Figure I.1. Clark Model. Representation of melanoma progression since the formation of a benign melanocytic lesion (nevus) to the formation of a metastatic melanoma[13].

Nevus growth has been attributed to a variety of mutations, being *BRAF* the most commonly found in until 50% of non-tumoral lesions[14]. Normally, nevus growth is limited, so its progression to a malignant lesion is infrequent. This limited growth has been explained by a process known as oncogene-induced senescence (OIS)[15]. Senescence is a key cellular protection against aberrant cell proliferation. In senescent nevi, genetic and epigenetic alterations can additionally occur allowing the cells to overcome senescence and resulting in the acquisition of malignancy and the consequent progression of the tumor[6].

Once tumor cells acquire the ability of radial growth, intra-epidermal lesions can occur. Then, cells can progress to the vertical-growth phase, driven by the regulation of different adhesion molecules. These changes will allow the tumor cells to penetrate through the basement membrane and invade the dermis. Finally, the regulation of critical factors that drive tumor cell motility and dissemination into lymphatic and vascular vessels will allow cells to dissociate from the primary lesion and spread to other areas in the skin or even to other organs, being able to proliferate and establish metastatic nests in distant sites[6].

It is important to highlight that not all melanomas start from the first step of the Clark model; more than 50% of melanoma tumors can be originated independently of the existence of a previous benign lesion[16,17].

Currently, the staging system adopted by clinicians no longer considers Clark's model, because it is less prognostic and more subjective than other alternatives, but it is still useful for the understanding of biological and genetic changes taking place during melanoma progression. More recent models are based in the TNM classification system established by American Joint Committee on Cancer (AJCC)[18].

Independently of the used model, prognosis is getting worse with every step being metastatic melanoma the most aggressive and difficult to treat. For this reason, most efforts in the field are focused on the study of acquisition of malignancy and progression mechanisms as well as the establishment of new therapeutic approaches for the targeted treatment of these advanced tumors.

2.3. Molecular characterization of melanoma

For the acquisition of malignancy, abnormal activation of the RAS-ERK1/2 pathway has been widely described, being *BRAF*, *NRAS* and *NF1*, a negative regulator of RAS, the most common genetic targets in melanoma (*TCGA database*). *BRAF* and *NRAS* are mutated in more than 70% of melanoma patients resulting in RAS-ERK1/2 pathway hyperactivation[19]. Moreover, deregulation of this pathway can also occur through the overexpression or hyperactivation of tyrosine kinase receptors (RTKs) such as proto-oncogene KIT[20], hepatocyte growth factor receptor (HGFR/MET)[21] and vascular endothelial growth factor receptor (VEGFR)[22]. KIT

alterations are more common in acral and mucosal melanomas[20] while GNAQ and GNA11, two G protein subunits involved in MAPK signaling, are frequently activated in uveal melanomas[23] (Figure I.2).

Other recurrent genetic alterations include upregulation of *AKT* and *PTEN* loss, what involves the activation of the phosphatidylinositol 3-kinase (PI3K) pathway[24,25] (Figure I.2).

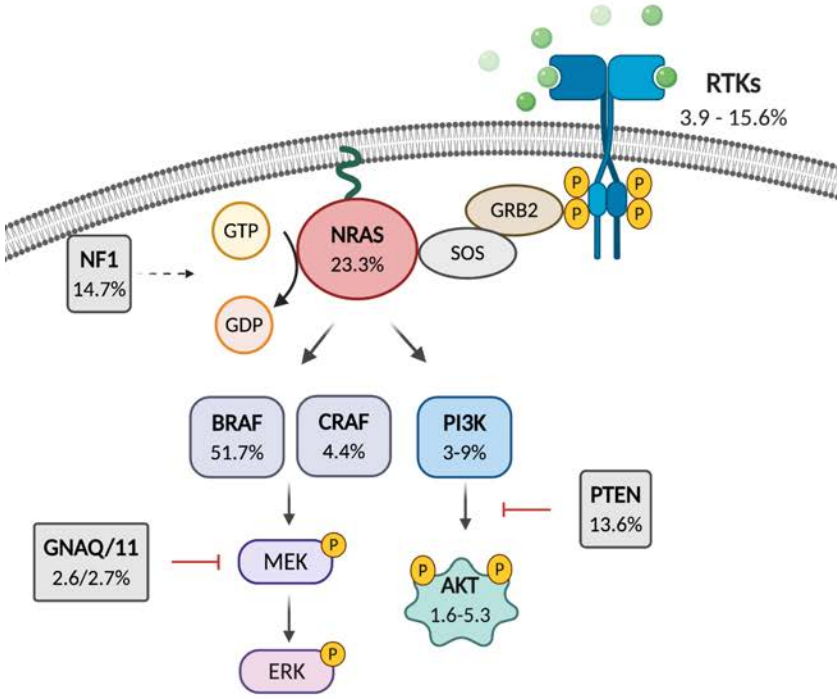

Figure I.2. RAS-ERK1/2 pathway. Percentages indicate mutational incidence in melanoma. Data obtained from *TCGA database*.

The MAPK pathway, or more specifically the RAS/RAF/MEK/ERK pathway, is involved in the transmission of the signal downstream of RTKs in response to growth factors. This signaling cascades start from the dimerization and intrinsic activation of the RTK and the consequent activation of RAS proteins, small GTPases that are recruited to the membrane and activates RAF (MAPKKK), that in turn activates MEK (MAPKK), which phosphorylates ERK (MAPK), resulting in gene expression regulation, cell division, metabolism, motility, survival, differentiation and apoptosis[26].

Three different members including HRAS, KRAS (two alternative splice variants: KRASa and KRASb[27]) and NRAS compose the RAS family. When RAS proteins bind to GTP, become activated and can transactivate its effector

molecules, including RAF proteins, that initiates a phosphorylation cascade[28].

The RAF family is composed by ARAF, BRAF and CRAF kinases, which are characterized by the presence of a RAS-binding domain (RBD) in the N-terminal region of the protein. Each of the members can dimerize with itself or with any other member of the family. This dimerization and consequent activation result in the phosphorylation and activation of MEK1/2, which in turns, phosphorylates and activates ERK1/2[26,29,30]. Activated ERK can phosphorylate multiple cytoplasmic and cytoskeletal proteins or can translocate to the nucleus, where it phosphorylates and activates several transcription factors[26]. Active ERK can also phosphorylate components of the RAS pathway attenuating the signal transmission and participating in its own regulation[31].

Upon normal conditions, the RAS pathway is subjected to a thigh regulation in order to modulate proliferation and survival mechanisms in non-malignant cells. However, there are many tumors where deregulation of growth factors-dependent signaling and mutations in the upstream effectors of the pathway have been observed, especially in melanoma[19–23]. Thus, understanding the behavior and regulation mechanisms of these altered genes is critical for the management of melanoma patients.

2.3.1. BRAF-mutant melanoma

BRAF mutant melanoma is the most common molecular subtype, reaching an incidence of more than 50% of the cases (*TCGA database*). Most oncogenic *BRAF* mutations, accounting for a 90% of the total, cause valine to glutamic acid substitutions at codon 600 ($BRAF^{V600E}$), which are the result of the point mutation T1799A and involves the constitutive activation of the BRAF kinase domain[19,32]. The second most common mutation, representing a 5-6% of the total, is $BRAF^{V600K}$, where a valine is substituted by a lysine. Other oncogenic mutations in the *BRAF* gene are $BRAF^{V600R}$ and $BRAF^{V600D}$ [32]. All these mutations result in the activation of BRAF and consequently, of the downstream molecules MEK and ERK, resulting in the hyperactivation of the RAS-ERK1/2 pathway and the regulation of cell growth and survival of tumoral cells[19] (Figure I.3).

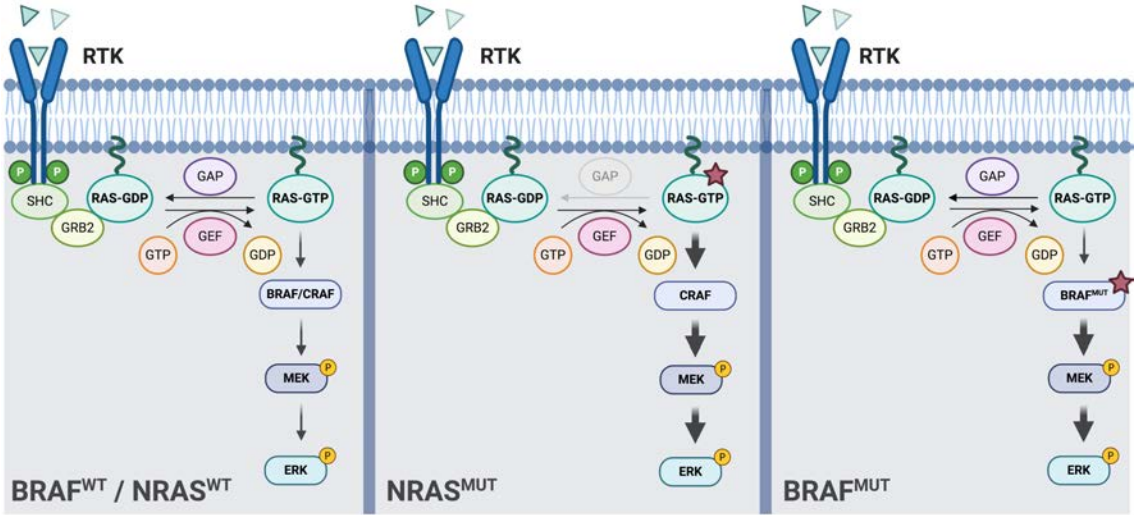

Figure I.3. RAS-ERK1/2 pathway regulation in *NRAS* and *BRAF* mutant tumors.

Since *BRAF* point mutations were discovered in 2002, the targeted therapy landscape for melanoma have changed dramatically and several therapies for the treatment of *BRAF* mutant melanomas have been proposed until now showing promising results. Small molecules that inhibit BRAF have been tested clinically alone and in combination with MEK inhibitors showing significant results in patients carrying *BRAF* mutations. These therapeutic strategies, even successful, have showed some limitations[29].

2.3.2. NRAS-mutant melanoma

The RAS protein family is constituted by HRAS, KRAS and NRAS. These members establish a superfamily of small GTPases that plays an essential role in the transduction of signals from the extracellular media through the activation of RTKs. Under physiological conditions, RAS proteins can exist in either an active (GTP-bound) or an inactive (GDP-bound) conformation. The exchange of GDP for GTP, and consequently, the activation of RAS, is catalyzed by guanine nucleotide exchange factors (GEFs), including SOS1, SOS2 and RasGRF10. On the other hand, GTPase-accelerating proteins (GAPs) are involved in switching RAS from the active to the inactive state[33,34]. Under normal conditions RAS activation typically proceeds following RTK activation upon ligand binding, what results in the autophosphorylation of the receptor and its consequent dimerization. Adaptor molecules carrying an SH2 domain, such as GRB2, are then recruited, followed by GEFs[33–35]. Once activated, RAS is recruited to the membrane, binds downstream

intracellular effectors and stimulates different signaling pathways, including the RAS-ERK1/2 and PI3K/AKT pathways, what results in the coordination of multiple cellular responses including proliferation, survival, differentiation, apoptosis, senescence and metabolism [28,34].

All isoforms share structural and functional similarities and, even are nearly ubiquitous and broadly conserved across species, they are differentially expressed depending on the tissue and the tumor type[36,37]. Regarding the sequence variability among the different isoforms, identical residues are found within the first half of the GTPase domain, while in the second half; an 82% of sequence identity can be appreciated. In the C-terminal domain, significant sequence variability can be observed, constituting the hypervariable region (HVR)[36,37].

In general, *KRAS* is the most frequently found mutated isoform in cancer, including colorectal, lung and pancreatic cancers, however, in the specific case of melanoma, activating mutations in *NRAS* are the most common ones, accounting for more than 20% of the cases[38]. This has been proposed to be due to a higher expression of the *NRAS* isoform in melanocytes, when compared to other cell types[39]. In this isoform, mutations typically occur at codons 12 ($NRAS^{G12}$) and 61 ($NRAS^{Q61}$). $NRAS^{G12}$ mutation affects the conformation of the protein and decreases its sensitivity to GTPase-accelerating proteins (GAPs) while $NRAS^{Q61}$ mutations usually involves a substitution of glutamine to leucine ($NRAS^{Q61L}$) and disrupts the GTPase activity of NRAS locking it in its active conformation[34,40] (Figure I.3). Both mutations are activating and involve the constitutive activation of the RAS-ERK1/2 cascade and the subsequent biological effect in cell proliferation and survival[41]. Furthermore, *NRAS* but not *BRAF* mutations, result in the regulation of additional signaling pathways, like PI3K/AKT pathway[34], supporting the relevance of NRAS in growth, motility and survival and, as a consequence, in tumorigenesis and cancer progression.

When compared with *BRAF* mutations, *NRAS* mutations also involve differences at molecular level that affects the regulation of the RAS-ERK1/2 pathway. It has been described that *NRAS* mutant cells signal preferentially through CRAF rather than BRAF[42]. CRAF-mediated MAPK signaling depends on two parallel mechanisms: the inactivation of BRAF and deregulation of PKA

signaling that prevents CRAF inactivation[42]. The inactivation of BRAF occurs through a negative feedback mechanism in which ERK phosphorylates BRAF at the inhibitory phosphorylation sites S151, T401, S750 and T753[43]. Regarding PKA, it can be inhibited by several mechanisms preventing CRAF phosphorylation at its inhibitory sites[42].

It has been widely described that constitutive activation of the pathway is essential for most melanomas but it is important to distinguish between the mutated agents within the pathway involved in this activation, as well as the molecular and phenotypic implications, in order to develop specific therapeutic strategies. Understanding molecular differences between both *BRAF* and *NRAS* mutant tumors would be essential to propose novel and/or more effective therapies.

2.3.3. Differences among BRAF and NRAS mutant tumors

As previously explained, *BRAF* and *NRAS* mutations involve the activation of the RAS-RAF-MEK-ERK signaling pathway. These mutations have been observed to be mutually exclusive (*TCGA database*) and even the consequences of the mutations seem to be similar, *BRAF* and *NRAS* mutant tumors have been described to be different entities at different levels, including molecular and clinical levels[40,44].

As described in Table I.3, *BRAF* and *NRAS* mutant tumors show different signaling patterns as well as different biological behavior. As previously mentioned, the incidence rate varies between both tumor types, being *BRAF* mutations more commonly found in both, malignant and non-malignant melanocytic lesions[44]. However, contrary to *NRAS* mutations, *BRAF* mutations are not found in congenital nevi[44,45]. While *NRAS* mutations appears in both, sun-exposed and sun-unexposed areas of the skin, *BRAF* mutations preferentially appears in those areas of the skin that have been intermittently exposed to UV radiation[44,46]. Differences in malignancy have been also described, being *NRAS* mutations the ones presenting worse prognosis, due to both, a high mitotic rate and a high metastatic capacity[44,47]. Molecularly, *NRAS* mutations are also involved in the activation of additional signaling pathways, including the PI3K/AKT pathway, whereas in the case of *BRAF* mutant tumors, additional mutations are required for PI3K pathway activation[48,49]. Furthermore, the age of diagnosis can

also differ between both types, being *NRAS* mutant tumors diagnosed in older patients[44,50,51]. An important final consideration is the availability of targeted therapy against *BRAF* mutant tumors, while *NRAS* mutant melanomas lack a specific line of treatment and are treated using other therapeutic alternatives, including chemotherapy and immunotherapy, showing low response rates and toxicity[29,34,40,44].

	***BRAF*^{mut}**	***NRAS*^{mut}**	**Reference**
Incidence	~50%	~20%	*TCGA database*
Location	Intermittently sun-exposed areas	Sun-exposed and sun-unexposed areas	44,46
Non-malignant melanocytic lesions (nevi)	Yes	No	44
Congenital nevi	No	Yes	44,45
Age at diagnosis	Younger	Older (>55 years old)	44,50,51
Malignancy	Lower mitotic rates and thinner primary tumors	Higher mitotic rate and thicker primary tumors	44
Prognosis	It depends on additional mutations	Bad (high metastatic rate)	44,47
Activation of additional signaling pathways	Additional mutations are required (e.g. PTEN)	PI3K/Akt	48,49
Targeted therapy	Yes	No	29,34,40,44

Table I.3. Differences among *BRAF* and *NRAS* mutant tumors.

Recently, it has been described that metabolic settings can be driven by *BRAF* mutations, suggesting an oncogene-dependent metabolic rewiring[52–57]. However, most of the findings are related to *BRAF* mutant tumors, and little is known about the role of *NRAS* mutations in metabolism reprogramming. Deciphering metabolic settings in *NRAS* mutant melanomas could provide new avenues for the establishment of specific therapeutic approaches.

2.4. Therapeutic strategies for the treatment of melanoma

Surgery is the first option for the treatment of melanoma patients at initial diagnosis since primary cutaneous lesions are usually easily removable. However, most melanomas are diagnosed at late stages when metastasis has already occurred. Until 2011, advanced melanomas had been treated using standard chemotherapeutic regimes, like Dacarbazine, showing almost no effects in the overall survival of patients[58]. Significant advances in the understanding of the biological and molecular basis of this disease have been made since then, what

have resulted in the establishment of successful treatments, including targeted therapy and immunotherapy. Nevertheless, only a subset of patients benefits from these approaches and is able to achieve durable responses. Within these groups, the majority experience resistance acquisition and disease relapse, highlighting the need of establishing improved and novel therapeutic strategies[59].

2.4.1. Targeted therapy

As previously established, deregulation of the RAS-ERK1/2 pathway takes place in the majority of melanomas; where *BRAF* mutations, especially $BRAF^{V600E}$, are found in approximately 50% of the cases. Vemurafenib and Dabrafenib were the two first BRAF inhibitors approved for the treatment of *BRAF* mutant melanoma in 2011 and 2013, respectively. In both cases survival benefit was demonstrated when compared to standard treatment (Dacarbazine)[60,61]. However, inhibition of BRAF alone has showed limited responses and has been associated with the development of resistance[62]. Furthermore, additional skin tumors such as cutaneous squamous carcinomas have been observed to appear after treatment[63,64].

Distinct and heterogeneous mechanisms of resistance to targeted therapy have been described; including the reactivation of the RAS-ERK1/2pathway by the acquisition of additional mutations[65], the upregulation of alternative pathways, like PI3K/AKT pathway[65,66], the regulation of cell cycle and apoptosis[67–69], the constitutive activation of receptor tyrosine kinases such as platelet-derived growth factor receptor β (PDGFRβ) or insulin-like growth factor 1 receptor (IGF1R)[70,71], and metabolic reprogramming[72,73]. Moreover, reactivation of the RAS-ERK1/2 pathway can also occur due to molecular switches within the pathway, also known as the "paradoxical activation of the pathway"[74]. This phenomenon results from the activation of CRAF in cells carrying wild type BRAF in response to RAS-ERK1/2 pathway inhibition and is based on the ability of RAF proteins forming dimers. In *BRAF* mutant tumors, upon BRAF inhibition, CRAF can dimerize with another CRAF molecule, or can also forms heterodimers with wild type BRAF, what allows the downstream activation of the pathway[74,75]. This activation is even higher due to the increased kinase activity of BRAF-CRAF heterodimers when compared to BRAF and CRAF homodimers[76].

In order to avoid the paradoxical activation of the pathway, as well as other mechanisms involving resistance acquisition, simultaneous inhibition of MEK and BRAF was proposed several years ago, leading to improved survival when compared to BRAF inhibitor monotherapy. When Dabrafenib, a BRAF inhibitor, and Trametinib, a MEK inhibitor, were administered together, increased clinical benefit and lower toxicity were observed[77]. Combined-treatment is now considered a standard therapeutic option for patients carrying *BRAF* mutations. Currently, several BRAF (Vemurafenib, Dabrafenib, Selumetinib) and MEK (Trametinib, Cobimetinib, Binimetinib) inhibitors have been approved by the FDA and different combinations of them are used in the clinics. Nevertheless, the efficacy of these combinations is restricted to the subset of patients with mutant *BRAF*. Moreover, combined therapies still results in the development of resistance and relapse after a limited period of time[77–79].

The second most common oncogenic mutation in melanoma occurs in *NRAS*. Due to the role of NRAS activation in melanomagenesis and melanoma progression, inhibiting it would provide improved outcome in melanoma patients. Because the activation of RAS depends on previous association to the inner face of the plasma membrane, several efforts have been made to target the hydrophobic modifications of the C-terminal domain necessary for its anchorage. Specifically, farnesyl transferase inhibitors, such as Tipifarnib and Lonafarnib, and S-transfarnesylthiosalicylic acid, also known as Salirasib, have been tested in order to try to prevent NRAS localization to the plasma membrane. Unsuccessful results have been observed[80,81], which can be explained by the presence of alternative modifications, such as geranylgeranyl that also allow NRAS association to the plasma membrane[82]. Moreover, toxicity has been observed due to the inhibition of a large family of proteins that also require farnesylation as a post-translational modification. An alternative mechanism for the specific inhibition of RAS proteins is the inhibition of its binding to the downstream effector RAF molecules. With this aim Rigosertib, a small molecule RAS mimetic, has been tested but no promising results have been obtained[81]. Additional efforts have been made trying to inhibit downstream RAS targets in order to mitigate the pathway activation but only partial responses have been observed[81].

KIT specific targeting has been also tested using Imatinib and other tyrosine kinase inhibitors such as Nilotinib. Some beneficial effects have been observed for those patients carrying KIT mutations, which are mainly those with acral and mucosal melanomas[83–85]. This approach may be promising but accurate selection of specific cohorts of patients with this molecular subtype is essential for treatment success.

Targeting other upstream elements of the RAS-ERK1/2 signaling cascade has been also contemplated and inhibition of several tyrosine kinase receptors (RTKs) has been tested for the treatment of melanoma. Lenvatinib, which targets VEGFR, fibroblast growth factor receptor (FGFR), KIT and proto-oncogene tyrosine-protein kinase receptor RET (RET); and Axitinib, targeting VEGFR1/3, KIT and PDGFR, are some examples. In general, even potential benefit in patients outcome has been observed, further and more complete studies are needed[59]. Even successful, these kind of inhibitors are not expected to have a high impact in this kind of tumors, since amplifications or activating mutations in RTKs are not that frequent in melanoma (*TCGA database*).

2.4.2. Immunotherapy

Until now, several efforts have been made for the modulation and activation of the immune response against tumors. Since first immunotherapy-based trials using IL-2 were performed in the 1980s, showing long-term remission in a few patients[86], several alternative therapies involving T-cells activation have been proposed.

Currently, the most effective immune-therapies are based in the inhibition of immunocheckpoints, specially the inhibition of PD-1/PD-L1 and CTLA-4 axis with Pembrolizumab/Nivolumab and Ipilimumab respectively[87–89]. This approach is based in the blockage of tumor-induced inhibitory effect on effector T cells in order to avoid immune tolerance. This way, effector T cells become active and are able to react against the malignant cells, therefore eliminating the tumor. The combination of different immunocheckpoint inhibitors has provided promising results during the last years, showing tumor regression and improved survival, what has been translated into a significant improve of clinical outcome[90,91].

The past decade has been a time of accelerated progress in this field and although immune-based approaches, specially the use of immunocheckpoint inhibitors, have through light to the field of advanced melanoma therapy, there are still several limitations. In one hand, there are a high percentage of non-responders showing a low objective response rate (ORR), added to the intrinsic toxicity of being targeting the immune system. On the other hand, when compared to targeted therapies, response rates are lower[92]. Moreover, despite promising initial responses in some patients are observed, resistance to immune-based therapies can be developed. Several strategies including genetically modified virus, antibody-mediated inhibition of immunocheckpoints, cytokine-based approaches, vaccines and adoptive cell transfer, are being developed and clinically tested in order to deal with low response rates, treatment-derived toxicity and resistance development[93].

Herpes simplex virus type I T-VEC is a genetically modified virus that preferentially replicates in tumor cells, enhances antigen loading of MHC class I and expresses granulocyte-macrophage colony-stimulating factor (GM-CSF), which results in an increased tumor-antigen presentation by dendritic cells (DCs). Combination with Ipilimumab and Pembrolizumab has showed an increase in the ORR in advanced melanoma patients. However, the majority of responses are limited to the site of injection, and the delivery to metastatic regions is limited[93].

Inhibitors against lymphocyte activation gene-3 (LAG-3), an inhibitor of T-cell response, activation and growth; and T-cell immunoglobulin and mucin-domain containing-3 (TIM-3), a suppressor of $FoxP3^+$ Treg-cells, macrophages and DCs, are now in clinical development. LAG-3 inhibition with different monoclonal antibodies (Relatlimab, LAG525 and MK-4280) has showed promising results in combination with Pembrolizumab or Nivolumab. Regarding TIM-3, trials are ongoing and potential synergistic effects are expected in combination with other immunocheckpoint inhibitors[94].

Several cytokines, including IL-12, IL-15, IL-18, IL-21 and GM-CSF have been tested showing reduction of tumor growth. However, the use of cytokine-based treatments as single agents is quite controversial due to their pleiotropic activity and derived-toxicity[93].

Peptide vaccines have been proposed as an alternative mechanism to induce specific immune response against tumor antigens. The results have showed some potential synergistic effects in combination with other immunocheckpoint inhibitors[93].

Adoptive cell transfer is emerging as a new strategy for the treatment of patients with non-functional tumor antigen-specific T-cells. Two different approaches, including transfer of expanded pre-existing anti-tumor T-cell populations and gene therapy based in the alteration of T-cells to express high affinity T-cell receptors (TCRs) becoming melanoma-specific have been described. CAR-T cells (chimeric antigen receptor T-cells) have been proposed for adoptive cell transfer, showing efficacy in hematological malignancies. However, lower responses have been described in solid tumors. Combination of CAR-T cells-based therapy with immunocheckpoint inhibitors is currently being tested[93].

Future promising strategies include the combination of different immune-based therapies among them and with targeted therapy agents. Even several trials are ongoing trying to increase response rates and to deal with toxicity and resistance-development, it seems that only certain subsets of patients would benefit from these approaches.

2.4.3. Therapeutic needs

Despite huge advances have been made in the landscape of metastatic melanoma treatment during the last decade, only a subset of patients achieves long-term responses. Moreover, there are still a significant percentage of patients that do not respond to any available therapy. Establishment of novel therapeutic approaches, together with the improvement of already available ones, are critical steps to further improve survival outcomes in patients with this disease.

Targeted therapies are only available for *BRAF* mutant tumors but, regarding those 50% of patients lacking *BRAF* mutations, few advances have been made in the development of specific targeted treatments. As already mentioned, the next most common mutation in melanoma occurs in *NRAS*, accounting for more than 20% of cases. *NRAS*-mutant patients have been observed to present a more aggressive disease that is associated with poorer prognosis[44,47]. Although the

relatively high incidence and relevance of this mutation in the disease, these tumors are still orphans in terms of therapy and are subjected to treatment with non-specific approaches, which includes chemotherapy and immunotherapy, resulting in low response rates and high toxicity. There is an urgent need to find new approaches for the treatment of *NRAS*-mutant melanoma in order to target these tumors in a more specific way, what will contribute to the improvement of patient's survival.

2.4.3.1. RAS: The undruggable oncogene

RAS proteins have been observed to be highly relevant in melanoma biology, being mutated in more than 20% of the cases and playing a key role in the regulation of the RAS-ERK1/2 pathway. As explained above, these proteins need to be post-translationally modified in order to acquire acyl groups that allow its localization to the plasma membrane[80–82]. During the last years different post-translational modification inhibitors have been proposed, however, none of them have produced benefits in patient's outcome and serious side effects have been observed.

Due to the failure observed upon direct inhibition of NRAS, efforts have been focused in the inhibition of critical signaling pathways driven by RAS-mediated transformation. The most studied approach has been the inhibition of the RAS-ERK1/2 pathway using MEK inhibitors. After several clinical trials testing different MEK inhibitors from first to third generation, no specific response has been observed in patients carrying *NRAS* mutations[95–98].

Next generation MEK inhibitors, such as Binimetinib and Pimasertib, have showed certain effects in progression-free survival (PFS) in *NRAS*-mutated advanced melanoma patients when compared to Dacarbazine, however, adverse effects are still observed[99,100]. In order to achieve more relevant clinical responses, MEK inhibitors are being tested in combination with additional agents. It is of especial interest the synergistic effect observed upon the combination with PI3K pathway inhibitors. Several clinical trials are ongoing in order to define the most efficient drug combination for the treatment of this molecular subtype[40]. For the moment, no clear effects are observed and further investigation is needed.

Although the currently implemented targeted and immunotherapeutic approaches may provide some benefit to patients with *NRAS*-mutant melanoma, none of these therapies are mutation specific and have shown partial responses and significant toxicity. In contrast with *BRAF* mutant melanoma, to date, there are no available specific and effective therapeutic strategies approved for *NRAS* mutant melanoma treatment. As a consequence, many clinicians do not perform mutational profiling of *NRAS* routinely although the presence of *NRAS* mutations may have prognostic implications and would facilitate patient management and clinical trial enrolment. A better understanding of the biological and signaling features of the *NRAS*-mutant melanoma subtype is urgently needed. This would help to the establishment of novel, specific and effective therapeutic strategies, what is essential to keep advancing in the management of this disease.

3. Cancer Metabolism: An Emerging Hallmark of cancer

3.1. Metabolic reprogramming in cancer

During the last two decades interest in how cancer cells regulate metabolism has growth considerably. Tumor cells have to deal with stressful situations like low nutrient and oxygen accessibility at the same time that they need to maintain high proliferation rates and tumor growth. In order to adapt to such stressful situation and sustain tumor mass, cells have to provide enough energy as well as building blocks, like amino acids, nucleotides and lipids[53,54]. As a result, metabolism regulation is frequently altered in transformed cells, what results in an opportunity for the specific targeting of them. One of the most studied and established cancer hallmarks is the adaptation of glucose metabolism, involving an increase in aerobic glycolysis or *Warburg effect* even in the presence of enough oxygen[53,54,101].

Tumor metabolism is a complex process that derives from intrinsic tumor properties together with tumor-microenvironment interactions and all the involved processes must be coordinated. The metabolic composition of the tumor microenvironment can determine the metabolic phenotype of the tumor cells, and vice versa. This fact results in high heterogeneity between different tumors or even within the same tumor[54,102]. Moreover, metabolic features of the tumor can also

change during time in order to adapt to the metabolic needs during cancer progression[102,103]. In this context, cancer cells are exposed to different levels of oxygen and nutrients, what determines the behavior of the cells that, depending on the location within the tumor, will rewire it metabolism in one way or another in order to adapt to these conditions[102]. Because of the complexity of this process, characterization of metabolic regulation in cancer has been a challenge during the last years.

Many studies indicate that targeting metabolism can result in the reduction of cancer growth. Furthermore, during the last years, evidence is growing about the fact that metabolic reprogramming can be subjected to regulation by oncogenes and/or tumor suppressors[102,103]. These discoveries open new avenues for therapeutic interventions based on targeting metabolism in tumor cells. Moreover, metabolic targeting could be combined with other anticancer drugs in order to improve the efficacy of the treatment, avoid resistance development and improve patient's outcome.

3.2. Oncogene-dependent metabolic settings

Metabolic reprogramming is the result of a complex interplay between oncogenes, tumor suppressors and components of the tumor microenvironment. These factors can modulate both the expression and the activity of a wide range of metabolic enzymes, giving rise to specific expression and activity patterns that differ from non-tumoral cells. These patterns will vary depending on the tissue of origin and the genetic and epigenetic features of the tumor cells.

Until now, several oncogenic drivers have been described to regulate different metabolic pathways. In the specific case of the RAS-ERK1/2 pathway, *BRAF* oncogenic mutations have been related to the regulation of several genes such as hypoxia-inducible factor 1 subunit α (*HIF1α)*, MYC proto-oncogene (*MYC)* and melanocyte inducing transcription factor (*MITF)*, which are responsible of the regulation of distinct metabolic pathways, including carbon metabolism, especially by regulating the balance between aerobic glycolysis and oxidative phosphorylation[57,104–106].

3.2.1. Metabolic regulation in BRAF mutant tumors

It is well established that oncogenic *BRAF* mutations regulate metabolic reprogramming in melanoma[52,53,57,107]. In *BRAF* mutant tumors, pyruvate has been defined as a pivotal metabolite. It can fuel alternative metabolic pathways, what will define the tumor destiny. If it is metabolized through the TCA cycle and the consequent oxidative phosphorylation, oncogene-induced senescence (OIS) will be activated[108,109]. This is the result of the regulation of pyruvate dehydrogenase complex (PDH) regulated by both, pyruvate dehydrogenase kinases (PDKs) and phosphatases (PDPs). In senescent cells, PDH activity is increased due to a higher phosphatase activity, which result in the maintenance of OIS[110]. On the other hand, induction of aerobic glycolysis would result in the development of tumorigenesis, in this case, due to an increase of kinase activity[108,109]. It has been described *in vivo* that PDK1 silencing (both, genetically and chemically), decreases tumorigenesis and promotes regression of already established tumors. Moreover, it enhances sensitivity to BRAF inhibitors, suggesting the combination of PDK1 and BRAF inhibitors as a novel therapeutic approach[111].

Another important metabolic pathway regulated in *BRAF* mutant tumors is ketogenesis. High expression of mitochondrial ketogenic enzymes, including HMG-CoA synthase 1/3 and hydroxyl-3-methylglutaryl-CoA lyase (HMGCL), have been described to cooperate with *BRAF* mutations[112]. In primary human melanomas, HMGCL overexpression on a $BRAF^{V600E}$ background is accompanied by elevated phosphorylation and activation of MEK and ERK in comparison to tumor cells with wild-type BRAF[112]. Importantly, HMGCL is required for BRAF-induced cell transformation, as knockdown of either mutant *BRAF* or *HMGCL* decreases cell proliferation and tumor growth in xenograft models[112]. Addition of acetoacetate, the HMGCL product, to the media of cultured cells selectively promoted proliferation of *BRAF* mutant cells and rescued growth phenotypes induced by *HMGCL* knockdown, what was accompanied by increased MEK and ERK phosphorylation[112].

Moreover, BRAF inhibition promotes the overexpression of MITF and peroxisome proliferator-activated receptor γ coactivator 1α (PGC1α) in order to adapt to low ATP levels and as a consequence, reduced glycolytic flow[57]. MITF

expression partially restores glycolysis through the induction of mitochondrial biogenesis and the increase of oxidative metabolism. ATP levels can be also restored through a PGC1α-driven mitochondrial generation program that results in the upregulation of oxidative phosphorylation. This induction limits BRAF inhibitor efficacy. Thus, combining BRAF inhibition with inhibitors of mitochondrial function is a promising approach to inhibit tumor cell proliferation[57].

Both, metformin and phenformin, known inhibitors of AMP-activated protein kinase (AMPK), have been described to enhance the therapeutic efficacy of $BRAF^{V600E}$ inhibitors in melanoma[113,114]. This efficacy is due to metformin- and phenformin-derived blockage of the boost in glycolytic and TCA cycle intermediates taking place during malignant transformation[115]. Moreover, $BRAF^{V600E}$ mutant tumors have been described to be insensitive to energy stress and consequently do not activate AMPK due to the uncoupling of liver kinase B1 (LKB1)-AMPK axis[107].

BRAF alterations are also involved in glutamine metabolism. BPTES, an inhibitor of the enzyme glutaminase, synergizes with BRAF inhibitors due to the increased reliance of $BRAF^{V600E}$-inhibited melanoma cells on glutamine[72,116].

Overall, these studies independently confirm that combined targeting of mitochondrial oxidative metabolism and oncogenic BRAF signaling has a synergistic effect in the inhibition of tumor growth and resistance development. However, even more than 20% of melanomas have activating mutations in *NRAS*, surprisingly, much less is known about the metabolic consequences of this genetic alteration. In the case of *KRAS* mutations, several studies support metabolic rewiring in different types of cancers which involves changes in glucose metabolism, glutamine utilization, mitochondrial metabolism and reactive oxygen species (ROS) metabolism[53].

3.3. Glucose metabolism

Glucose metabolism involves different metabolic pathways including glycolysis, which transform glucose to pyruvate with the consequent ATP generation; the pentose phosphate pathway (PPP), which generates ribulose-5-phosphate and

pentose phosphates for RNA and DNA synthesis, as well as NADPH; the hexosamine pathway, required for protein glycosylation; glycogenesis, which storage glucose for future needs; the serine biosynthesis pathway, involved in the generation of aminoacids; and the one-carbon metabolism cycle, required for purine and glutathione biosynthesis, as well as for NADPH generation[103].

Until now, glycolysis has been the most studied and cancer-related metabolic pathway. It is a multistep process in which glucose is transformed into pyruvate in the cytoplasm (Figure I.4). First of all, glucose is internalized into the cell through specific transporters known as GLUT1-4. The different isoforms present different affinities for glucose and its expression can vary depending on the cell type and tissue[103]. Interestingly, certain oncogenes can regulate glucose uptake by switching from one isoform to another in tumor cells. For example both, *KRAS* and *BRAF* mutations, are known to induce the expression of GLUT1[117,118]. Nevertheless, targeting glucose carriers as a way of targeting cancer is not a good approach because of the derived toxicity from non-tumoral cells also expressing these same isoforms[103].

The glycolytic pathway is composed by several reversible enzymatic reactions and three irreversible or committed steps, which are the most relevant ones in terms of regulation. Once glucose is internalized, it is phosphorylated by hexokinase (HK) to produce glucose 6-phosphate (G6P) in the first committed step. At this point glucose is trapped inside the cell. G6P is then rearranged to fructose 6-phosphate (F6P) by glucose phosphate isomerase (GPI). Fructose can also enter to the glycolytic pathway by phosphorylation at this point. The second committed step of glycolysis is driven by phosphofructokinase 1 (PFK-1) and catalyzes the conversion of F6P into fructose 1,6-bisphosphate (F 1,6-biP). The obtained hexose is split in two trioses: glyceraldehyde 3-phosphate (GA3P) and dihydroxyacetone phosphate (DHAP) by aldolase (ALDO). DHAP can be quickly converted into GA3P by a triosephosphate isomerase enzyme (TPI). Then, glyceraldehyde 3-phosphate dehydrogenase (GAPDH) catalyzes the conversion of GA3P into 1,3-bisphosphoglycerate (1,3-biPG). Subsequently, 1,3-biPG is converted into 3-phosphoglycerate (3PG) by phosphoglycerate kinase (PGK) in a reaction that generates ATP. Phosphoglycerate mutase (PGAM) isomerizes 3PG into 2-

phosphoglycerate (2PG). Enolase next converts 2PG to phosphoenolpyruvate (PEP) and finally PEP results in pyruvate upon pyruvate kinase (PKM) activation in the third and last committed step of the pathway, also involving the production of ATP[103].

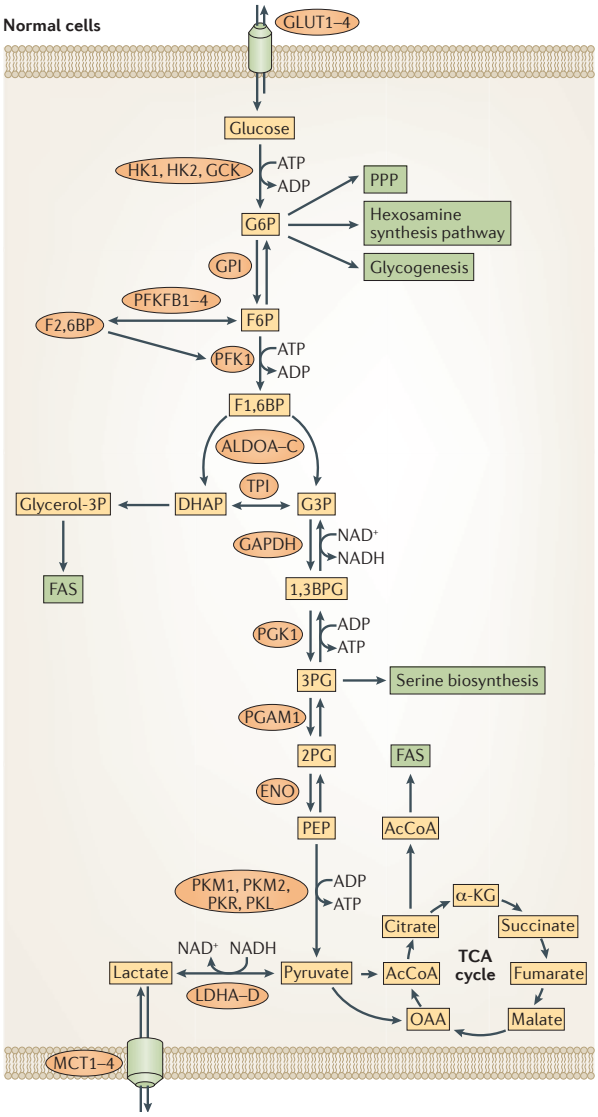

Figure I.4. Glycolysis pathway. Enzymes that catalyze the metabolic reactions are shown in ovals. GLUT=Glucose transporter; HK=Hexokinase; GCK=Glucokinase; G6P=Glucose 6-phosphate; GPI=Glucose 6-phosphate isomerase; F6P=Fructose 6-phospate; PFKFB=6-Phosphofructo 2-kinase/fructose-2,6-bisphosphatase; F 2,6-biP=Fructose 2,6-bisphosphate; PFK-1=Phosphofructokinase; F 1,6-biP= Fructose 2,6-bisphosphate; ALDO=Aldolase; DHAP=Dihydroxyacetone-phosphate; TPI=Triosephosphate isomerase; G3P=Glyceraldehyde 3-phosphate; GAPDH=Glyceraldehyde 3-phosphate dehydrogenase; 1,3-biPG=1,3-bisphosphoglycerate; PGK=Phosphoglycerate kinase; 3PG=3-phosphoglycerate; PGAM=phosphoglycerate mutase; 2PG=2-phosphoglycerate; ENO=Enolase; PEP=Phosphoenol pyruvate; PK=Pyruvate kinase; LDH=Lactate dehydrogenase; MCT=Monocarboxylate transporter; AcCoA=acetyl-CoA; α-KG=α-ketoglutarate; OAA=Oxaloacetate; FAS=Fatty acids synthesis; PPP=Pentose phosphate pathway; TCA=Tricarboxylic acid. *Hay et al., 2016*[103].

The energetic balance of the pathway results in the consumption of two molecules of ATP during the first half or preparatory phase of the pathway and the generation of four molecules of ATP during the second or payoff phase of the pathway. Moreover, two molecules of NADH are generated.

3.3.1. Glycolysis regulation

The conversion of glucose into pyruvate is regulated to meet two major cellular needs: the production of ATP and the provision of building blocks to sustain cell proliferation and tumor growth. As previously explained, glycolysis involves several enzymatic reactions that can be classified into reversible and irreversible. Irreversible steps, which are known to be critical for the regulation of the process, are catalyzed by hexokinases (HKs), phosphofructokinases (PFKs) and pyruvate kinases (PKMs). These enzymes are subjected to a rigorous control by a wide range of mechanisms.

There are five different human hexokinases whose expression varies depending on the tissue. HK2 is the most expressed isoform in cancer cells, resulting in an increased glycolytic flux[119]. This step is known as the first committed step of glycolysis mainly for two reasons: it traps glucose inside the cell and it is the converging point of glycolysis, the pentose phosphate pathway (PPP), the hexosamine pathway and glycogen biosynthesis. Hexokinases can be allosterically inhibited by its own product glucose 6-phosphate (G6P)[103].

In the case of phosphofructokinases, regulation is more complex. PFK-1 can be allosterically regulated (activated) by fructose 2,6-bisphosphate (F 2,6-biP), which is generated from fructose 6-phosphate (F6P) by 6-phosphofructo-2-kinase/fructose-2,6-bisphosphatase (PFK-2 or PFKFB) enzymes. Different downstream products of glycolysis, including phosphoenol pyruvate (PEP), lactate, citrate, palmitoyl-CoA and ATP, can also negatively regulate this enzyme. Moreover, PFK-1 activity can be inhibited by glycosylation at position S529 avoiding the binding to F 2,6-biP[120]. Regulation of this enzyme is essential for the control of metabolites derivation to branching pathways[103].

Pyruvate kinases catalyze the last glycolytic step. There are four different pyruvate kinases: PKM1, PKM2, PKR and PKL. They can be activated by direct

binding of both, F 1,6-biP and serine; and inhibited by phosphorylation at Y105 or binding to phosphotyrosine peptides. PKM activity can be also modulated by high levels of reactive oxygen species (ROS), resulting in the derivation of metabolites to alternative pathways in order to generate NADPH to combat oxidative stress[103,121]. Cancer cells usually express pyruvate kinase PKM2, which is characterized by its low affinity for PEP and results in the attenuation of this step[122]. This suggests the existence of an alternative mechanism for the conversion of PEP into pyruvate. This reaction depends on PGAM1, the enzyme that catalyzes the conversion of 3PG into 2PG in the pathway. This enzyme, moreover, is able to generate pyruvate from PEP[123]. The attenuation of this step diverts metabolites into the branching pathways, such as the PPP and the serine biosynthesis pathway, in order to produce enough metabolic intermediates to sustain cell growth and proliferation.

3.3.2. Regulation of glucose metabolism in cancer

There is not a common mechanism for all cancer cells to regulate and reroute glucose metabolism, but some frequent strategies have been observed to occur in a significant number of tumors[103].

Many malignant cells are characterized by an increased glucose uptake. Moreover, there are additional mechanisms that modify the glycolytic flux for an efficient adaptation to the changeable metabolic needs. These mechanisms are mainly focused in the regulation of the expression and activity of the three glycolytic pivotal enzymes. In one way, higher expression of hexokinases, being HK2 the most relevant isoform in cancer, has been described[119]. The second committed step of glycolysis is dependent on PFK-1, which catalyzes the conversion of F6P into F 1,6-biP. Cancer cells show increased activity of this enzyme due to the regulation of PFKFB1-4 enzymes, which produces F 2,6-biP, an allosteric regulator of PFK-1, being PFKFB3 isoform the most expressed one in tumor cells due to the higher kinase/phosphatase activity ratio of this isoform[124,125]. The third pivotal step of the glycolytic pathway is catalyzed by pyruvate kinases, converting PEP into pyruvate. In the case of this step, an attenuation of the reaction has been described in cancer cells, what is explained by a preference for cancer cells of using PKM2, an isoform presenting a lower affinity

for PEP[122]. This attenuation results in higher flux of glycolysis-derived metabolites to branching pathways.

As previously mentioned, one of the most relevant mechanisms involved in the adaptation of general metabolism and specifically, glucose metabolism, is oncogene-dependent metabolic rewiring. Some of the most studied oncogenes until now, including *KRAS*, *BRAF*, *AKT and MYC*, have been described to regulate glucose transporters[117,118,126]. Tumor suppressors also play an important role in the regulation of metabolism. *TP53* induces the expression of TP53-induced glycolysis and apoptosis regulator (TIGAR)[127], which can decrease the levels of F 2,6-biP, and as a consequence decrease PFK-1 activity. *TIGAR* can also regulate HK2, promoting its activity in a PFKFB-independent manner[128]. PFKFB isozymes have been described to be relevant for malignancy acquisition, specifically *PFKFB2* and *PFKFB3*, which have been observed to be upregulated in cancer cells, are under the control of AKT[129].

Environmental stressors, like hypoxia, and one of the most well-known hypoxia inducible factors, HIF1α, have been also described to accelerate glucose metabolism by a wide range of different mechanisms. One example is the increase in the expression of *GLUT1* and *HK2*[130].

Events following glycolysis are also differentially regulated in cancer cells. Pyruvate conversion into lactate is increased in tumoral versus non-tumoral cells by an increased expression of lactate dehydrogenases (LDHs)[131]. These enzymes are bidirectional and different isoforms present different affinity for pyruvate and lactate. LDHA has higher affinity for pyruvate while LDHB present higher affinity for lactate. Depending on the most expressed isoform, the flux will go in one sense or another. The most expressed isoform in cancer is LDHA, what explains the increased flux from pyruvate to lactate in these cells. The produced lactate is mainly secreted to the extracellular media thanks to the presence of specific carriers known as monocarboxylate transporters (MCTs). Diminishing intracellular accumulation of lactate is essential in order to maintain low acidic environment as well as to avoid PFK-1 inhibition by this metabolite[132]. Lactate secretion also has some advantages for the extracellular environment including regulation of invasion[133] and its use as an energy source for adjacent cells[134]. Both,

LDHA and MCTs, can be regulated by HIF1α and MYC[130,135].

GAPDH, even it is not considered a pivotal enzyme in glycolysis regulation, is also relevant in terms of glucose diversification as its inhibition can reroute glucose to the PPP in order to generate reduction power. Under oxidative stress conditions, the channeling of metabolites to the PPP is further increased by the oxidative inhibition of GAPDH activity[136].

Moreover, glycolytic enzymes present alternative functions that are not related to metabolism and promote malignant transformation[137] (Figure I.5). These functions are mainly associated with transcriptional regulation, cell cycle regulation and chemoresistance.

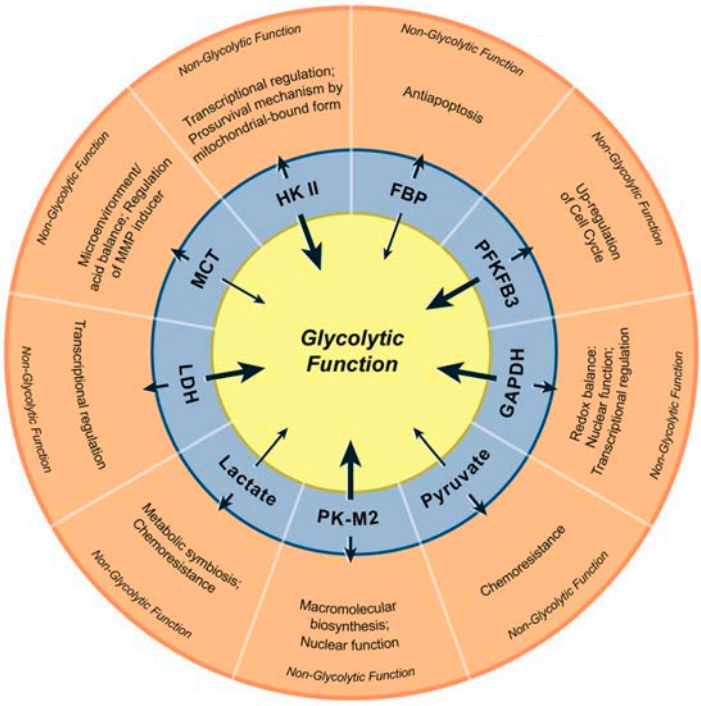

Figure I.5. Non-metabolic functions of glycolytic enzymes and metabolic intermediates in cancer cells. *Ganapathy-Kanniappan and Geschwind, 2013.*

3.3.2.1. Warburg effect

All these molecular changes taking place in malignant cells lead to an increase in glycolytic flux. However, this does not always result in an increase in oxidative phosphorylation (OXPHOS). Otto Warburg described this phenomenon in the late 1920s and since then it has been known as *Warburg effect* and it has been considered one of the most accepted and well-described cancer hallmarks[101].

The rationale of regulating glucose metabolism in this way is that cancer cells present a high demand of energy, reduction power and building blocks for anabolic processes in order to sustain high proliferation rates and tumor growth. This means that glycolysis is accelerated in cancer cells to feed the branching pathways that generate enough biomass to sustain nucleic acid, protein and membrane synthesis, allowing tumor maintenance and growth. Even the yield of ATP per glucose molecule consumed is lower than through complete OXPHOS, it can surpass that produced from OXPHOS if the glycolytic flux is high enough. In summary, the *Warburg effect* has a positive impact on energy production, biomass generation and detoxification of reactive oxygen species (ROS) through the generation of reduction power[138].

This discovery has been contemplated as an opportunity for the specific targeting of these cells and has been also used for many years for the development of tumor detection using image techniques. This difference in glucose consumption in tumoral versus non-tumoral cells can be used for the specific detection of tumors through positron emission tomography (PET), which is based in the use of labeled glucose analogue [^{18}F] fluorodeoxyglucose (FDG), whose uptake is higher by high proliferative cells[139].

3.3.2.2. Glucose deprivation

Glucose deprivation is one of the most common environmental factors affecting tumor cells. This occurs in tumors with high growth rate, where cells that stay in the middle of the tumor mass are not well irrigated. This situation is especially harmful for cancer cells due to its dependence on glucose to maintain cell proliferation and survival. At the molecular level, glucose starvation results in the reduction of intracellular ATP and NADPH, generating an energetic imbalance and a stress condition derived from ROS intracellular accumulation, what can lead to cell death. In order to overcome this situation, cells activate AMP-activated protein kinase (AMPK). AMPK inhibits acetyl-CoA carboxylase 1/2 (ACC1/2), an essential enzyme for the regulation fatty acid synthesis (FAS) and fatty acid oxidation (FAO). As a consequence of this change in fatty acids synthesis regulation, NADPH consumption decreases. Moreover, NADPH synthesis is promoted upon FAO

induction and the activation of the folate pathway[140]. Glucose starvation can also promote the use of other alternative energy sources, like aminoacids. Many tumor cells rely on glutamine metabolism to fuel their cellular bioenergenicts, especially under energy stress conditions. Through conversion from glutamine to glutamate and α-ketoglutarate, cells can fuel the TCA cycle. Glutamine metabolism has been described to be regulated by MYC, which can promote glutamine uptake, as well as glutamine catabolism. Serine and glycline are some other examples of alternative energy sources for cancer cell metabolism[53,106].

3.3.3. Targeting metabolism as a novel therapeutic approach

The exploitation of metabolic reprogramming may provide attractive and effective therapeutic approaches for the selective targeting of cancer cells. However, to be effective, there are different issues to consider: the efficacy of metabolic routes, in particular glycolysis, is in part due to the existence of several isoforms of the different glycolytic enzymes. Additionally, inhibitors may not distinguish between the cancer-specific isoform and the isoforms expressed by normal cells, and even if specificity could be achieved, the expression of the other isoforms could be induced in response to inhibition of the cancer-specific isoform, what would compensate the function of the inhibited isoform. Another concern is related to metabolic heterogeneity of the tumors. This condition can overwrite the inhibition of one metabolic pathway by the upregulation of alternative routes. To avoid this, different metabolic pathways should be inhibited at the same time.

4. Phosphofructokinase (PFK-1)

4.1. Isozymes and structure

PFK-1 enzymes, kinases involved in the phosphorylation of F6P to F 1,6-biP, are expressed by three different tissue-specific genes: *PFKM* in muscle, *PFKL* in liver and *PFKP* in platelets. The molecular weight of each subunit varies being 82.5 kDa, 77 and 86.5 respectively[124]. For the enzyme to be active, each subunit has to dimerize with three more subunits forming homo- or hetero-tetramers, depending on the cell type[141]. The main isoenzymes expressed in tumor cells are PFKP and PFKL. On the other hand, fructose 1,6-bisphosphatases (FBPases) catalyzes the opposite reaction in which F 1,6-biP is dephosphorylated back to F6P during the

gluconeogenesis pathway[124] (Table I.4).

Gene name	Chromosomal location (human)	Kinase/phosphatase activity	Regulation
PFKM	12q13.11	Kinase	PKA, PKC, AMPK
PFKL	21q22.3	Kinase	RAS, Src, HIF1α
PFKP	10p15.2	Kinase	AKT, EGFR, HIF1α, Glycosylation, Snail
FBPase1	9q22.32*	Phosphatase	Snail
FBPase2	9q22.32*	Phosphatase	Not described

Table I.4. Phosphofructokinase (PFK-1) and fructose-1,6-bisphosphate (FBPase) isoforms. Table includes chromosomal location, enzyme acvtivity and known regulation mechanisms. *Same chromosomal region, different locus. *Modified from Bartrons et al., 2018*[124].

4.2. *Regulation* and role in cancer

As previously mentioned, glycolysis is a tightly regulated process where the irreversible steps are key for the control of the pathway. The step catalyzed by PFK-1 is the most important one due to its role in the redirection of the glycolytic metabolites to branching metabolic pathways, which is essential for rapid proliferating cells to generate enough reduction power and biomass to sustain tumor growth.

This enzyme is subjected to a complex regulation process. Its functionality and regulatory characteristics depend on the composition of the different subunits forming the active tetramer. Furthermore, PFK-1 can be also regulated by different allosteric effectors, including negative (citrate, ATP, PEP, and $[H^+]$) and positive effectors (F 2,6-biP, AMP, F 1,6-biP, G 1,6-biP, NH_4^+, and P_i). This fact results in the coordination of the response to the energy status of the cell[141]. Moreover, the presence of high amounts of lactate induces the dissociation of the tetramers reducing its enzymatic activity and consequently, reducing glycolytic flux[132].

PFK-1 activity can be also induced by different oncogenes as well as cancer-related transcription factors. Overexpression of RAS, Src or HIF1α has been described to be involved in the regulation of PFK activity[142,143]. The transcriptional repressor Snail can also reprogram glucose metabolism by suppressing lactate production and, as a consequence, PFKP[144].

Postranslational modifications, such as glycosylation and phosphorylation, also modulate the activity of this enzyme. Glycosylation can occur in response to hypoxic stress, which results in the inhibition of PFK-1 activity and the consequent redirection of the glycolytic flux toward the PPP[120]. PFK-1 isozymes can be phosphorylated by different kinases but this does not have significant effects in the enzyme activity[145,146]. AKT can bind to and phosphorylate PFKP at S386, which inhibits its binding to TRIM21 E3. This results in the inhibition of PFKP polyubiquitylation and subsequent degradation, so an increase in glycolytic flux can be observed[147]. The enzyme location is also important for its regulation. PFKM activity has been observed to increase upon localization to the actin filaments of the cytoskeleton[148].

PFKFB1-4 enzymes, which are characterized by dual kinase/phosphatase activity, as well as TIGAR, catalyze fructose-6-phosphate/fructose-2,6-bisphosphate cycle, thus playing a key role in the control of PFK-1 and consequently, of the glycolytic rate[124] (Figure I.6).

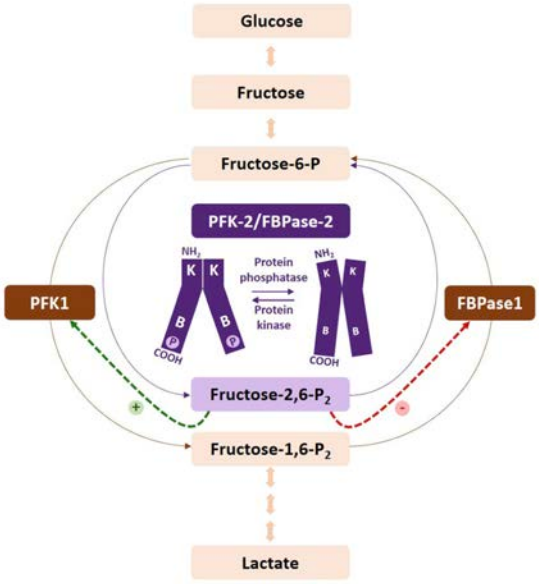

Figure I.6. Regulation of the F6P/F 1,6-BP substrate cycle. *Bartrons et al. 2018.*

As stated above, targeting metabolic enzymes as a therapeutic strategy against tumor cells may not be a good approach as normal cells also express the same enzymes and it could result in non-tolerable toxicity. Targeting specific mechanisms involved in the regulation of these enzymes in tumor cells, instead of directly targeting the glycolytic enzymes, could overcome these unspecific effects. Following this rational, PFK-1 enzyme could be inhibited by directly targeting

PFKFB enzymes, specifically those isoforms preferentially expressed by cancer cells. PFKFB enzymes product F 2,6-biP concentration inside the cell depends on the relative kinase and phosphatase activities of the different PFKFB isoforms so, specific inhibition of the kinase activity would result in a decrease of F 2,6-biP amount and the subsequent inhibition of PFK-1 activity. Thus, the use of small-molecule inhibitors that inhibit the kinase activity of cancer-specific PFKFB isoforms has been proposed as a possible therapeutic approach for the inhibition of PFK-1 in cancer cells[149].

5. PFKFB (6-phosphofructo-2-kinase/fructose-2,6-bisphosphatase) enzymes

5.1. Isoenzymes and structure

PFKFB enzymes are structured in two tandem domains with opposing activities. The first one, with kinase activity, is able to phosphorylate F6P to F 2,6-biP; and the second one, with phosphatase activity, dephosphorylates F 2,6-biP back to F6P. Because F 2,6-biP has an allosteric effect in PFK-1 activity, the relative kinase to phosphatase activity ratio of PFKFB enzymes plays an essential role in the regulation of PFK-1 activity, modulating the intracellular levels of F6P and F 1,6-biP and consequently, regulating the glycolytic flux.

Gene name	Chromosomal location (human)	Kinase/phosphatase ratio	Regulation
PFKFB1	Xp11.21	1.2 (bovine liver), 2.5 (rat liver), 0.4 (rat muscle)	PKA, PP2A
PFKFB2	1q32.1	1.8 (bovine liver)	AMPK, PKA, AKT, PKC, RSK, Glucocorticoids, Androgens
PFKFB3	10p15.1	710 (human placenta), 3.1 (bovine brain)	AMPK, PKA, AKT, PKC, Smad, RSK, p38-MK2, Estrogens, Adenosine, LPS, P53, S-glutathionylation, demethylation
PFKFB4	3p21.31	0.9 (human testis), 4.1 (rat testis)	HIF1α, P-PPARγ, testosterone, p53

Table I.5. Phosphofructokinase-2 isoforms. Table includes information regarding chromosomal localization of the different PFKFB isoforms, kinase to phosphatase activity ratio and known regulators. *Modified from Bartrons et al., 2018*[124].

There are four isoforms of PFKFB (PFKFB1–4), each one encoded by a separate gene. The relative kinase to phosphatase activity of each isoform varies as well as their relative expression levels, which are tissue-specific (Table I.5, Figure I.6). It is important to remark the higher kinase to phosphatase ratio of PFKFB3

(710) in comparison with the rest of the isoforms, what explains why cancer cells preferentially express it.

PFKFB proteins are known to be homodimeric, composed of two 55 KDa subunits. Each monomer present both kinase and phosphatase domains within the same polypeptide chain, with the kinase domain at the N-terminal end of the protein and the phosphatase domain at the C-terminal end[150].

5.2. Regulation and role in cancer

As previously explained, PFKFB enzymes are regulators of PFK-1 through the generation of fructose 2,6-bisphosphate. This metabolite is a known allosteric regulator of PFK-1, which results in the increase of the affinity of PFK-1 for F6P and the modulation of ATP-mediated inhibition of PFK-1. It can also synergistically increase the affinity of PFK-1 for AMP, a positive allosteric effector of the enzyme. Moreover, it is involved in the inhibition of the phosphatase activity of the enzyme[124]. Furthermore, F 2,6-biP stabilizes PFK-1 and promotes its association into tetramers and higher oligomers with enhanced activity[124,141,148]. Therefore, changes in the concentration of this metabolite regulate the activity of PFK-1 and FBPase1, thereby conferring a key role of F 2,6-biP in the regulation of the glycolytic flux. These enzymes are mainly regulated by phosphorylation and its regulation varies depending on the isoform[124] (Figure I.7).

PFKFB1 can be phosphorylated at residue S32 by cAMP-dependent protein kinase (PKA), in response to glucagon, and dephosphorylated by protein phosphatase 2A (PP2A), activating the bisphosphatase and inhibiting the kinase activity respectively. This one is the only isoform that has not been found to be overexpressed in cancer cells[124].

PFKFB2 has been described to be expressed in cancer cells[151,152]. This enzyme can undergo phosphorylation in different sites, integrating signals from many pathways. S466, T475 and S483 can be phosphorylated by 3-phosphoinositide-dependent kinase 1 (PDPK-1), AMP-activated protein kinase (AMPK), PKA, PKB/AKT, PKC, p70 ribosomal protein S6 kinase (S6K1), calcium-calmodulin-dependent protein kinase (Ca/CAMK) and p90 ribosomal protein S6 kinase (RSK). Phosphorylation at these residues results in the activation of the

enzyme[150]. This enzyme is also subjected to transcriptional regulation. Regarding promotion of cancer phenotype, it has been described that PFKFB2 can contribute to metabolic reprogramming through the activation of the SLIT2/ROBO1 axis promoting proliferation, apoptosis and inducing the *Warburg effect* through the activation of the Src/ERK/MYC/PFKFB2 axis[153]. Additional regulation mechanisms, like non-coding RNAs can be also involved in PFKFB2 regulation[154,155].

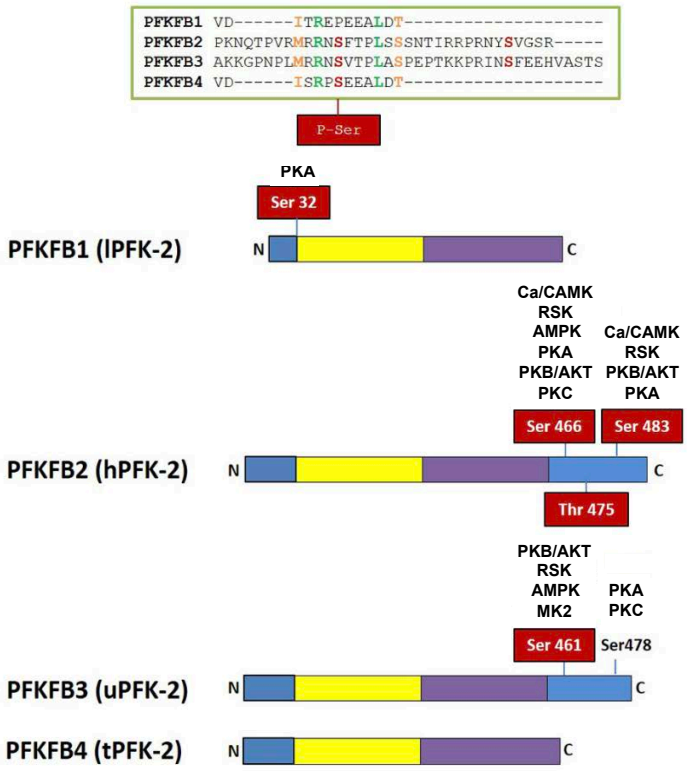

Figure I.7. Domains organization of PFKFB enzymes. Regulatory regions with residues susceptible of phosphorylation by different protein kinases are shown in blue**.** *Modified from Bartrons et al., 2018.*

PFKFB3 is the most expressed isoform in cancer cells. Like many proto-oncogenes PFKFB3 has many copies of the AUUUA sequence in their 3'UTR, which confers instability and enhanced translational activity[156]. PFKFB3 expression has been described to be regulated by several mechanisms, including response to stress, pro-inflamatory molecules and hormones, among others[156–158]. As well as the other isoforms, PFKFB3 activity can be modulated by phosphorylation at distinct sites. Different protein kinases, such as AMPK, PKA, AKT, PKC and RSK have been described to phosphorylate PFKFB3. Additional mechanisms of PFKFB3

regulation includes ROS-mediated S-glutathionylation and demethylation, both resulting in the inhibition of PFKFB3 kinase activity and the derivation of glycolysis intermediates to the pentose phosphate pathway (PPP)[124,159]. Due to its role in metabolism reprogramming in cancer cells, PFKFB3 has been proposed as a possible target for the establishment of novel therapeutic approaches[149]. Indeed, downregulation of *PFKFB3* expression with siRNAs has been reported to decrease cell viability in cancer cells[160]. Moreover, PFKFB3 small molecule inhibitors have been developed[149]. Recent studies in patients suggest significant effects in combination with standard chemotherapeutics in the treatment of recurrent tumors[161].

PFKFB4 has been described to be upregulated in cell lines coming from prostate, liver, colon, bladder, stomach and pancreas tumors and its expression can be modulated by HIF1α, PPARϒ and p53[124,151].

HYPOTHESIS AND OBJECTIVES

BRAF and *NRAS* are the most commonly found mutated genes in melanoma, with an incidence of 50% and 20%, respectively. In both cases, alterations in these genes result in the constitutive activation of the RAS-ERK1/2 pathway, with a consequent increase in proliferation and survival deriving in increased tumorigenesis. However, even the same signaling pathway is affected, both types of tumors have been widely described to be different entities at clinical and molecular levels, which results in distinct signaling patterns as well as different biological behavior. Until now, several therapies against *BRAF* mutant tumors have been developed with some of them showing a high success rate. Surprisingly, for *NRAS* mutant tumors, there are no available specific therapies and these tumors are currently treated using more general approaches, including chemotherapy and immunotherapy, showing low response rates and toxicity.

Previous results in our group, together with additional investigations, have highlighted the presence of different metabolic settings subjected to *BRAF* oncogene regulation. However, little is known about the role of *NRAS* mutations in metabolic rewiring. Deciphering metabolic settings in *NRAS* mutant melanomas could provide new avenues for the establishment of specific therapeutic approaches against these, until now, untargetable tumors.

For this reason, the main aim of this thesis is to unveil new metabolic targets for therapy by the establishment of different metabolic settings under *NRAS* regulation.

Metabolic stress, specifically energy stress induced by either glucose removal or metformin treatment, has been observed to promote a differential response in $BRAF^{V600E}$ vs. $NRAS^{Q61}$ mutant cells, which results in the acquired sensitivity of $NRAS^{Q61}$ mutant cells to Sorafenib treatment, a multi-kinase inhibitor. To further study the differential metabolic settings among both groups of cells, and the molecular implications of energy stress, together with the its relationship with RAS-ERK1/2 pathway regulation, the following objectives are proposed.

Objectives:

1. To elucidate the underlying mechanism in the differential response to metabolic stress of melanoma cells harboring $NRAS^{Q61}$ and $BRAF^{V600E}$ mutations and to establish the impact of glucose starvation in the regulation of the RAS-ERK1/2 pathway.
2. To study differences existing in the metabolic settings of $NRAS^{Q61}$ and $BRAF^{V600E}$ mutant melanoma cells.
3. To describe the link existing between metabolic stress, RAS-ERK1/2 pathway regulation, and cell death, as well as its differential regulation in $NRAS^{Q61}$ and $BRAF^{V600E}$ mutant melanoma cells.
4. To establish therapeutic approaches based on the differential metabolic features of $NRAS^{Q61}$ mutant tumors.

RESULTS

The RAS-ERK1/2 pathway is differentially regulated in NRAS^{Q61R} and BRAF^{V600E} mutant cells in response to metabolic stress

Previous results from our group established that BRAF^{V600E} mutant cells are not able to sense low energy levels due to an uncoupling in the LKB1-AMPK axis[107]. Consequently, these cells do not activate the expected apoptotic response under energy stress conditions. This phenotype, which is oncogene-dependent, was rescued upon treatment with Sorafenib, a multi-kinase inhibitor that targets vascular endothelial growth factor receptors (VEGFR) 2/3, platelet-derived growth factor receptor β (PDGFRβ), KIT, Fms related receptor tyrosine kinase 3 (FLT3), BRAF and CRAF proteins. This phenomenon was interpreted as an opportunity for the specific targeting of these cells as combination of energy stress (glucose starvation, metformin, phenformin) and RAS-ERK1/2 pathway inhibition (Sorafenib plus U0126, a MEK inhibitor) triggered apoptosis[107]. Effects of the combination of metformin, an AMPK activator mimicking low energy stress, and the inhibition of the RAS-ERK1/2 pathway, were evaluated in cells carrying mutations in *NRAS* and *BRAF*, the two most commonly altered components of the RAS-ERK1/2 pathway (*TCGA database*). The combined treatment resulted in cytotoxicity in both NRAS^{Q61} and BRAF^{V600E} mutant cells but surprinsingly, NRAS^{Q61} mutant cells showed higher sensitivity to the combined treatment (*Esteve-Puig R. Doctoral thesis 2011*).

To further analyze the molecular implications of metabolic stress in the regulation of the RAS-ERK1/2 pathway, the role of RAS-ERK1/2 pathway regulating the metabolic response to the stress, as well as the oncogene-mediated contributions to this process, we analyzed the effect of glucose withdrawal in different cell lines carrying mutations in *NRAS* and *BRAF.*

RAS-ERK1/2 pathway activation status was evaluated in *SKMel103* (NRAS^{Q61R}), *SKMel147* (NRAS^{Q61R}), *SKMel28* (BRAF^{V600E}) and *UACC903* (BRAF^{V600E}) cells in response to glucose starvation. To that end, cells were subjected to glucose withdrawal during 30 minutes, 1 hour, 2 hours, 3 hours and 4 hours and ERK1/2 phosphorylation at residues T202/Y204 was analyzed by Western Blot. Quantification of the obtained signal showed that NRAS^{Q61} mutant cells experiment

a more than twenty-fold increase of ERK1/2 phosphorylation after 30 minutes of glucose starvation and that this activation is sustained during time. $BRAF^{V600E}$ mutant cells, which already present high-phosphorylated ERK1/2 amounts, did not respond to the treatment (Figure R.1). Thus, these data suggest an oncogene-mediated differential regulation of the RAS pathway in response to metabolic stress.

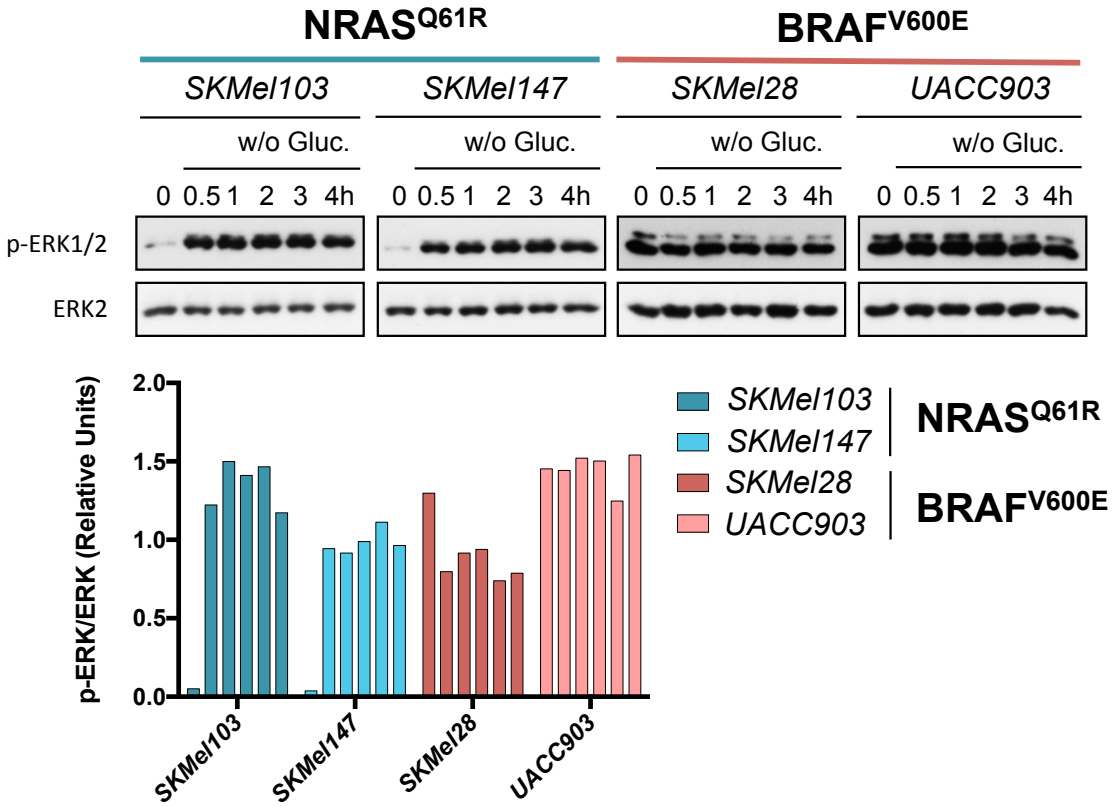

Figure R.1. RAS-ERK1/2 regulation upon metabolic stress in $NRAS^{Q61R}$ and $BRAF^{V600E}$ mutant melanoma cells. Western Blot showing ERK1/2 phosphorylation in response to glucose starvation. The bars graph represents quantification of ERK1/2 phosphorylation. Gluc.=Glucose.

Activated ERK1/2 localization upon metabolic stress is predominantly cytoplasmic

In order to determine the correct function of ERK after its activation we analyzed ERK1/2 localization in response to metabolic stress. In resting conditions, ERK localizes in the cytoplasm due to its interactions with anchoring proteins. Upon stimulation, it is activated by phosphorylation at residues T202 and Y204. This phosphorylation induces conformational changes and ERK is released from anchoring proteins and translocated to the nucleus. Nuclear translocation is

required to active ERK1/2 nuclear substrates and regulates proliferation and other relevant cellular processes[162].

To establish ERK1/2 localization within the cell we proceeded to the fractionation of protein lysates. *SKMel103* ($NRAS^{Q61R}$), *SKMel147* ($NRAS^{Q61R}$), *SKMel28* ($BRAF^{V600E}$) and *UACC903* ($BRAF^{V600E}$) cells were subjected to glucose starvation for 1 and 3 hours and both, nuclear a cytoplasmic protein lysates were obtained. Protein extracts were subjected to electrophoresis and ERK1/2 phosphorylation was analyzed by Western Blot. In all cell lines phosphorylated ERK1/2 was observed to be located in both, nucleus and cytoplasm. Interestingly, phosphorylation increase was observed to be more evident in the cytoplasmic fraction of $NRAS^{Q61R}$ mutant cells. Lamin A/C and GAPDH, used as nuclear and cytoplasmic markers, confirmed the purity of the protein extracts (Figure R.2). Hence, these data indicates that activated ERK1/2 localization upon metabolic stress is predominantly cytoplasmic in $NRAS^{Q61R}$ mutant cells.

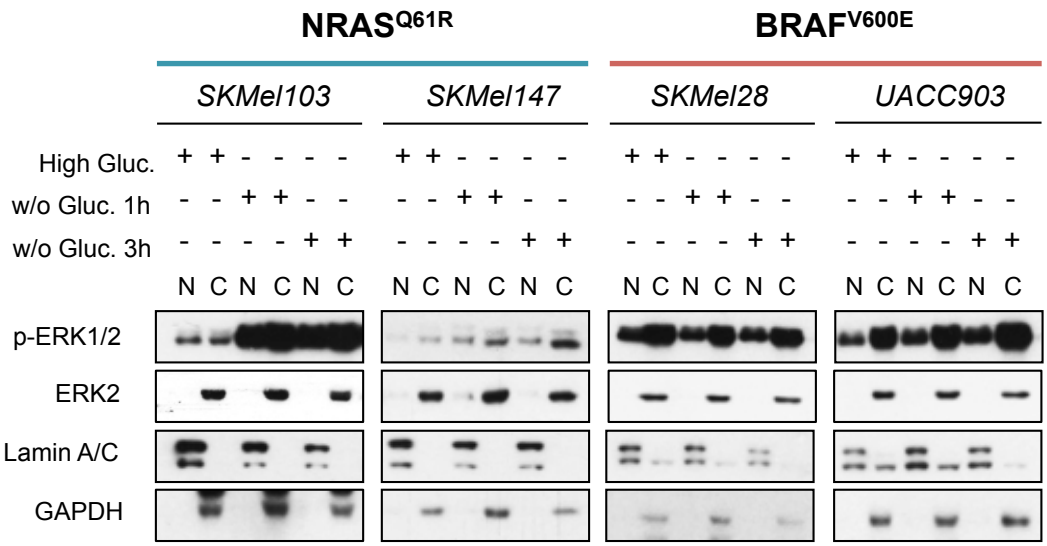

Figure R.2. Subcellular localization of p-ERK1/2 upon metabolic stress. Western Blot showing ERK1/2 phosphorylation in nuclear and cytoplasmic protein extracts in response to metabolic stress. Lamin A/C and GAPDH are used as nuclear and cytoplasmic markers, respectively. Gluc.=Glucose, N=Nucleus, C=Cytoplasm.

Hyperactivation of the RAS-ERK1/2 pathway sensitizes $NRAS^{Q61R}$ *mutant cells to treatment with the multi-kinase inhibitor Sorafenib*

As previously explained, Sorafenib, a multi-kinase inhibitor targeting RAF molecules, is able to sensitize *BRAF* mutant cells to low energy conditions[107]. Moreover, it has been observed that *NRAS* and *BRAF* mutant cells undergo a

differential response to glucose starvation regarding the hyperactivation of the RAS-ERK1/2 pathway. We wondered then if this differential behavior could have any impact in cell sensitivity in respect to the inhibition of the pathway.

Thus, *SKMel103* ($NRAS^{Q61R}$), *SKMel147* ($NRAS^{Q61R}$), *SKMel28* ($BRAF^{V600E}$) and *UACC903* ($BRAF^{V600E}$) cells were subjected to Sorafenib treatment in the presence and absence of glucose during 4 hours and pathway activation was determined analyzing ERK1/2 phosphorylation by Western Blot. Hyperactivation of the pathway upon glucose withdrawal was confirmed in $NRAS^{Q61R}$ mutant cells. Surprisingly, glucose starvation resulted in the sensitization of these cells to Sorafenib treatment and the complete ablation of ERK1/2 phosphorylation in response to the combined treatment. This effect, even less accentuated was also observed in $BRAF^{V600E}$ mutant cells, which are known to be sensitive to RAS pathway inhibition upon normal conditions[29] (Figure R.3). Altogether, the data suggest that $NRAS^{Q61R}$ mutant cells are sensitized to treatment with Sorafenib upon glucose starvation conditions.

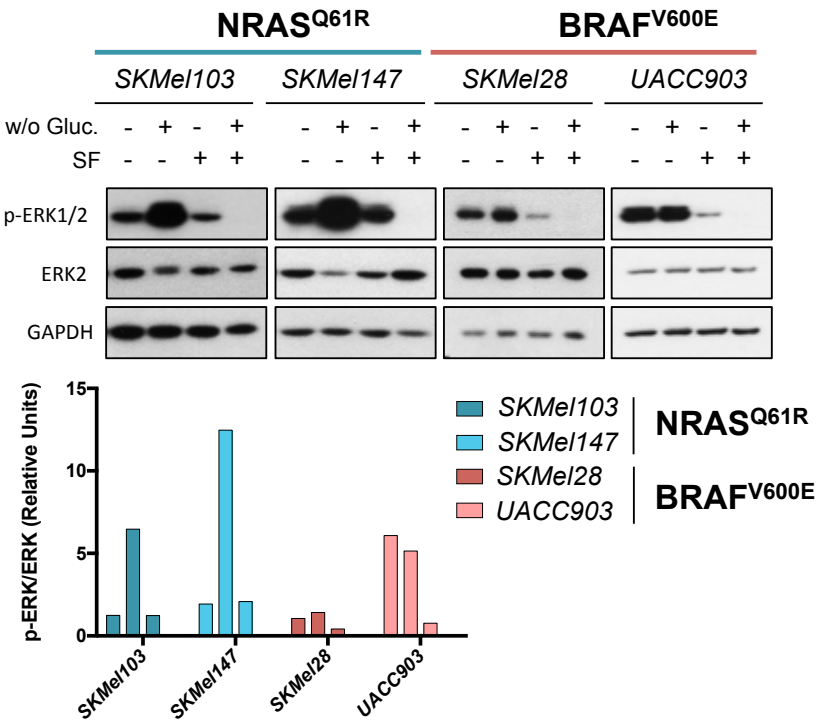

Figure R.3. Glucose withdrawal sensitizes $NRAS^{Q61R}$-mutated melanoma cells to treatment with Sorafenib. Western Blot showing ERK1/2 phosphorylation in response to glucose starvation and treatment with Sorafenib (15 μM, 4 hours). GAPDH is shown as a loading control. The bars graph represents quantification of ERK1/2 phosphorylation. Gluc.=Glucose, SF=Sorafenib.

Sorafenib is the only inhibitor promoting synthetic lethality in NRAS^{Q61R} mutant cells

To determine whether the different targets of Sorafenib could be responsible of the hyperactivation of the RAS pathway and the consequent inhibition upon glucose starvation plus Sorafenib conditions we tested the effect of different inhibitors against the different Sorafenib targets. Thus, *SKMel103* (NRAS^{Q61R}), *SKMel147* (NRAS^{Q61R}), *SKMel28* (BRAF^{V600E}) and *UACC903* (BRAF^{V600E}) cells were subjected to glucose starvation in combination with Sorafenib (SF), Vemurafenib (VE), Trametinib (TR), Axitinib (AX), Avastin (AV), Lenvatinib (LEN), Sunitinib (SU) and CCT196969 (CCT). The rationale for the use of these inhibitors was to cover the whole range of Sorafenib targets. AX, AV, LEN and SU were used for the inhibition of receptor tyrosine kinases (RTKs). AX targets vascular endothelial growth factor receptors (VEGFR) 1/2/3, platelet-derived growth factor receptors (PDGFR) α/β and KIT. AV is an anti VEGF-A antibody. LEN targets VEGFR1/2/3, PDGFR α/β, KIT, Fibroblast growth factor receptor 1 (FGFR1) and RET. SU targets VEGFR2, PDGFRβ, KIT and FLT3. CCT is a PanRAS inhibitor. VE was used for the specific targeting of BRAF^{V600E}, TR was used for the inhibition of MEK and SF was used for the inhibition of both RTKs and RAF proteins, including BRAF^{V600E}.

Analysis of ERK1/2 phosphorylation by Western Blot showed ERK1/2 inhibition by SF, TR and CCT in all cell lines. VE effect, as expected, was only appreciated in cells carrying the BRAF^{V600E} mutation. AX, AV, SU and LEN, did not show inhibition at ERK1/2 level, even more, an increase was appreciated in all cell lines with the exception of *UACC903* in the case of AX and AV, probably due to the upregulation of alternative RTKs and other elements of the pathway in response to the treatment (Figure R.4 and Supplementary Figure 1).

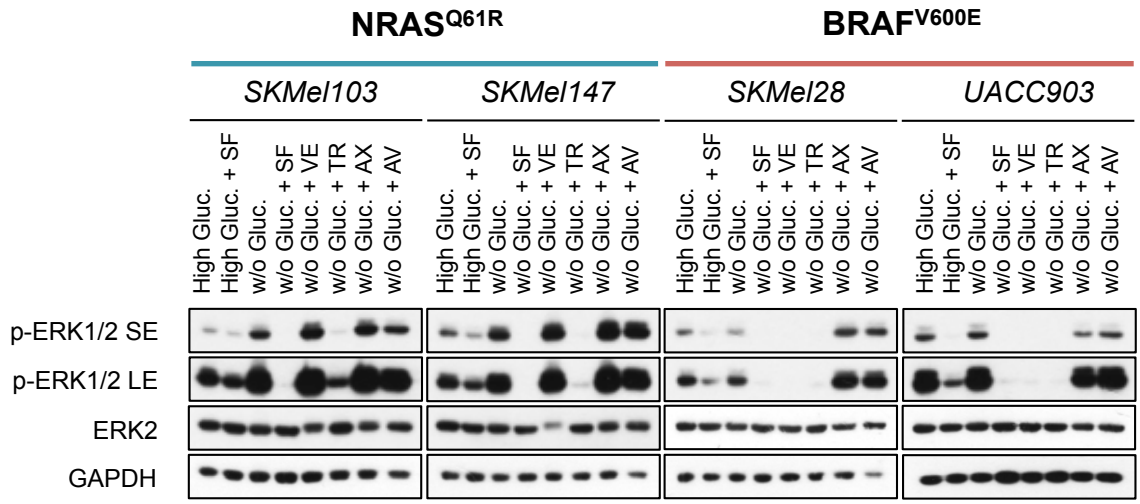

Figure R.4. Molecular response to RAS-ERK1/2 pathway inhibition. Western Blot showing ERK1/2 phosphorylation in response to glucose starvation and RAS-ERK1/2 pathway inhibition. Cells were treated with SF (15 μM), VE (5 μM), TR (100 nM), AX (10 μM) and AV (0.5 mg/ml) during four hours, either with and without glucose. GAPDH is shown as a loading control. Gluc.=Glucose, SF=Sorafenib, VE=Vemurafenib, TR=Trametinib, AX=Axitinib, AV=Avastin, SE=Short exposure, LE=Long exposure.

Concomitant to the inhibition of ERK1/2 by Sorafenib upon metabolic stress, $NRAS^{Q61R}$ mutated cells were detached from the plate showing a phenotype compatible with cell death. Thus, we evaluated simultaneously by flow cytometry the apoptosis triggered by the different assayed conditions. All the samples showed between 1-4% of basal cell death. Neither glucose starvation nor Sorafenib treatment produced any effect in cell viability. However, the combination of both resulted in an increase of cell death in $NRAS^{Q61R}$ mutant cells (42.7% and 46.88% in *SKMel103* and *SKMel147*, respectively), generating a condition of *synthetic lethality*. This behavior was not observed in $BRAF^{V600E}$ mutant cells, where cell death did not increase in response to combined treatment (3.92% and 3.40% in *SKMel28* and *UACC903*, respectively). Regarding the rest of the inhibitors, cell death percentages from 2 to 7% were detected in $NRAS^{Q61R}$ mutant cells, showing no synergy between glucose starvation and the different inhibitors. $BRAF^{V600E}$ mutant cells showed between 2 and 12% of cell death, being VE and TR the most lethal inhibitors (Figure R.5). Overall, these data support the higher sensitivity of $BRAF^{V600E}$ mutant cells to the inhibition of the RAS-ERK1/2 pathway and propose Sorafenib as the only inhibitor promoting *synthetic lethality* in $NRAS^{Q61R}$ mutant cells upon metabolic stress.

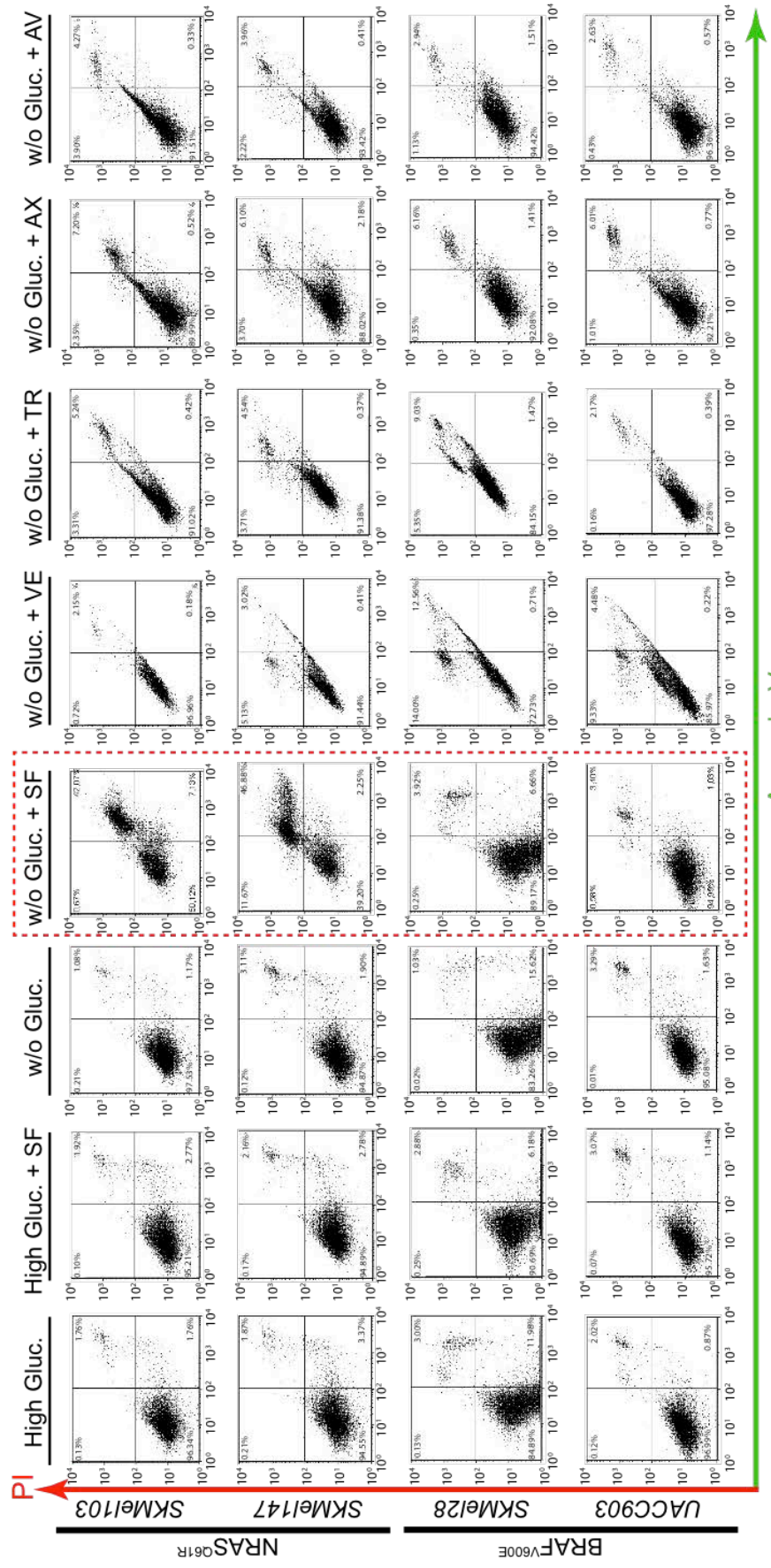

Figure R.5. Sorafenib is the only inhibitor promoting synthetic lethality in NRAS^{Q61R} mutant cells. Graphs showing cell apoptosis measured by flow cytometry. Cells were treated with SF (15 μM), VE (5 μM), TR (100 nM), AX (10 μM) and AV (0.5 mg/ml) during four hours, either with and without glucose. Gluc.=Glucose, SF=Sorafenib, VE=Vemurafenib, TR=Trametinib, AX=Axitinib, AV=Avastin, PI=Propidium Iodide, Annexin V=GFP-annexin V.

Hyperactivation of the RAS-ERK1/2 pathway is NRAS^{Q61R}-dependent and involves a switch from CRAF- to BRAF-dependent signaling

Altogether these results suggest the existence of oncogene-dependent metabolic settings in NRAS^{Q61R} mutant cells. To investigate NRAS^{Q61R} role in the ERK1/2 hyperactivation upon glucose starvation, we depleted NRAS^{Q61R} oncogene using specific siRNAs in *SKMel103* and *SKMel147* NRAS^{Q61R} mutant cells. Three different siRNAs were used for *NRAS* knockdown and a scrambled siRNA was used as a negative control. NRAS downregulation at protein level and the status of the RAS-ERK1/2 pathway activation under the different conditions were analyzed by Western Blot.

Both, non-transfected (N/T) and scramble-transfected NRAS^{Q61R} mutant cell lines (*SKMel103* and SKMel147) showed ERK1/2 hyperactivation upon glucose withdrawal. In contrast, in NRAS depleted cells this response to metabolic stress was dramatically decreased. The observed effect associated to the knockdown of *NRAS* was consistent within the three different siRNAs, confirming the specificity of the assay (Figure R.6). Thus, the hyperactivation of the RAS-ERK1/2 pathway upon metabolic stress seems to be *NRAS* oncogene-dependent.

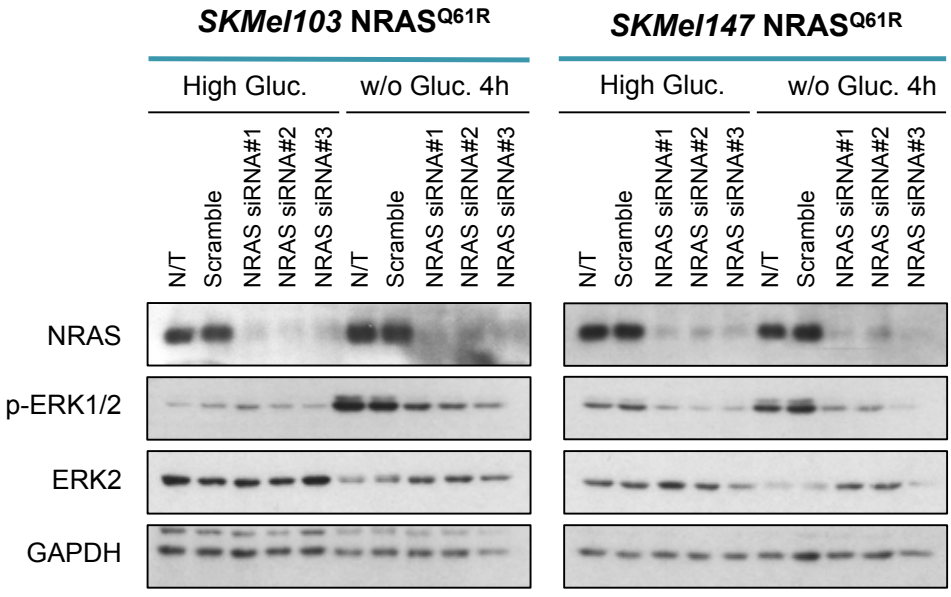

Figure R.6. NRAS^{Q61R} mutant cells do not respond to metabolic stress upon NRAS downregulation. Western Blot showing ERK1/2 phosphorylation in response to metabolic stress upon NRAS silencing with three different siRNAs (NRAS siRNA#1, NRAS siRNA#2 and NRAS siRNA#3). GAPDH is shown as a loading control. Gluc.=Glucose. N/T=Non-transfected cells, Scramble=Cells transfected with scrambled siRNA.

The above results suggested the direct participation of the oncogene in the observed response. To further investigate the molecular mechanisms involved in the hyperactivation of the pathway we measured changes in NRAS activation in response to metabolic stress. As previously explained NRAS belongs to a family of small GTPases and it is activated upon binding to GTP. $NRAS^{Q61}$ mutation disrupts GTPase activity of NRAS. Thus, when $NRAS^{Q61}$ is activated in response to any stimulus, it binds to GTP and it becomes locked in its active conformation[33,34]. To establish NRAS activation status we performed a RAS activation assay based in RAS-GTP precipitation using agarose beads bound to a RAS-binding domain (RBD-agarose). Once precipitated, lysates were resolved by electrophoresis and NRAS was detected by Western Blot (Figure R.7A).

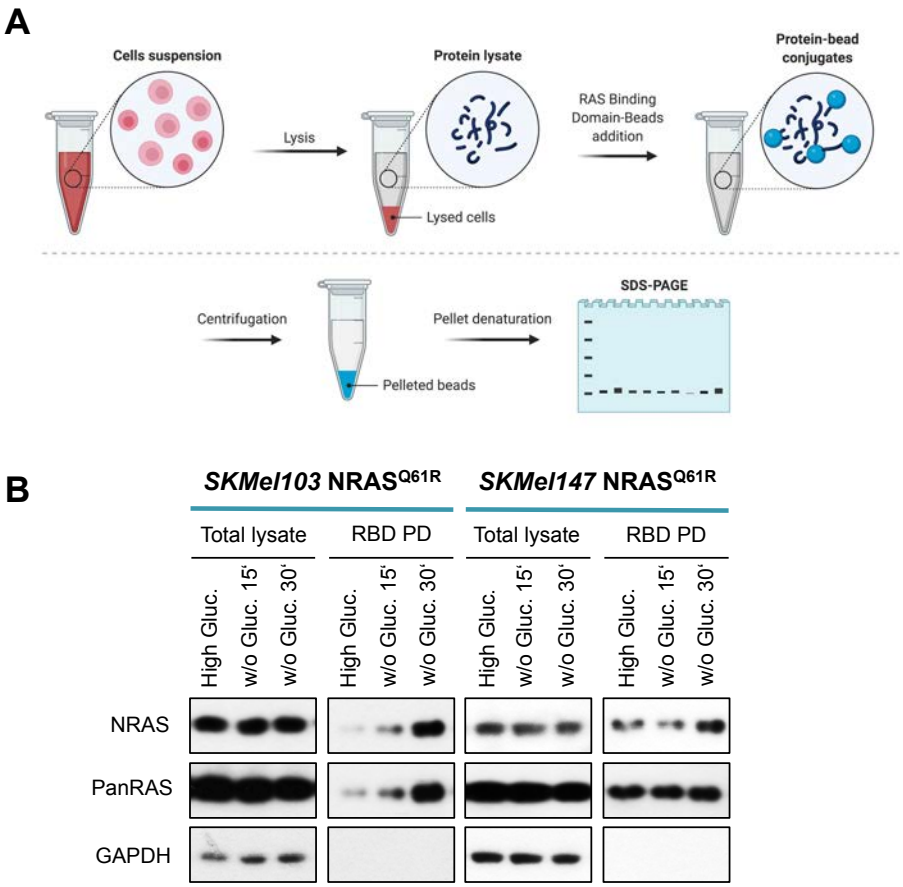

Figure R.7. NRAS activation in response to metabolic stress. (A) Diagram representing the experimental procedure followed to determine RAS activation. (B) Western Blot showing NRAS activation upon metabolic stress. GAPDH is shown as a loading control. Gluc.=Glucose, RBD=RAS binding domain, PD=Pull down.

To assess RAS activation at early time point cells were subjected to glucose withdrawal for 15 and 30 minutes. An increase in RAS binding to GTP was observed after 30 minutes of glucose starvation in both, *SKMel103* and *SKMel147* $NRAS^{Q61R}$ mutant cell lines (Figure R.7B), confirming NRAS activation in response to metabolic stress.

As stated above one of the characteristics of *NRAS* mutant cells is the molecular switch taking place from BRAF- to CRAF-dependent signaling[42]. We wondered if the observed $NRAS^{Q61R}$-dependent metabolic settings and the acquisition of RAS-ERK1/2 inhibition sensitivity derived from them could involve changes in *NRAS* mutant cells signaling regulation.

It is widely described that CRAF is tightly regulated by activating and inhibiting phosphorylation at different sites. One of the key modifications involved in the regulation of CRAF is inactivating phosphorylation at S259, which can be driven by AKT and PKA. Phosphorylation at this point results in the binding to inhibitory 14-3-3 proteins and the disruption of the RAS-RAF complexes, thus resulting in the inhibition of CRAF catalytic activity[30,42] (Figure R.8A). In order to establish CRAF S259 phosphorylation status *SKMel103* $NRAS^{Q61R}$ mutant cells were subjected to glucose starvation for 4 hours and CRAF phosphorylation at residue S259 was analyzed by Western Blot. Phosphorylation was observed to increase in response to metabolic stress, suggesting the inhibition of CRAF activity upon this condition (Figure R.8B).

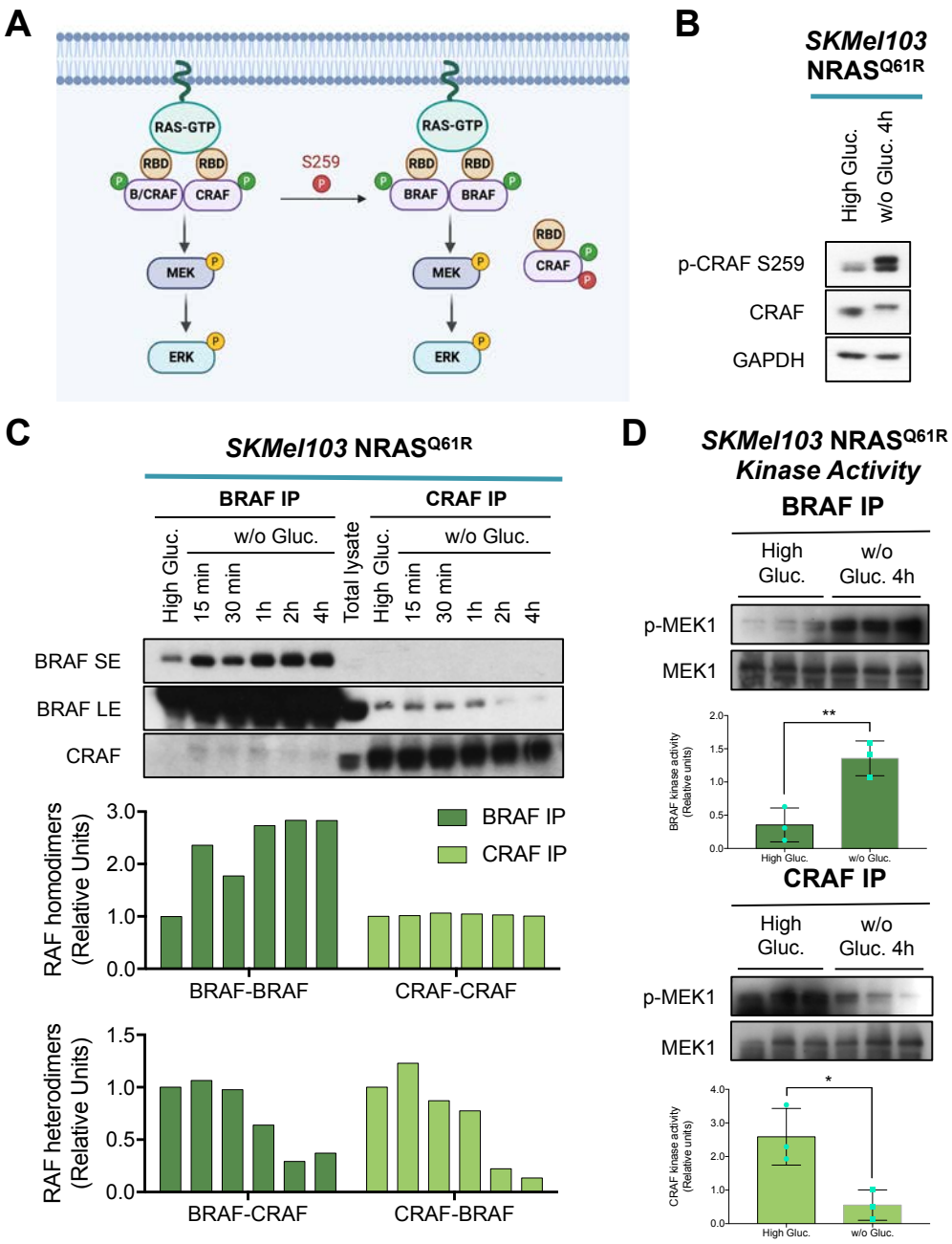

Figure R.8. Metabolic stress promotes a switch from CRAF to BRAF signaling in NRAS^{Q61R} melanoma cells. (A) Scheme indicating RAF dimerization regulation in response to phosphorylation at S259. (B) Western Blot showing CRAF phosphorylation at residue Ser259 in response to metabolic stress. GAPDH is shown as a loading control. (C) Western blot showing immunoprecipitated BRAF and CRAF in response to metabolic stress. The bars graphs represent quantification of BRAF and CRAF proteins amount. (D) Kinase assay showing MEK phosphorylation as a readout of BRAF and CRAF kinase activity in the presence and absence of glucose. The bars graphs represent quantification of phosphorylated MEK amount upon BRAF and CRAF immunoprecipitation. Three different replicates are showed. RBD=RAS Binding Domain, IP=Immunoprecipitation, Gluc.=Glucose, SE=Short exposure, LE=Long exposure, *=*p-value<0.05*, **=*p-value<0.01*.

To investigate the consequences of CRAF inactivation in the dimerization of RAF proteins and the activation of the pathway we analyzed the composition of the dimers under normal conditions and in response to metabolic stress in *SKMel103* $NRAS^{Q61R}$ mutant cells. To that end we immunoprecipitated BRAF and CRAF upon 15 minutes, 30 minutes, 1 hour, 2 hours and 4 hours of glucose starvation and a Western Blot was performed. BRAF-immunocomplexes showed an increasing amount of BRAF molecules in response to metabolic stress, concomitant to a decrease of CRAF molecules bound to BRAF after 2 and 4 hours of glucose withdrawal (Figure R.8C). This observation suggested an increase in BRAF homodimers together with a decrease in BRAF-CRAF heterodimers. CRAF homodimers amount did not change (Figure R.8C). The decrease in BRAF-CRAF heterodimers formation could be also appreciated in this case (CRAF immunocomplexes). Altogether, the data suggest that, in $NRAS^{Q61}$ mutant cells, metabolic stress promotes a switch in the use RAF signaling isoforms from CRAF to BRAF. This observation was confirmed by an increased BRAF kinase activity and a decreased CRAF kinase activity in $NRAS^{Q61R}$ mutant cells subjected to four hours of glucose starvation (Figure R.8D).

$NRAS^{Q61R}$ and $BRAF^{V600E}$ mutant cells differentially express metabolism-related genes

Next, we aim to characterize *NRAS mutant cells*-specific metabolic settings. To that end, we performed a microarray study in two different $NRAS^{Q61R}$ mutant cells (*SKMel103* and *SKMel147*) and two different $BRAF^{V600E}$ mutant cells (*SKMel28* and *UACC903*), upon normal conditions and in response to glucose starvation. Data analysis showed that the 400 top differentially expressed genes among $NRAS^{Q61R}$ and $BRAF^{V600E}$ mutant cells under basal conditions were significantly associated with metabolism-related categories, including cellular components organization or biogenesis, metabolic processes and detoxification (Figure R.9A and Supplementary Table 1).

Moreover, response to metabolic stress was observed to be differential when comparing $NRAS^{Q61R}$ and $BRAF^{V600E}$ mutant cells (Figure R.9B and Supplementary Table 2). Comparison of upregulated and downregulated genes among $NRAS^{Q61R}$ and $BRAF^{V600E}$ mutant cells indicated than only a small

percentage of genes was common to both groups of cells (26.9% and 5.5% of upregulated genes in *NRAS* and *BRAF* mutant cells, respectively, and 22.9% and 7.8% of downregulated genes in *NRAS* and *BRAF* mutant cells). These data support the existence of metabolic settings that are under the regulation of the oncogene.

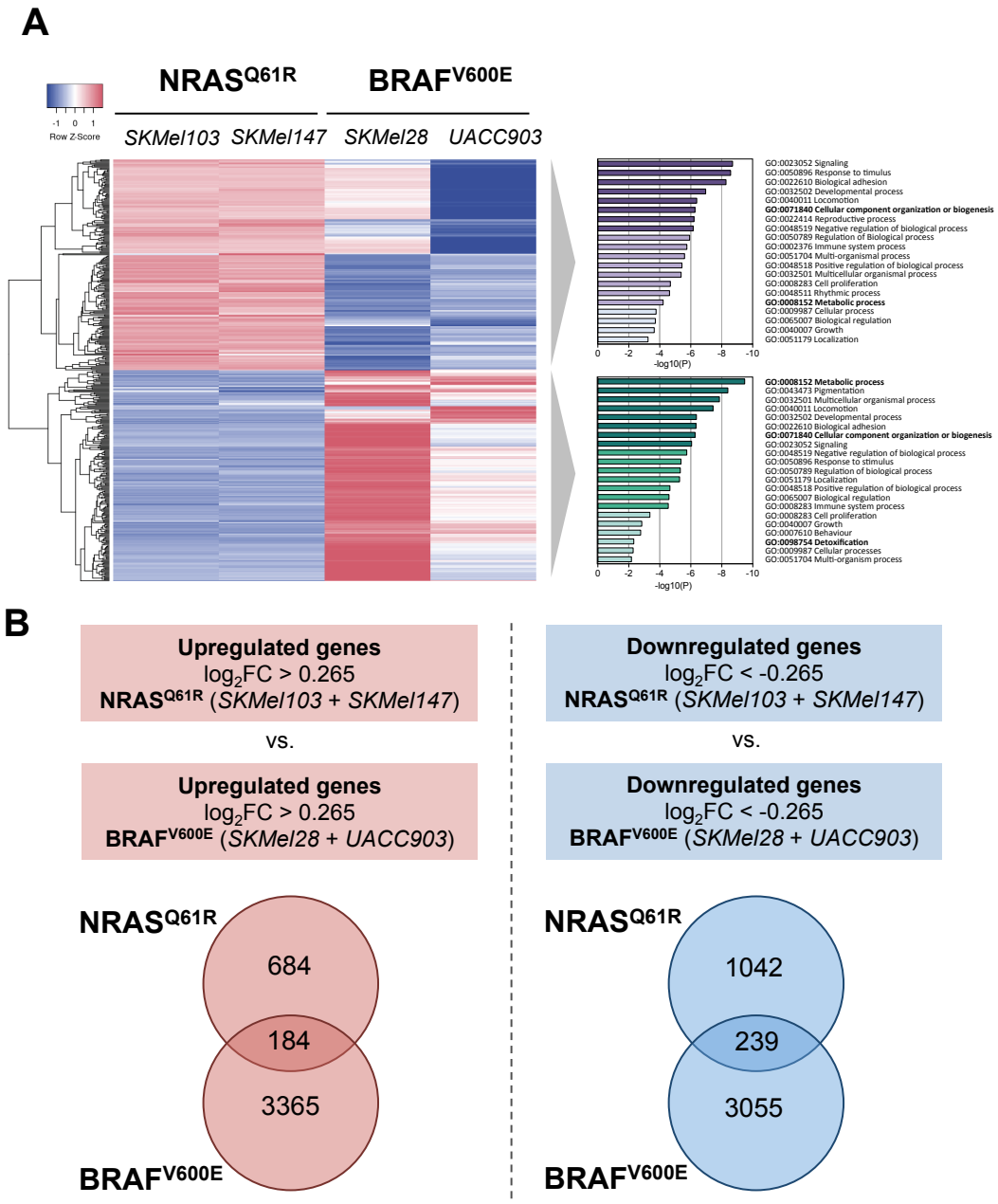

Figure R.9. Differential expression of metabolism-related genes among NRAS and BRAF mutant cells. (A) On the left, a heatmap representing the 400 most differentially expressed genes under basal conditions in *NRAS* vs. *BRAF* mutant melanoma cell lines (n=3). On the right, gene ontology (GO) processes obtained from the analysis of upregulated and downregulated genes using *Metascape.org*. (B) On the top, scheme showing the flow followed to compare *NRAS* and *BRAF* mutant cells regulated genes in response to metabolic stress. On the bottom, Venn diagrams indicating upregulated ($log_2FC > 0.265$) and downregulated ($log_2FC < -0.265$) genes in response to glucose withdrawal in $NRAS^{Q61R}$ and $BRAF^{V600E}$ mutant melanoma cells.

Mitochondrial response capacity *is compromised in NRAS^{Q61} mutant cells*

To further characterize the NRAS^{Q61} oncogene-dependent metabolic features, we used Seahorse technology to profile the functional mitochondrial capacity of melanoma cells according to their mutational status (NRAS^{Q61} vs. BRAF^{V600E}). This technology is based in the establishment of key parameters of mitochondrial function by directly measuring the oxygen consumption rate (OCR) of cultured cells. To modulate the respiratory chain we added different regulators of respiration including oligomycin, phenylhydrazona (FCCP), rotenone and antimycin A to cells in culture. Olygomycin is used for the inhibition of ATP synthase (Complex V). It is involved in the decrease of electron flow through the respiratory chain resulting in the reduction of mitochondrial respiration and as a consequence the OCR. This decrease in OCR is linked to cellular ATP production. FCCP is an uncoupling agent that collapses the proton gradient and disrupts the mitochondrial membrane potential. It reverses the inhibition of respiratory chain and oxygen consumption by complex IV reaches the maximum. This allows the calculation of spare capacity, defined as the ability of the cell to respond to increased energy demand. Finally, rotenone and antimycin A are complex III inhibitors, which shut down mitochondrial respiration and enable the calculation of non-mitochondrial respiration driven by processes outside the mitochondria.

Cells were treated first with oligomycin following basal measurements. Then, FCCP, rotenone and antimycin were added successively. We measured mitochondrial respiration related parameters in *SKMel103* (NRAS^{Q61R}), *SKMel147* (NRAS^{Q61R}), *SKMel28* (BRAF^{V600E}), *UACC903* (BRAF^{V600E}), *A375* (BRAF^{V600E}) and *G361* (BRAF^{V600E}), as well as in patient-derived cell lines *Mmln9* (NRAS^{Q61}) and *Mmln10* (NRAS^{Q61}). Mitochondrial response capacity of NRAS^{Q61} mutant cells was much more reduced when compared with BRAF^{V600E} mutant cells (Figure R.10A). Furthermore, NRAS^{Q61} mutant cells showed lower maximal and ATP-linked respiration together with an increased proton leak (Figure R.10B). Overall, this data highlight that NRAS^{Q61} mutant cells have a reduced mitochondrial response capacity in comparison with BRAF^{V600E} mutant cells.

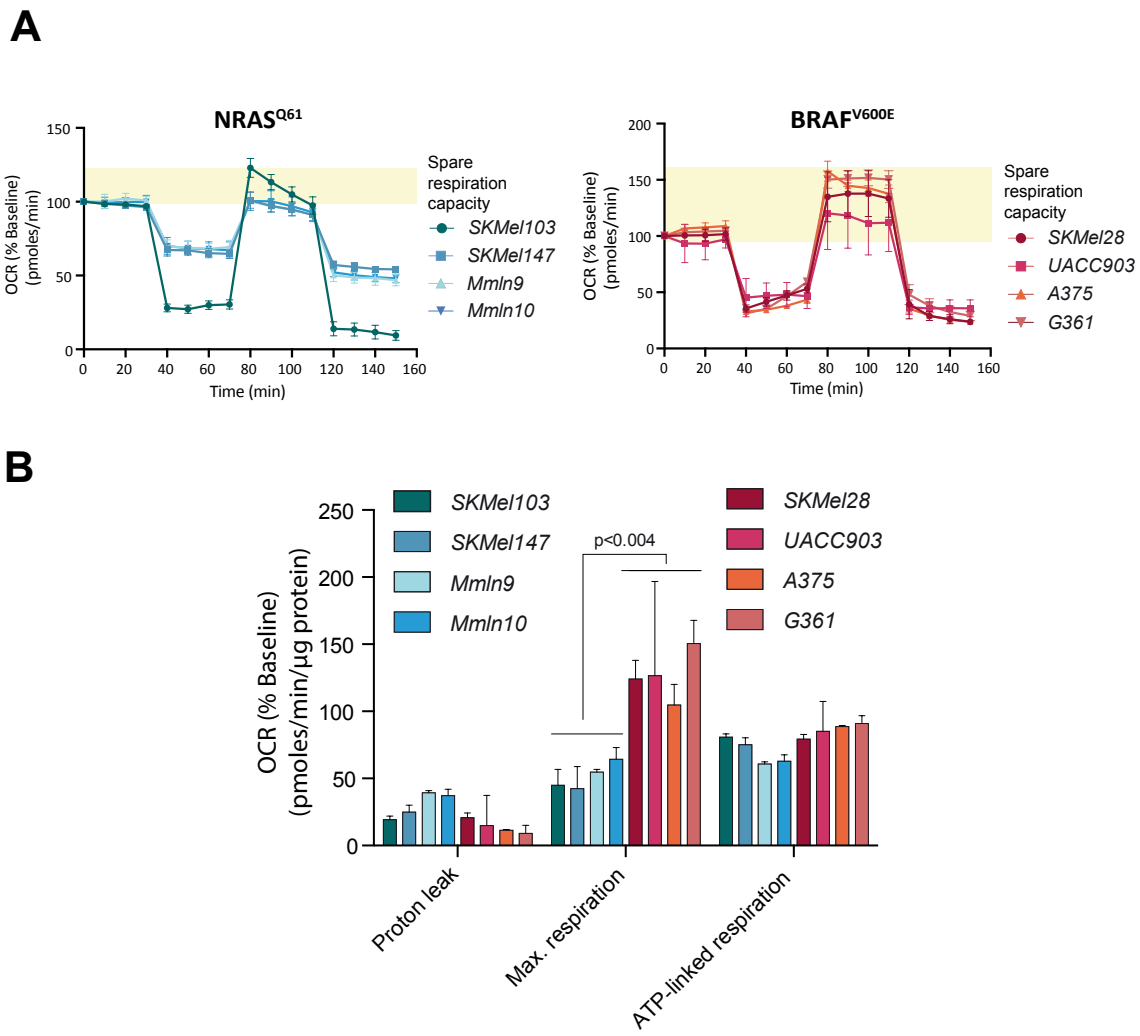

Figure R.10. Mitochondrial response capacity is compromised in NRAS^{Q61} mutant cells. (A) Graphs representing oxygen consumption rate (OCR) in NRAS^{Q61} (blue) and BRAF^{V600E} (red) mutant melanoma cells. The yellow area represents the spare respiration capacity. (B) Graph showing quantification of oxygen consumption-associated parameters including proton leak, mitochondrial maximal respiration and ATP-linked respiration. (n=5 ± SD; p-value was calculated by Student's t-test).

NRAS^{Q61R} mutant cells are less flexible than BRAF^{V600E} mutant cells using alternative fuels in the absence of glucose

Metabolic plasticity characterize tumor cells, as they need to rewire metabolic settings in an attempt to adapt to stress and low energy conditions at the same time that they have to maintain high proliferation rates to sustain tumor growth. This plasticity is possible due to tumor cells high capacity and flexibility metabolizing different energy sources. As these cells need to adapt to continuously changeable environments, in the absence of any metabolite or energy source, cells have to reprogram its metabolism settings in order to survive[53,54,103].

We assessed then how dependent, capable and flexible, *NRAS* and *BRAF* mutant cells were metabolizing the three most important energy sources for human cells metabolism: glucose, glutamine and long-chain fatty acids. Thus, we performed OCR measurements using Seahorse technology to determine the rate of oxidation of each fuel in the presence and absence of inhibitors of the different metabolic pathways: UK5099, an inhibitor of the mitochondrial pyruvate carrier (MPC), that inhibits glucose oxidation; BPTES, an inhibitor of glutaminase (GLS1) and consequently of glutamine oxidation; and etomoxir, a carnitine palmitoyl-transferase 1A (CPT1A) inhibitor that promotes the inhibition of long chain fatty acids oxidation. All measurements were taken in the presence and absence of glucose in the culture media. Inhibition of the pathway of interest followed by the two alternative pathways enabled the establishment of how cells depend on the pathway of interest to meet energy demand. Inhibiting the two alternative pathways followed by the pathway of interest enabled the establishment of cell capacity. Fuel flexibility was calculated subtracting fuel dependency from fuel capacity for each metabolic pathway.

Interestingly, $NRAS^{Q61}$ mutant cells were less efficient using alternative fuels in the absence of glucose than $BRAF^{V600E}$ mutant cells (Figure R.11), suggesting higher limitations of $NRAS^{Q61}$ mutant cells to meet energy demand upon glucose starvation conditions.

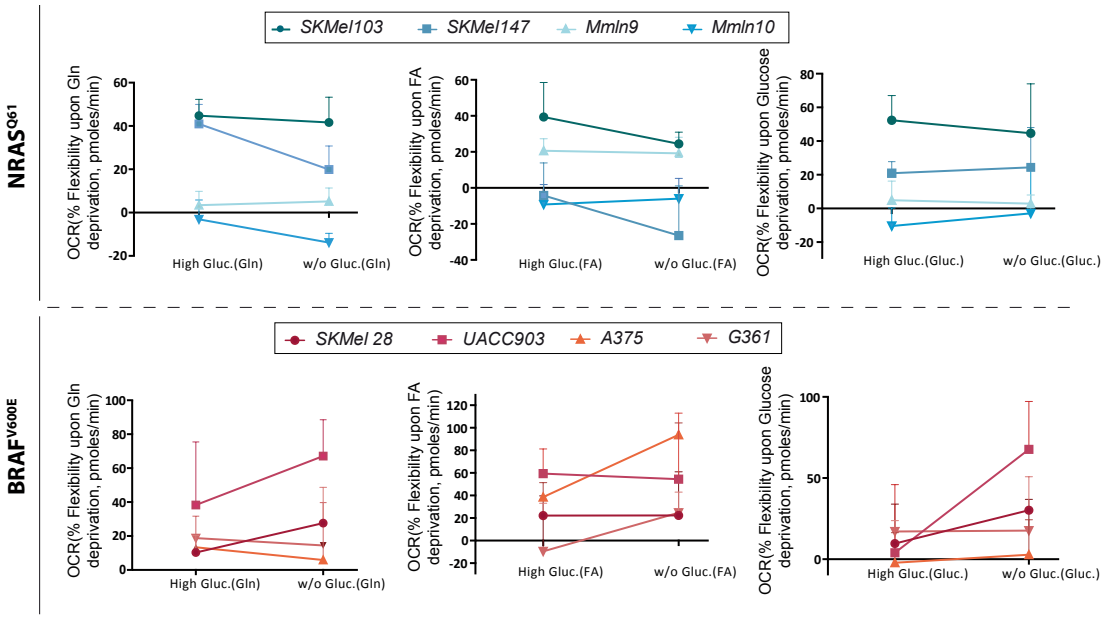

Figure R.11. NRAS^{Q61} mutant cells are less flexible using alternative fuels in the absence of glucose than BRAF^{V600E} mutant cells. On the top, from left to right, graphs represent NRAS^{Q61} mutant cells flexibility metabolizing alternative fuels upon inhibition of glutamine (Gln), fatty acids (FA) and Glucose (Gluc.) metabolism. On the bottom, from left to right, graphs represent BRAF^{V600E} mutant cells flexibility metabolizing alternative fuels upon inhibition of glutamine (Gln), fatty acids (FA) and Glucose (Gluc.) metabolism (n=5).

Addition of glucose but not pyruvate is able to revert the RAS-ERK1/2 hyperactivation observed upon metabolic stress, as well as Sorafenib-induced apoptosis

The above data suggests that NRAS^{Q61} mutant cells depend on glucose as an energy source, but it seems that glucose is not oxidized to carbon dioxide and water through the TCA, due to the low mitochondrial response capacity previously demonstrated within these cells. This is also supported by the observation showing that they are not capable to compensate the lack of glucose through the use of alternative energy sources. As stated by Otto Warburg, cancer cells are characterized by an increased aerobic glycolysis, meaning that even in the presence of enough oxygen, glucose is metabolized until pyruvate and then converted to lactate but it does not go through oxidative phosphorylation[101]. The objective of this metabolic strategy is to produce enough reduction power and building blocks for the maintenance of high proliferative rates.

If glucose were oxidized to carbon dioxide and water, addition of either glucose or pyruvate to starved cells would result in the reconstitution of the

phenotype. However, this reconstitution would not be observed in response to pyruvate addition if glucose were derived to branching pathways, what would support the use of glucose essentially to generate building blocks and/or reduction power.

To confirm $NRAS^{Q61}$ mutant cells behavior regarding glucose metabolism and its relationship with RAS-ERK1/2 pathway regulation and sensitivity acquisition to Sorafenib, we followed two different strategies. In one hand we treated cells with Sorafenib and increasing concentrations of glucose or pyruvate in culture media lacking both, glucose and pyruvate. On the other hand, we tested whether inhibition of first and last glycolytic steps could mimic the lack of glucose. Combination of Sorafenib and agents mimicking low glucose conditions should result in the induction of apoptosis. Thus, cells were treated with 3-bromopyruvate (3BP), an hexokinase 2 inhibitor, and dichloroacetate (DCA), an inhibitor of pyruvate dehydrogenase (Figure R.12A) and cell viability was assessed upon fluorescence detection after addition of acridine orange (AO) and ethidium bromide (EB) (Figure R.12B). Addition of glucose was related with an increase of cell viability in a dose-dependent manner, an effect that was not observed upon pyruvate addition to the cells (Figure R.12C). In line with this, 3BP and Sorafenib combined treatment resulted in a dose-dependent increase of cell death while DCA addition did not produce any change in cell phenotype (Figure R.12D). These results indicated an important role of glycolysis in $NRAS^{Q61}$ mutant cells, likely involving the upper glycolytic steps rather than the lower part of the pathway and consequently glucose derivation to branching pathways rather than oxidative phosphorylation.

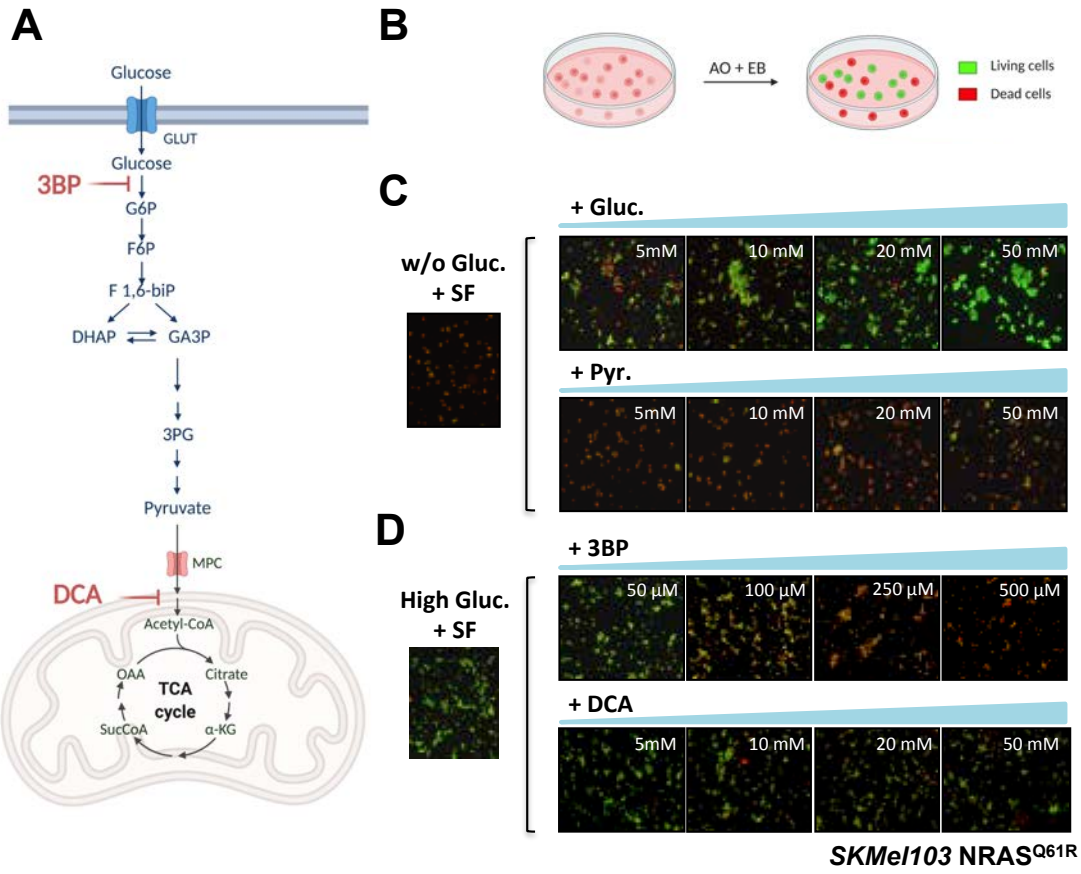

Figure R.12. Sorafenib effects in combination with glucose, pyruvate, 3-bromopyruvate (3BP) and dichloroacetate (DCA). (A) Schematic representation of the glycolytic pathway. (B) Scheme showing the procedure used for the analysis of cell death. (C) Cell pictures showing cell viability in response to Sorafenib (15 µM) either alone or in combination with increasing concentrations of glucose and sodium pyruvate. (D) Cell pictures showing cell viability in response to Sorafenib (15 µM) either alone or in combination with increasing concentrations of 3-bromopyruvate (3BP) and dichloroacetate (DCA). G6P=Glucose 6-phosphate, F6P=Fructose 6-phosphate, F1,6-biP=Fructose 1,6-bisphosphate, DHAP=Dihydroxyacetone phosphate, GA3P=Glyceraldehyde 3-phosphate, 3PG=3-Phosphoglycerate, OAA=Oxaloacetate, SucCoA=Succinyl-CoA, α-KG=α-ketoglutarate, AO=Acridine Orange, EB=Ethidium Bromide, Gluc.=Glucose, Pyr.=Pyruvate.

To investigate whether the observed changes in cell viability correlated with the loss of cell sensitivity to the inhibition of the RAS-ERK1/2 pathway with Sorafenib, we also studied the phosphorylation status of ERK1/2 in Sorafenib-treated cells upon the addition of increasing concentrations of either glucose or pyruvate (Figure R.13A).

Addition of glucose, but not pyruvate resulted in the decrease of RAS-ERK1/2 pathway hyperactivation in a dose-dependent manner, and the loss of sensibility to Sorafenib. These molecular effects were not appreciable in pyruvate-treated cells (Figure R.13B).

Overall, these data highlight the relevance of glucose metabolism in NRAS^{Q61} mutant cells. Moreover, the data provide evidence regarding the preferential glucose derivation to branching pathways rather than conversion to pyruvate for oxidative phosphorylation.

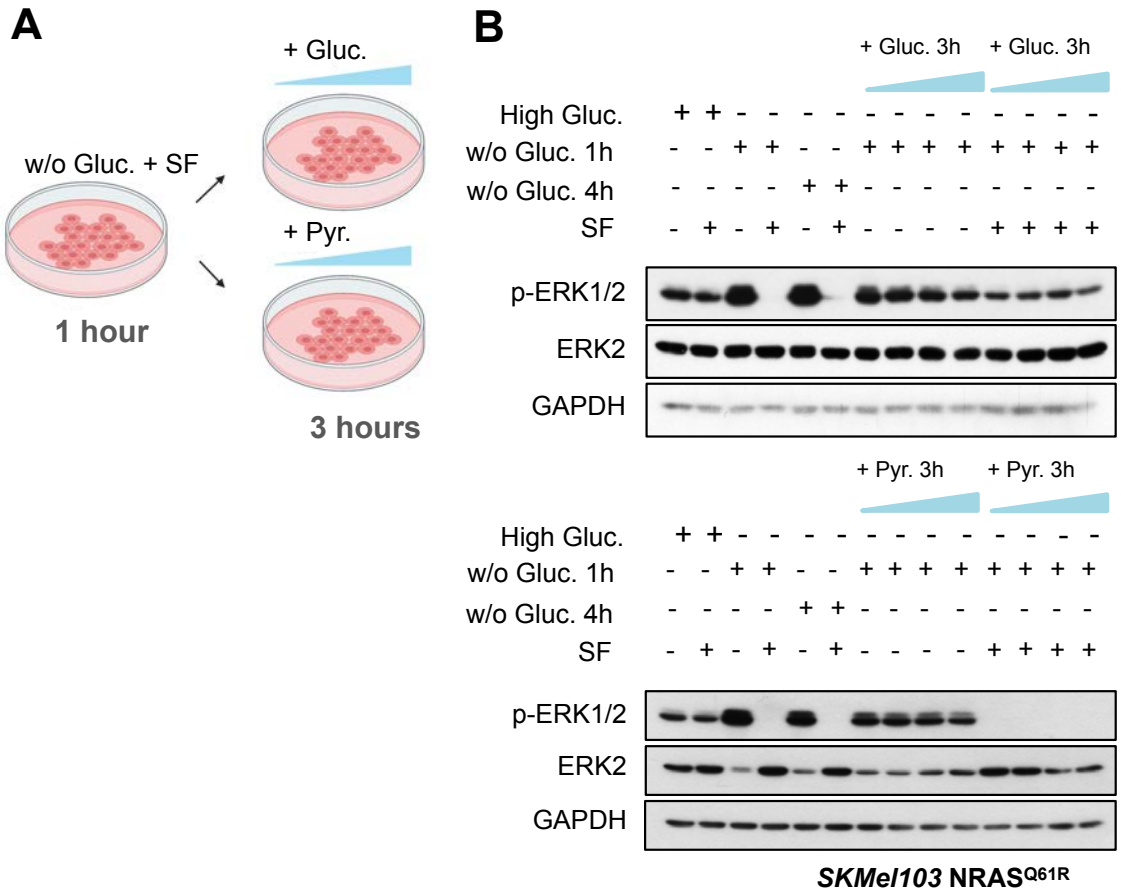

Figure R.13. Sorafenib does not produce ERK1/2 inhibition in combination with glucose but it does when combined with sodium pyruvate. (A) Scheme showing the followed experimental procedure. (B) Western Blot showing ERK1/2 phosphorylation in response to Sorafenib treatment, either alone or in combination with metabolic stress. Glucose and pyruvate concentrations correspond to 5 mM, 10 mM, 20 mM and 50 mM. Sorafenib was added at 15 μM. GAPDH is shown as a loading control. Gluc.=Glucose, Pyr.=Pyruvate, SF=Sorafenib.

Several glycolytic (ALDOB, ENO2, ENO3, G6PC2, PGAM2 and PKLR) and glucose metabolism-related genes (FBP1, FBP2, G6PD, LDHC, MPC2, PFKFB2 and PFKFB4) are regulated in NRAS^{Q61R} mutant cells in response to metabolic stress

Due to the observed relevance of the glycolytic pathway in NRAS^{Q61R} mutant cells and using the gene expression profiles generated, we investigated the transcriptional regulation of several glycolytic enzymes involved in the conversion from glucose to pyruvate (purple) and the derivation to branching pathways (orange) in NRAS^{Q61R} mutant cells (*SKMel103* and *SKMel147*) (Figure R.14A).

PGAM2, *PFKFB2*, *G6PD*, *G6PC2*, *FBP2*, *FBP1* and *ENO2* were upregulated in glucose-starved versus non-starved cells in at least one NRAS^{Q61R} mutant cell line ($log_2FC > 0.265$). On the other hand *PKLR*, *PFKFB4*, *MPC2*, *LDHC* and *ALDOB* were downregulated ($log_2FC < -0.265$) upon glucose starvation. *ENO3* was regulated oppositely in the two investigated NRAS^{Q61R} mutant cells, being upregulated in *SKMel147* and downregulated in *SKMel103* cells (Figure R.14B). Interestingly, upregulated genes were related with the metabolization of glucose to pyruvate or derivation of glycolysis intermediates to branching pathways. However, downregulated genes were mainly related to the use of pyruvate in the mitochondria (OXPHOS) or the conversion of pyruvate to lactate. Thus, metabolic stress is involved in the regulation of several glycolytic and glucose metabolism-related genes in NRAS^{Q61R} mutant cells suggesting an increased glycolytic phenotype in response to glucose starvation.

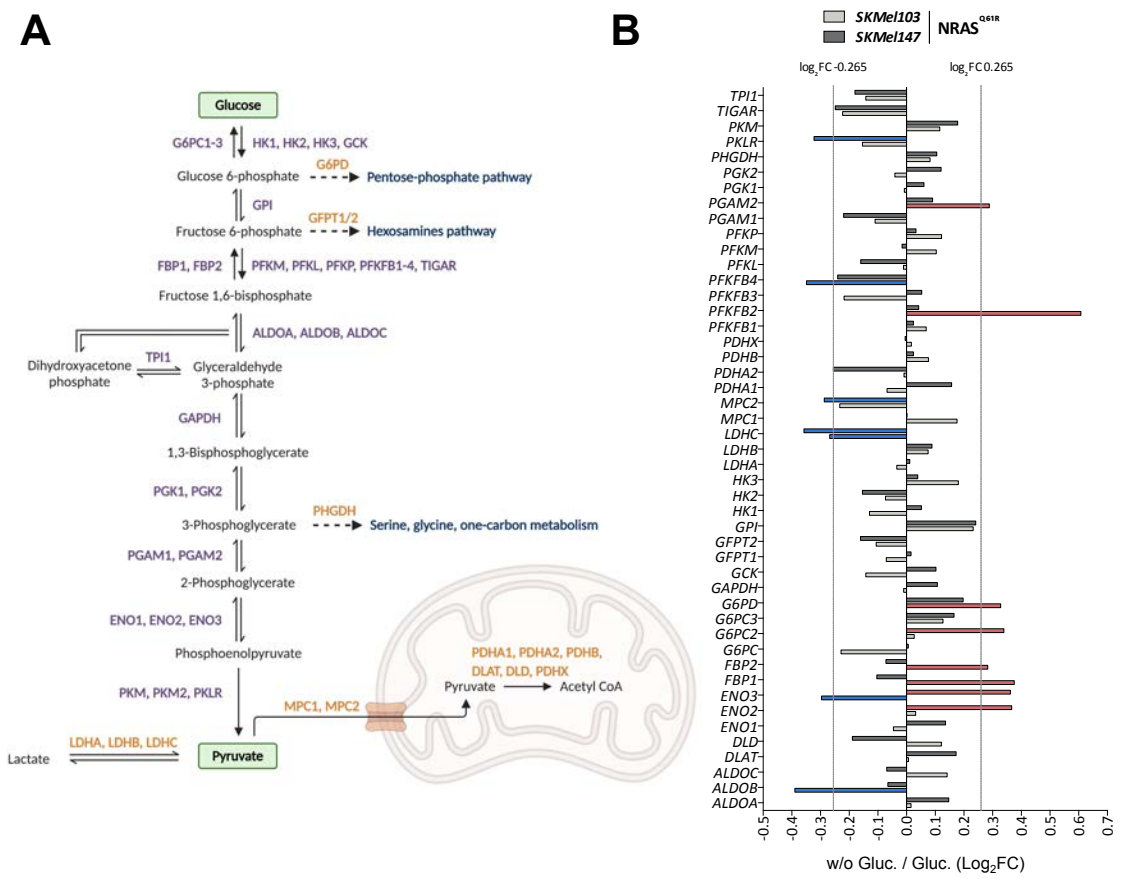

Figure R.14. Glycolysis-related genes regulation in response to metabolic stress. (A) Schematic representation of the glycolytic pathway, highlighting enzymes involved in glucose to pyruvate conversion (purple) and the derivation to branching pathways (orange). (B) Graph showing glycolysis-related genes regulation upon metabolic stress in NRAS^{Q61R} mutant cells. In red, significantly upregulated genes ($log_2FC > 0.265$) in starved vs. non-starved cells. In blue, significantly downregulated genes ($log_2FC < -0.265$) in starved vs. non-starved cells. Gluc.=Glucose, FC=Fold change.

Upregulation of PFKFB2 enzyme, which is regulated in response to metabolic stress, shows a significant tendency to co-occur with NRAS^{Q61} mutations

Upregulated enzymes in response to metabolic stress were subjected to a deeper analysis with the objective to establish its role in human melanoma biology. To this end, the enzymes genetic status was investigated in the *TCGA database* (*Melanoma Firehose Legacy study*, 287 complete samples). *PKLR*, *PFKFB2* and *MPC2* were observed to be altered, mainly upregulated, in more than 10% of melanoma cases (Figure R.15A). Moreover, *PFKFB2* showed a significant tendency (*q-value<0.05*) to co-occur with *NRAS* mutations (Figure R.15B), what suggested a relevant role of this enzyme in *NRAS* mutant backgrounds.

A

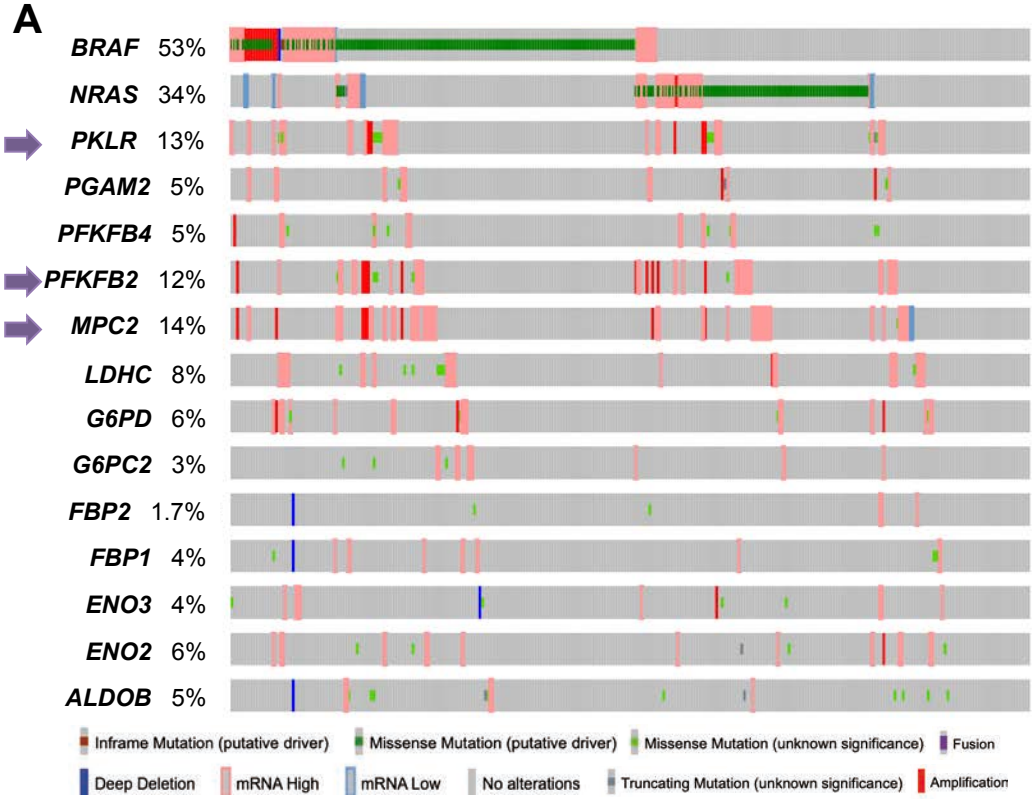

B

A	B	Neither	A Not B	B Not A	Both	q-Value	Tendency
BRAF	NRAS	56	133	78	20	< 0.001	Mutual exclusivity
NRAS	PFKFB2	174	78	15	20	0.044	Co-ocurrence

Figure R.15. Mutational status of glycolysis-related genes in human cutaneous melanoma. (A) Genetic alterations of glycolysis-related genes in human samples obtained from *TCGA (Firehose Legacy study, 287 complete samples*). Purple arrows indicate those genes altered in >10% of the samples. (B) Table showing co-ocurrence tendency of *PFKFB2* and *NRAS* genetic alterations. Data obtained from *TCGA (Firehose Legacy study,* 287 complete samples).

This co-occurrence was confirmed at the copy-number variant level, where a positive correlation tendency could be observed more clearly in *NRAS* mutant tumors than in *BRAF* mutant tumors (Figure R.16).

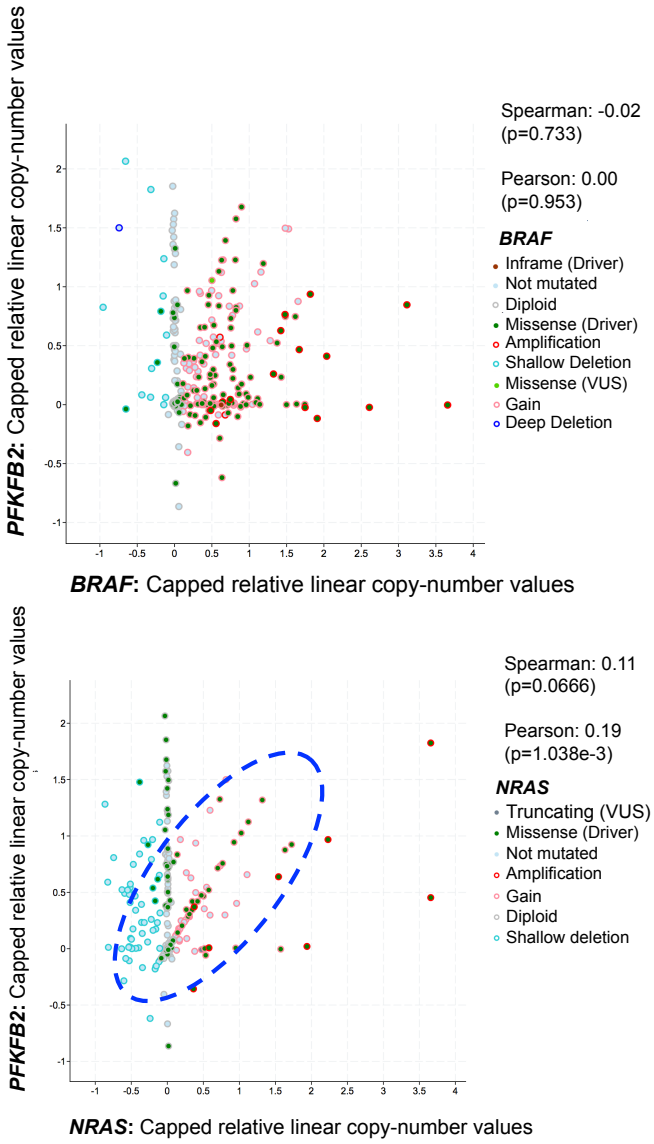

Figure R.16. Positive correlation of *NRAS* and *PFKFB2* copy number variations in human cutaneous melanoma. Graphs represent *BRAF* copy number variation (CNV) relationship with *PFKFB2* CNV (top) and *NRAS* CNV relationship with *PFKFB2* CNV (bottom). Data obtained from *TCGA database (Firehose Legacy study,* 287 complete samples).

PFKFB2 is an important enzyme in terms of glycolytic regulation, as it is involved in the conversion from F6P to F 2,6-biP, an important allosteric regulator of PFK-1. PFK-1 is involved in one of the three most important steps in glycolysis regulation, being responsible of the redirection of metabolites to glycolysis branching pathways when reduction power and biomass are needed[124].

To further confirm *PFKFB2* upregulation taking place in *NRAS* mutant cells we analyzed PFKFB2 expression at protein level in two cell line panels, including

patient-derived cell lines. Cell lines were classified in non-tumoral cells (N-T), *BRAF* mutant cells ($BRAF^{V600E}$), *NRAS* mutant cells ($NRAS^{Q61}$) and tumor cells lacking both, *NRAS* and *BRAF* mutations ($NRAS^{WT}/BRAF^{WT}$). A clear tendency of $NRAS^{Q61}$ mutant cells expressing higher PFKFB2 amounts was observed in both panels (Figure R.17). Altogether, these data provide evidence about co-ocurrence of *NRAS* mutations and PFKFB2 upregulation at protein level.

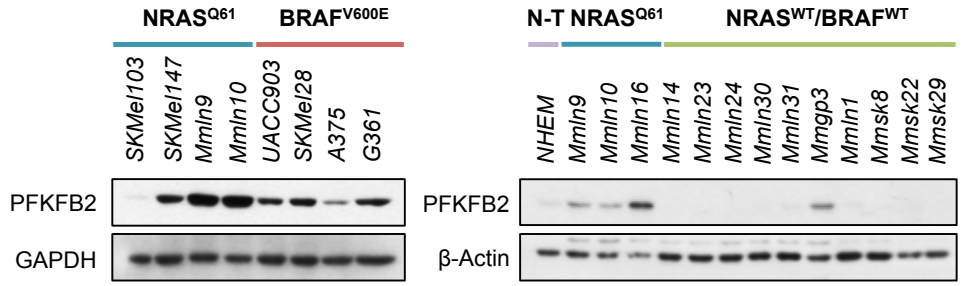

Figure R.17. PFKFB2 is upregulated in $NRAS^{Q61}$ mutant cells. On the left, commercial melanoma human cell lines panel. On the right, non-tumoral (N-T) human melanocytes and patient-derived cells. GAPDH and β-Actin are shown as loading controls.

PFKFB2 phosphorylation is regulated in response to metabolic stress and Sorafenib treatment

Once established PFKFB2 relevance in *NRAS* mutant cells we investigated its regulation in response to metabolic stress and RAS-ERK1/2 pathway inhibition conditions. PFKFB2 has a dual role in glucose metabolism. Depending on its phosphorylation status it can act as a kinase, increasing the glycolytic flux, or as a phosphatase, promoting gluconeogenesis. It has been described that PFKFB2 kinase activity is mainly regulated by phosphorylation at residue S483, and that this regulation can be driven by PKA PKC, AKT, Ca/CAMK, S6K1 and RSK[124].

In order to determine whether RAS-ERK1/2 pathway activation could be involved in PFKFB2 regulation, phosphorylation at S483 was analyzed by Western Blot in *SKMel103* ($NRAS^{Q61R}$), *SKMel147* ($NRAS^{Q61R}$), *SKMel28* ($BRAF^{V600E}$) and *UACC903* ($BRAF^{V600E}$) cell lines. Cells were subjected to one, two, three and four hours of glucose starvation alone and in combination with the RAS-ERK1/2 pathway inhibitors Sorafenib (SF) and Trametinib (TR). PFKFB2 phosphorylation at residue S483 was increased in all cell lines in response to metabolic stress; being *SKMel147* ($NRAS^{Q61R}$) the cells showing the highest response with a 2-fold

increase of PFKFB2 phosphorylation (Figure R.18A). Moreover, phosphorylation was completely inhibited by Sorafenib upon glucose starvation in all cell lines (Figure R.18B). This phosphorylation inhibition was not observed in the rest of the treatments.

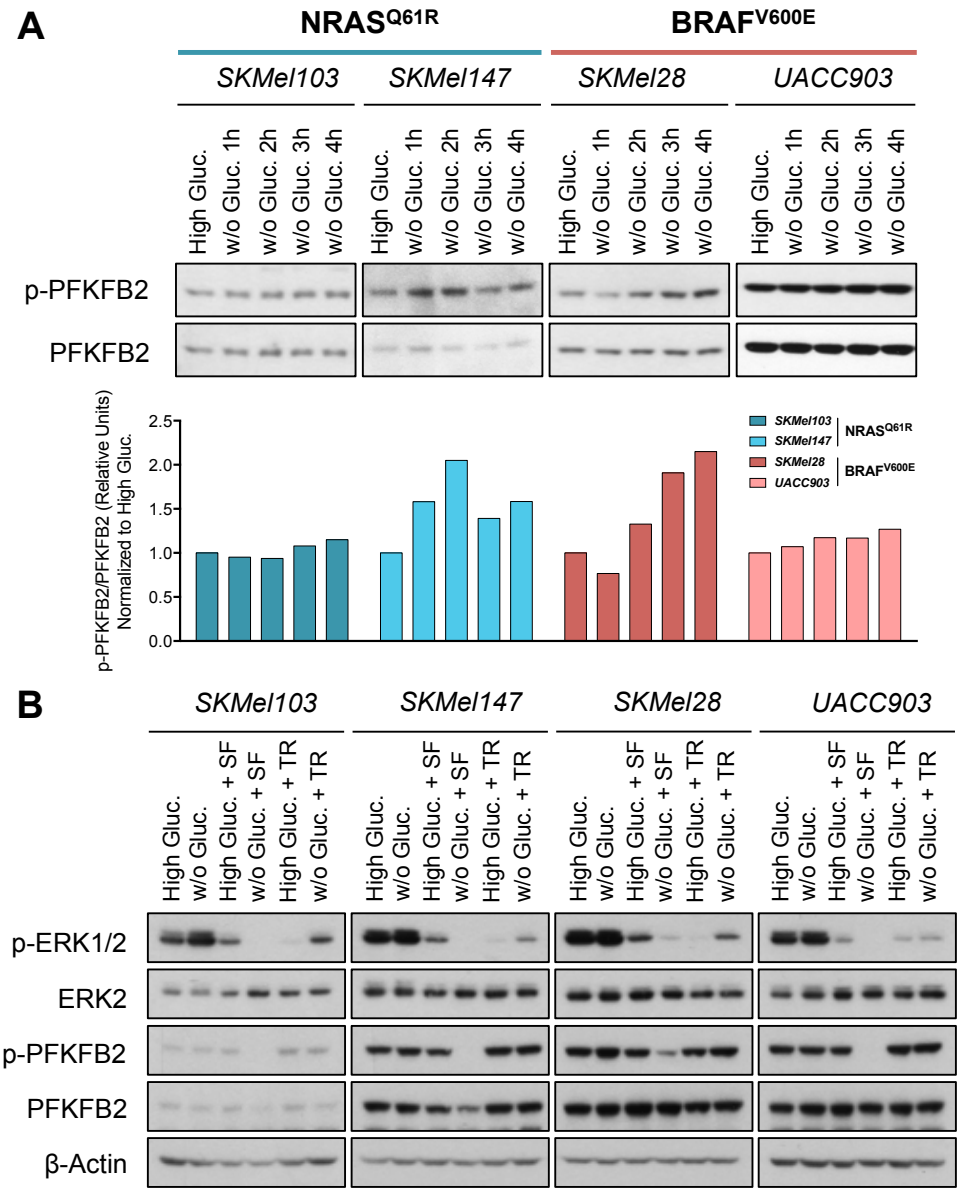

Figure R.18. PFKFB2 regulation upon metabolic stress and RAS-ERK1/2 inhibition. (A) Western Blot showing PFKFB2 phosphorylation at residue S483 and total PFKFB2 amount. The bars graph represents quantification of PFKFB2 phosphorylation. (B) Western Blot showing ERK1/2 and PFKFB2 phosphorylation at residue S483 in response to glucose starvation, Sorafenib (SF) and Trametinib (TR). Gluc.=Glucose.

These results suggest the existence of a link between glycolysis and the RAS-ERK1/2 pathway. In one hand, PFKFB2 could be mediating the hyperactivation of the RAS-ERK1/2 pathway in response to metabolic stress and

on the other hand, RAS-ERK1/2 inhibition with Sorafenib but not with Trametinib promotes inhibition of PFKFB2 phosphorylation, suggesting that RAS-ERK1/2-driven regulation of PFKFB2 is likely, carried out by the RAF family of protein kinases.

Glucose withdrawal induces PFK-1 activation through co-localization with actin fibers

As previously mentioned, PFKFB2 is involved in the synthesis of one of the main regulators of PFK-1, fructose 2,6-bisphosphate. It has been described that PFK-1 tetramerization and co-localization with actin fibers has been associated with enzyme activation[148]. In order to prove that changes in PFKFB2 phosphorylation were related to changes in PFK-1 activity (Figure R.19A), we analyzed whether metabolic stress caused differential changes in PFK-1 localization according to the cells genotype (*SKMel103* ($NRAS^{Q61R}$), *SKMel147* ($NRAS^{Q61R}$), *SKMel28* ($BRAF^{V600E}$) and *UACC903* ($BRAF^{V600E}$)).

The results showed that while $NRAS^{Q61R}$ mutant cells (*SKMel103* and *SKMel147*) increased PFK-1 activity in response to metabolic stress according to its co-localization with actin fibers, no changes were detected in $BRAF^{V600E}$ mutant cells (*SKMel28* and *UACC903*) (Figure R.19B). Thus, these results indicate that glucose starvation induces PFK-1 activation through co-localization with actin fibers in $NRAS^{Q61R}$ mutant cells.

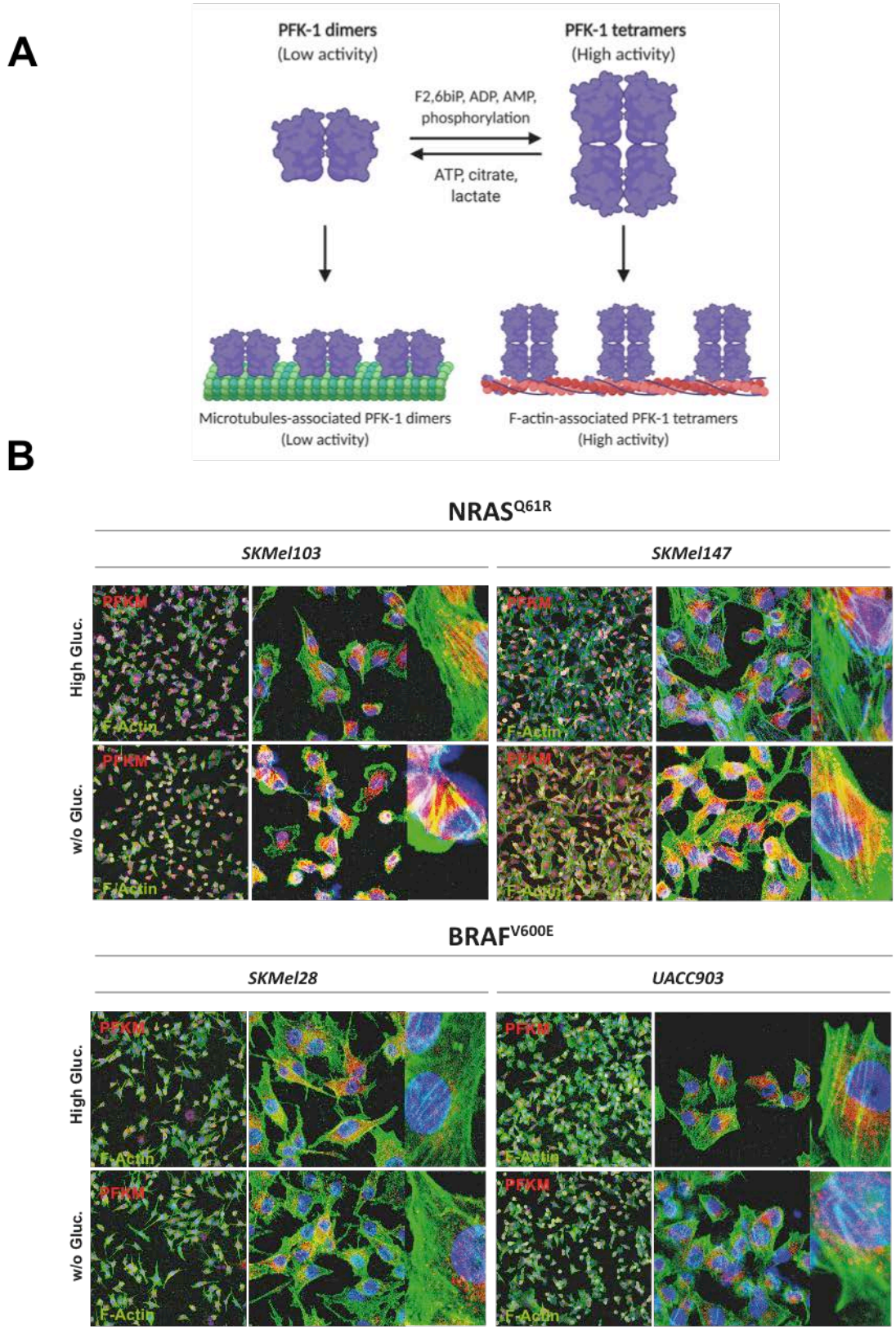

Figure R.19. PFKM and actin fibers co-localization in response to metabolic stress. (A) Schematic representation of activation mechanisms of PFK-1 activity. (B) Representative immunofluorescence images showing PFKM (Red) and actin fibers (Green) co-localization in $NRAS^{Q61R}$ and $BRAF^{V600E}$ mutant cells in response to glucose starvation.

Fructose 1,6-bisphosphate produces an increase in ERK1/2 phosphorylation

Fructose 1,6-bisphosphate, the product of PFK-1 has been described to activate RAS through the activation of *Cdc25*, the yeast ortholog of *SOS1* (Figure R.20A)[163]. The above results demonstrated that PFK-1 activity is upregulated upon metabolic stress. Thus, we investigated whether the increased production of F 1,6-biP could be part of the mechanism responsible for RAS pathway activation upon glucose starvation. To that end, we mimicked PFK-1 activation by the treatment of cells with F 1,6-biP and investigated whether we could recapitulate the activation of the RAS-ERK1/2 pathway.

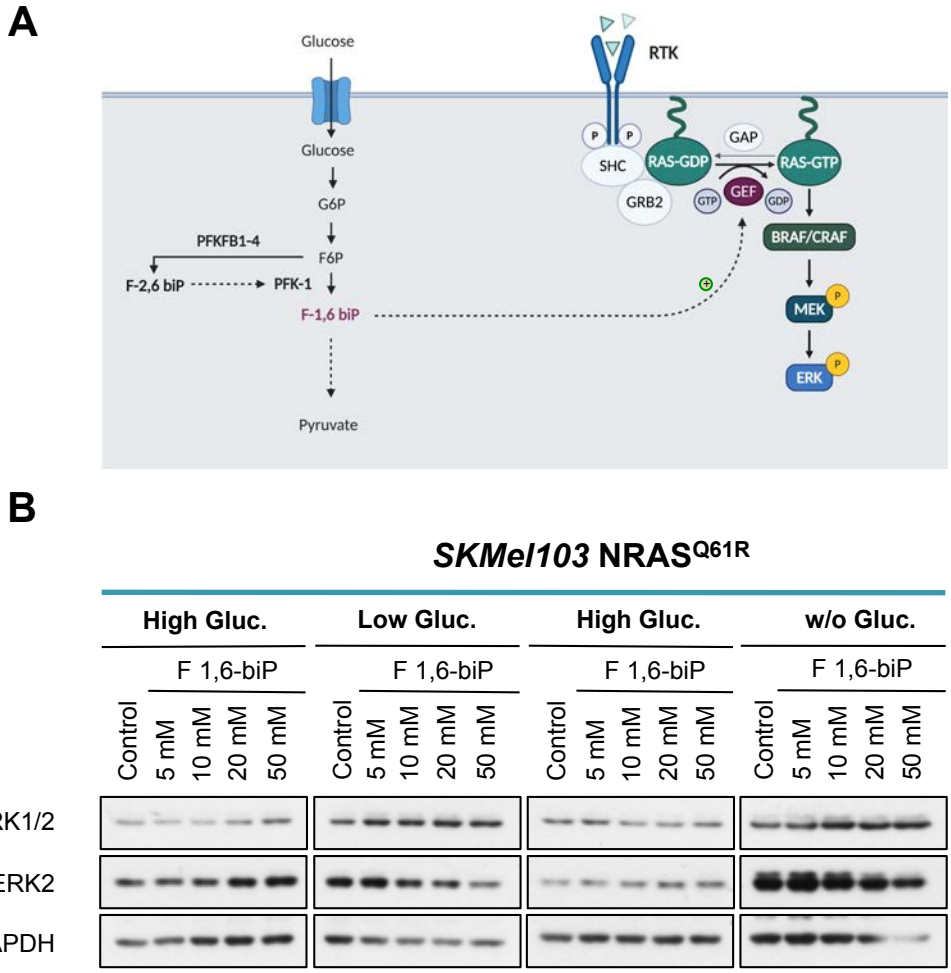

Figure R.20. Fructose 1,6-bisphosphate induces RAS-ERK1/2 pathway activation. (A) Schematic representation of glycolysis and the RAS-ERK1/2 pathway and possible described link among them. (B) Western Blot showing ERK1/2 phosphorylation regulation upon treatment with Fructose 1,6-bisphosphate (F 1,6-biP) at 5, 10, 20 and 50 mM in combination with high glucose (25 mM), low glucose (5 mM) and no glucose conditions. GAPDH is shown as a loading control.

SKMel103 cells ($NRAS^{Q61R}$) were treated with increasing concentrations of F 1,6-biP in media containing no glucose, low glucose (5 mM) or high glucose (25 mM). The results showed that ERK1/2 phosphorylation increased in cells treated with F 1,6-biP plus no glucose and low glucose containing media (Figure R.20B). Thus, these results indicate that increased production of F 1,6-biP derived from increased PFK-1 activity promotes the hyperactivation of the RAS-ERK1/2 pathway in response to metabolic stress.

In silico analysis shows PFKFB2 putative target sequences for confirmed kinases and new phosphorylation sites that may be regulated by RAF and ERK1/2 phosphorylation

These findings link glycolytic activation through PFK-1 activation and increased production of F 1,6-biP with the hyperactivation of the RAS-ERK1/2 pathway. Moreover, we have previously demonstrated that RAS-ERK1/2 inhibition with Sorafenib in combination with metabolic stress results in the inhibition of PFKFB2 phosphorylation. As PFKFB2 regulation is mainly governed by phosphorylation at different residues (Figures R.21A and R.21B), we wondered whether RAF or downstream kinases might be involved in the regulation of PFKFB2 by direct phosphorylation.

We performed an *in silico* phosphorylation analysis of PFKFB2 using the *GPS 5.0* software[164,165]. This algorithm has the ability of predicting potential protein kinase-specific phosphorylation sites from protein sequences. The prediction resulted in the generation of several parameters including score and cutoff for each predicted phosphorylation site. The score parameter represents the possibility that a specific sequence is a phosphorylation site peptide for a given kinase. If the score of a peptide sequence is high enough to bypass the cutoff value, we may estimate that it is a potential phosphorylation site of the analyzed kinase. The analysis was performed using the high threshold, which corresponds to a theoretically maximal false positive rate (FPR) of 2% for serine/threonine kinases and 4% for tyrosine kinases. Ten kinases showing the highest score after subtracting the cutoff value were represented for each phosphorylation site. Some of the already described kinases phosphorylating PFKFB2 came out from the analysis, including CAMK, RSK and AKT. Interestingly, ERK1/2 and RAF proteins

also appeared as possible regulators, being ERK1 the kinase showing the highest score at position S493, a PFKFB2 residue that had not been previously described to be involved in its regulation (Figure R.21C). Hence, *in silico* analysis proposed ERK1/2 and RAF proteins as possible kinases phosphorylating PFKFB2, highlighting the possible role of ERK1/2 in the phosphorylation of residue S493, a phosphorylation site that has not been described so far.

A

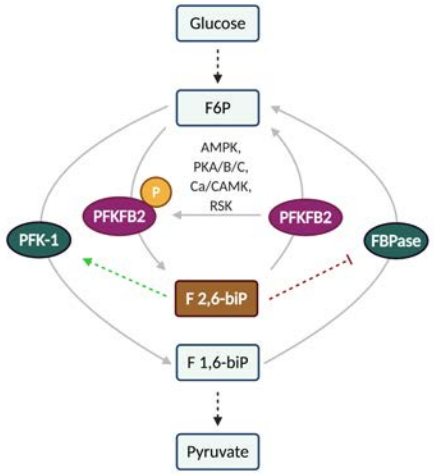

B

	PFKFB2		
	S466	T475	S483
AMPK	X		
PKA	X		X
PKB/ Akt	X		X
PKC	X	X	
Ca/ CAMK	X		X
RSK	X		X

C

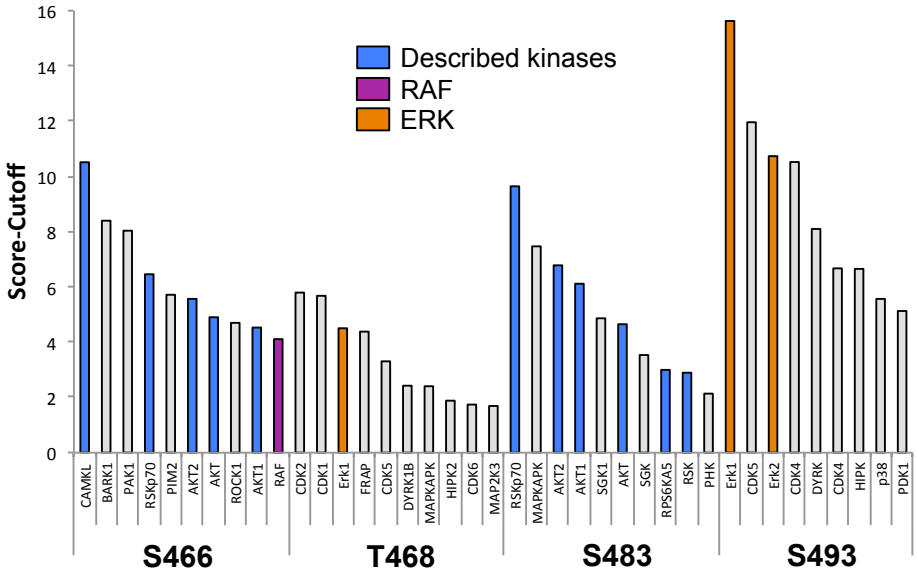

Figure R.21. Computational prediction of kinases involved in PFKFB2 phosphorylation. (A) Schematic representation of PFKFB2 regulation and its consequences in glycolysis regulation through modulation of PFK-1 activity. (B) Table indicating PFKFB2 already described phosphorylation sites and kinases involved in its phosphorylation. (C) Barr graph indicating the probability for each kinase to phosphorylate PFKFB2 at each specific site. Analysis performed using *GPS 5.0 software.*

Mass Spectrometry analysis reveals ERK2 and PFKFB3 as possible PFKFB2-interacting proteins as well as novel PFKFB2 phosphorylation sites, which are regulated in response to metabolic stress and Sorafenib treatment

To confirm RAF and ERK proteins as interacting partners of PFKFB2, as well as to further study PFKFB2 phosphorylation regulation, we performed a mass spectrometry assay. To that end we generated an inducible lentiviral construct expressing His-tagged PFKFB2 (*pLenti-rtTA2-His-PFKFB2-IRES-GFP)* (Supplementary Figure 2A). *SKMel103* ($NRAS^{Q61R}$) and *UACC903* ($BRAF^{V600E}$) cells were infected with this construct and upon induction with doxycycline His-tagged PFKFB2 was expressed together with GFP, which was used for the establishment of infection and expression efficacy (Supplementary Figure 2B).

Next, cells were subjected to metabolic stress and to treatment with Sorafenib; and His-tagged PFKFB2 was pulled down using magnetic beads (Supplementary Figure 2C). Total lysates were analyzed by Western Blot to confirm RAS-ERK1/2 pathway hyperactivation in response to glucose starvation and ERK1/2 inhibition upon Sorafenib treatment (Supplementary Figure 3) and pulled down samples were subjected to mass spectrometry analysis.

Mass spectrometry analysis of obtained lysates after His-tag PFKFB2 pull down in *SKMel103* ($NRAS^{Q61R}$) and *UACC903* ($BRAF^{V600E}$) cell lines revealed the presence of ERK2 and PFKFB3 as possible direct or indirect interacting partners of PFKFB2 (Figure R.22A and Supplementary Table 3). Further validation by Western Blot in *SKMel103* ($NRAS^{Q61R}$), *SKMel147* ($NRAS^{Q61R}$), *SKMel28* ($BRAF^{V600E}$) and *UACC903* ($BRAF^{V600E}$) cell lines confirmed the presence of both proteins (Figure R.22B) and also revealed BRAF as a possible PFKFB2 interacting partner. Interestingly, BRAF-PFKFB2 immunocomplex was stabilized in response to Sorafenib treatment in $NRAS^{Q61R}$ mutant cells and not in $BRAF^{V600E}$ mutant cells. These results suggest the presence of BRAF and ERK2 as possible PFKFB2 phosphorylating kinases in *NRAS* mutant melanoma cells. Moreover, PFKFB3 may be forming heterodimers with PFKFB2, what would have implications at functional level due to the differential kinase/phosphatase activity ratio of these enzymes[124],

and what would involve a novelty in the field, as PFKFB2 has been only described to homodimerize in order to be active[124].

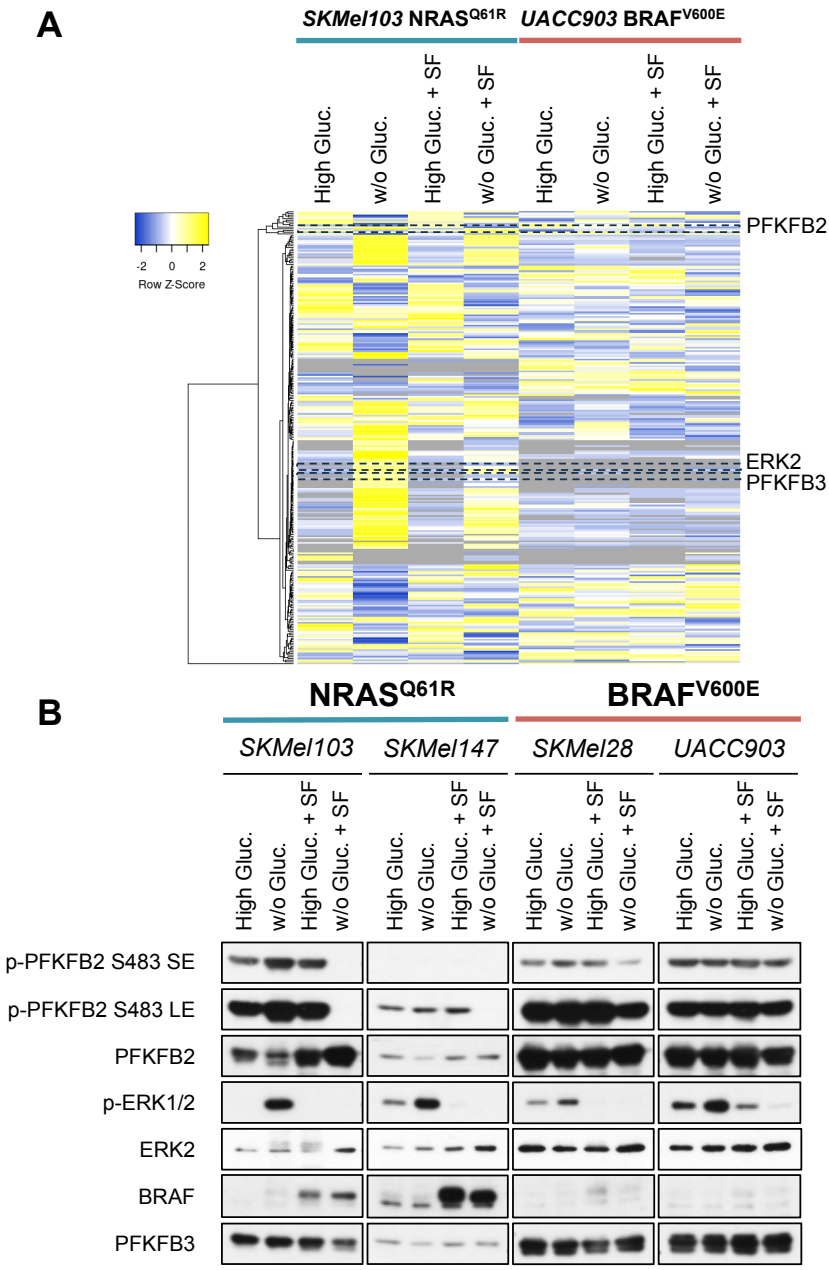

Figure R.22. ERK2 and PFKFB3 are present in the same immunocomplex than PFKFB2. (A) Heatmap representing mass spectrometry peptide counts (B) Western Blot showing proteins detected after His-tagged PFKFB2 pull down in response to metabolic stress and Sorafenib treatment (15 μM, 4 hours). Gluc.=Glucose, SF=Sorafenib, SE=Short Exposure, LE=Long Exposure.

Enrichment in phosphorylated peptides using titanium dioxide (TiO_2) followed by mass spectrometry and semi-quantitative analysis allowed us to infer phosphorylated changes of PFKFB2 in response to glucose starvation and Sorafenib treatment. Phosphorylation of PFKFB2 at residues S466, T468, S483,

S486 and S493 was detected, confirming S493 as a new PFKFB2 phosphorylation site (Figure R.23 and Supplementary Table 4). Moreover, S483 and S493 were found to be simultaneously phosphorylated (Figure R.23 and Supplementary Table 4).

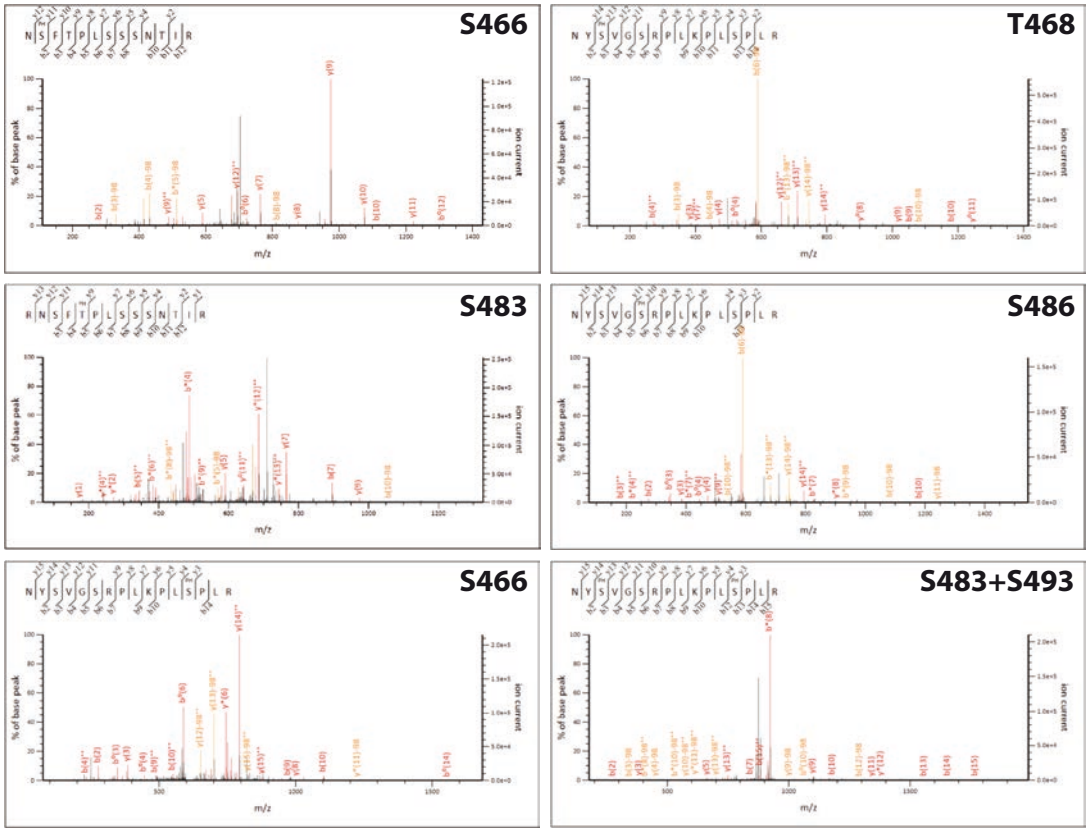

Figure R.23. Identification of novel PFKFB2 phosphorylation sites. Graphs showing the fragmentation spectrum of the phosphorylated PFKFB2 peptides identified by mass spectrometry. m/z=mass/charge ratio.

Phosphorylation at S466 was observed to increase in response to glucose withdrawal, as well as in response to Sorafenib, however, it was inhibited by the combination of both treatments. T468 residue could not be individually analyzed due to technical issues and obtained data could not discriminate among S466 and T468 phosphorylation. Something similar occurred in the case of S483, S486 and S493 residues, where phosphorylated peptides in either residue were indistinguishable. Analysis of all residues together showed the same tendency previously observed, an increase upon metabolic stress together with a marked decrease upon metabolic stress and Sorafenib treatment. Phosphorylation regulation at S483 and S493 residues could not be individually investigated however, S483 and S493 biphosphorylated peptides were detected and the

amount of them was increased in response to metabolic stress and decreased upon both, Sorafenib treatment and the combination of metabolic stress and RAS-ERK1/2 pathway inhibition (Figure R.24).

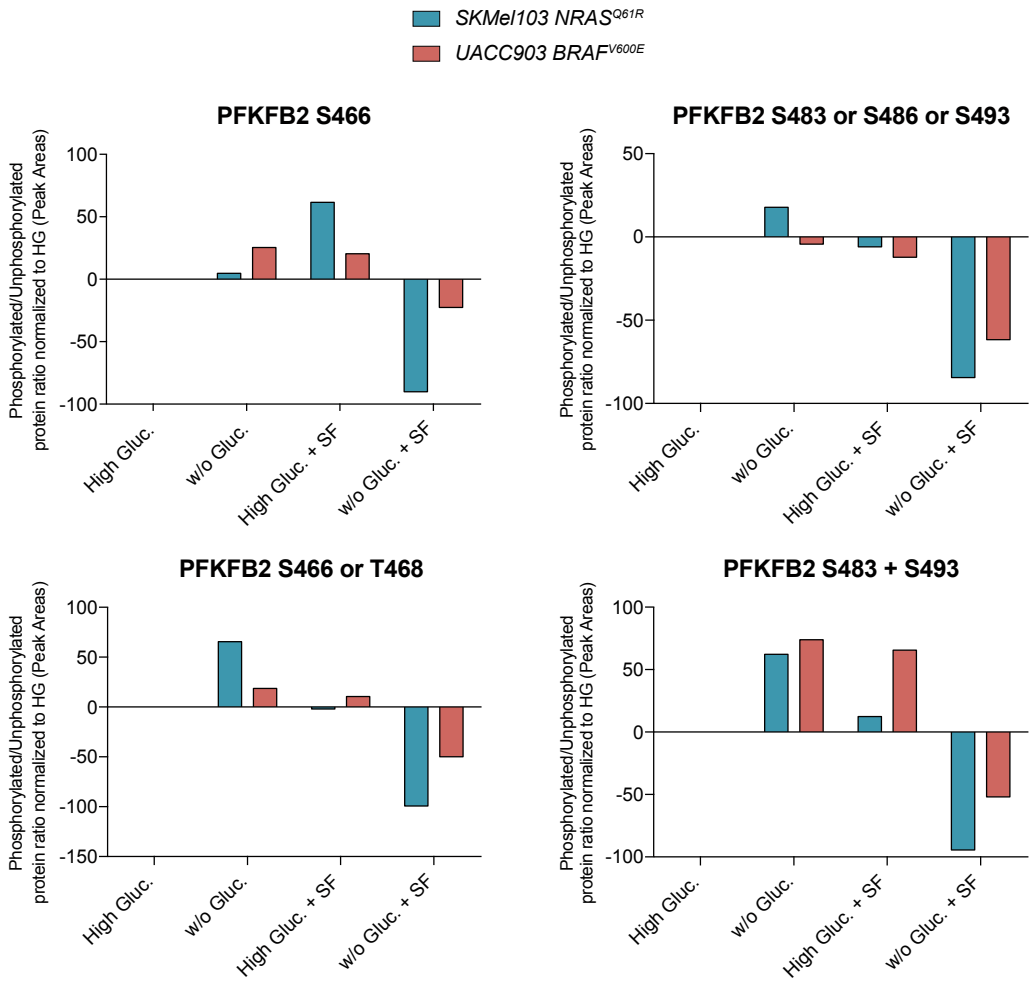

Figure R.24. PFKB2 phosphorylation regulation in response to metabolic stress and treatment with Sorafenib. Graphs indicate the ratio of phosphorylated/unphosphorylated PFKFB2 at residues S466, T468, S483, S486 and S493 in response to metabolic stress and Sorafenib (15 μM, 4 hours). Gluc.=Glucose, SF=Sorafenib.

Overall, these data confirm that PFKFB2 phosphorylation is regulated in response to metabolic stress and RAS-ERK1/2 pathway inhibition. This regulation involves phosphorylation changes in residues S466, S483 and S493, being this last residue an unknown PFKFB2 phosphorylation site until now. Mass spectrometry analysis, followed by Western Blot validation, also identified BRAF, ERK2 and PFKFB3 as putative interaction partners of PFKFB2.

PFKFB2 and PFKFB3 seem to be able to form heterodimers

As previously explained, PFKFB family of enzymes (PFKFB1-PFKFB4 isoforms), which shows around 70% of sequence identity approximately among its members (Figure R.25A), has been described to be activated through homodimerization[124]. The above results generated from mass spectrometry analysis and Western Blot, suggest the possible heterodimers formation of PFKFB2-PFKFB3 isoforms in four different melanoma cell lines.

To confirm the existence of PFKFB2-PFKFB3 heterodimers we designed an inducible lentiviral construct expressing Flag-tagged PFKFB3 (*pLenti-rtTA2-Flag-PFKFB3-IRES-GFP)*. *SKMel103* ($NRAS^{Q61R}$) mutant cells were simultaneously infected with both *pLenti-rtTA2-His-PFKFB2-IRES-GFP* and *pLenti-rtTA2-Flag-PFKFB3-IRES-GFP*. Infection and expression efficacy were assessed by Western Blot and GFP detection (Figure R.25B and Figure R25C). Both, His-tag and Flag-tag pull down assays were performed. Moreover, a double consecutive pull down was performed in order to assure the interaction between both proteins (Figure R.25D).

Presence of both, PFKFB2 and PFKFB3 was detected by Western Blot after His-tag pull down and Flag-tag pull down. Double His-tag pull down followed by Flag-tag pull down also revealed the presence of both proteins, supporting the previous observation that PFKFB2-PFKFB3 proteins may be interacting forming heterodimers (Figure R.25E).

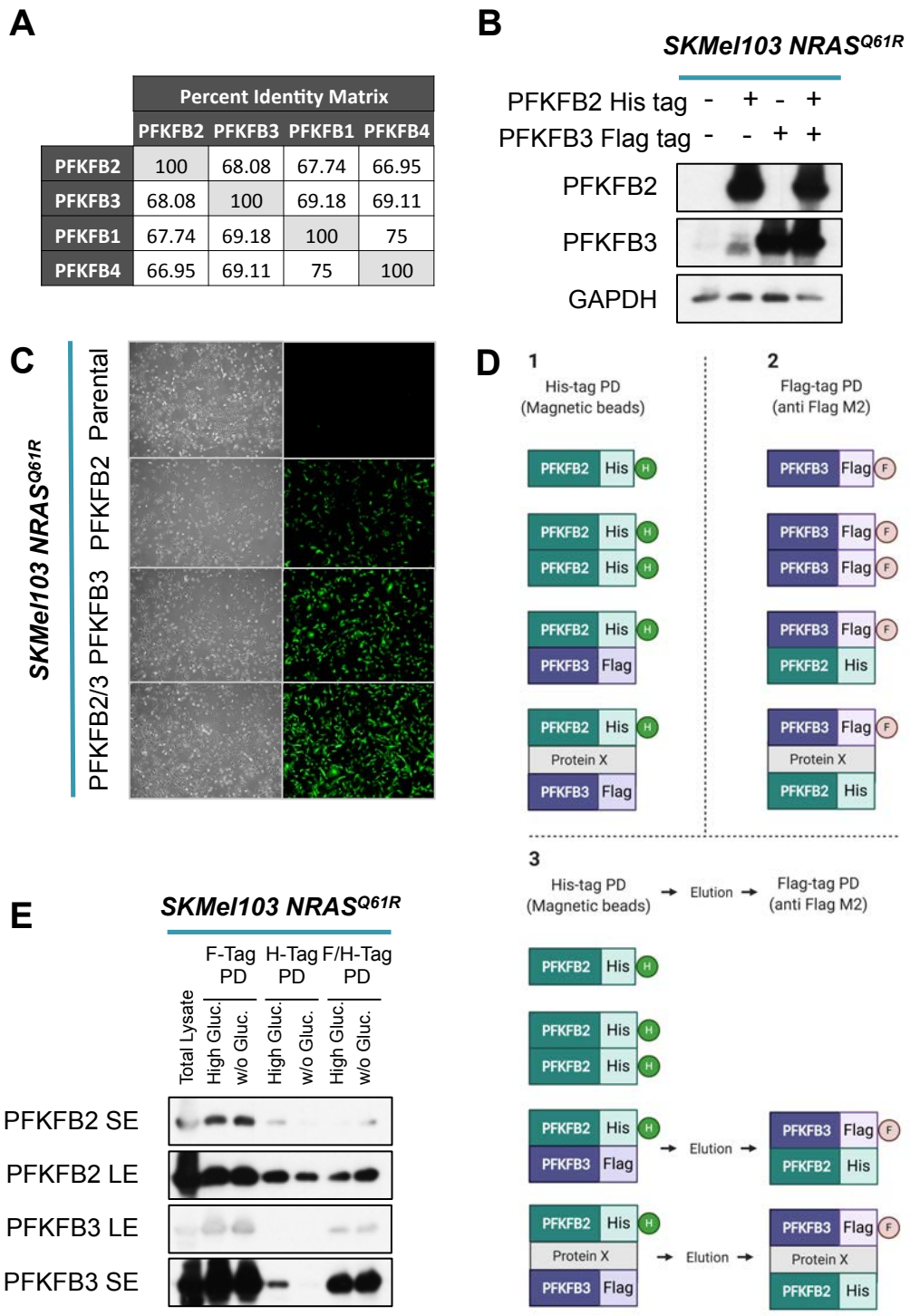

Figure R.25. PFKFB2 dimerizes with PFKFB3. (A) Table showing identity percentages obtained from the comparison between PFKFB2 and PFKFB3 isozymes. (B) Western Blot showing cells infected with His-tagged PFKFB2 and Flag-tagged PFKFB3 constructs. GAPDH is shown as a loading control. (C) Expression of GFP in induced cells infected with the different constructs. (D) Scheme representing possible scenarios after His-tag (D1), Flag-tag (D2) and double pull down (D3) assays. (E) Western Blot showing obtained proteins after flag-tagged PFKFB3 pull down, His-tagged PFKFB2 pull down and Flag-tagged PFKFB3 followed by His-tagged PFKFB2 pull down, in response to one hour of glucose starvation. Gluc.=Glucose, PD=Pull down, SE=Short exposure, LE=Long exposure.

PFKFB2 and PFKFB3 downregulation produces a decrease in ERK1/2 phosphorylation upon metabolic stress in NRAS^{Q61R} *mutant cells*

Taking into account the possible interaction between PFKFB2 and PFKFB3 which would promote the upregulation of PFK-1 activity in response to metabolic stress and consequently the RAS-ERK1/2 pathway activation due to increased levels of F 1,6-biP, we wondered whether the depletion of PFKFB2 or PFKFB3 could have any impact in the observed ERK1/2 hyperactivation in response to glucose deprivation.

To that end we transfected *SKMel103* (NRAS^{Q61R}) and *UACC903* (BRAF^{V600E}) cell lines with *PFKFB2* and *PFKFB3* siRNAs. Activation status of the RAS-ERK1/2 pathway, as well as efficacy of the siRNAs, were analyzed by Western Blot. Depletion of either PFKFB2 or PFKFB3 resulted in the inhibition of RAS-ERK1/2 pathway hyperactivation in response to metabolic stress in NRAS^{Q61R} mutant cells, while no effect was observed in BRAF^{V600E} mutant cells (Figure R.26). This effect appeared to be more pronounced when we depleted PFKBF3, which has been described to have the highest kinase activity of all isoforms of the PFKFB family. Thus, these results confirm the role of PFKFB2 and PFKFB3 in the hyperactivation of the RAS-ERK1/2 pathway in response to metabolic stress.

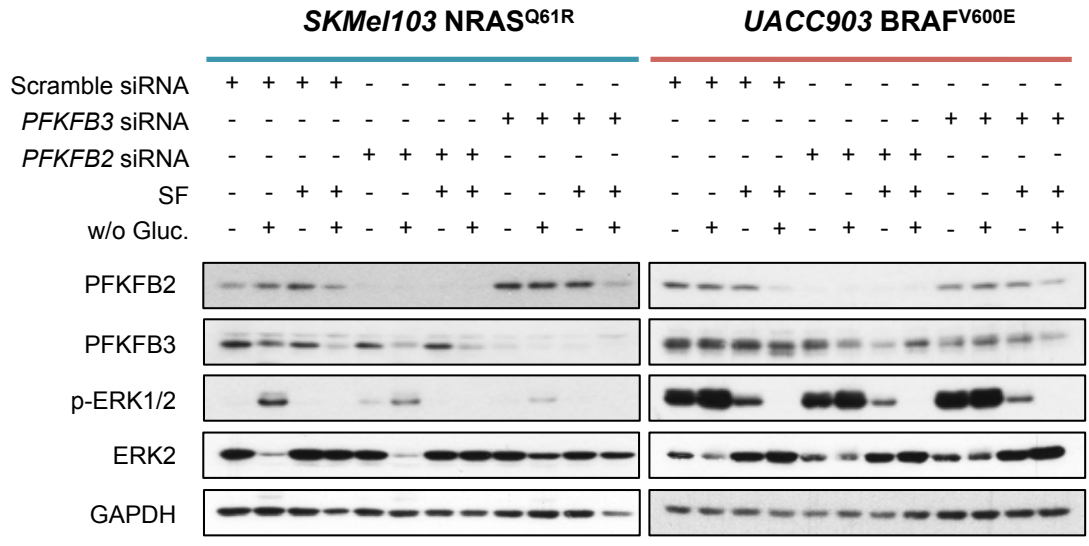

Figure R.26. PFKFB2 and PFKFB3 downregulation impedes RAS-ERK1/2 activation upon metabolic stress in NRAS^{Q61R} mutant cells. Western Blot showing PFKB2/PFKFB3 expression and ERK1/2 phosphorylation upon transient *PFKFB2* and *PFKFB3* silencing using specific siRNAs, both under basal conditions and in response to metabolic stress and treatment with Sorafenib (15 μM, 4 hours). GAPDH is shown as a loading control. Gluc.=Glucose. SF=Sorafenib.

2-Deoxy-D-glucose (2DG) mimics the low glucose effect in vitro.

The above results suggested that a therapeutic strategy combining metabolic stress and Sorafenib treatment might be an effective treatment against *NRAS* mutant melanomas. To translate the observed mechanism to an *in vivo* system we tested the efficacy of 2-deoxy-D-glucose (2DG) in an attempt to mimic glucose starvation derived effects. Over the last years, 2DG has been tested in clinical trials and overall, well toleration and non significant effects in tumor growth have been described when administered as a single agent[166].

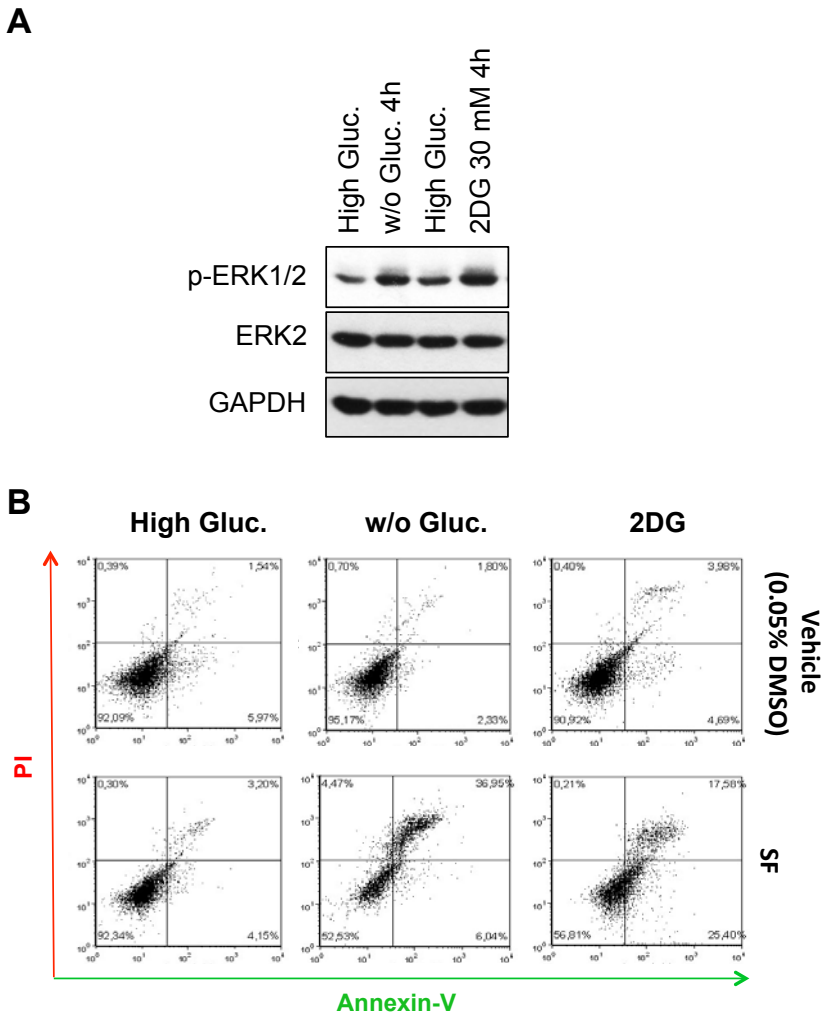

Figure R.27. 2-Deoxy-D-glucose (2DG) mimics the glucose starvation effect *in vitro*. (A) Western Blot showing ERK1/2 phosphorylation in response to glucose starvation and 2-Deoxy-D-glucose (2DG) treatment. (B) Graphs showing cell apoptosis measured by flow cytometry comparing glucose withdrawal and 2DG treatment (30 mM) in combination with either vehicle (0.05% DMSO) or Sorafenib (15 µM, 4 hours). Gluc.=Glucose, SF=Sorafenib, PI=Propidium Iodide, Annexin V=GFP-annexin V.

To confirm 2DG efficacy *in vitro SKMel103* $NRAS^{Q61R}$ cells were treated with 30 mM 2DG and subjected to Western Blot and flow cytometry analysis. In a similar manner than glucose starvation, 2DG treatment increased ERK1/2 phosphorylation (Figure R.27A). Moreover, combination of 2DG and Sorafenib resulted in an increase in cell death (17.58%) (Figure R.27B). These results support the potential use of 2DG as a glucose starvation-mimicking agent for *in vivo* treatment.

Combination of 2DG and Sorafenib has a synergistic effect in $NRAS^{Q61}$ mutant cells in vivo, including patient-derived cells

SKMel103 ($NRAS^{Q61R}$) and *SKMel28* ($BRAF^{V600E}$) cells were subcutaneously inoculated in immunosuppressed mice for the evaluation of 2DG and Sorafenib treatments *in vivo*. When the tumors reached a volume between 50-100 mm^3, mice with similarly sized tumors were randomized into treatment groups (*n*= 5 per group). Treated groups received glucose starvation treatment by the addition of 1000 mg/kg 2DG to drinking water and an intraperitoneal injection of 10 mg/kg Sorafenib every day. Control groups were treated with vehicle (PBS with 5% (v/v) DMSO).

Either Sorafenib or 2DG single treatment promoted a decrease in tumor growth in both, $NRAS^{Q61R}$ and $BRAF^{V600E}$ mutant cells. However, in the case of $NRAS^{Q61R}$ mutant cells a significant additive effect was observed in response to the combination of both treatments, metabolic stress and Sorafenib (*q-value<0.0001* compared to 2DG and *q-value<0.001* compared to SF) (Figure R.28A). Further analysis of obtained tumors by immunohistochemistry confirmed ERK1/2 hyperactivation in response to 2DG in $NRAS^{Q61R}$ mutant cells and the expected inhibition of this phosphorylation upon combined treatment. These data correlated with a decrease in Cyclin D1 expression in treated cells, confirming the inhibition of cell division capacity in response to 2DG, SF and 2DG + SF treatments. In contrast, no regulation of these markers was appreciated in $BRAF^{V600E}$ mutant cells (Figure R.28B).

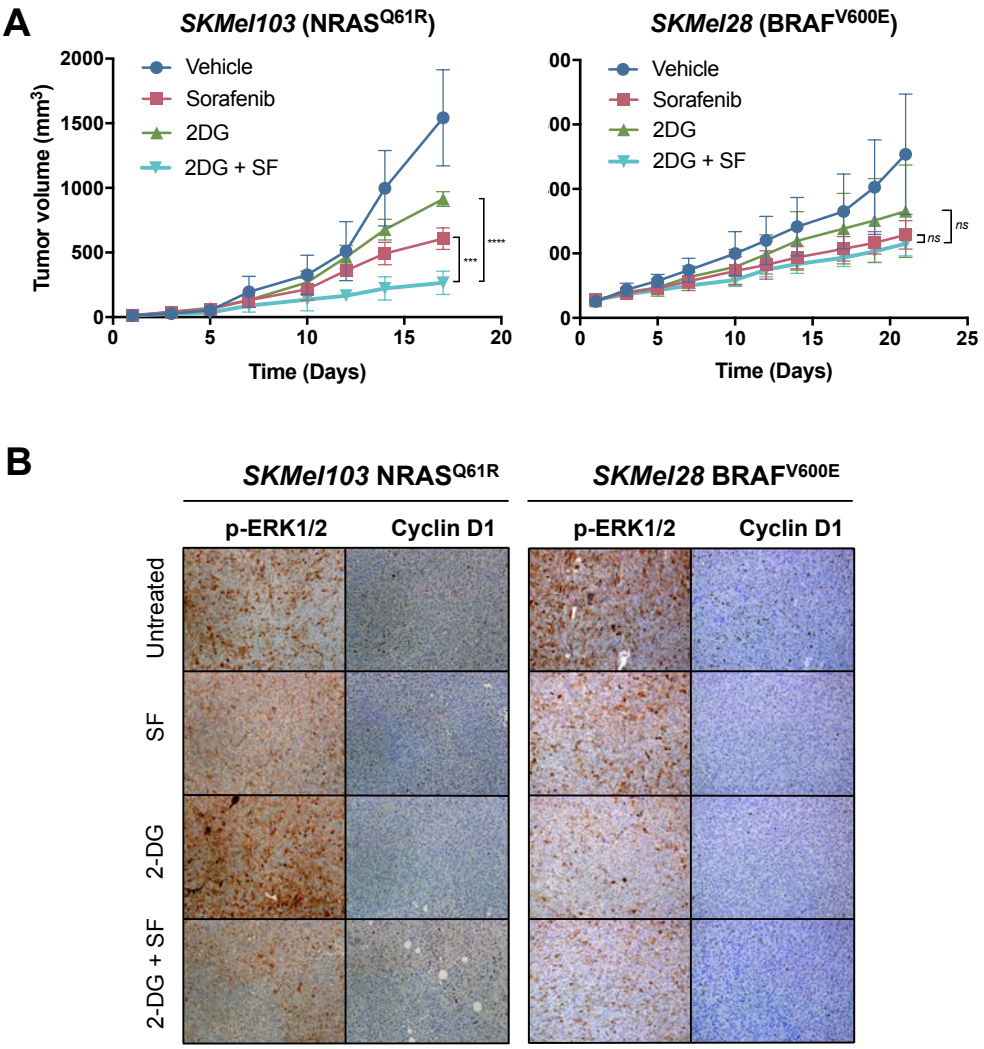

Figure R.28. Combination of 2-Deoxy-D-glucose (2DG) and Sorafenib has a synergistic effect *in vivo* in NRAS^{Q61R} mutant cells. (A) Graphs showing *in vivo* tumor growth upon treatment with Sorafenib, 2DG and the combination of both (n=5± SD). Vehicle-treated cells are shown as control cells. (B) Representative images of p-ERK1/2 and Cyclin D1 immunostaining of tumors are shown. SF=Sorafenib; ns=non-significant;***=*q-value<0.001*; ****=*q-value<0.0001.*

To further validate the efficacy and specificity of the proposed combined therapy in a patient-derived xenograft (PDX) model, we used NRAS^{Q61} mutant patient-derived cells (*Mmln9*). As expected, significant decrease in tumor growth could be observed when we compared the combination of 2DG and SF with individual treatments (*q-value<0.001* compared to 2DG and *q-value<0.01* compared to Sorafenib). Moreover, necrotic areas could be detected in those tumors resulting for the double-treated mice (Figure R.29).

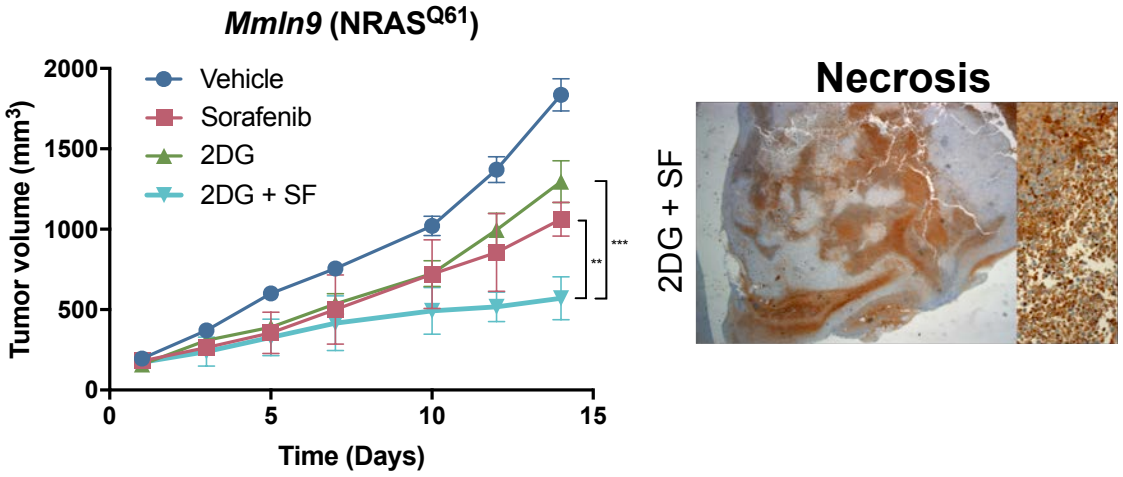

Figure R.29. Combination of 2-Deoxy-D-glucose (2DG) and Sorafenib has a synergistic effect *in vivo* in patient-derived NRAS^{Q61R} mutant cells. On the left, graph shows *in vivo* tumor growth of *Mmln9* (patient-derived) cells upon treatment with Sorafenib, 2DG and the combination of both (n=5± SD). Vehicle-treated cells are shown as control cells. On the right, a representative tumor picture of a necrotic tumor from mice treated with 2DG + SF. SF=Sorafenib; **=*q-value<0.01*; ***=*q-value<0.001.*

Overall, these data support the *in vivo* tolerability and efficacy of the combination of 2DG and Sorafenib, which involves a dramatic decrease of tumor growth in NRAS^{Q61} mutant cells while non-significant effects are observed in BRAF^{V600E} mutant cells.

DISCUSSION

Activating mutations in *BRAF* and *NRAS* oncogenes are the most common genetic alterations in cutaneous melanoma (*TCGA database*). Both modifications lead to the constitutive activation of the RAS-ERK1/2 pathway[19], however, it has been also noticed that *BRAF* and *NRAS* mutant tumors constitute two different tumoral entities at molecular and clinical levels[40,44]. An important consequence of this molecular scenario is the availability of targeted therapies against *BRAF* mutant melanomas, while *NRAS* mutant tumors are treated with the standard of care, showing low response rates and high toxicity[29,34,40,44]. Thus, understanding the molecular mechanisms governing *NRAS* mutated melanomas compared to *BRAF* mutant tumors would be essential to improve the therapeutic opportunities for the treatment of patients carrying *NRAS* mutations.

During the last years, an increased interest in how cancer cells regulate metabolism has emerged[53,54]. Moreover, evidence is growing on the fact that metabolic reprogramming can be subjected to regulation by oncogenes[102,103]. Recently, it has been described that metabolic settings can be driven by oncogenes in melanoma[52,53,57,107], nevertheless, these findings are almost totally related to *BRAF* oncogenic activation, and little is known about the role of *NRAS* mutations in metabolism rewiring. In this matter, deciphering the metabolic settings of *NRAS* mutant melanomas could provide new avenues for the establishment of specific therapeutic approaches against these tumors.

Adaptation of glucose metabolism has been established as the most important cancer hallmark regarding metabolic reprogramming. In fact, glucose starvation is one of the most relevant stressors affecting tumor cells, due to its dependence on glucose to maintain cell proliferation. Previous results from our group established that $BRAF^{V600E}$ mutant cells are not able to sense low energy levels derived from glucose deprivation due to an uncoupling in the LKB1-AMPK axis promoted by $BRAF^{V600E}$ oncogene. In turn, these cells do not activate the expected apoptotic response under energy stress conditions[107]. This phenotype is BRAF-dependent and it can be restored upon treatment with Sorafenib, a multi-kinase inhibitor targeting RAF. Overall, this phenomenon was interpreted as an opportunity for the specific targeting of these cells, since the combination of energy stress and RAS-ERK1/2 pathway inhibition triggered apoptosis[107].

Surprisingly, combination of metformin, an AMPK activator mimicking low energy stress, and the inhibition of the RAS-ERK1/2 pathway, resulted in an unexpected increased cytotoxicity in $NRAS^{Q61}$ mutant cells compared to *BRAF* mutant cells[167]. These results showed a differential response to metformin in $NRAS^{Q61}$ and $BRAF^{V600E}$ mutant cells that may be exploited for the direct targeting of tumors carrying *NRAS* mutations. Interestingly, these results are in agreement with improved disease control rate in *KRAS* mutant non-small cell lung cancer patients treated with metformin plus Sorafenib in comparison with Sorafenib as a single agent[168]. Thus, we investigated the molecular implications of glucose starvation in $NRAS^{Q61}$ mutant cells in order to establish whether the presence of NRAS-dependent metabolic settings can be exploited for the development of targeted therapies against *NRAS* mutant melanomas.

Our results confirmed that $NRAS^{Q61}$ and $BRAF^{V600E}$ mutant melanoma cells experiment a differential response to glucose deprivation that results in the hyperactivation of the RAS-ERK1/2 pathway in $NRAS^{Q61}$ mutant cells. Upon activation, phosphorylated ERK1/2 translocates to the nucleus[162], however, $NRAS^{Q61}$ mutant cells subjected to metabolic stress showed a predominant cytoplasmic localization of activated ERK1/2. This unexpected localization may be related to the regulation of ERK1/2 cytoplasmic substrates and/or the saturation of the translocation systems to the nucleus within the cell. These results are in agreement with the described increased ERK1/2 cytoplasmic activity in myeloid leukemia cells describing a protection mechanism against apoptosis caused by prolonged serum starvation[169]. Moreover, deregulation of reactive oxygen species (ROS), a situation that can be promoted by glucose starvation, could be involved in the regulation of ERK1/2 activity in the cytoplasm[170].

In line with previous results and the above data[107,167], metabolic stress resulted in $NRAS^{Q61}$ mutant cells acquisition of sensitivity to Sorafenib treatment. Intriguingly, inhibition of the different Sorafenib targets using receptor tyrosine kinases inhbitors Axitinib, Avastin, Lenvatinib and Sunitinib; $BRAF^{V600E}$ inhibitor Vemurafenib; PanRAS inhibitor CCT196969; and MEK inhibitor Trametinib, did not mimic Sorafenib effect *in vitro*. The resulting phenotype may be the consequence of a higher Sorafenib efficiency in the inhibition of one or more of its

targets upon glucose starvation. It is important to remark that contrary to the rest of the tested inhibitors, Sorafenib is a known type II inhibitor, able to bind targets in their inactive conformation (*DGF-out*) occupying the hydrophobic pocket adjacent to the ATP binding site[171]. This feature, that has been demonstrated to confer efficacy and specificity, would explain why Sorafenib is so effective against certain molecular scenarios. Conformational changes of the different Sorafenib targets in response to metabolic stress may explain different affinity and consequently higher efficacy of Sorafenib in $NRAS^{Q61}$ mutant glucose-deprived cells. In line with this, Verlande et al. have described differential response to several metabolic stressors governed by RAF-KSR dimerization (CRAF in *NRAS* mutant cells and BRAF in *BRAF* mutant cells). The authors suggest that this differential association may be responsible of either conformational changes that involve regulation of RAF susceptibility to phosphorylation, or the stabilization of active-CRAF. Both events contemplate the hyperactivation of ERK1/2 in response to metabolic stress in *NRAS* mutant cells. However, contrary to our data, the authors describe this process as an *NRAS*-independent process[172].

Concomitant to the inhibition of ERK1/2, sensitivity acquisition of $NRAS^{Q61}$ mutant cells resulted in the generation of a *synthetic lethality* condition, being cell death detected exclusively in $NRAS^{Q61}$ mutant cells subjected to glucose starvation and Sorafenib treatment. Remarkably, this effect was not observed in $BRAF^{V600E}$ mutant cells, which are known to be sensitive to the inhibition of the RAS-ERK1/2 pathway under normal conditions. The synergistic effect of Sorafenib and metabolic stress observed in $NRAS^{Q61}$ mutant cells provide a new therapeutic opportunity for the targeting of *NRAS* mutant melanomas, repurposing the use of drugs previously discarded for this disease[173].

At the molecular level, these results suggest the existence of oncogene-dependent metabolic settings in $NRAS^{Q61R}$ mutant cells. In fact, the extraordinary decrease of ERK phosphorylation observed in *NRAS*-depleted cells in response to metabolic stress confirmed that the hyperactivation of the RAS-ERK1/2 pathway is an *NRAS* oncogene-dependent process.

Mutation of *NRAS* at residue Q61 is responsible for the disruption of the GTPase activity of the protein. Upon GTP binding to NRAS, this modification locks

the protein it in its active conformation resulting in the constitutive activation of the RAS-ERK1/2 cascade and the subsequent biological effects in cell proliferation and survival[34,40]. Thus, $NRAS^{Q61}$ mutations do not involve the direct activation of RAS. In other words, RAS has to be previously recruited to the membrane and activated (GTP-charged) by different stimuli within the cell and then, $NRAS^{Q61}$ mutation will be responsible for the sustained signal blocking RAS in the active or RAS-GTP conformation. Analysis of RAS-GTP binding in response to glucose starvation revealed an increased RAS binding to GTP, which correlates with previously obtained data and highlights the direct participation of RAS in the response to metabolic stress.

One of the molecular peculiarities of *NRAS* mutant cells is the use of CRAF instead of BRAF to transmit the downstream signal[42]. Our results demonstrate that there is a switch in the use of the RAF isoforms from CRAF to BRAF in response to glucose deprivation. This is supported by the increased phosphorylation of CRAF at S259 residue in response to metabolic stress, which leads CRAF to an inhibitory state[30,42]. In addition to this, CRAF inactivation is associated to the disruption of BRAF-CRAF heterodimers concomitant to the formation of BRAF homodimers. Moreover, the regulation of RAF activity and dimerization patterns upon glucose deprivation results in an increased BRAF kinase activity and a decreased CRAF kinase activity. Altogether, these data strongly support the existence of a specific NRAS-dependent signaling regulation in response to metabolic stress.

The analysis of the top 400 differentially expressed genes among $NRAS^{Q61}$ and $BRAF^{V600E}$ mutant cells in basal conditions, shows a significant association of these genes with metabolism-related processes, including metabolic process, cellular component organization or biogenesis and detoxification GO categories, thus involving *NRAS* mutant cells-specific metabolic settings. Moreover, in response to metabolic stress, only a small percentage of regulated genes were common to $NRAS^{Q61}$ and $BRAF^{V600E}$ mutant cells. To further analyze the metabolic implications of these molecular differences, we used a total of four $BRAF^{V600E}$ and four $NRAS^{Q61}$ mutant cell lines, including patient-derived cells. We have established that $NRAS^{Q61}$ mutant cell lines show a consistent reduced mitochondrial response capacity compared to $BRAF^{V600E}$ mutant cells. Several

studies have highlighted the presence of high mitochondrial capacity of $BRAF^{V600E}$ mutant cells, involving high oxidative phosphorylation rates, especially in response to $BRAF^{V600E}$ inhibition with Vemurafenib[174–176]. Regarding regulation of mitochondrial function in *RAS*-mutated backgrounds, attenuation of mitochondrial capacity has been described in glioblastoma, due to the inhibition of PDH phosphatase (PDP)[177]. Moreover, additional studies[178,179] have demonstrated a relationship existing between the presence of *KRAS* mutations and both, general autophagy and selective mitophagy, involving a glycolytic metabolic shift in breast and pancreatic cancers. Altogether these data strongly support that cells carrying *NRAS* mutations are characterized by a compromised mitochondrial capacity, contrary to $BRAF^{V600E}$ mutant cells. Furthermore, cells carrying *NRAS* mutations are not very efficient metabolizing alternative energy sources in the absence of glucose. This low metabolic flexibility is manifested in glucose deprived $NRAS^{Q61}$ mutant cells subjected to the metabolic inhibition of glucose, glutamine and long chain fatty acids catabolism, the most relevant energy sources used to meet energy demand in human cells. Overall, these data provide strong evidence supporting glycolysis regulation as a key process for $NRAS^{Q61}$ mutant cells.

It is important to highlight that glucose seems not to be preferentially metabolized to CO_2 and H_20 due to the low mitochondrial capacity characterizing these cells. The importance of glucose as a fuel source resides in the different steps of glycolysis rather than in the full oxidation of glucose through oxidative phosphorylation, a phenomenon known as "Warburg effect"[101]. Increased glycolytic flux either can derive in glucose conversion to pyruvate and then to lactate; or glucose can be derived to glycolysis branching pathways in order to generate reduction power and building blocks for the maintenance of high proliferation rates. The addition of glucose but not pyruvate to cells growing in glucose and pyruvate free media in the presence of Sorafenib, is able to rescue the apoptosis induced by the combination of metabolic stress and Sorafenib, increasing cell viability in a dose-dependent manner. This piece of data allowed us to reinforce the fact that glucose is not fully metabolized through oxidative phosphorylation. Moreover, it can neither be converted into pyruvate and lactate, being likely derived to the branching pathways of the glycolysis to generate reduction power and tumor biomass. Consequently, the addition of 3BP, an

hexokinase 2 (HK2) inhibitor, is able to mimic glucose starvation-induced cell death in combination with Sorafenib, while DCA, a pyruvate dehydrogenase inhibitor, is not. Importantly, these phenotypic effects (increased cell viability and the loss of sensitivity to Sorafenib) also correlated with molecular changes in the RAS-ERK1/2 pathway. In this matter, the addition of glucose but not pyruvate is able to restore ERK1/2 phosphorylation. Moreover, in combination with Sorafenib, glucose addition can recover ERK1/2 phosphorylation basal levels while pyruvate can not. Thus, these data emphasize glucose metabolism relevance in $NRAS^{Q61}$ mutant cells and support the preferential metabolization of glucose to the branching pathways rather than conversion to pyruvate and later oxidative phosphorylation. These results are in agreement with previously described glycolysis intermediates channeling to the pentose phosphate pathway and hexosamine pathway in *KRAS* mutant pancreatic and colorectal cancers[180,181].

Transcriptional analysis of the regulation of glycolytic and glycolysis-related genes has revealed *PFKFB2* as a key player in the regulation of glycolysis in $NRAS^{Q61R}$ mutant cells, which becomes upregulated in response to glucose deprivation. PFKFB2 has dual kinase and phosphatase activity and it is involved in the conversion from F6P to F 2,6-biP and vice versa. F 2,6-biP is an allosteric regulator of PFK-1. PFK-1 catalyzes one of the three most important steps in glycolysis regulation[124]. We have investigated the incidence of PFKFB2 alterations in human melanoma. PFKFB2 appears to be altered, mainly amplified, in 12% of cutaneous melanoma patients (*TCGA database*). Interestingly, these alterations show a significant tendency to co-occur with *NRAS* mutations (*q-value < 0.05*). This observation has been confirmed at the protein level, where $NRAS^{Q61}$ mutant cells tend to express larger amounts of PFKFB2. Furthermore, PFKFB2 activity is regulated by increased phosphorylation at residue S483, a phosphorylation site promoting kinase activity, in response to metabolic stress. Of note, these changes in PFKFB2 phosphorylation promote the activation of PFK-1 through co-localization with actin fibers in $NRAS^{Q61R}$ mutant cells and not in $BRAF^{V600E}$ mutant cells. This observation is in agreement with previous reports that have correlated PFK-1 tetramerization and co-localization to cytoskeleton with higher activity rates[148].

A possible link existing among phosphofructokinase increased activity and RAS-ERK1/2 pathway activation has been described by Peeters et al[163]. The authors established that F 1,6-biP, the product of PFK-1 activity, can activate RAS through the activation of Cdc25 (yeast ortholog of SOS1), a GTPase accelerating protein[163]. We have reinforced these data by demonstrating ERK1/2 hyperactivation in response to F 1,6-biP treatment, providing a possible mechanism by which the activation of the kinase activity of PFKFB2 upon metabolic stress and the consequent allosteric activation of PFK-1 by F 2,6-biP, results in the increased production of F 1,6-biP leading to the hyperactivation of the RAS pathway. The activation mechanism is NRAS-dependent and involves increased RAS binding to GTP, likely mediated by SOS1, as well as changes in NRAS-dependent signaling patterns.

In addition to this, combination of metabolic stress and Sorafenib results in the inhibition of PFKFB2 phosphorylation establishing that activation of PFKFB2 is related with RAS-ERK1/2 pathway regulation. Intriguingly, combination of metabolic stress and RAS-ERK1/2 pathway inhibition downstream RAF with Trametinib does not have any effect in PFKFB2 phosphorylation. Known kinases phosphorylating PFKFB2 include PKA, PKB/AKT, PKC, Ca/CAMK, S6K1 and RSK[124]. Among these enzymes, the only one targetable by Sorafenib would be RSK[182], which can be activated by ERK. We discarded this possibility because ERK inhibition with Trametinib does not have any effect in PFKFB2 phosphorylation. Our data provide new evidence about the existence of alternative protein kinases involved in PFKFB2 phosphorylation under certain metabolic situations, and these kinases may be targetable by Sorafenib and not by Trametinib.

A predictive phosphorylation analysis to establish putative kinases able to modify specific PFKFB2 residues, not only showed already described kinases including CAMK, RSK and AKT, but also disclosed ERK1/2 and RAF proteins as possible kinases of PFKFB2. In relation to this, ERK1 was the kinase showing the highest score able to phosphorylate the S493 position, a residue that has not been previously described to be involved in its regulation. Mass spectrometry and Western Blot analyses have confirmed the presence of BRAF and ERK2 in the same immunocomplex than PFKFB2, suggesting a new role of BRAF and ERK2 in the

phosphorylation and regulation of PFKFB2. This observation is in agreement with previously described cytoplasmic localization of ERK1/2 in $NRAS^{Q61}$ mutant cells subjected to metabolic stress.

Mass spectrometry analysis also highlighted the changes in PFKFB2 phosphorylation in response to both, metabolic stress and RAS-ERK1/2 pathway inhibition with Sorafenib. In line with the observed post-translational modifications of PFKFB2 by Western Blot, PFKFB2 phosphorylation is increased in response to glucose starvation and inhibited in cells subjected to glucose deprivation and Sorafenib treatment. Mass spectrometry data also confirms the existence of residue S493 as a new PFKFB2 phosphorylation site, whose regulation can be driven by metabolic stress and RAS-ERK1/2 pathway inhibition. Moreover, we provide evidence of simultaneous phosphorylation of S483 and S493. Additional investigation about the specific role of each phosphorylation site under both, basal and glucose starvation conditions will provide new insights into the regulation mechanisms of PFKFB2.

It has been widely described that PFKFB proteins are activated upon homodimerization[124]. Surprinsingly, mass spectrometry analysis also showed PFKFB3 as a possible interacting protein partner of PFKFB2. Presence of PFKFB3 in PFKFB2 immunocomplex was further confirmed by Western Blot after PFKFB2 pull down, PFKFB3 pull down and consecutive double pull down. This observation, together with the fact that all PFKFB family members share around 70% of identity, strongly suggest the formation of PFKFB2-PFKFB3 heterodimerization capability. However, with these data we cannot conclude direct interaction between both molecules. Heterodimers formation capability would have an enormous impact in cell biology. As previously explained, PFKFB3 is the isoform showing the highest kinase to phosphatase activity ratio within the family, thus increased activation of this isoform would result in increased glycolytic flux. Depletion of either PFKFB2 or PFKFB3 results in the inhibition of the RAS pathway hyperactivation in response to metabolic stress in $NRAS^{Q61}$ mutant cells, highlighting the role of both isoforms in response to glucose starvation. Altogether, these data emphasize PFKFB2 and PFKFB3 as key players, probably forming

heterodimers, of glycolysis regulation in $NRAS^{Q61}$ mutant cells, especially under glucose starvation stress.

To translate the generated knowledge into a possible therapeutic strategy we used 2-deoxy-D-glucose (2DG) as a glucose starvation-mimicking agent. 2DG treatment not only promoted the hyperactivation of the RAS-ERK1/2 pathway, but also sensitizes cells to Sorafenib treatment inducing apoptosis. In line with previous *in vitro* data, Sorafenib treatment in combination with 2DG promotes a significant decrease of tumor growth in $NRAS^{Q61R}$ mutant cells (*q-value<0.001*) but not in $BRAF^{V600E}$ mutant cells (*q-value=ns*). Interestingly, these results have been confirmed in an $NRAS^{Q61R}$ mutated patient-derived xenograft model (PDX) (*q-value<0.01*). Moreover, ERK1/2 phosphorylation in tumors follows the same regulation pattern previously described in response to both, metabolic stress and RAS-ERK1/2 pathway inhibition. The synergistic effect of Sorafenib and metabolic stress observed in $NRAS^{Q61}$ mutant cells provide a new therapeutic opportunity for the targeting of *NRAS* mutant melanomas. It is important to remark that both, 2DG and Sorafenib, have been already tested in clinical trials for the treatment of different tumors. In fact, synergistic effect of 2DG plus Sorafenib has been observed both, *in vitro* and *in vivo*, in papillary thyroid carcinoma and hepatocellular carcinoma. However, 2DG plus Sorafenib efficacy has been attributed to Sorafenib-induced mitochondrial damage and derived-energetic shift toward aerobic glycolysis in these particular type of cells, which results in increased glucose consumption and thereby, sensitivity to glucose metabolism inhibition by 2DG, and not to *RAS* mutant genetic backgrounds[183–187]. Moreover, the observed Sorafenib-induced metabolic reprogramming has been confirmed in patients by an increased [^{18}F] fluorodeoxyglucose consumption[188]. These and other studies have shown that, in both cases (2DG and Sorafenib), tolerability has been acceptable but low efficacy has been achieved by its individual administration[166,173,189–192]. However our investigation posit the combination of 2DG and Sorafenib as a treatment for the specific targeting of *NRAS* mutant melanomas. This become particularly relevant knowing that both drugs are safe and have been authorized for human use.

Additionally, due to the described role of PFKFB2 and PFKFB3 in the regulation of the RAS-ERK1/2 pathway in response to stress, the development of inhibitors targeting these enzymes or their heterodimerization could be also relevant and effective. In the case of PFKFB3, some inhibitors are already available[193]. Due to the observed PFKFB2 activation in response to metabolic stress, as well as PFKFB2 and PFKFB3 dependency in the hyperactivation of the RAS pathway, an alternative approach would be to combine metabolic stress with the inhibition of PFKFB2 and/or PFKFB3.

Overall, in this study we have demonstrated the presence of *NRAS* oncogene-dependent metabolic settings. $NRAS^{Q61}$ mutant cells show a differential response to metabolic stress that results in the hyperactivation of the RAS-ERK1/2 pathway and the sensitization to the multi-kinase inhibitor Sorafenib. PFKFB2, PFKFB3 and PFK-1 are key players in the regulation of this process, which is NRAS-dependent and involves NRAS activation and changes in the signaling and dimerization patterns of RAF proteins. We also provide evidence about the possibility of PFKFB2 regulation by BRAF and ERK2 phosphorylation. Furthermore, we propose for the first time the possible formation of PFKFB2-PFKFB3 heterodimers. Finally, we have suggested a therapeutic approach for the specific targeting of *NRAS* mutant melanoma tumors, based on the combination of 2DG and Sorafenib. Interestingly, most of the described mechanisms are specific for *NRAS* mutant cells, highlighting that *NRAS* and *BRAF* mutant tumors are different entities at different levels, not only at molecular and clinical levels but also at metabolic level.

CONCLUSIONS

1. The RAS-ERK1/2 pathway is hyperactivated in response to metabolic stress in $NRAS^{Q61R}$ mutant cells, generating a *synthetic lethal* condition that sensitizes these cells to Sorafenib.

2. Hyperactivation of the RAS-ERK1/2 pathway is *NRAS* oncogene-dependent and involves a switch from CRAF- to BRAF-dependent signaling.

3. $NRAS^{Q61}$ and $BRAF^{V600E}$ mutant cells present distinct metabolic settings and differentially regulate glycolytic enzymes as well as glucose metabolism-related genes in response to metabolic stress.

4. $NRAS^{Q61}$ mutant cells seem to have a compromised mitochondrial respiration capacity response and a diminished flexibility in metabolizing alternative energy sources in the absence of glucose.

5. PFKFB2 and PFK-1 are activated in response to metabolic stress in $NRAS^{Q61R}$ mutant cells resulting in the hyperactivation of the RAS-ERK1/2 pathway likely promoted by an increase in fructose 1,6-bisphosphate amount.

6. Phosphorylation of PFKFB2 residues related to its activity is regulated in response to metabolic stress and Sorafenib treatment, likely involving BRAF and ERK2 protein kinases.

7. PFKFB2 and PFKFB3 are involved in RAS-ERK1/2 hyperactivation in response to glucose starvation, probably through the formation of heterodimers.

8. 2-Deoxy-D-glucose (2DG) is able to mimic glucose starvation effect *in vitro* and *in vivo*, resulting in an additive effect in tumor growth inhibition in combination with Sorafenib in $NRAS^{Q61}$ mutant tumors, including patient-derived xenografts (PDX), but not in $BRAF^{V600E}$ mutant tumors.

METHODOLOGY

Cell culture and treatments

SKMel103 and *SKMel147* cells were obtained from M. Soengas (CNIO Madrid, Spain). *UACC903* cells were a gift from J. Trent (P. Pollock, Tgen, Phoenix, AZ, USA). *SKMel28*, *A375* and *G361* were purchased from the American Type Culture Collection (ATCC, Manassas, VA, USA). *NHEM* were purchased from PromoCell (Heidelberg, Germany). Patient-derived cell lines, including *Mmln1*, *Mmln9*, *Mmln10*, *Mmln14*, *Mmln16*, *Mmln23*, *Mmln24*, *Mmln30*, *Mmln31*, *Mmgp3*, *Mmsk8*, *Mmsk22* and *Mmsk29,* were derived from patients after tumor surgery (Supplementary Table 5). All samples were obtained upon the informed consent of the patients and the Vall d'Hebron Hospital ethical committee approval. Tumors were disaggregated by mechanical disruption and cultured in Dulbecco's Modified Eagle Media (DMEM) (Biowest, Riverside, MO, USA) supplemented with 20% fetal bovine serum (FBS) (Gibco, Waltham, MA, USA), 2 mM L-Glutamine (Gibco), 100 U/ml penicillin, 100 µg/m streptomycin (Gibco) and 5 µg/ml Plasmocin (InvivoGen, Toulouse, France).

SKMel103, *SKMel147*, *A375* and *G361* cells were grown in Dulbecco's Modified Eagle Media (DMEM). *UACC903* cells were cultured in Roswell Park Memorial Institute (RPMI) media (Biowest). *SKMel28* cells were cultured in Eagle's Minimum Essential Media (EMEM)(ATCC). In all the cases media was supplemented with 10% FBS, 2 mM L-Glutamine, 100 U/ml penicillin, 100 µg/m streptomycin and 5 µg/ml Plasmocin. All cells were maintained at 37°C in a 5% CO_2 incubator.

For glucose starvation experiments cells were cultured in DMEM without glucose (Gibco). Sorafenib was obtained from Santa Cruz Biotecnology (SCBT, Santa Cruz, CA, USA). Trametinib was purchased from Deltaclon (Deltaclon, Madrid, Spain). Vemurafenib, Axitinib, Avastin, Lenvatinib, Sunitinib and CCT196969 were obtained from Selleckchem (Selleckchem, Houston, TX, USA). Sodium Pyruvate was purchased from Biowest. D-Glucose, Dichloroacetate (DCA), Fructose 1,6-bisphosphate (F 1,6-biP) and 2-Deoxy-D-Glucose (2DG) were obtained from Sigma (Sigma, St Louis, MO, USA). 3-Bromopyruvate (3BP) was obtained from Millipore (Millipore, Burlington, MA, USA).

Protein isolation and Immunoblotting

Cells were washed twice with phosphate-buffered saline (PBS) and lysed using a scraper in NP-40 lysis buffer (150 mM NaCl, 50 mM Tris, 1 mM EDTA and 1% (v/v) NP-40) containing protease and phosphatase inhibitor cocktails (Millipore). After an incubation of 20 minutes on ice for a highly efficient cell lysis, samples were centrifuged 30 minutes at 15.000 rpm. Then, supernatant was collected into a new tube and protein concentration was calculated using the Pierce BCA Protein Assay Kit (Thermo Fisher, Waltham MA, USA). Equal amounts of protein (30-50 µg) were denatured by addition of Laemmli sample buffer 1X (62.5 mM Tris-HCl, 25% (v/v) glycerol, 2% (w/v) SDS, 0.01% (w/v) Bromophenol Blue and 5% (v/v) β-mercaptoethanol) and incubated at 95 °C during 5 minutes. Samples were next subjected to 8-12% SDS-PAGE and proteins were transferred to a previously activated PVDF membrane (Millipore) at a voltage of 400 mA during 90 minutes. Membranes were activated with methanol (Sigma) for one minute. Both electrophoresis and transfer were performed using mini-gel Bio-Rad (Bio-Rad, Hercules, CA, USA) equipment. Membranes were blocked with 5 % non-fat dry milk (SCBT) dissolved in 0.1% (v/v) Tween (Sigma) Tris-buffered saline (TBS-T) for one hour at room temperature. The membrane was rinsed three times with TBS-T and incubated with the primary and secondary horseradish peroxidase (HRP)-conjugated antibodies at the optimized concentrations (Table M.1). Primary antibodies against p-ERK1/2 T202/Y204, p-CRAF S259, PFKFB2 and p-PFKFB2 S483 were purchased from Cell Signaling (Cell Signaling, Danvers, MA, USA). ERK2, Lamin A/C, NRAS, BRAF and CRAF were purchased from SCBT. PFKFB3 and GAPDH were obtained from Proteintech (Rosemont, IL, USA). PanRAS was obtained from Millipore. β-Actin was obtained from Sigma. Secondary antibodies were obtained from GE Healthcare (Chicago, IL, USA). Incubation was at 4°C overnight for primary antibodies and one hour at room temperature for secondary antibodies. After incubation protein was detected using ECL (GE Healthcare).

Antibody	Application	Dilution	Commercial Reference	Commercial Source
BRAF	WB/IP	1:500/1ug/ml	sc-5284	SCBT
p-CRAF S259	WB	1:1000	#9421	Cell Signaling
CRAF	WB/IP	1:500/1ug/ml	sc-133	SCBT
p-ERK1/2	WB	1:1000	#9101	Cell Signaling
ERK2	WB	1:1000	sc-154	SCBT
NRAS	WB	1:200	sc-31	SCBT
PanRAS	WB	1:1000	05-516	Millipore
p-PFKFB2 S483	WB	1:1000	#13064	Cell Signaling
PFKFB2	WB	1:1000	#13029	Cell Signaling
PFKFB3	WB	1:1000	13763-1-AP	Proteintech
Lamin A/C	WB	1:500	sc-6215	SCBT
GAPDH	WB	1:10000	60004-1	Proteintech
β-Actin	WB	1:10000	A3854	Sigma
PFK-1	ICC	1:100	sc-67028	SCBT
Actin	ICC	1:100	sc-1615	SCBT
p-ERK 1/2	IHC	1:400	#4370	Cell Signaling
Cyclin D1	IHC	1:50	#2926	Cell Signaling
Rabbit igG HRP-linked	WB/IHC	1:10000	NA934	GE Healthcare
Mouse IgG HRP-linked	WB/IHC	1:10000	NA931	GE Healthcare

Table M.1. Antibodies information. In this table it is showed antibodies dilutions used in this work for the different applications, including Western Blot (WB), Immunohistochemisty (IHC), Immunocytochemistry (ICC) and immunoprecipitation (IP). Commercial references and sources are also indicated.

Nuclear/Cytoplasmic protein purification

SKMel103, *SKMel147*, *SKMel28* and *UACC903* cells were plated in p100 plates (VWR, Radnor, PA, USA) at a 70% confluence, incubated overnight and subjected to treatment with glucose starvation for one and three hours. Nuclear and cytoplasmic protein lysates were obtained using the NE-PER Extraction Kit from Thermo Fisher following manufacturer's indications. The procedure is based on a first membrane disruption and release of cytoplasmic contents using a hypotonic buffer (CERI and CERII). Then, nuclei are recovered from the cytoplasmic extract by centrifugation, and independently lysed using NER buffer. This way, two different protein lysates (nuclear and cytoplasmic) were obtained from each condition. Then, lysates were subjected to quantification and immunoblot as

previously explained.

Apoptosis assays

SKMel103, *SKMel147*, *SKMel28* and *UACC903* cells were plated in p60 plates (Sarstedt, Nümbrecht, Germany) at a 70% confluence and incubated overnight. Then, cells were subjected to treatment with glucose starvation and the different RAS-ERK1/2 pathway and upstream inhibitors including Sorafenib (SF), Vemurafenib (VE), Trametinib (TR), Axitinib (AX) and Avastin (AV) for four hours.

Apoptosis detection is based on the observation that early apoptotic cells translocate the membrane phospholipid phosphatidylserine (PS) from the inner face to the cell surface. Once on the cell surface, PS can be easily detected by annexin V, a protein showing a strong natural affinity for PS. Thus, annexin V-EGFP fusion allows specific staining of apoptotic cells. Further distinction among apoptotic and necrotic cells is possible when combining annexin V with propidium iodide (PI). PI is a DNA-binding molecule that can enter to the cells depending on the membrane permeability. Alive and early apoptotic cells, with intact plasma membrane, cannot be stained with PI. However, ruptured membranes, which characterize late apoptotic and necrotic cells, allow PI to pass and intercalate into nucleic acids.

Cells were detached using trypsin and washed twice with PBS. To measure apoptosis, cells were stained with annexin V–EGFP and PI according to the manufacturer's protocol (Biovision, Milpitas, CA, USA). Apoptosis was then evaluated by flow cytometry using the analyzer FACSCalibur (BD Biosciences, San Jose, CA, USA).

siRNA transfection

SKMel103 and *SKMel147* cells were plated in p100 plates at a 70% confluence and incubated overnight. Transfection was performed during 8 hours with Lipofectamine® RNAiMAX (Thermo Fisher) following manufacturer's recommendations and cells were incubated for 60 hours before performing glucose starvation treatments. For *NRAS* downregulation three different siRNAs against *NRAS* were used (Table M.2). A total amount of 100 nM of siRNA was

transfected into the recipient cells. For *PFKFB2* and *PFKFB3* downregulation, 5 nM of siRNA were transfected to the cells (Table M.2). A scrambled siRNA was used as a control of cell transfection. All siRNAs were purchased from Invitrogen (Thermo Fisher). After the treatments, cells were subjected to protein isolation and western blotting as explained above.

siRNAs	Sense sequence (5' → 3')	C. Reference	C. Source
NRAS	CAAGUGUGAUUUGCCAACAAGGACA	HSS181572	Thermo Fisher
	CAAGAGUUACGGGAUUCCAUUCAU	HSS181573	Thermo Fisher
	AGUCAUUUGCGGAUAUUAACCUCUA	HSS107313	Thermo Fisher
PFKFB2	CCAAGAAACUAACACGCUA	s10356	Thermo Fisher
PFKFB3	GAGGAUCAGUUGCUAUGAA	s10358	Thermo Fisher

Table M.2. siRNAs information. Table includes sense siRNA sequences, commercial references and commercial sources.

Ras activation Assay

SkMel103 and *SKMel147* cells were seeded at a 70% confluence in p100 plates and incubated overnight. After glucose starvation treatment (15 minutes and 30 minutes), it was proceeded to measure RAS activation using the RAS Activation Assay Kit #17-218 (Millipore) following the manufacturer's recommendations.

RAS activation assay is based in RAS-GTP precipitation using agarose beads bound to the CRAF RAS-binding domain (RBD-agarose). To do so, protein lysates from untreated and treated cells were obtained. For cell lysis, culture media was removed and cells were rinsed twice with ice-cold PBS. Then, ice-cold MLB buffer containing proteases and phosphatases inhibitor cocktail (Millipore) was added to cells on ice and cells were detached using a cell scraper. Lysates were then transferred to microcentrifuge tubes on ice and cleared of insoluble cell debris by centrifugation (5 minutes, 14.000xg, 4°C). Immediately after centrifugation, supernatant was recovered and protein was quantified as explained above. 1 mg of total protein lysate was diluted in 500 µl ofbuffer. To each condition, 7.5 µl of the CRAF RBD-agarose reagent were added and reaction mixtures were incubated at 4°C for 45 minutes with gentle agitation. Agarose beads were then pelleted by brief centrifugation (10 seconds, 14000xg, 4°C). After discarding the supernatant, beads were washed three times with MLB buffer and boiled in Laemmli buffer 2X at 95°C

for 5 minutes. Finally, the supernatant and the agarose pellet were mixed and loaded and resolved by electrophoresis, transferred to a PVDF membrane and probed with anti-NRAS and PanRAS antibodies as previously explained.

Immunoprecipitation (IP)

Immunoprecipitations were performed in NP-40 lysis buffer after the addition of Protein A/G agarose PLUS (SCBT). Immunoprecipitated samples were subjected to electrophoresis and proteins were visualized by Western Blot as described above.

SKMel103 cells were seeded in p100 plates at a 70% confluence and incubated overnight. Cells were subjected to glucose starvation for 15 minutes, 30 minutes, 1 hour, 2 hours and 4 hours. Then, protein was isolated and quantified as previously explained. 800 µg of total protein were incubated with 10 µl of agarose beads for one hour at 4°C in order to avoid unspecific binding of the beads. After incubation, samples were centrifuged (300 rpm, 5 minutes) and supernatant was transferred to a clean tube. At that point, BRAF and CRAF antibodies were added to each sample at a concentration of 1 µg/ml and samples were incubated overnight at 4°C. The following day, 20 µl of beads were added to each condition and incubated 1 hour at 4°C. Samples were centrifuged in order to isolate the incubated beads-antibody-protein complexes. Then, supernatant was discarded and centrifuged beads were washed three times with NP-40 lysis buffer. Next, samples were subjected to denaturing conditions, including the addition of Laemmli buffer 2X and the incubation of the samples at 95°C during 5 minutes, and subjected to following applications.

Kinase activity assay

RAF kinases assays were performed with immunoprecipitated BRAF or CRAF as described in Wan et al.[194] The kinase activity of these proteins was determined by measuring their ability to directly phosphorylate kinase dead GST-MEK (^{KD}MEK).

SKMel103 cells were seeded in p100 plates at a 70% confluence. After overnight incubation, cells were subjected to glucose starvation for four hours. BRAF and CRAF proteins were immunoprecipitated as described above. The obtained immunoprecipitates were washed 3 times using 500 µl of wash buffer

(30 mM Tris HCl, 0.2 mM EDTA, 0.3% (v/v) β-mercaptoethanol, 10% (v/v) glycerol, 0.1% (v/v) Triton X-100, 5 mM NaF and 0.2 mM Na_3VO_4) containing decreasing concentrations of KCl (1.0 M, 0.1 M and 0 M). Immunoprecipitates were resuspended in 25 µl A/B Buffer (50 mM Tris [pH 7.5], 100 mM NaCl, 0.1% TX-100, 0.1 mM EDTA, 3% (v/v) β-mercaptoethanol, 50 mM NaF, 1 mM Na_3VO_4 and 36 µM GST-^{KD}MEK (kinase dead MEK)) and reactions were initiated by the addition of 5 µl ATP buffer (500 µM ATP, 75 mM $MgCl_2$ in A/B buffer w/o MEK kinase). Obtained products were resolved by SDS-PAGE and an immunoblot was performed against p-MEK1/2 as previously described. All experiments were performed in triplicates.

RNA isolation, quantification and quality control

SKMel103, *SKMel147*, *SKMel28* and *UACC903* cells were seeded in p60 plates at a 70% confluence and incubated overnight. Cells were subjected to glucose withdrawal for one hour and total RNA was isolated. For RNA purification the Direct-Zol RNA kit (Zymo Research, Irvine, CA, USA) was used. The isolation procedure was performed according to the manufacturer's recommendations. RNA was analyzed using a 2100 Bioanalyzer (Agilent, Santa Clara, CA, USA) to confirm amount and integrity of the sample. Only high quality samples (RNA Integrity Number (RIN) ≥ 9) were used for following applications. Each condition was performed in triplicates in order to obtain statistically significant data.

Microarray

Gene expression was analyzed using a *Clariom S Human Array* (Affymetrix Santa Clara, CA, USA). Raw data generated from the array were processed using the free-source software R studio. Intensity values were converted into gene expression values using Robust Multi-array Average (RMA) through the *BioConductor* package *oligo*, which consists on background correction, logarithmic transformation, quantile normalization and probe normalization.

Identification of differentially expressed genes (DEG) was carried out using the *limma* package. A moderated *t-test* was applied for each comparison based on the empirical *Bayes* method. Then, top tables were generated, with genes sorted from most to least differentially expressed genes according to the log_2FC value.

For functional analysis of the obtained differentially expressed genes *Metascape* was used (metascape.org)[195]. Heatmaps were generated using *Heatmapper* (heatmapper.ca)[196].

Metabolic profiling

Mitochondrial efficiency and metabolic features of *BRAF* and *NRAS* mutant cells were assessed using Seahorse technology: Seahorse XF Cell Mito Stress Kit and Seahorse XF Mito Fuel Flex Kit (Agilent, Santa Clara, CA, USA).

The Agilent XF Mito Stress Kit measures key parameters of mitochondrial function by directly measuring the oxygen consumption rate (OCR) of cultured cells. Different modulators of respiration, including oligomycin, phenylhydrazone (FCCP), rotenone and antimycin A are added to cells (Figure M.1) to modulate the respiratory chain.

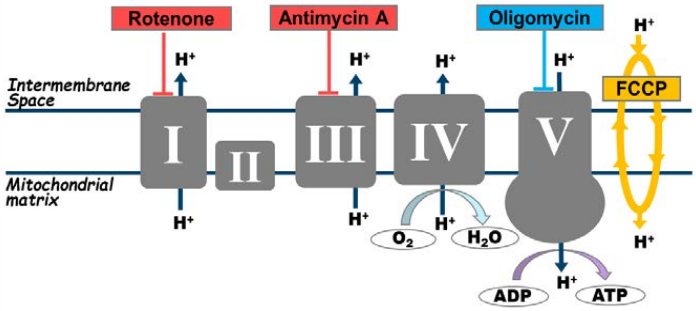

Figure M.1. Agilent Seahorse XF Cell Mito Stress Modulators of the electron transport chain. *Seahorse, Agilent.*

SKMel103, *SKMel147*, *Mmln9*, *Mmln10*, *SKMel28*, *UACC903*, *A375* and *G361* cells were cultured on Seahorse XFe-24 plates (Agilent) at a density of 80.000 cells per well. On the day of metabolic flux analysis, cells were changed to unbuffered DMEM (DMEM base medium supplemented with, 1 mM sodium pyruvate, 2 mM Glutamine, pH 7.4)(Agilent) with or without 10 mM glucose (Sigma), and incubated at 37 °C in a non-CO_2 incubator for 1 h. Four baseline measurements of OCR were taken before and after sequential injection of mitochondrial inhibitors (1 µM oligomycin, 0.5 µM FCCP, 0.5 µM rotenone and 0.5 µM antimycin A). OCR was automatically calculated and recorded by the Seahorse XF-24 software (Figure M.2). After the assay, plates were saved and protein readings were measured for each well to normalize obtained data. The percentage of change

compared with the basal rates was calculated as the value of change divided by the average value of baseline readings.

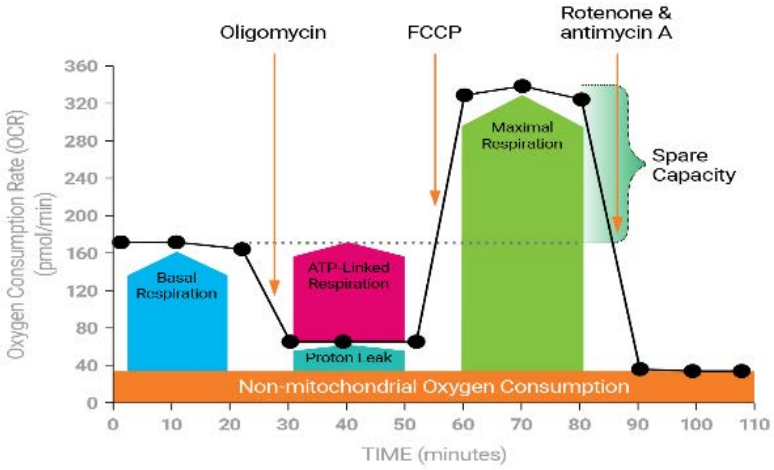

Figure M.2. Seahorse XF Cell Mito Stress Test profile. Parameters related to mitochondrial function are showed. *Seahorse, Agilent.*

For the study of dependency, capacity and flexibility of the different cell lines we used the XF Mito Fuel Flex Kit following manufacturer's recommendations. This assay determines the rate of oxidation of each fuel, including glucose, fatty acids and glutamine, by measuring cells OCR in the presence or absence of the different pathways inhibitors (Figure M.3).

Inhibition of the pathway of interest followed by the two alternative pathways enable the establishment of how cells depend on the pathway of interest to meet energy demand. Dependency indicates that cells are unable to compensate for the blocked pathway by metabolizing other fuels. Inhibiting the two alternative pathways followed by the pathway of interest enables the establishment of cell capacity. Fuel flexibility can be calculated by subtracting fuel dependency from fuel capacity for the pathway of interest. It indicates the cells ability to compensate for the inhibited pathways by using alternative energy sources. High dependency rates combined with absence of flexibility indicate that the mitochondria require that fuel pathway to maintain basal OCR.

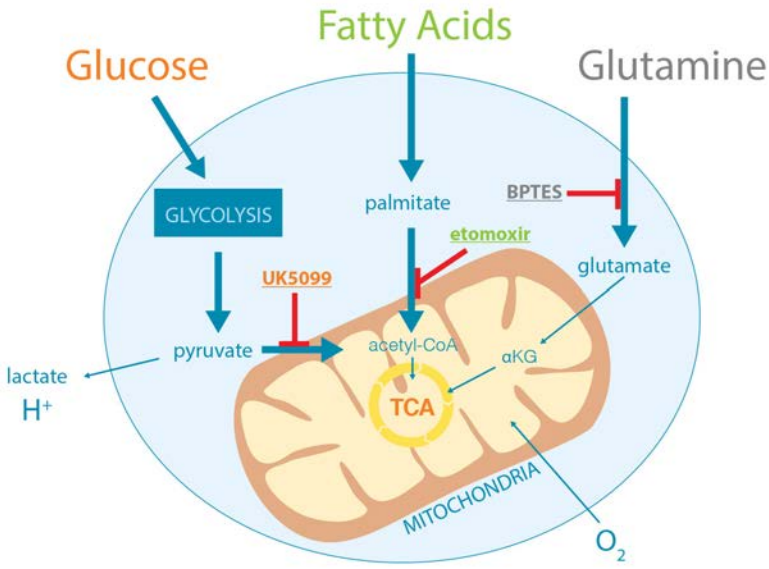

Figure M.3. Agilent Seahorse XF Mito Fuel Flex Test. Alternative sources for mitochondrial respiration and energy production. *Seahorse, Agilent.*

Three different inhibitors were used in order to establish dependency, capacity and flexibility of *NRAS* and *BRAF* mutant cells for glucose, glutamine and long chain fatty acids metabolism; UK5099, which blocks the mitochondrial pyruvate carrier (MPC), thus inhibiting glucose oxidation; BPTES, which inhibits glutamine oxidation by inhibiting glutaminase (GLS1) and etomoxir, an inhibitor of long chain fatty acid oxidation through the inhibition of carnitine palmitoyl-transferase 1A (CPT1A), a critical step for the translocation of fatty acids from the cytosol to the mitochondria for β-oxidation.

For the assay *SKMel103*, *SKMel147*, *Mmln9*, *Mmln10*, *SKMel28*, *UACC903*, *A375* and *G361* cells were cultured on Seahorse XFe-24 well plates at a density of 80.000 cells per well and incubated overnight at 37°C in a 5% CO_2 incubator. On the day of the assay, cells were changed to unbuffered DMEM (DMEM base medium supplemented with, 1 mM sodium pyruvate, 2 mM Glutamine, pH 7.4) with or without 10 mM glucose, and incubated at 37 °C in a non-CO_2 incubator for 1 h. All medium and injection reagents were adjusted to pH 7.4 on the day of assay. Four baseline measurements of OCR were taken before and after sequential injection of inhibitors, including UK5099 (3 μM), BPTES (4 μM) and etomoxir (2 μM). Inhibitors were added following all possible sequence combinations in order to determine the different parameters for the three different assayed fuels:

glucose, glutamine and long chain fatty acids. OCR was automatically calculated and recorded by the Seahorse XF-24 software. After the assay, plates were saved and protein readings were measured for each well to normalize obtained data. Dependency, capacity and flexibility parameters were calculated using the following formulas:

$$Dependency\ \% = \left[\frac{Baseline\ OCR - Target\ inhibitor\ OCR}{Baseline\ OCR - All\ inhibitors\ OCR} \right] * 100$$

$$Capacity\ \% = [\ 1 - \left[\frac{Baseline\ OCR - Other\ two\ inhibitors\ OCR}{Baseline\ OCR - All\ inhibitors\ OCR} \right]] * 100$$

$$Flexibility\ \% = Capacity\ \% - Dependency\ \%$$

Cell viability

Acridine orange (AO) is a vital dye that stains both alive and dead cells. Ethidium bromide (EB) stains only cells that have lost membrane integrity, meaning apoptotic cells. Untreated and treated *SKMel103* cells were detached with trypsin and 500.000 cells were resuspended in 50 µl PBS. Cell suspension was stained with 50 µl of staining solution (5 µg/ml AO and 3 µg/ml EB in PBS) and placed on a microscope slide with a glass coverslip. Live cells appeared uniformly green while apoptotic cells also incorporated ethidium bromide and therefore stained red.

Immunocytochemistry (ICC)

SKMel103, *SKMel147*, *SKMel28* and *UACC903* cells were seeded directly on cover slides in a 24-well plate (Sarstedt) at a 50% confluence and incubated overnight. Once attached cells were subjected to glucose withdrawal for four hours. After treatment, cells were rinsed twice with PBS and fixed with 4% paraformaldehyde (PFA) in PBS for ten minutes at room temperature. Once fixated, cells were washed three times with PBS (5 minutes/each), permeabilized using TBS 0.2% Triton for 5 minutes and blocked with TBS containing 1% BSA (Sigma) and 10% Horse Serum (ATCC) for one hour at room temperature. Following blocking incubation the primary antibody (diluted in TBS 1% BSA) was added to the samples at the optimized concentrations (Table M.1) and incubated overnight at 4°C. After two five minute-washes with TBS 0.025 % (v/v) Triton X-100 (Sigma) (TBS-Triton) samples were incubated with TBS-Triton containing the secondary antibody and 1 mg/ ml Hoescht for one hour at room temperature. To finish, covers were washed

three times with TBS-Triton and mounted with Vectashield fluorescent media (Vector Laboratories, Burlingame, CA, USA). Image acquisition was performed using the Spectral confocal microscope FV1000 (Olympus).

Computational analysis of phosphorylation sites

Analysis of PFKFB2 putative phosphorylation sites was performed using the *GPS 5.0* software[164,165]. This algorithm, known as Group-based Prediction System (GPS) has the ability of predicting potential protein kinases-specific phosphorylation sites from protein sequences by the combination of two different methods: position weight determination (PWD) and scoring matrix optimization (SMO).

The algorithm is based in 617 single predictors for the computational identification of specific phosphorylation sites of 479 human protein kinases. The prediction results in the generation of several parameters including position, protein kinase, flanking peptide, score and cutoff for each predicted phosphorylation site. The score parameter represents the possibility that a specific sequence is a phosphorylation site peptide for a given kinase. If the score of a peptide sequence is high enough, bypassing the cutoff value, we may estimate that it is a potential phosphorylation site of the analyzed kinase. The analysis was performed using the high threshold, which corresponds to a theoretically maximal false positive rate (FPR) of 2% for serine/threonine kinases and 4% for tyrosine kinases.

Lentiviral Transduction for overexpression of PFKFB2 and PFKFB3

The *pLenti-rtTA2-IRES-H2B-GFP* doxycycline-inducible plasmid was obtained from *S. Tenbaum, HG Palmer's Laboratoty* (Vall d´Hebron Institute of Oncology, VHIO). Human *PFKFB2* and *PFKFB3* sequences were subcloned from *pCR4-TOPO-PFKFB2* (MHS6278-202856883) and *pBluescriptR-PFKFB3* (MHS6278-202808447) (Horizon Discovery, Cambridge, UK) to obtain *pLenti-rtTA2-His-PFKFB2-IRES-GFP* and *pLenti-rtTA2-Flag-PFKFB3-IRES-GFP*, respectively. During the cloning process a His-tag was added to the N-terminal end of the PFKFB2 protein and a Flag-tag was added to the N-terminal end of the PFKFB3 protein. Obtained constructs were validated by restriction analysis and sequencing.

To produce lentivirus, three millions *HEK-293-T* cells were seeded in p100 plates in 8 ml of DMEM supplemented with 10% FBS. One hour before transfection, media was replaced by DMEM supplemented with 10% FBS (Complement Inactivated) and Chloroquine (Sigma) at 25 μM final concentration. 50 μg of total DNA (25 μg lentiviral vector, 18.75 μg pPAX2 and 6,25 μg pMD2.G) were added to 150 mM sodium chloride (NaCl) in a final volume of 800 μl. Then, 200 μl of PEI transfection reagent (1mg/ml) (Sigma) were added to the DNA solution and the mix was incubated at room temperature for 15 minutes. The mix was added to the cells drop by drop and incubated overnight at 37°C. Medium was then replaced by DMEM supplemented with 2% FBS (Complement Inactivated) and 5 mM Sodium Butyrate (Sigma). After 24 hours the supernatant containing the produced virus was collected and fresh media was added back to the cells. The collected supernatant was centrifuged five minutes at 1000 rpm and passed through a 0.2 μm filter (Sarstedt). Cells were incubated for another 24 hours and the collection procedure was repeated. For cell infection, the processed supernatant containing 8 μg/ml polybrene (SCBT) was added to the recipient cell lines. Infection efficacy was assessed after doxycycline (Sigma) induction through detection of the GFP signal.

His-tag pull down

SKMel103, *SKMel147*, *SKMel28* and *UACC903* cells were infected with the doxycycline-inducible construct *pLenti-rtTA2-His-PFKFB2-IRES-GFP* as previously explained. Infected cells were plated in p100 plates at a 50% confluence and induced with 1 μg/ml doxycycline (Sigma) for 24 h. Then, cells were subjected to glucose withdrawal and Sorafenib treatment (15 μM) for one hour and it was proceeded to the pull down of the His-tagged PFKFB2 proteins.

For the pull down Dynabeads™ (Invitrogen, Thermo Fisher) were used. This technology is based in optimized cobalt-based immobilized metal affinity chromatography (IMAC). Cells were washed twice with PBS and lysed with 500 μl of Wash/Binding buffer (100 mM sodium-phosphate pH 8.0, 600 mM NaCl, 0.02% (v/v) Twenn-20). 40 μl of Dynabeads were added to each condition and samples were incubated 10 minutes at 4°C. After incubation, samples were cleared using a magnet. Beads were washed four times with Wash/Binding buffer and 50 μl of His

elution buffer (300 mM imidazole, 50 mM sodium-phosphate pH 8.0, 300 mM NaCl, 0.01 % Tween-20) were added to elute the His-tagged proteins from the magnetic beads. Eluted His-tagged proteins were used for following applications, including immunoblot and mass spectrometry.

Flag- tag pull down

SKMel103 cells were infected with the doxycycline-inducible construct *pLenti-rtTA2-Flag-PFKFB3-IRES-GFP* as previously explained. Infected cells were plated in p100 plates at a 50% confluence and induced with 1 µg/ml doxycycline for 24 h. Then, cells were subjected to glucose withdrawal for one hour and it was proceeded to the pull down of the Flag-tagged PFKFB3 proteins.

To pull down Flag-tagged proteins, anti Flag M2 Affinity Gel Kit was used (Invitrogen, Thermo Fisher). Cells were washed twice with PBS, lysed in NP-40 lysis buffer and centrifuged 30 minutes at 15000 rpm. Supernatant was transferred to a new tube and it was proceeded to the pull down assay. 40 µl of resin were used for each condition. Before adding the beads they were washed twice with TBS. Quantified cell lysates were added to the washed resin and incubated two hours at 4°C with constant agitation. Solution was then centrifuged (30 seconds, 8000xg) and supernatant was discarded. After three washes with TBS proteins were eluted by competition with Flag peptide. Flag-peptide stock elution solution was prepared by dissolving the Flag peptide in 0.5 M Tris HCl pH 7.5, 1 M NaCl at a concentration of 5 µg/µl. For elution, 3 µl of 5 µg/µl peptide stock solution were diluted in 100 µl of TBS (150 ng/µl final concentration) and added to the washed resin. Samples were incubated at 4°C during 30 minutes with gentle shaking. Finally, resin was centrifuged for 30 seconds and supernatant containing eluted proteins was transferred to a new tube.

For combined pull down assays cells were infected with both constructs (*pLenti-rtTA2-His-PFKFB2-IRES-GFP and pLenti-rtTA2-Flag-PFKFB3-IRES-GFP)* and His-tag pull down procedure started from the Flag-tagged eluted proteins.

Mass Spectrometry

After infection with *pLenti-rtTA2-His-PFKFB2-IRES-GFP*, *SKMel103* and *UACC903* cells were subjected to one hour of glucose withdrawal and/or Sorafenib

treatment (15 μM) and a His-tag pull down was performed for both, untreated and treated cells following the procedure explained above. Obtained lysates were subjected to proteomic analyses following two different approaches, a first one looking for PFKFB2 protein partners and a second one following phosphorylated peptides enrichment to analyze changes in PFKFB2 phosphorylation in response to glucose starvation and Sorafenib treatment.

Sample preparation and trypsion digestion

His-tagged PFKBF2 was enriched by Ni-IMAC chromatography using His-Trap columns (Sigma). Samples were concentrated and buffer exchanged to 6 M Urea 50 mM ammonium bicarbonate using 0.5 ml 3KDa cut-off Amicon Ultra ultrafiltration devices (Millipore). Total protein content was quantified using RCDC kit (Bio-Rad), and around 5 mg of each sample were taken for tryptic digestion. Samples were first reduced with dithiothreitol (DTT) to a final concentration of 10mM, for 1h at room temperature, and then alkylated with 20 mM of iodoacetamide (IAA) for 30 min at room temperature in the dark. Carbamidomethylation reaction was quenched by addition of N-acetyl-L-cysteine to a final concentration of 35 mM followed by incubation for 15 min at room temperature in the dark. Samples were diluted with 50 mM ammonium bicarbonate to a final concentration of 1 M Urea, and then modified porcine trypsin (Promega) was added in a ratio of 1:10 (w/w), and the mixture was incubated overnight at 37°C. The reaction was stopped with formic acid to a final concentration of 0.5%. The digests were finally purified on reverse phase C18 micro columns (ZipTip, Millipore), and kept at -20°C until further analysis.

Phosphopeptide enrichment using titanium dioxide

Phosphopeptide enrichment was performed according to Thingholm and Larsen[197], with some modifications. TiO_2 beads at 0.50 mg/μl were previously equilibrated in 1M glycolic acid, 80% acetronitrile (ACN) and 1% trifluoroacetic acid (TFA). Peptides were diluted in 60% ACN with 1% TFA and added to 0.5 mg TiO_2. The suspension was incubated during 20 minutes at room temperature, with end-over-end rotation for phosphopeptide binding. The mixture was then centrifuged at 13000 rpm and supernatant containing non-phosphorylated peptides was discarded. TiO_2 beads with phosphopeptides were loaded on

previously prepared home made constructed stage tips (made using high performance C18 extraction disks into pipette tips). After two successive washes with 60% ACN and 1% TFA, bound phosphopeptides were eluted first with 5% NH_4OH and then with 10% NH_4OH with 25% ACN. Eluted phosphopeptides were evaporated, resuspended in 0.1% FA and stored at -20°C until further analysis.

LC-MS analysis

Tryptic digests were analyzed using a linear ion trap Velos-Orbitrap mass spectrometer (Thermo Fisher Scientific). Instrument control was performed using Xcalibur software package, version 2.2.0 (Thermo Fisher Scientific). Peptide mixtures were fractionated by on-line nanoflow liquid chromatography using an EASY-nLC 1000 system (Proxeon Biosystems, Thermo Fisher Scientific) with a two-linear-column system. Digests (aprox. 500 ng) were loaded onto a trapping guard column (Acclaim PepMap 100 nanoviper, 2 cm long, inner diameter 75 µm packed with C18, 3 µm particle size from Thermo Fisher Scientific) at 4 ml/min. Then, samples were eluted from the analytical column (25 cm long, inner diameter 75 µm packed with Reprosil Pur C18-AQ, 3 µm particle size, *Dr. Maisch*). Elution was achieved by using a mobile phase from 0.1% FA (Buffer A) and 100% acetonitrile with 0.1% FA (Buffer B) and applying a linear gradient from 0 to 35% of buffer B for 60 min at a flow rate of 300 nl/min. Ions were generated applying a voltage of 1.9 kV to a stainless steel nano-bore emitter (Proxeon, Thermo Fisher Scientific), connected to the end of the analytical column, on a Proxeon nano-spray flex ion source.

The LTQ Orbitrap Velos mass spectrometer was operated in data-dependent mode. A scan cycle was initiated with a full-scan MS spectrum (from m/z 300 to 1600) acquired in the Orbitrap with a resolution of 30.000. The 20 most abundant ions were selected for collision-induced dissociation fragmentation in the linear ion trap when their intensity exceeded a minimum threshold of 1000 counts, excluding singly charged ions. Accumulation of ions for both MS and MS/MS scans was performed in the linear ion trap, and the automatic gain control (AGC) target values were set to 1×10^6 ions for survey MS and 5000 ions for MS/MS experiments. The maximum ion accumulation time was 500 and 200 ms in the MS and MS/MS modes, respectively. The normalized collision energy was set to

35%, and one microscan was acquired per spectrum. Ions subjected to MS/MS with a relative mass window of 10 ppm were excluded from further sequencing for 20 s. For all precursor masses a window of 20 ppm and isolation width of 2 Da was defined. Orbitrap measurements were performed enabling the lock mass option (m/z 445.120024) for survey scans to improve mass accuracy.

Bioinformatics for peptide and protein identification and quantitation

LC-MS/MS data were analyzed using the Proteome Discoverer software (Thermo Fisher Scientific) to generate mgf files. Processed runs were loaded to ProteinScape software (Bruker Daltonics, Bremen, Germany) and peptides were identified using Mascot (Matrix Science, London UK) to search the SwissProt database, restricting taxonomy to human proteins. MS/MS spectra were searched with a precursor mass tolerance of 10 ppm, fragment tolerance of 0.8 Da, trypsin specificity with a maximum of 2 missed cleavages, cysteine carbamidomethylation set as fixed modification and methionine oxidation, serine, threonine or tyrosine phosphorylation as variable modifications. Significance threshold for the identifications was set to $p<0.05$ for the probability-based Mascot score, minimum ions score of 20, and the identification results were filtered to 1% FDR at peptide level, based on searches against a Decoy database. Relative quantification of the peptides corresponding to PFKFB2 phosphorylation sites was based on the integrated areas of the extracted ion chromatograms for each of the corresponding observed m/z values. The areas for the signals corresponding to both the unphosphorylated and phosphorylated peptides observed were measured for each of the samples.

In vivo

All mice were cared for and maintained in accordance with animal welfare regulations under an approved protocol by the Institutional Animal Care and Use Committee of Vall d'Hebron Research Institute (VHIR). For xenograft animal models, 5×10^5 human *SKMel103*, *SKMel28*, or *Mmln9* cells were subcutaneously implanted in eight-week-old athymic Nude-*Foxn1*^{nu} mice (Envigo, Indianapolis, IN, USA). Tumors were measured with a digital Vernier caliper, and the mice were weighed twice a week. Tumor volume was calculated as *L x w x h*, where "*L"* was the major diameter, "*w"* the minor diameter and "*h*" the third axis of the tumor

mass.

When the tumors reached a volume between 50-100 mm^3, mice with similarly sized tumors were randomized into treatment groups (*n*= 5 per group). Treated groups received glucose starvation treatment by the addition of 1000 mg/kg 2DG to drinking water and an intraperitoneal injection of 10 mg/kg Sorafenib every day. Control groups were treated with vehicle (PBS with 5% (v/v) DMSO).

Representative tumor pictures were taken and tumor samples were obtained for further analysis. The results are presented as tumor volume mean ± SD.

Immunohistochemistry (IHC)

Paraffin-embedded tumor samples were subjected to immunohistochemistry according the manufacturer's antibody protocol. Samples were developed using secondary antibodies linked to horseradish peroxidase (HRP).

At the endpoint of the *in vivo* experiment, tumors were excised and fixed for 24 hours in formaldehyde (Sigma). Then, samples were embedded in paraffin blocks and sections of 4 µm of thickness were obtained using Microm HM355S microtome (Thermo Fisher). Previous staining, samples were deparaffinated and rehydrated. To that end, paraffin sections were incubated at 56°C overnight. The deparaffination step was performed by two incubations in 100% xylol for 10 minutes at room temperature, followed by the ethanol rehydration chain, consisting in 5 minute-washes with 100% (v/v), 96% (v/v) and 70% (v/v) ethanol. Finally, samples were incubated 10 minutes in water. Then, samples were subjected to antigen retrieval using pH6 antigen retrieval solution (Agilent,) at 100 °C. After cool down samples were permeabilized. To do so, slides were washed with TBS 0.2% (v/v) Triton for 5 minutes at room temperature and samples were blocked for 1 hour in TBS containing 1% (w/v) BSA and 10% (v/v) goat serum. Then, slides were incubated overnight at 4°C with the primary antibody diluted in 1% (v/v) BSA, washed twice with TBS 0.025% (v/v) Triton (5 minutes/each) and incubated with HRP-linked secondary antibodies (Table M.1). Slides were developed using the Vector Laboratories 3-3'-diaminobenzidine (DAB) substrate

Kit. Substrate working solution was prepared by adding 2 drops of buffer stock solution, 4 drops of DAB stock solution and 2 drops of hydrogen peroxide solution to 5 ml of distilled water. Samples were incubated from 2 to 10 minutes at room temperature with the substrate working solution and washed in distilled water for 5 minutes. Finally samples were mounted by the addition of mounting media (Vector Laboratories). p-ERK 1/2 T202/Y204 antibody (Cell Signaling #4370) was used to confirm the response to glucose starvation and Sorafenib treatment; and Cyclin D1 (Cell Signaling #2926) was used as an indicator of proliferating cells.

Statistical analysis

ImageJ software was used for the quantification of the Western Blot signal and GraphPad Prism v6.0c was used for the graphic representation and statistical analysis of the data. Comparisons between groups were performed with Student's t test using GraphPad Prism v6.0c. The differences were considered significant if the *p-value* or *q-value* was ≤ 0.05.

SUPPLEMENTARY INFORMATION

ABBREVIATIONS LIST

1,3-biPG: 1,3-bisphosphoglycerate
2DG: 2-deoxy-D-glucose
2PG: 2- phosphoglycerate
3'UTR: 3' untranslated region
3BP: 3-bromopyruvate
3PG: 3-phosphoglycerate
ACC: Acetyl-Coa carboxylase
ACN: Acetonitrile
AGC: Automatic gain control
AJCC: American joint committee on cancer
AKT/PKB: Protein kinase B
ALDO: Aldolase
AMPK: AMP-activated kinase
AO: Acridine orange
ARAF: ARAF serine/threonine kinase
ATP: Adenosine triphosphate
AV: Avastin
AX: Axitinib
BCC: Basal cell carcinoma
BPTES: bis-2-(5-phenylacetamido-1,3,4-thiadiazol-2-yl)ethyl sulfide
BRAF: BRAF serine/threonine kinase
BSA: Bovine serum albumin
Ca/CAMK: Calcium-calmodulin-dependent protein kinase
cAMP: Cyclic adenosine monophosphate
CAR-T: Chimeric antigen receptor T-cells
CCT: CCT196969
Cdc25: RAS-specific nucleotide exchange factor Cdc25
CNV: Copy number variation
CPT1A: Carnitine palmitoyl-transferase 1A
CRAF: CRAF serine/threonine kinase
CTLA-4: Cytotoxic T-lymphocyte associated protein 4
DAB: 3,3'-diaminobenzidine
DCA: Dichloroacetate
DCs: Dendritic cells
DEG: Differentially expressed genes
DGF: Aspartic acid-phenylalanine-Glycine
DHAP: Dehydroxyacetone phosphate
DMEM: Dulbecco's modified Eagle media
DMSO: Dimethyl sulfoxide
DNA: Deoxyribonucleic acid
DTT: Dithiothreitol
EB: Ethidium bromide
EDTA: Ethylenediaminetetraacetic acid
EGFP: Enhanced green fluorescent protein
EMEM: Eagle's Minimum Essential Media
ERK: Extracellular signal-regulated kinase
F 1,6-biP: Fructose 1,6-bisphosphate
F 2,6-biP: Fructose 2,6-bisphosphate
F6P: Fructose 6-phosphate
FAO: Fatty acid oxidation
FAS: Fatty acid synthesis
FBP/FBPase: Fructose 1,6-bisphosphatase
FBS: Fetal bovine serum
FC: Fold change
FCCP: Trifluoromethoxy carbonylcyanide phenylhydrazone
FDA: Food and drug administration
FDG: Fluorodeoxyglucose
FDR: False discovery rate
FGFR: Fibroblast growth factor receptor
FLT3: Fms related receptor tyrosine kinase 3
FoxP3: Forkhead box P3
FPR: False positive rate
G 1,6-biP: Glucose 1,6-bisphosphate
G6P: Glucose 6-phosphate
G6PC: Glucose 6-phosphatase catalytic subunit
G6PD: Glucose 6-phosphate dehydrogenase
GA3P: Glyceraldehyde 3-phosphate
GAP: GTPase-accelerating proteins
GAPDH: Glyceraldehyde -3-phosphate dehydrogenase
GDP: Guanosine diphosphate
GEF: GDP exchange factor
GFP: Green fluorescent protein

GLS1: Glutaminase 1
Gluc.: Glucose
GLUT: Glucose Transporter
GM-CSF: Granulocyte-macrophage colony-stimulating factor
GNA11: G protein subunit alpha 11
GNAQ: G protein subunit alpha Q
GO: Gene ontology
GPI: Glucose phosphate isomerase
GPS: Group-based prediction system
GRB2: Growth factor receptor bound protein 2
GST: glutathione S-transferase
GTP: Guanosine triphosphate
H2B: Histone 2B
HGFR/MET: Hepatocyte growth factor receptor.
HIF1α: Hypoxia inducible factor 1 subunit α
HK: Hexokinase
HMGCL: Hydroxyl-3-methylglutaryl-CoA lyase
HRAS: Harvey Rat Sarcoma Viral Oncogene Homolog
HVR: Hypervariable Region
IAA: Indolacetamide
ICC: Immunocytochemistry
IGF1R: Insulin-like growth factor 1 receptor
IHC: Immunohistochemistry
IL: Interleukin
IMAC: Immobilized metal affinity chromatography
IP: Immunoprecipitation
IRES: Internal ribosome entry site
^{KD}MEK: Kinase dead MEK
KIT: KIT tyrosine kinase
KRAS: Kirsten Rat Sarcoma Viral Oncogene Homolog
LAG-3: Lymphocyte activation gene-3
LDH: Lactate dehydrogenase
LE: Long exposure
LEN: Lenvatinib
LKB1: Liver kinase B1
MAPK: Mitogen-activated protein kinase
MCT: Monocarboxylate transporter
MEK: Mitogen-activated protein kinase kinase
MHC: Major histocompatibility complex
MITF: Melanocyte inducing transcription factor
MPC: Mitochondrial pyruvate carrier
MYC: MYC proto-oncogene
NADPH: Nicotinamide adenine dinucleotide phosphate
NF1: Neurofibromin 1
NHEM: Normal human epidermal melanocytes
NP-40: Nonidet P-40
NRAS: Neuroblastoma RAS viral oncogene homolog
OAA: Oxaloacetate
OCR: Oxygen consumption rate
OIS: Oncogene-induced senescence
ORR: Objective response rate
OXPHOS: Oxidative phosphorylation
PBS: Phosphate-buffered saline
PD-1: Programmed cell death protein 1
PD-L1: Programmed cell death 1 ligand 1
PDGFR: Platelet-derived growth factor receptor
PDH: Pyruvate dehydrogenase
PDK: Pyruvate dehydrogenase kinase
PDP: Pyruvate dehydrogenase phosphatase
PDPK-1: 3-phosphoinositide-dependente kinase 1
PEP: Phosphoenolpyruvate
PET: Positron emission tomography
PFA: Paraformaldehyde
PFK-1: Phosphofructokinase 1
PFKFB/PFK-2: 6-phosphofructo, 2-kinase/fructose, 2,6-bisphosphatase
PFKL: Phosphofructokinase, liver
PFKM: Phosphofructokinase, muscle
PFKP: Phosphofructokinase, platelet
PFS: Progression-free survival
PGAM: Phosphoglycerate mutase
PGC1α: Peroxisome proliferator-activated receptor gamma coactivator 1α
PGK: Phosphoglycerate kinase
PI3K: Phosphatidylinositol 3-kinase

PKA: cAMP-dependent protein kinase catalytic subunit α
PKC: Protein kinase C
PKLR: Pyruvate kinase isozyme L/R
PKM: Pyruvate kinase
PP2A: Protein phosphatase 2A
PPARγ: Peroxisome proliferator activated receptor γ
ppm: Parts per million
PPP: Pentose phosphate pathway
PS: Phosphatidylserine
PTEN: Phosphatase and tensin homolog
PVDF: Polyvinylidene difluoride
PWD: Position weight determination
Pyr.: Pyruvate
RASGRF10: RAS protein specific guanine nucleotide releasing factor 10
RBD: RAS binding domain
RET: Proto-oncogene tyrosine-protein kinase receptor RET
RET: Receptor tyrosine kinase RET
RIN: RNA integrity number
RMA: Robust multi-array average
RNA: Ribonucleic acid
ROS: Reactive oxygen species
Rpm: Revolutions per minute
RPMI: Roswell Park Memorial Institute
RSK: Ribosomal protein S6 kinase
RTK: Receptor Tyrosine Kinase
rtTA2: Tetracycline-controlled transcriptional activator 2
S6K1: P70 ribosomal S6 kinase
SCC: Squamous cell carcinoma
SD: Standard deviation
SDS-PAGE: SDS–polyacrylamide gel electrophoresis
SDS: Sodium dodecyl sulfate
SE: Short exposure
SF: Sorafenib
SH2: Src homology 2 domain
siRNA: small interfering RNA
SMO: Scoring matrix optimization
SOS: Son of sevenless homolog
Src: Tyrosine kinase Src
SU: Sunitinib
SucCoA: Succinyl-CoA
T-VEC: Talimogene laherparepvec
TBS: Tris-buffered saline saline
TCA cycle: Tricarboxylic acid cycle
TCGA: The cancer genome atlas
TCR: T-cell receptors
TFA: Trifluoroacetic acid
TIGAR: TP53-induced glycolysis and apoptosis regulator
TIM-3: T-cell immunoglobulin and mucin-domain containing-3
TP53: Tumor suppressor P53
TPI: Triosephosphate isomerase
TR: Trametinib
TRIM21 E3: E3 ubiquitin-protein ligase TRIM21
UV radiation: Ultraviolet radiation
VE: Vemurafenib
VEGF: Vascular endothelial growth factor
VEGFR: Vascular endothelial growth factor receptor
VHIO: Vall d'Hebron oncology institute
VHIR: Vall d'Hebron research institute
α-KG: α –Ketoglutarate

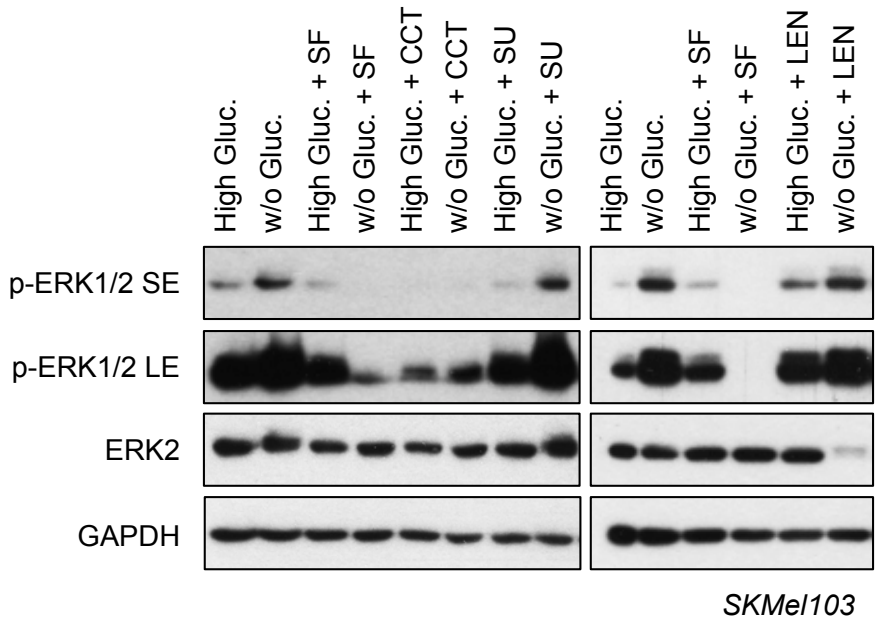

Supplementary Figure 1. RAS-ERK1/2 pathway activation status upon inhibition with Sorafenib (SF), CCT196969 (CCT), Sunitinib (SU) and Lenvatinib (LEN). Western Blot showing ERK1/2 phosphorylation status in response to glucose starvation in combination with SF (15 μM), CCT (10 μM), SU (10 μM) and LEN (20 μM)(4 hours). GAPDH is shown as a loading control. Gluc.=Glucose; SE=Short exposure; LE=Long exposure.

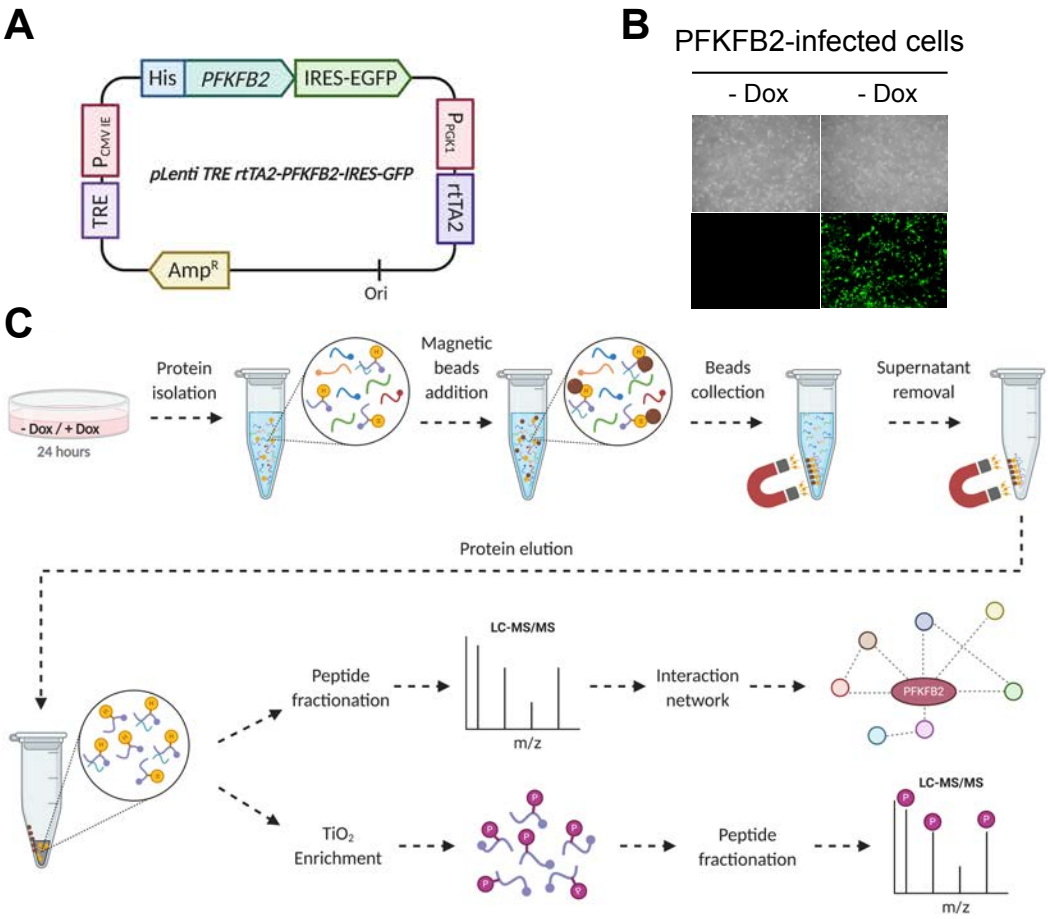

Supplementary Figure 2. His-tagged PFKFB2 obtention and pull down. (A) Lentiviral inducible His-*PFKFB2* IRES-EGFP vector map. (B) Representative pictures of uninduced and induced infected cells. (C) Schematic representation of the procedure followed to pull down His-tagged PFKFB2 for further identification of interacting proteins and phosphorylation status.

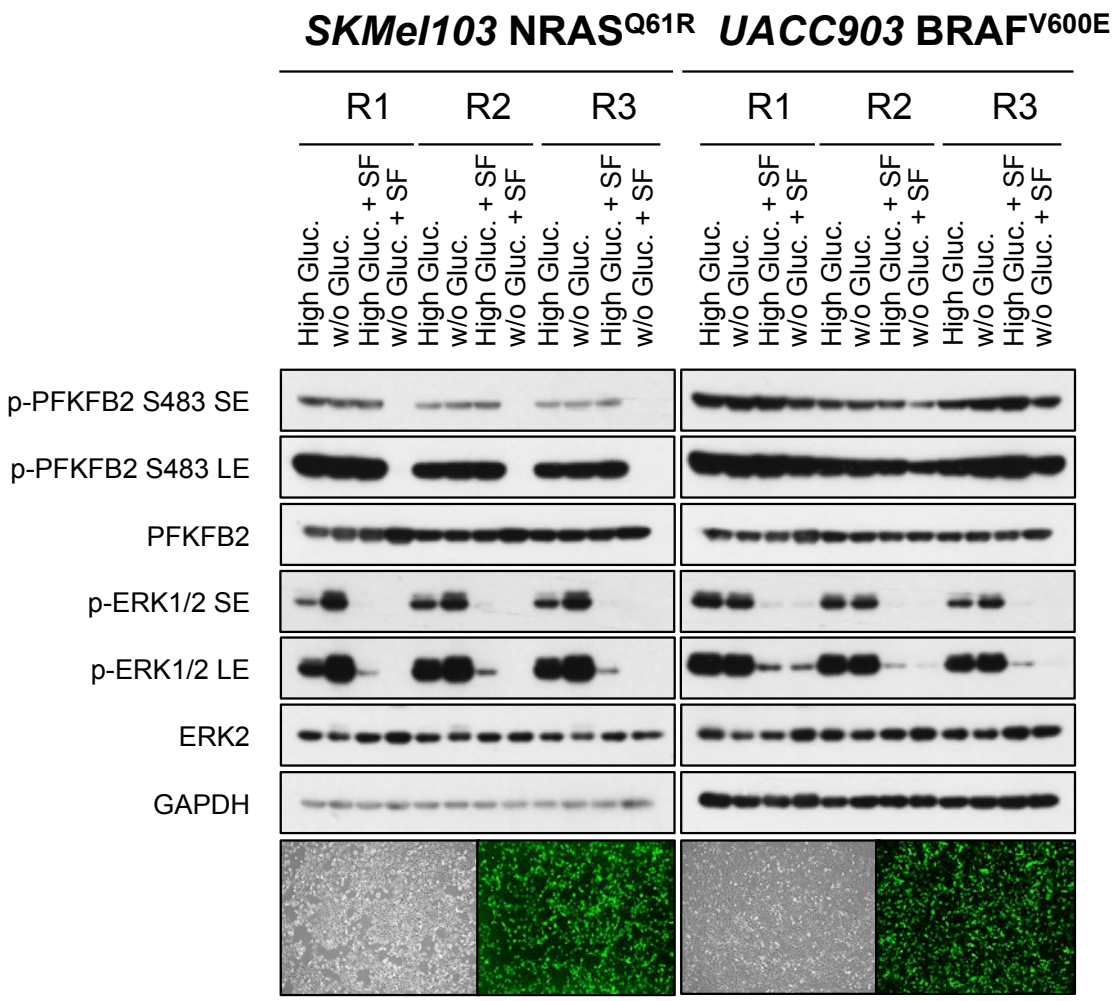

Supplementary Figure 3. His-tagged PFKFB2 infected cells. Western Blot showing regulation of PFKFB2 phosphorylation at residue Ser483 and ERK1/2 phosphorylation in response to metabolic stress and treatment with Sorafenib (15 μM, 1 hour). Three different biological replicates are represented (R1, R2 and R3). GAPDH is shown as a loading control. At the bottom representative pictures of infected induced cells are shown. Gluc.=Glucose, SF=Sorafenib, SE=Short Exposure, LE=Long Exposure.

Symbol	Gene description	log_2FC	p-value	adj.p-value
TGFBI	transforming growth factor beta induced	-7.721	3.2E-16	9.6E-13
SLC14A1	solute carrier family 14 member 1 (Kidd blood group)	-6.476	5.5E-17	2.2E-13
S100A16	S100 calcium binding protein A16	-6.379	2.7E-20	7.4E-16
TMPRSS15	transmembrane serine protease 15	-6.212	3.9E-10	9.2E-08
GLIPR1	GLI pathogenesis related 1	-6.116	5.4E-11	1.9E-08
MT1E	metallothionein 1E	-6.065	5.5E-13	4.5E-10
LY6K	lymphocyte antigen 6 family member K	-5.835	1.1E-11	5.7E-09
HLA-DRA	major histocompatibility complex, class II, DR alpha	-5.795	6.2E-05	1.5E-03
PNP	purine nucleoside phosphorylase	-5.756	5.8E-11	2.0E-08
SERPINB7	serpin family B member 7	-5.558	5.7E-17	2.2E-13
DKK3	dickkopf WNT signaling pathway inhibitor 3	-5.493	1.1E-12	8.3E-10
VEPH1	ventricular zone expressed PH domain containing 1	-5.448	9.3E-11	2.9E-08
PDE1C	phosphodiesterase 1C	-5.380	2.0E-12	1.4E-09
BCAT1	branched chain amino acid transaminase 1	-5.355	2.7E-13	2.4E-10
PRTFDC1	phosphoribosyl transferase domain containing 1	-5.265	1.0E-09	2.1E-07
IL24	interleukin 24	-5.204	3.5E-11	1.3E-08
MMP2	matrix metallopeptidase 2	-5.165	2.2E-16	7.5E-13
GALNT14	polypeptide N-acetylgalactosaminyltransferase 14	-5.158	7.8E-13	6.1E-10
PAX6	paired box 6	-5.028	1.7E-15	3.0E-12
HLA-DRB1	major histocompatibility complex, class II, DR beta 1	-4.992	3.3E-17	2.2E-13
ARNTL2	aryl hydrocarbon receptor nuclear translocator like 2	-4.961	1.8E-14	2.7E-11
S100A2	S100 calcium binding protein A2	-4.955	1.1E-10	3.2E-08
NCAM1	neural cell adhesion molecule 1	-4.953	2.2E-09	4.1E-07
XAGE1A	X antigen family member 1A	-4.913	2.9E-10	7.3E-08
TRHDE	thyrotropin releasing hormone degrading enzyme	-4.859	1.9E-12	1.3E-09
CDKN1A	cyclin dependent kinase inhibitor 1A	-4.853	1.2E-14	2.1E-11
XAGE1B	X antigen family member 1B	-4.852	2.0E-10	5.5E-08
ERRFI1	ERBB receptor feedback inhibitor 1	-4.785	8.1E-04	1.0E-02
RUNX1	RUNX family transcription factor 1	-4.746	5.8E-11	2.0E-08
MECOM	MDS1 and EVI1 complex locus	-4.737	5.9E-12	3.4E-09
ODC1	ornithine decarboxylase 1	-4.729	5.3E-05	1.4E-03
FERMT1	fermitin family member 1	-4.727	1.6E-14	2.6E-11
LAYN	layilin	-4.702	1.1E-13	1.1E-10
SPTLC3	serine palmitoyltransferase long chain base subunit 3	-4.675	1.3E-11	6.0E-09
KRTAP2-3	keratin associated protein 2-3	-4.666	7.3E-08	7.5E-06
KRT80	keratin 80	-4.632	1.2E-11	5.8E-09
NGFR	nerve growth factor receptor	-4.614	1.9E-10	5.2E-08
STEAP3	STEAP3 metalloreductase	-4.605	4.3E-13	3.6E-10
NRP1	neuropilin 1	-4.564	1.3E-09	2.5E-07
PMEPA1	prostate transmembrane protein, androgen induced 1	-4.563	4.7E-11	1.7E-08
ADGRL4	adhesion G protein-coupled receptor L4	-4.549	2.9E-07	2.2E-05
ZEB1	zinc finger E-box binding homeobox 1	-4.529	1.2E-15	2.4E-12
S1PR1	sphingosine-1-phosphate receptor 1	-4.512	4.9E-06	2.2E-04
DDAH1	dimethylarginine dimethylaminohydrolase 1	-4.503	1.1E-05	4.2E-04
GPRC5A	G protein-coupled receptor class C group 5 member A	-4.503	2.2E-10	5.7E-08
TM4SF1	transmembrane 4 L six family member 1	-4.493	8.4E-03	4.6E-02
IL7R	interleukin 7 receptor	-4.474	5.7E-09	9.2E-07
SAMHD1	SAM and HD domain containing dNTP triphosphohydrolase 1	-4.461	5.7E-11	2.0E-08
FADS2	fatty acid desaturase 2	-4.446	1.7E-11	7.2E-09
ITGA3	integrin subunit alpha 3	-4.433	1.7E-08	2.4E-06
TBX3	T-box 3	-4.426	3.2E-10	8.1E-08
LAPTM5	lysosomal protein transmembrane 5	-4.415	8.9E-11	2.8E-08
SERPINE1	serpin family E member 1	-4.356	2.6E-08	3.4E-06
HLA-DPB1	major histocompatibility complex, class II, DP beta 1	-4.318	2.8E-09	5.1E-07
WDR66	WD repeat domain 66	-4.299	2.1E-11	8.4E-09
INHBA	inhibin subunit beta A	-4.292	4.3E-07	3.1E-05
IL31RA	interleukin 31 receptor A	-4.289	2.4E-14	3.1E-11
DKK1	dickkopf WNT signaling pathway inhibitor 1	-4.280	2.4E-07	2.0E-05
IFITM3	interferon induced transmembrane protein 3	-4.208	8.4E-06	3.3E-04
CLMP	CXADR like membrane protein	-4.197	3.1E-09	5.5E-07
DBNDD2	dysbindin domain containing 2	-4.184	5.3E-16	1.4E-12
NID1	nidogen 1	-4.184	8.9E-09	1.4E-06
CLDN4	claudin 4	-4.154	1.1E-11	5.7E-09
IL1B	interleukin 1 beta	-4.123	1.7E-03	1.7E-02
SLFN11	schlafen family member 11	-4.122	1.6E-09	3.0E-07
ANXA1	annexin A1	-4.120	7.9E-03	4.5E-02
BEX1	brain expressed X-linked 1	-4.116	1.5E-11	6.7E-09
RPS24	ribosomal protein S24	-4.086	1.7E-02	6.8E-02
TGFB2	transforming growth factor beta 2	-4.078	1.8E-10	4.9E-08
NRG1	neuregulin 1	-4.074	3.7E-14	4.4E-11
SMURF2	SMAD specific E3 ubiquitin protein ligase 2	-4.053	2.6E-08	3.4E-06
NFASC	neurofascin	-4.039	1.4E-10	4.1E-08
ANXA3	annexin A3	-4.033	1.5E-05	5.3E-04
CDH13	cadherin 13	-4.025	1.2E-09	2.5E-07
TPM1	tropomyosin 1	-4.006	1.2E-09	2.5E-07
E2F4	E2F transcription factor 4	-3.994	1.8E-04	3.5E-03
ADAM12	ADAM metallopeptidase domain 12	-3.993	6.9E-06	2.9E-04
ELL2	elongation factor for RNA polymerase II 2	-3.988	2.2E-07	1.8E-05
PAQR3	progestin and adipoQ receptor family member 3	-3.976	6.1E-06	2.6E-04
FLI1	Fli-1 proto-oncogene, ETS transcription factor	-3.955	2.0E-14	2.9E-11
UCP2	uncoupling protein 2	-3.939	2.2E-13	2.1E-10
PDGFA	platelet derived growth factor subunit A	-3.929	7.3E-06	3.0E-04
AXL	AXL receptor tyrosine kinase	-3.925	1.1E-05	4.1E-04
MDK	midkine	-3.925	5.8E-06	2.5E-04
KCNMA1	potassium calcium-activated channel subfamily M alpha 1	-3.923	1.1E-10	3.5E-08
STC1	stanniocalcin 1	-3.909	1.3E-09	2.7E-07
NEXN	nexilin F-actin binding protein	-3.893	1.0E-15	2.2E-12
THBS1	thrombospondin 1	-3.878	2.6E-03	2.2E-02
AMIGO2	adhesion molecule with Ig like domain 2	-3.877	9.6E-16	2.2E-12
DCBLD2	discoidin, CUB and LCCL domain containing 2	-3.859	3.8E-03	2.8E-02
TMEM154	transmembrane protein 154	-3.858	1.2E-12	8.6E-10
CLU	clusterin	-3.854	4.1E-11	1.5E-08
SNRPB2	small nuclear ribonucleoprotein polypeptide B2	-3.845	9.6E-03	5.0E-02
SMN1	survival of motor neuron 1, telomeric	-3.831	1.8E-03	1.7E-02
ADAMTSL1	ADAMTS like 1	-3.828	3.0E-06	1.5E-04
RABGGTB	Rab geranylgeranyltransferase subunit beta	-3.828	2.3E-03	2.1E-02
IFI16	interferon gamma inducible protein 16	-3.790	5.6E-03	3.6E-02
CALB2	calbindin 2	-3.788	4.6E-07	3.3E-05
CD24	CD24 molecule	-3.766	2.8E-08	3.6E-06
MX2	MX dynamin like GTPase 2	-3.759	3.0E-09	5.4E-07

Supplementary Table 1 (1/4). 400 top differentially expressed genes in $BRAF^{V600E}$ vs. $NRAS^{Q61R}$ mutant cells.

Symbol	Gene description	log_2FC	p-value	adj.p-value
MRPL51	mitochondrial ribosomal protein L51	-3.759	6.7E-03	4.1E-02
TXNL4B	thioredoxin like 4B	-3.738	8.6E-05	2.0E-03
STC2	stanniocalcin 2	-3.735	4.7E-09	7.8E-07
HLA-DMA	major histocompatibility complex, class II, DM alpha	-3.729	9.0E-04	1.1E-02
MLLT11	MLLT11 transcription factor 7 cofactor	-3.727	9.4E-05	2.1E-03
UBE2T	ubiquitin conjugating enzyme E2 T	-3.722	4.5E-03	3.1E-02
ABCA13	ATP binding cassette subfamily A member 13	-3.720	9.9E-09	1.5E-06
KRTAP2-1	keratin associated protein 2-1	-3.713	9.8E-06	3.8E-04
RPS29	ribosomal protein S29	-3.709	9.8E-03	5.0E-02
SKP2	S-phase kinase associated protein 2	-3.709	4.3E-04	6.4E-03
TFB2M	transcription factor B2, mitochondrial	-3.704	2.7E-04	4.6E-03
TPM2	tropomyosin 2	-3.699	3.8E-12	2.4E-09
TMEM123	transmembrane protein 123	-3.693	1.4E-02	6.0E-02
ALCAM	activated leukocyte cell adhesion molecule	-3.692	4.6E-05	1.2E-03
SLC38A1	solute carrier family 38 member 1	-3.686	2.2E-06	1.2E-04
GJA1	gap junction protein alpha 1	-3.678	5.4E-05	1.4E-03
CCL2	C-C motif chemokine ligand 2	-3.672	6.7E-03	4.1E-02
TMEM14B	transmembrane protein 14B	-3.665	1.4E-02	6.2E-02
SDC4	syndecan 4	-3.664	7.8E-05	1.8E-03
CACNA2D4	calcium voltage-gated channel auxiliary subunit alpha2delta 4	-3.661	6.5E-11	2.2E-08
AOX1	aldehyde oxidase 1	-3.661	3.4E-09	6.1E-07
ZNF804A	zinc finger protein 804A	-3.647	3.7E-11	1.4E-08
CLDND1	claudin domain containing 1	-3.643	3.7E-03	2.8E-02
MCL1	MCL1 apoptosis regulator, BCL2 family member	-3.643	1.9E-03	1.8E-02
LIMCH1	LIM and calponin homology domains 1	-3.641	7.1E-09	1.1E-06
AADAT	aminoadipate aminotransferase	-3.636	3.9E-07	2.9E-05
PDZD8	PDZ domain containing 8	-3.628	9.4E-04	1.1E-02
FOSL1	FOS like 1, AP-1 transcription factor subunit	-3.624	3.2E-05	9.3E-04
UQCRQ	ubiquinol-cytochrome c reductase complex III subunit VII	-3.623	1.5E-02	6.4E-02
TSPAN5	tetraspanin 5	-3.615	1.0E-10	3.1E-08
HIGD1A	HIG1 hypoxia inducible domain family member 1A	-3.613	1.5E-02	6.4E-02
CRIM1	cysteine rich transmembrane BMP regulator 1	-3.608	9.5E-10	2.0E-07
SLC38A2	solute carrier family 38 member 2	-3.603	8.8E-04	1.1E-02
KRTAP2-2	keratin associated protein 2-2	-3.601	3.0E-06	1.5E-04
FABP6	fatty acid binding protein 6	-3.594	1.6E-08	2.3E-06
HIST1H4C	histone cluster 1 H4 family member c	-3.588	2.9E-02	8.8E-02
DIS3	DIS3 homolog, exosome endoribonuclease and 3'-5' exoribonuclease	-3.587	2.9E-08	3.7E-06
OCIAD2	OCIA domain containing 2	-3.584	7.0E-13	5.6E-10
PRPF4	pre-mRNA processing factor 4	-3.583	1.4E-03	1.4E-02
SLC43A3	solute carrier family 43 member 3	-3.569	2.4E-02	8.1E-02
CDC123	cell division cycle 123	-3.569	4.0E-03	2.9E-02
NEGR1	neuronal growth regulator 1	-3.565	1.1E-12	8.3E-10
RFPL4A	ret finger protein like 4A	-3.552	3.8E-10	9.0E-08
CAPN2	calpain 2	-3.549	1.7E-02	6.9E-02
SYT1	synaptotagmin 1	-3.546	1.2E-06	7.1E-05
SH3BGRL2	SH3 domain binding glutamate rich protein like 2	-3.535	5.3E-12	3.2E-09
TBL1X	transducin beta like 1 X-linked	-3.535	2.3E-07	1.9E-05
ZNF146	zinc finger protein 146	-3.530	4.8E-03	3.3E-02
TMEM14C	transmembrane protein 14C	-3.529	8.6E-03	4.7E-02
H1F0	H1 histone family member 0	-3.524	1.2E-06	7.1E-05
ITPRIPL1	ITPRIP like 1	-3.524	4.2E-08	4.9E-06
ZNHIT6	zinc finger HIT-type containing 6	-3.524	5.3E-05	1.4E-03
RPL3	ribosomal protein L3	-3.523	2.4E-02	8.1E-02
COL12A1	collagen type XII alpha 1 chain	-3.521	1.5E-10	4.3E-08
PHLDB2	pleckstrin homology like domain family B member 2	-3.516	8.1E-12	4.6E-09
DMKN	dermokine	-3.509	4.1E-04	6.2E-03
GDI2	GDP dissociation inhibitor 2	-3.504	1.9E-02	7.1E-02
BASP1	brain abundant membrane attached signal protein 1	-3.503	3.5E-04	5.6E-03
KNSTRN	kinetochore localized astrin (SPAG5) binding protein	-3.501	1.3E-03	1.4E-02
PTX3	pentraxin 3	-3.496	1.1E-07	1.1E-05
KRT18	keratin 18	-3.492	1.9E-06	1.0E-04
TAF9	TATA-box binding protein associated factor 9	-3.492	5.7E-03	3.7E-02
PRKACB	protein kinase cAMP-activated catalytic subunit beta	-3.482	2.0E-03	1.9E-02
UTP4	UTP4 small subunit processome component	-3.482	4.0E-04	6.1E-03
CYB5R2	cytochrome b5 reductase 2	-3.477	8.4E-10	1.8E-07
MRFAP1	Morf4 family associated protein 1	-3.472	9.1E-04	1.1E-02
NTM	neurotrimin	-3.467	5.9E-08	6.3E-06
ZNF883	zinc finger protein 883	-3.458	4.6E-11	1.7E-08
HLA-DQA1	major histocompatibility complex, class II, DQ alpha 1	-3.456	1.2E-07	1.1E-05
AKAP12	A-kinase anchoring protein 12	-3.436	7.2E-03	4.2E-02
FLRT3	fibronectin leucine rich transmembrane protein 3	-3.431	3.6E-10	8.7E-08
SRP72	signal recognition particle 72	-3.430	1.0E-02	5.1E-02
PAK1IP1	PAK1 interacting protein 1	-3.425	8.4E-04	1.0E-02
NGDN	neuroguidin	-3.423	5.7E-04	7.7E-03
SLIRP	SRA stem-loop interacting RNA binding protein	-3.421	5.6E-03	3.6E-02
EBNA1BP2	EBNA1 binding protein 2	-3.419	1.9E-02	7.2E-02
SDHD	succinate dehydrogenase complex subunit D	-3.417	8.0E-03	4.5E-02
LDHB	lactate dehydrogenase B	-3.408	2.4E-02	8.1E-02
TOMM5	translocase of outer mitochondrial membrane 5	-3.399	6.0E-03	3.8E-02
NREP	neuronal regeneration related protein	-3.399	9.3E-09	1.4E-06
HLA-DPA1	major histocompatibility complex, class II, DP alpha 1	-3.398	2.8E-03	2.4E-02
JUN	Jun proto-oncogene, AP-1 transcription factor subunit	-3.390	4.1E-13	3.6E-10
NUP188	nucleoporin 188	-3.390	4.7E-03	3.3E-02
NIFK	nucleolar protein interacting with the FHA domain of MKI67	-3.389	8.9E-03	4.8E-02
SERPINB2	serpin family B member 2	-3.384	3.9E-08	4.7E-06
CIAO2B	cytosolic iron-sulfur assembly component 2B	-3.362	7.5E-04	9.5E-03
TXN	thioredoxin	-3.362	2.4E-02	8.0E-02
SMAD5	SMAD family member 5	-3.355	1.1E-02	5.2E-02
RPS13	ribosomal protein S13	-3.353	4.7E-02	1.1E-01
HIST1H2BK	histone cluster 1 H2B family member k	-3.351	9.8E-03	5.0E-02
ADORA2B	adenosine A2b receptor	-3.344	6.7E-16	1.7E-12
SUB1	SUB1 homolog, transcriptional regulator	-3.338	3.6E-03	2.8E-02
KIF20A	kinesin family member 20A	-3.337	5.0E-03	3.4E-02
DLGAP5	DLG associated protein 5	-3.333	1.6E-02	6.6E-02
HACD2	3-hydroxyacyl-CoA dehydratase 2	-3.327	4.7E-03	3.3E-02
DPYD	dihydropyrimidine dehydrogenase	-3.326	6.1E-09	9.9E-07
MRPL42	mitochondrial ribosomal protein L42	-3.322	1.3E-03	1.4E-02
SCML1	Scm polycomb group protein like 1	-3.321	1.6E-09	3.0E-07
MT2A	metallothionein 2A	-3.321	1.8E-02	7.0E-02
C12orf75	chromosome 12 open reading frame 75	-3.320	5.1E-04	7.1E-03

Supplementary Table 1 (2/4). 400 top differentially expressed genes in $BRAF^{V600E}$ vs. $NRAS^{Q61R}$ mutant cells.

Symbol	Gene description	log_2FC	p-value	adj.p-value
NR4A3	nuclear receptor subfamily 4 group A member 3	2.560	3.3E-03	2.6E-02
ASRGL1	asparaginase like 1	2.562	4.8E-05	1.3E-03
RNLS	renalase, FAD dependent amine oxidase	2.563	7.6E-05	1.8E-03
RAB11FIP4	RAB11 family interacting protein 4	2.568	1.4E-04	2.8E-03
HERC5	HECT and RLD domain containing E3 ubiquitin protein ligase 5	2.571	1.2E-03	1.3E-02
LPAR1	lysophosphatidic acid receptor 1	2.574	4.9E-06	2.2E-04
FRAS1	Fraser extracellular matrix complex subunit 1	2.581	2.9E-08	3.6E-06
ARPC1B	actin related protein 2/3 complex subunit 1B	2.587	1.7E-11	7.2E-09
CKMT1B	creatine kinase, mitochondrial 1B	2.599	5.0E-07	3.6E-05
TNFRSF19	TNF receptor superfamily member 19	2.601	1.5E-04	3.0E-03
ELOVL2	ELOVL fatty acid elongase 2	2.620	3.1E-04	5.0E-03
CPT1A	carnitine palmitoyltransferase 1A	2.635	5.8E-05	1.5E-03
ATP6V0D2	ATPase H+ transporting V0 subunit d2	2.640	7.5E-03	4.3E-02
CA8	carbonic anhydrase 8	2.641	6.7E-03	4.1E-02
ST8SIA6	ST8 alpha-N-acetyl-neuraminide alpha-2,8-sialyltransferase 6	2.645	1.1E-07	1.0E-05
RGMA	repulsive guidance molecule BMP co-receptor a	2.648	2.2E-02	7.7E-02
NR4A1	nuclear receptor subfamily 4 group A member 1	2.650	2.2E-05	7.1E-04
SLC22A23	solute carrier family 22 member 23	2.659	1.1E-03	1.2E-02
GSTM2	glutathione S-transferase mu 2	2.660	1.9E-05	6.2E-04
CHST11	carbohydrate sulfotransferase 11	2.673	1.4E-04	2.9E-03
LCP2	lymphocyte cytosolic protein 2	2.684	2.9E-04	4.8E-03
EIF1AY	eukaryotic translation initiation factor 1A Y-linked	2.687	6.6E-07	4.5E-05
RPS4Y1	ribosomal protein S4 Y-linked 1	2.690	8.8E-03	4.7E-02
LRRK1	leucine rich repeat kinase 1	2.691	1.0E-06	6.2E-05
COBL	cordon-bleu WH2 repeat protein	2.698	1.8E-08	2.5E-06
TFAP2A	transcription factor AP-2 alpha	2.698	1.3E-13	1.3E-10
FBLN5	fibulin 5	2.710	4.4E-08	5.1E-06
GATA4	GATA binding protein 4	2.712	2.1E-10	5.5E-08
CD200	CD200 molecule	2.717	2.2E-02	7.6E-02
PRKG2	protein kinase cGMP-dependent 2	2.719	2.6E-05	7.8E-04
SPSB1	splA/ryanodine receptor domain and SOCS box containing 1	2.722	9.7E-05	2.2E-03
TRPM1	transient receptor potential cation channel subfamily M member 1	2.728	2.0E-04	3.7E-03
CASP1	caspase 1	2.740	6.9E-03	4.1E-02
IL16	interleukin 16	2.750	2.3E-03	2.1E-02
TMEM198	transmembrane protein 198	2.758	9.4E-04	1.1E-02
ITGB3	integrin subunit beta 3	2.760	1.0E-03	1.2E-02
GPM6B	glycoprotein M6B	2.763	8.1E-05	1.9E-03
PNKD	PNKD metallo-beta-lactamase domain containing	2.767	2.2E-08	2.9E-06
LHX8	LIM homeobox 8	2.768	2.1E-03	2.0E-02
HIST1H3I	histone cluster 1 H3 family member i	2.768	2.5E-07	2.0E-05
LRRC61	leucine rich repeat containing 61	2.776	5.3E-10	1.2E-07
ANKRD30B	ankyrin repeat domain 30B	2.778	1.6E-02	6.6E-02
PPP2R5A	protein phosphatase 2 regulatory subunit B'alpha	2.779	3.7E-07	2.8E-05
TMEM167B	transmembrane protein 167B	2.780	1.3E-06	7.7E-05
SESN3	sestrin 3	2.783	2.3E-03	2.1E-02
KAZN	kazrin, periplakin interacting protein	2.790	1.6E-11	7.1E-09
CYP7B1	cytochrome P450 family 7 subfamily B member 1	2.790	4.7E-04	6.9E-03
FNDC10	fibronectin type III domain containing 10	2.796	6.2E-08	6.5E-06
GPC4	glypican 4	2.797	7.9E-04	9.9E-03
TBC1D16	TBC1 domain family member 16	2.799	9.1E-05	2.1E-03
ACP5	acid phosphatase 5, tartrate resistant	2.814	8.9E-06	3.5E-04
FCRLA	Fc receptor like A	2.818	1.2E-07	1.1E-05
HIST1H3G	histone cluster 1 H3 family member g	2.821	2.5E-04	4.3E-03
LURAP1	leucine rich adaptor protein 1	2.822	1.5E-05	5.4E-04
VAMP8	vesicle associated membrane protein 8	2.825	6.0E-05	1.5E-03
BMT2	base methyltransferase of 25S rRNA 2 homolog	2.830	2.2E-04	3.9E-03
SLC17A9	solute carrier family 17 member 9	2.831	5.4E-05	1.4E-03
CSPG4	chondroitin sulfate proteoglycan 4	2.842	4.2E-06	2.0E-04
VAV3	vav guanine nucleotide exchange factor 3	2.844	4.1E-03	3.0E-02
IL12RB2	interleukin 12 receptor subunit beta 2	2.849	1.1E-04	2.4E-03
HENMT1	HEN methyltransferase 1	2.852	9.6E-04	1.1E-02
CCNA1	cyclin A1	2.855	3.6E-10	8.7E-08
TRIM63	tripartite motif containing 63	2.859	2.2E-03	2.0E-02
MERTK	MER proto-oncogene, tyrosine kinase	2.868	7.0E-03	4.2E-02
SLC2A11	solute carrier family 2 member 11	2.871	2.4E-05	7.5E-04
GLB1L2	galactosidase beta 1 like 2	2.871	4.3E-06	2.0E-04
BCL2A1	BCL2 related protein A1	2.875	5.3E-02	1.2E-01
CKMT1A	creatine kinase, mitochondrial 1A	2.901	3.3E-06	1.6E-04
GNG7	G protein subunit gamma 7	2.907	6.0E-05	1.5E-03
NFATC2	nuclear factor of activated T cells 2	2.922	4.1E-03	3.0E-02
OCA2	OCA2 melanosomal transmembrane protein	2.923	5.1E-04	7.2E-03
ENOSF1	enolase superfamily member 1	2.931	1.9E-05	6.3E-04
MITF	melanocyte inducing transcription factor	2.931	7.6E-03	4.4E-02
GRAMD4	GRAM domain containing 4	2.933	9.4E-03	4.9E-02
BMP7	bone morphogenetic protein 7	2.947	2.7E-07	2.1E-05
COL19A1	collagen type XIX alpha 1 chain	2.950	9.5E-03	5.0E-02
SGCD	sarcoglycan delta	2.970	1.8E-03	1.7E-02
OSR1	odd-skipped related transcription factor 1	2.976	4.0E-02	1.0E-01
MASP1	mannan binding lectin serine peptidase 1	2.979	1.9E-02	7.2E-02
PTPN3	protein tyrosine phosphatase non-receptor type 3	2.984	1.9E-04	3.5E-03
ZNF280B	zinc finger protein 280B	3.010	2.8E-04	4.7E-03
GABARAPL1	GABA type A receptor associated protein like 1	3.011	2.6E-04	4.5E-03
RXRG	retinoid X receptor gamma	3.018	1.6E-04	3.2E-03
H2AFJ	H2A histone family member J	3.021	8.2E-07	5.4E-05
SLCO2B1	solute carrier organic anion transporter family member 2B1	3.035	2.1E-06	1.1E-04
IDH2	isocitrate dehydrogenase (NADP(+)) 2, mitochondrial	3.036	1.2E-11	5.8E-09
ATP10B	ATPase phospholipid transporting 10B (putative)	3.041	5.2E-05	1.4E-03
P3H2	prolyl 3-hydroxylase 2	3.041	1.0E-02	5.1E-02
LXN	latexin	3.044	1.0E-02	5.1E-02
TSTD1	thiosulfate sulfurtransferase like domain containing 1	3.045	1.6E-04	3.1E-03
ITGA9	integrin subunit alpha 9	3.053	1.0E-07	9.8E-06
LAMA4	laminin subunit alpha 4	3.056	9.7E-07	6.1E-05
NDN	necdin, MAGE family member	3.066	2.3E-05	7.2E-04
FN1	fibronectin 1	3.075	1.4E-02	6.1E-02
CYP27A1	cytochrome P450 family 27 subfamily A member 1	3.077	2.4E-02	8.0E-02
TGFBR3	transforming growth factor beta receptor 3	3.088	9.1E-04	1.1E-02
CEACAM5	carcinoembryonic antigen related cell adhesion molecule 5	3.095	4.4E-03	3.1E-02
BIRC7	baculoviral IAP repeat containing 7	3.108	3.0E-10	7.6E-08
CTNNBIP1	catenin beta interacting protein 1	3.120	5.3E-10	1.2E-07
TRIB2	tribbles pseudokinase 2	3.126	1.8E-04	3.5E-03

Supplementary Table 1 (3/4). 400 top differentially expressed genes in $BRAF^{V600E}$ vs. $NRAS^{Q61R}$ mutant cells.

Symbol	Gene description	log_2FC	p-value	adj.p-value
FYN	FYN proto-oncogene, Src family tyrosine kinase	3.133	9.3E-12	5.2E-09
HTR2B	5-hydroxytryptamine receptor 2B	3.135	9.1E-04	1.1E-02
ALDH1A1	aldehyde dehydrogenase 1 family member A1	3.161	4.7E-04	6.8E-03
SPRR2D	small proline rich protein 2D	3.179	1.7E-05	5.8E-04
PSCA	prostate stem cell antigen	3.184	1.3E-04	2.7E-03
DAPK1	death associated protein kinase 1	3.193	1.2E-07	1.1E-05
ABCB5	ATP binding cassette subfamily B member 5	3.197	2.8E-04	4.7E-03
GDF15	growth differentiation factor 15	3.210	2.1E-07	1.7E-05
CST1	cystatin SN	3.212	1.1E-02	5.3E-02
QPRT	quinolinate phosphoribosyltransferase	3.245	5.9E-06	2.6E-04
SYNM	synemin	3.251	3.6E-07	2.7E-05
KREMEN1	kringle containing transmembrane protein 1	3.256	3.2E-12	2.0E-09
MMP17	matrix metallopeptidase 17	3.257	4.4E-06	2.0E-04
A2M	alpha-2-macroglobulin	3.265	1.7E-04	3.3E-03
DIPK1B	divergent protein kinase domain 1B	3.268	3.3E-05	9.6E-04
PYCARD	PYD and CARD domain containing	3.273	4.4E-05	1.2E-03
SIRPA	signal regulatory protein alpha	3.303	4.0E-03	2.9E-02
IGFBP7	insulin like growth factor binding protein 7	3.305	8.3E-05	1.9E-03
BAMBI	BMP and activin membrane bound inhibitor	3.315	9.4E-05	2.1E-03
FRMD4B	FERM domain containing 4B	3.324	4.2E-03	3.0E-02
GPRC5B	G protein-coupled receptor class C group 5 member B	3.327	6.3E-14	7.1E-11
ABCC2	ATP binding cassette subfamily C member 2	3.329	8.6E-04	1.0E-02
PCDH7	protocadherin 7	3.339	4.2E-07	3.1E-05
SLC1A4	solute carrier family 1 member 4	3.354	3.9E-03	2.9E-02
APOE	apolipoprotein E	3.372	8.5E-07	5.5E-05
MIR6809	microRNA 6809	3.374	5.0E-07	3.6E-05
ZNF518B	zinc finger protein 518B	3.376	1.9E-05	6.3E-04
PI15	peptidase inhibitor 15	3.387	2.8E-04	4.7E-03
LAMA1	laminin subunit alpha 1	3.414	1.4E-02	6.2E-02
SLC45A2	solute carrier family 45 member 2	3.434	7.8E-04	9.8E-03
IGSF11	immunoglobulin superfamily member 11	3.435	2.4E-05	7.5E-04
ITIH5	inter-alpha-trypsin inhibitor heavy chain 5	3.439	1.7E-08	2.3E-06
ADAMTS17	ADAM metallopeptidase with thrombospondin type 1 motif 17	3.440	1.7E-13	1.7E-10
MYLIP	myosin regulatory light chain interacting protein	3.445	7.9E-07	5.2E-05
TNFRSF14	TNF receptor superfamily member 14	3.454	9.4E-05	2.1E-03
TBX2	T-box 2	3.462	1.7E-08	2.4E-06
SCML4	Scm polycomb group protein like 4	3.483	4.4E-06	2.0E-04
PDE4B	phosphodiesterase 4B	3.505	1.8E-07	1.5E-05
SCIN	scinderin	3.528	7.1E-03	4.2E-02
PCSK2	proprotein convertase subtilisin/kexin type 2	3.546	1.1E-03	1.2E-02
GOLPH3L	golgi phosphoprotein 3 like	3.565	5.8E-11	2.0E-08
CPN1	carboxypeptidase N subunit 1	3.571	9.0E-04	1.1E-02
DAAM2	dishevelled associated activator of morphogenesis 2	3.598	9.7E-04	1.1E-02
NEO1	neogenin 1	3.618	9.4E-07	6.0E-05
BAIAP2L2	BAI1 associated protein 2 like 2	3.626	9.7E-05	2.2E-03
HAS2	hyaluronan synthase 2	3.634	1.5E-03	1.5E-02
PMP2	peripheral myelin protein 2	3.644	1.1E-03	1.2E-02
PLXNC1	plexin C1	3.676	2.9E-03	2.4E-02
CTSH	cathepsin H	3.679	7.8E-03	4.4E-02
SOX6	SRY-box 6	3.698	2.2E-05	7.1E-04
MMP8	matrix metallopeptidase 8	3.725	1.7E-02	6.8E-02
CTSK	cathepsin K	3.732	2.0E-04	3.7E-03
SDC3	syndecan 3	3.733	5.9E-03	3.7E-02
SLC27A3	solute carrier family 27 member 3	3.747	3.3E-04	5.3E-03
GMPR	guanosine monophosphate reductase	3.758	2.1E-03	1.9E-02
PRDM7	PR/SET domain 7	3.762	7.2E-05	1.7E-03
NRCAM	neuronal cell adhesion molecule	3.797	6.5E-05	1.6E-03
LGALS3	galectin 3	3.799	8.6E-03	4.7E-02
RUNX3	RUNX family transcription factor 3	3.850	5.6E-06	2.5E-04
CARD16	caspase recruitment domain family member 16	3.890	1.9E-05	6.4E-04
C1orf21	chromosome 1 open reading frame 21	3.908	4.1E-08	4.8E-06
IRF4	interferon regulatory factor 4	3.921	6.1E-07	4.2E-05
ENTPD1	ectonucleoside triphosphate diphosphohydrolase 1	3.992	1.2E-03	1.3E-02
RCN3	reticulocalbin 3	4.009	7.2E-06	3.0E-04
DCT	dopachrome tautomerase	4.019	1.6E-02	6.5E-02
SNX10	sorting nexin 10	4.020	2.1E-04	3.9E-03
ST6GALNAC2	ST6 N-acetylgalactosaminide alpha-2,6-sialyltransferase 2	4.022	6.3E-06	2.7E-04
BEST1	bestrophin 1	4.025	7.5E-04	9.5E-03
GYG2	glycogenin 2	4.045	4.6E-03	3.2E-02
C10orf90	chromosome 10 open reading frame 90	4.059	1.3E-03	1.4E-02
TTYH2	tweety family member 2	4.109	1.3E-07	1.2E-05
CELF2	CUGBP Elav-like family member 2	4.118	2.4E-05	7.5E-04
FXYD3	FXYD domain containing ion transport regulator 3	4.155	2.3E-05	7.3E-04
S100B	S100 calcium binding protein B	4.183	1.0E-03	1.2E-02
TMTC1	transmembrane and tetratricopeptide repeat containing 1	4.234	2.2E-05	7.1E-04
GAPDHS	glyceraldehyde-3-phosphate dehydrogenase, spermatogenic	4.266	9.4E-04	1.1E-02
S100A1	S100 calcium binding protein A1	4.297	2.4E-06	1.3E-04
GPR143	G protein-coupled receptor 143	4.409	8.4E-04	1.0E-02
LINC00504	long intergenic non-protein coding RNA 504	4.411	3.3E-03	2.6E-02
SLC16A6	solute carrier family 16 member 6	4.424	1.5E-03	1.5E-02
TYRP1	tyrosinase related protein 1	4.512	2.4E-05	7.5E-04
CAPN3	calpain 3	4.590	1.7E-03	1.7E-02
GJB1	gap junction protein beta 1	4.745	2.9E-04	4.8E-03
SEMA6A	semaphorin 6A	4.900	5.6E-08	6.3E-06
GPNMB	glycoprotein nmb	5.065	1.5E-04	3.1E-03
PLA1A	phospholipase A1 member A	5.078	5.0E-04	7.1E-03
TYR	tyrosinase	5.101	6.5E-06	2.8E-04
ERBB3	erb-b2 receptor tyrosine kinase 3	5.230	6.7E-11	2.2E-08
SLC24A5	solute carrier family 24 member 5	5.237	1.8E-04	3.5E-03
TSPAN7	tetraspanin 7	5.275	2.7E-06	1.4E-04
KCNAB2	potassium voltage-gated channel subfamily A regulatory beta subunit 2	5.288	1.4E-05	4.9E-04
CEACAM1	carcinoembryonic antigen related cell adhesion molecule 1	5.312	3.9E-03	2.9E-02
APOD	apolipoprotein D	5.366	1.8E-04	3.5E-03
CAPG	capping actin protein, gelsolin like	5.573	2.7E-07	2.1E-05
QPCT	glutaminyl-peptide cyclotransferase	5.621	1.1E-03	1.2E-02
SLC7A8	solute carrier family 7 member 8	5.964	1.9E-05	6.4E-04
MLANA	melan-A	6.195	1.6E-03	1.6E-02
MBP	myelin basic protein	6.244	1.0E-07	9.8E-06
PLP1	proteolipid protein 1	6.412	2.4E-19	3.3E-15
PMEL	premelanosome protein	6.797	1.4E-04	2.9E-03

Supplementary Table 1 (4/4). 400 top differentially expressed genes in $BRAF^{V600E}$ vs. $NRAS^{Q61R}$ mutant cells.

A

Upregulated in NRAS^{Q61R} mutant cells						
A2M	CEACAM8	FCHSD2	KCNJ11	NR5A1	RHBDD1	TFCP2L1
ABAT	CEL	FFAR1	KCNQ4	NRG3	RHO	TFEB
ABCC6	CER1	FGF11	KCTD18	NSUN5P2	RILP	TFPI
ACE	CES1P1	FGF2	KCTD8	NUP210	RNASE13	THEG
ACO2	CFAP43	FGR	KIAA1107	NYX	RNASE7	THNSL2
ACP5	CFAP52	FIGLA	KIZ	OARD1	RNASEK	THTPA
ACSS2	CFAP74	FLT3LG	KLF1	OASL	RND3	TM4SF18
ACTG2	CGA	FOLH1B	KLHL10	OGFOD1	RNF19A	TM6SF2
ADAD1	CGB1	FOS	KLHL30	OPN3	RPH3A	TMCO2
ADAMTS17	CGB2	FOXI3	KNDC1	OR10H5	RPP40	TMEM11
ADGRF5	CGB3	FOXQ1	KRT27	OR10W1	RSPO2	TMEM132C
ADIPOR1	CGB5	FRAS1	KRTAP3-1	OR1D2	RTCB	TMEM139
ADM	CGB8	FRRS1L	LAMA1	OR1J4	RTL4	TMEM150A
ADM2	CHCHD2	FRZB	LANCL3	OR1S1	RTN1	TMEM151B
ADORA2A	CHRDL1	FSCB	LAT	OR2AP1	SAA2	TMEM156
ADRB2	CKMT1A	FST	LAYN	OR2F1	SAMD5	TMEM198
AGTRAP	CLDN1	FUT10	LCE1D	OR2L3	SAP25	TMEM234
AGXT2	CLEC4A	GABRA1	LCE1F	OR2T33	SBSN	TMEM38B
AIFM3	CLEC4D	GABRA5	LCN10	OR2V1	SCGB3A2	TMEM74
AIMP2	CLEC4G	GABRB2	LEAP2	OR2Y1	SELENOM	TMEM8B
ALDH1L1	CLIC2	GADD45B	LETMD1	OR4C6	SELP	TNIP3
ALG10B	CLIP2	GALNT16	LGALS3	OR4E2	SERINC2	TNNT1
AMBN	CMBL	GALNT6	LGI3	OR51G2	SERPINA6	TOP3B
AMBP	CMC4	GAREM1	LILRA1	OR52R1	SERPINA9	TPP1
AMN1	CNTNAP3B	GAREM2	LINC00504	OR5B12	SERPINB3	TPSB2
AMY2A	CNTNAP5	GATA6	LINC01235	OR5K2	SERPINC1	TRAIP
ANKRD1	COL16A1	GDF15	LINC01588	OR8B8	SH2D1B	TRAP1
ANKRD6	COL1A1	GDF9	LMF2	OSBPL1A	SH3BGRL3	TSLP
APC2	COL8A1	GFI1B	LNX1	OSTF1	SH3D21	TSSK6
APOC3	CPM	GIMAP2	LOC100505841	OTOF	SHCBP1L	TST
AQP1	CPNE9	GIN1	LOC100652768	OXER1	SHISA5	TTLL2
AQP10	CPVL	GJA4	LOC286238	PBXIP1	SHKBP1	TUBA3E
AQP3	CRACR2B	GJA5	LOC389602	PCDHB11	SHMT2	TUBA4A
ARC	CRAT	GJB3	LOC650293	PCSK2	SIAE	TYW1
ARMCX4	CRYGN	GKN1	LOR	PDE10A	SIGLEC15	UBALD2
ARRDC3	CSRNP3	GLB1	LRATD1	PDE6G	SIGLEC7	UBTFL1
ARSE	CST9	GLCCI1	LRP5L	PDIA2	SIK1	UMODL1
ART1	CT47A10	GLIS1	LRRC6	PEAR1	SIX2	UNC93B1
ART4	CT47A12	GNA15	LRRC71	PEX3	SLC10A6	UPK3BL1
ASAP3	CT47A3	GNG3	LRTM1	PFKFB2	SLC12A5	URAD
ASIC2	CT47A6	GNGT2	LTA4H	PHGR1	SLC13A1	USP17L15
ASXL3	CT47A7	GP6	LTBP1	PI15	SLC17A7	USP17L28
ATF3	CT47A9	GPAA1	LTK	PIGV	SLC1A4	USP28
ATOH7	CTSE	GPR158-AS1	LURAP1	PITX2	SLC20A2	USP51
ATP11AUN	CTSF	GPR174	LUZP2	PKNOX2	SLC25A14	UTS2B
ATP5F1D	CXCL2	GPR42	LYPLA1	PLA2G2D	SLC26A1	VAX2
ATP6V0D2	CXCL5	GPR45	LYZ	PLA2G4E	SLC26A10	VPS28
ATP8A2	CXCL8	GPR89B	MAB21L1	PLA2G5	SLC26A4	VPS9D1
B3GALT2	CYB5R1	GPRASP2	MAB21L3	PLAC4	SLC30A2	VSNL1
BBOF1	CYLC2	GPX6	MAGEB17	PLAGL1	SLC30A3	VSTM4
BBS12	CYP2J2	GRB7	MAGED4B	PLCL2	SLC35D3	VXN
BCKDK	DBX1	GRIA2	MAMDC2	PLEKHN1	SLC35F2	WBP2
BDKRB2	DCAF17	GRM5	MAN2A2	PLP1	SLC38A3	WDR13
BMPER	DCHS2	GRM8	MAPK11	PLPPR2	SLC38A8	WDR48
BOLA1	DECR2	GRN	MAPK3	PMEL	SLC44A2	WDR60
BRINP1	DEFB106B	GSDMA	MAPT	POC1A	SLC6A19	WFDC10B
BRSK1	DEFB109B	HAPLN2	MATN2	POU3F4	SLC6A4	WFDC13
BTNL8	DEFB126	HCG2040054	MBD3L3	PPM1M	SLC7A10	WFDC2
C10orf90	DEFB4B	HCN2	MCTP1	PPP1R1B	SLC7A14	WIPF3
C16orf71	DEPDC4	HCN4	MDH2	PPP4R1	SLC8A3	WNT10B
C16orf86	DEPTOR	HEXA	MDP1	PRAC2	SLCO1B3	XG
C16orf90	DLX3	HEXB	METTL7B	PRB2	SMIM22	XKR9
C16orf92	DMRT2	HHIP	MFGE8	PRDM1	SMIM27	YIPF6
C1orf127	DNAAF4	HINFP	MFNG	PRDM16-DT	SNAP47	YPEL1
C1orf54	DNAL1	HIST3H3	MIR205HG	PROC	SOX15	ZBTB22
C1QL4	DOCK8-AS1	HLA-DQA2	MIR22HG	PROK1	SOX9	ZC3H12D
C21orf62	DRD1	HMOX1	MIR99AHG	PROK2	SPATA12	ZC3H6
C3	DUSP5	HMX2	MMGT1	PROM1	SPDYE5	ZC4H2
C4orf50	DUSP6	HOPX	MORN2	PRR23B	SPEF2	ZFP36
C8orf89	DUX4	HPN	MOSPD1	PRR5	SPINK1	ZFPL1
CA4	ECEL1	HPS1	MROH8	PRSS27	SPINT3	ZNF154
CACNA1A	EFS	HSD3B1	MRPL4	PRSS38	SPIRE1	ZNF280A
CACNG8	ELF5	HYAL3	MTHFD2L	PRSS56	SPNS1	ZNF296
CALML3	ELOVL2	IFIH1	MTM1	PRUNE2	SPRY1	ZNF423
CAMK2A	EMC9	IFIT2	MTRNR2L4	PSG9	SRPK2	ZNF442
CAMK4	EML5	IFITM1	MTRNR2L9	PTCD3	SRPX2	ZNF501
CARD16	EPPIN-WFDC6	IFNA4	MVK	PTCHD3	SRR	ZNF503
CASKIN1	ERGIC1	IFT22	MVP	PTGER4	SRRM5	ZNF541
CASP1	ERLIN2	IGDCC3	MYC	PTH1R	SSTR4	ZNF577
CASQ1	ERVFRD-1	IL15RA	MYCT1	PTN	SSX3	ZNF593
CBFA2T2	ESRP2	IL17A	MYLK3	PTOV1	SSX5	ZNF596
CBS	ETV2	IL17REL	MYOG	PTPN3	ST8SIA5	ZNF705B
CCDC102B	EXD1	IL18RAP	MYOM1	PTPN5	SUN3	ZNF729
CCDC142	F2RL2	IL27RA	N4BP2L1	PTPRE	SUPT20HL2	ZYG11A
CCDC169	FABP4	IL2RA	NALCN	PTPRR	SYNPO2L	
CCDC173	FAM107A	IL6	NAPSA	PTPRT	SYNPR	
CCDC96	FAM151B	IL7R	NBPF7	PYCARD	SYT8	
CCL3	FAM189A2	IL9	NDUFA4L2	RAB15	TAGLN	
CCN2	FAM189B	INHBB	NENF	RABAC1	TAGLN3	
CCR7	FAM215A	INKA1	NFKBIZ	RABGGTA	TAS1R2	
CCR9	FAM25G	INO80B	NINJ1	RAC2	TBC1D10C	
CD248	FAM30A	IRF3	NIPAL2	RAPGEF4	TBX1	
CD300C	FAM53A	ISLR2	NKX2-4	RASSF3	TBX5	
CD79A	FAM83A	ITIH3	NLGN4X	RBMY1J	TCIM	
CDH16	FAM98B	ITLN1	NMBR	RBP1	TCN1	
CDH7	FBXO16	KBTBD11	NME9	RCE1	TCTE1	
CDIPT	FBXO41	KCNA5	NOS1AP	REG1B	TECTB	
CDS1	FBXW4	KCNA6	NPW	REXO1L2P	TENT5D	
CEACAM1	FCGR1A	KCNE2	NPY1R	RFESD	TESK2	
CEACAM3	FCGR2A	KCNH7	NR0B2	RGS2	TESPA1	

B

Upregulated in NRAS^{Q61R} and BRAF^{V600E} mutant cells	
AGRP	MDFI
ALDH5A1	MGAM
ALKBH6	MRGPRX4
ANKFN1	MS4A15
APOC1	MT1HL1
ARHGAP6	MUC6
ATP5MF-PTCD1	MXRA8
ATP6V0E2	NCR3
BAG6	NDRG2
BAIAP2	NIM1K
BCKDHA	NR4A3
BCL6	NRM
C1QL1	OIT3
C1orf56	OPRD1
C9orf116	OSCP1
CACNG7	PAEP
CADM3	PARM1
CALHM3	PDE9A
CAPN5	PEBP4
CASTOR1	PEX16
CBLC	PHOX2B
CCDC140	PIGU
CCDC17	PIWIL2
CCDC180	PLAAT1
CCL23	PNMA2
CD207	PNPLA6
CD300E	POLR2E
CD84	POR
CDH18	PORCN
CDH20	PPDPF
CEACAM5	PPP1R15A
CHAC1	PRSS50
CLDN17	PSG1
CLEC2D	PXMP4
CLN6	REC114
CLPTM1	RELA
CLTRN	S100A4
CNNM3	SCD5
COMTD1	SDCBP2
COX7A1	SEC14L5
CPA4	SEMA4G
CT47A5	SERPINB9
CXCL3	SIM1
DDIT3	SLC10A2
DEFB119	SLC25A1
DET1	SLC36A1
DEXI	SLC4A11
DHRS12	SLCO2A1
DIRAS1	SMPD3
DMRTC1	SNCAIP
DNAL4	SNTG2
DPYSL5	SPACA9
DRD5	SPANXC
DUSP1	SPHKAP
EFCAB11	SPRN
EGR1	STIM2
EHF	SULT6B1
EMD	TBC1D21
EPB41L4B	TBCE
EPHB2	TCF7
FAM180A	TCP10L
FAM219A	TCTN2
FFAR3	TEX29
FOLR1	TEX36
FOXD4L5	TEX38
FXYD1	TLR7
GADD45A	TMC2
GATA1	TMEM102
GCFC2	TMEM170B
GLMP	TMEM174
GLYATL2	TMEM179B
GPR12	TMEM247
GPR162	TMUB1
GPR89A	TNFSF9
HHLA3	TOM1L1
HINT2	TP53INP2
HMGN5	TRIM64B
HSPA12B	TRIM7
HTRA1	TRY2P
IFNL4	TTYH2
IGFBP1	VPS52
ITIH4	WDR72
KBTBD8	WNT3
KCNG4	XPO4
KCNK2	
KIAA1211L	
KL	
KRT38	
KRTAP3-2	
LAMA4	
LAMB4	
LCN2	
LOC388780	
LRRC20	
LRRC72	
LRRC8E	
LTB	
LY6G6D	
LYVE1	
MBD3L2	

Supplementary Table 2 (1/9). Upregulated genes in response to metabolic stress ($Log_2FC>0.265$) (A) NRAS^{Q61R} mutant cells. (B) NRAS^{Q61R} and BRAF^{V600E} mutant cells.

Upregulated in BRAF^{V600E} mutant cells											
AGO2	AKR7A3	ARL5C	BLOC1S2	CACHD1	CDC25A	CLINT1	CXCL16	DLG2	EIF3F	FAM170B	FRK
AGO3	AKT1S1	ARL6IP1	BLOC1S3	CACNA1B	CDC25C	CLIP3	CXCL6	DLGAP2	EIF3G	FAM177B	FRMD4B
AADACL2	AKTIP	ARMC12	BMERB1	CACNA1I	CDC42EP2	CLK1	CXCL9	DLGAP4	EIF4E1B	FAM180B	FRMD6
AADACL4	ALAS1	ARMC3	BMP6	CACNB1	CDC42SE1	CLN8	CXCR5	DLK2	EIF4E3	FAM181A	FRMPD1
AADAT	ALDH18A1	ARMC4	BOD1	CACNG1	CDCA2	CLNK	CYB561	DLL4	EIF5AL1	FAM181B	FRMPD3-AS1
AAGAB	ALDH9A1	ARMC9	BOK	CACNG3	CDCP1	CLRN2	CYBRD1	DLST	EIF6	FAM182B	FRYL
AAK1	ALLC	ARMH3	BORCS7	CACTIN-AS1	CDH12	CLTC	CYLD	DLX4	ELAVL2	FAM184A	FTCD
AAMDC	ALOX15B	ARPIN-AP3S2	BORCS8	CACYBP	CDH22	CMC1	CYP19A1	DLX5	ELAVL4	FAM204A	FTH1P18
AARS	ALOXE3	ARVCF	BPIFA2	CADPS2	CDH23	CMSS1	CYP1A1	DMD	ELK3	FAM20C	FUBP3
AATF	ALPL	ARX	BPIFB1	CALB1	CDH3	CMTM5	CYP21A1P	DMGDH	ELL3	FAM210A	FUCA2
ABCA10	ALPP	AS3MT	BPY2B	CALB2	CDH4	CNDP1	CYP21A2	DMWD	ELMOD2	FAM210B	FUT11
ABCA13	ALX3	ASAH1	BRAF	CALHM4	CDIP1	CNGA4	CYP24A1	DNAAF5	ELMSAN1	FAM217B	FUT9
ABCA2	AMBRA1	ASAP2	BRAP	CALN1	CDK11B	CNGB3	CYP2A7	DNAJA4	ELOA	FAM221B	FXN
ABCC12	AMIGO1	ASB14	BRD2	CAMK2D	CDK15	CNIH1	CYP2C19	DNAJB11	ELOB	FAM222A	FXYD7
ABCF1	AMIGO3	ASB16	BRF2	CAMSAP3	CDKL5	CNIH3	CYP2S1	DNAJB2	ELOVL3	FAM227B	FYB1
ABCG1	AMZ1	ASB2	BRICD5	CAND1	CDKN2D	CNOT10	CYP2U1	DNAJB3	ELP5	FAM228B	FZD3
ABCG4	ANAPC10	ASB8	BRK1	CAND1.11	CDO1	CNOT3	CYP46A1	DNAJB6	ELSPBP1	FAM234B	FZD9
ABHD1	ANAPC11	ASPHD1	BRPF3	CAPN1	CDON	CNOT9	CYP4A22	DNAJB9	EMC1	FAM241B	GABPA
ABHD13	ANAPC16	ASS1	BSND	CAPN6	CDRT15	CNPPD1	CYP4B1	DNAJC18	EMC2	FAM25A	GABRA6
ABHD16A	ANAPC4	ASTE1	BST1	CAPSL	CDRT15L2	CNPY4	CYP4F11	DNAJC19	EMC8	FAM27E5	GABRD
ABHD17B	ANGPT2	ATAD5	BTBD10	CAPZA2	CDSN	CNR1	CYP4F12	DNAJC22	EMCN	FAM3B	GABRE
ABHD2	ANGPTL3	ATF4	BTBD3	CARD10	CDX2	CNTN4	CYP4F22	DNAJC5	EME1	FAM3D	GABRG2
ABHD3	ANGPTL4	ATF5	BTF3L4	CARD14	CEACAM6	CNTROB	CYP4V2	DNAJC6	EML2	FAM47C	GABRG3
ABHD6	ANGPTL6	ATF7IP	BTG4	CARD18	CEBPZ	COBLL1	CYP51A1	DNASE1	EMP3	FAM49A	GABRR2
ABI1	ANGPTL7	ATG14	BTNL10	CARHSP1	CEBPZOS	COCH	DAAM1	DNASE2B	EN2	FAM50B	GABRR3
ABI3	ANK1	ATG7	BUB1B-PAK6	CARMIL2	CECR2	COG1	DAB2IP	DNER	ENC1	FAM57A	GAD2
ABR	ANK2	ATOH8	BUD13	CARNMT1	CELA3B	COG2	DACH2	DNLZ	ENDOG	FAM57B	GADD45GIP1
ABRACL	ANKHD1	ATP10A	C10orf142	CARS	CELF3	COG5	DAOA	DNM2	ENG	FAM71B	GAGE10
ABRAXAS1	ANKRA2	ATP13A5-AS1	C11orf65	CASC1	CELSR1	COG6	DARS	DNM3	ENPP1	FAM71E2	GALC
ACACA	ANKRD10	ATP1A4	C11orf86	CASD1	CELSR2	COL11A2	DAZL	DNMT1	ENPP3	FAM78A	GALNTL5
ACAD10	ANKRD13D	ATP1B3	C11orf87	CASP10	CELSR3	COL19A1	DBF4	DNMT3L	ENTPD4	FAM86B1	GAMT
ACADVL	ANKRD23	ATP2B2	C11orf94	CASP8	CENPF	COL27A1	DBNDD1	DNPEP	ENTPD7	FAM89A	GAN
ACBD5	ANKRD34B	ATP2C1	C11orf97	CASS4	CENPJ	COL4A5	DBNDD2	DOCK10	EOMES	FAM92B	GAPVD1
ACBD6	ANKRD36C	ATP2C2	C12orf29	CATIP	CENPP	COL6A6	DCAF10	DOCK3	EP400P1	FANCC	GASK1A
ACCS	ANKRD40	ATP4A	C12orf50	CATSPER1	CENPW	COL9A3	DCAF12	DOCK5	EPAS1	FANK1	GATA2
ACCSL	ANKRD40CL	ATP5F1C	C12orf54	CATSPER3	CEP112	COLGALT1	DCAF12L1	DOP1B	EPB41L1	FARSA	GATD1
ACKR1	ANKRD42	ATP5F1EP2	C12orf65	CATSPERB	CEP120	COMMD1	DCAF4	DPCD	EPB41L2	FATE1	GATD3A
ACOX2	ANKRD44	ATP5MPL	C12orf75	CATSPERE	CEP128	COMMD8	DCAF5	DPH7	EPGN	FBL	GATM
ACSBG1	ANKRD46	ATP5PB	C14orf132	CATSPERZ	CEP152	COPG1	DCAF8L1	DPP9-AS1	EPHA1	FBP1	GBP1
ACSM3	ANKRD52	ATP6AP1L	C15orf54	CBL	CEP170	COPZ1	DCC	DPY19L4	EPHA3	FBXL14	GC
ACTBL2	ANKRD63	ATP6AP2	C16orf46	CBLB	CEP63	COX11	DCD	DPYD	EPHA7	FBXL3	GCA
ACTL6A	ANKS1B	ATP6V0B	C16orf89	CBLIF	CEP72	COX4I1	DCDC2	DRAM1	EPHB1	FBXO31	GCAT
ACTL7B	ANKS3	ATP6V1B1	C17orf107	CBR1	CEP85L	COX7B2	DCHS1	DRC3	EPHX2	FBXO32	GCDH
ACTN2	ANKZF1	ATP6V1C2	C17orf75	CBWD6	CERCAM	CPA3	DCLK1	DRG2	EPHX3	FBXO36	GCGR
ACTR10	ANO1	ATP6V1F	C17orf80	CBX8	CERS6	CPAMD8	DCLK2	DSCAM	EPN1	FBXO42	GCNA
ACTR3B	ANO3	ATP7A	C17orf98	CCDC105	CETN1	CPB1	DCLRE1B	DSCR4	EPRS	FBXO5	GCNT7
ACTR6	ANO4	ATP9B	C19orf47	CCDC107	CETN2	CPB2	DCLRE1C	DSEL	EPS15L1	FBXW12	GCOM1
ACVR1	ANO9	ATPAF1	C1D	CCDC112	CFAP126	CPNE2	DCP1A	DSTN	EPS8L1	FCAR	GCSH
ACVR2B	ANP32D	ATRIP	C1orf105	CCDC12	CFAP157	CPO	DCTN1	DTD2	EPS8L2	FCF1	GDA
ADAD2	ANTXR1	ATXN1	C1orf162	CCDC122	CFAP44	CPSF3	DCTN2	DTNB	ERAL1	FCGRT	GDI1
ADAL	ANTXR2	ATXN2	C1orf167	CCDC183	CFAP46	CPSF4	DCUN1D2	DTWD2	ERAP2	FCN2	GDNF-AS1
ADAM11	ANXA2R	ATXN7	C1orf198	CCDC185	CFAP77	CPSF4L	DCXR	DTX3L	ERBIN	FCRL2	GFER
ADAM12	ANXA8	ATXN7L1	C1orf216	CCDC187	CFAP97	CPT2	DDAH1	DTX4	ERCC1	FDFT1	GFOD1
ADAM15	AP1G1	AURKAIP1	C1orf220	CCDC188	CFDP1	CPXM1	DDAH2	DUS2	ERCC4	FEM1A	GGA1
ADAM7	AP1M1	AVPI1	C1orf43	CCDC197	CHAC2	CRACR2A	DDHD2	DUS3L	ERFE	FEM1B	GGACT
ADAMTS14	AP1M2	AWAT1	C1orf50	CCDC30	CHD5	CRAMP1	DDI1	DUSP18	ERH	FER1L6	GGH
ADAMTS2	AP2A2	B3GALT4	C1orf61	CCDC33	CHD9	CREG1	DDIT4	DUSP22	ERI1	FER1L6-AS1	GGT7
ADAMTS5	AP2M1	B3GALT6	C1orf94	CCDC47	CHEK1	CREG2	DDRGK1	DUXAP10	ERMARD	FERMT2	GHR
ADAMTS7	AP3D1	B3GNT5	C1QL2	CCDC50	CHFR	CRHR1	DDX12P	DXO	ERVV-1	FFAR2	GHRHR
ADAMTSL1	AP3M2	B3GNT6	C1QTNF5	CCDC51	CHGB	CRK	DDX18	DYNC1H1	ESM1	FGB	GIMAP8
ADAMTSL4	AP4B1	B3GNT7	C1QTNF7	CCDC59	CHID1	CRLF1	DDX19A	DYNC1I1	ESR1	FGF17	GIPC2
ADAT2	AP4E1	B3GNTL1	C2	CCDC60	CHM	CRP	DDX19B	DYRK1B	ESR2	FGF7	GIPR
ADCY10	APAF1	B4GALT7	C20orf173	CCDC63	CHMP2B	CRTC1	DDX28	DYRK2	ESRP1	FGFR4	GJB6
ADCY7	APBB2	B4GAT1	C20orf78	CCDC65	CHMP3	CRYBB1	DDX41	DZANK1	ETAA1	FGFRL1	GKAP1
ADD1	APCDD1	B9D2	C20orf85	CCDC74B	CHMP7	CRYBG1	DDX43	E2F1	ETNPPL	FGL1	GLA
ADGRD1	APCS	BACH1	C22orf39	CCDC77	CHODL	CRYBG3	DDX51	E2F4	ETV5	FHDC1	GLB1L3
ADGRE2	APH1B	BAG1	C2CD3	CCDC8	CHPF	CRYM	DDX60	E2F5	ETV6	FHL1	GLDC
ADGRE3	APOA1	BAHCC1	C2CD4D	CCDC80	CHRM1	CSF2RA	DEAF1	E2F6	EVA1C	FIBCD1	GLS
ADGRF1	APOA2	BAHD1	C2orf50	CCDC81	CHRNA10	CSPG4P1Y	DEF8	E2F7	EVC	FILIP1L	GLT8D2
ADH7	APOBEC2	BAK1	C2orf66	CCDC88A	CHRNA5	CST1	DEFB104A	EAF2	EVI2A	FITM2	GLTPD2
ADHFE1	APOBEC3F	BANF2	C2orf69	CCKAR	CHRNB3	CST7	DEFB108B	EAPP	EVI5L	FJX1	GMEB2
ADORA1	APOC2	BAP1	C2orf74	CCL26	CHRNB4	CSTA	DEFB123	EARS2	EXO5	FKBP11	GMIP
ADPRM	APOF	BATF	C2orf83	CCL3L3	CHRNG	CSTF1	DEFB131B	EBF4	EXOC3L4	FKBP14	GNAL
ADRA2B	APOL2	BATF2	C3orf35	CCL4L2	CHSY3	CT45A10	DEFB132	EBI3	EXOC5	FKBP15	GNAQ
ADRB3	APOL3	BAZ2B	C3orf36	CCL5	CHTF18	CT45A2	DENND2A	EBPL	EXOSC7	FKBP3	GNAT3
AFAP1L1	APOL4	BBC3	C3orf49	CCL8	CIAPIN1	CT45A3	DENND2C	ECE1	EXOSC9	FKBP4	GNAZ
AFF1	APPBP2	BBS4	C3orf56	CCN1	CIB2	CT45A5	DENND5A	ECH1	EXPH5	FKBP5	GNB5
AFF3	APPL1	BCAR1	C4orf17	CCND3	CIB3	CT45A6	DENND6B	ECHDC2	EXT2	FLG2	GNL2
AFP	APPL2	BCAS4	C4orf19	CCNF	CIC	CT45A7	DEPDC1B	ECM1	EYA1	FLI1	GNPAT
AGBL3	AQP12A	BCAT1	C4orf33	CCNI	CIP2A	CT45A8	DERL3	EDIL3	F13B	FLJ45513	GNRH1
AGL	AQP12B	BCHE	C5orf30	CCNT1	CIRBP	CT45A9	DGAT1	EDN2	FA2H	FMO4	GOLGA1
AGR2	AQP4	BCL10	C5orf49	CCP110	CIT	CT47B1	DGCR6	EEF1B2	FAAP100	FMO5	GOLGA2P5
AGR3	AREL1	BCL2L10	C5orf52	CCR2	CITED2	CTBP1	DGKK	EEF1E1-BLOC1S5	FAAP24	FMO6P	GOLGA3
AGT	ARGLU1	BCL2L15	C6	CCR5	CKB	CTBP1-DT	DGKZ	EEF2KMT	FAH	FMOD	GOLGA4
AGTR1	ARHGAP24	BCO1	C6orf89	CCT4	CKS1B	CTDSP2	DHRS1	EEFSEC	FAM104A	FN1	GOLGA6A
AHSP	ARHGAP26	BCR	C7orf25	CCT8	CLDN11	CTLA4	DHRS4L1	EFCAB12	FAM110D	FN3K	GOLGA8DP
AJAP1	ARHGAP27	BDH2	C7orf26	CCT8L2	CLDN20	CTNNBL1	DHRS7B	EFCAB7	FAM114A2	FNDC3A	GOLGA8S
AK2	ARHGAP35	BDKRB1	C7orf50	CD1D	CLDN6	CTNND1	DHX34	EFEMP1	FAM120B	FNIP2	GOLGB1
AK4	ARHGAP44	BECN2	C7orf69	CD200R1L	CLDN8	CTPS1	DHX58	EFHB	FAM122C	FNTB	GOLIM4
AK5	ARHGAP5	BEGAIN	C8orf31	CD244	CLDN9	CTR9	DHX8	EFL1	FAM124B	FOLR2	GOLPH3L
AK8	ARHGDIG	BEST4	C8orf33	CD2AP	CLDND1	CTRC	DIAPH3	EFTUD2	FAM131A	FOPNL	GORASP2
AKAIN1	ARHGEF28	BEX5	C8orf87	CD300LF	CLEC12A	CTSA	DIDO1	EGFLAM	FAM131C	FOXA3	GOT1L1
AKAP10	ARHGEF39	BHLHE22	C9orf135	CD34	CLEC14A	CTSW	DIP2A	EGLN3	FAM135A	FOXE3	GP2
AKAP12	ARHGEF6	BICD2	C9orf50	CD3G	CLEC17A	CUL2	DIP2B	EGR2	FAM135B	FOXF2	GPATCH1
AKAP13	ARID3B	BICDL1	C9orf57	CD4	CLEC1A	CUTA	DIS3	EGR3	FAM149A	FOXI1	GPATCH4
AKAP14	ARID4A	BICRAL	CA1	CD40LG	CLEC3A	CWF19L2	DIS3L	EHD2	FAM149B1	FOXK1	GPC4
AKR1A1	ARL13A	BIRC5	CAB39L	CD72	CLEC3B	CXADR	DIS3L2	EIF2B2	FAM155A	FOXL1	GPD1
AKR1B15	ARL13B	BLCAP	CABCOCO1	CD99	CLEC6A	CXCL10	DKK2	EIF2D	FAM155B	FOXL2	GPR101
AKR1C3	ARL17B	BLK	CABP5	CDC14A	CLEC7A	CXCL12	DKK3	EIF3A	FAM169A	FOXRED1	GPR108
AKR1E2	ARL2	BLM	CABYR	CDC14B	CLGN	CXCL14	DLD	EIF3C	FAM170A	FPR3	GPR132

Supplementary Table 2 (2/9). Upregulated genes in response to metabolic stress ($Log_2FC>0.265$) in BRAF^{V600E} mutant cells.

Upregulated in BRAF^{V600E} mutant cells											
GPR146	HIST2H2AA3	INO80E	KIF23	LINC00612	MAGEC1	MPC1L	NDNF	NUDT3	PDPN	POMK	PSMG3-AS1
GPR15	HIST2H2AB	INPP1	KIF26B	LINC00663	MAGEC2	MPDU1	NDOR1	NUDT8	PDYN	POP7	PSORS1C1
GPR150	HIST2H2BE	INSM2	KIF2A	LINC00668	MAGED4	MPEG1	NDRG1	NUP155	PDZD2	POSTN	PSPC1
GPR160	HIST3H2BB	INTS14	KIF5C	LINC00851	MAGIX	MPHOSPH8	NDRG4	NUP188	PDZD8	POT1	PSPH
GPR171	HIVEP2	INTS2	KIFAP3	LINC00934	MALT1	MPP4	NDUFAF2	NUP43	PEBP1	POTEB2	PSPN
GPR180	HLA-B	INTS6	KIRREL2	LINC01126	MAN1A2	MPPED1	NDUFB6	NUP54	PELI1	POTEB3	PTCD2
GPR20	HLA-DMA	INTS7	KISS1R	LINC01205	MAN1B1	MPPED2	NDUFS3	NUPR1	PELI2	POTEC	PTDSS1
GPR34	HLA-DRB1	INVS	KITLG	LINC01276	MANF	MRGBP	NDUFV1	NXNL2	PELI3	POTED	PTDSS2
GPR37	HLA-DRB5	IP6K1	KLC1	LINC01342	MAP1LC3B	MRGPRF	NDUFV3	OAS2	PENK	POTEE	PTER
GPR6	HLCS	IP6K2	KLC2	LINC01359	MAP2K1	MRLN	NECAP2	OCA2	PER3	POTEG	PTF1A
GPR68	HMGB2	IPO4	KLF12	LINC01496	MAP2K5	MROH1	NEDD4	OCIAD1	PES1	POTEH	PTGDR
GPR88	HMGB4	IQCA1	KLF6	LINC01549	MAP3K13	MROH2A	NEGR1	ODAM	PEX11A	POU3F3	PTGER3
GPRC5C	HMGCL	IQCF1	KLHDC2	LINC01590	MAP3K19	MROH2B	NEIL3	ODC1	PEX12	POU4F3	PTGES
GPS2	HMGCLL1	IQCF4	KLHL1	LINC01630	MAP3K4	MROH7	NEK4	OLFM4	PFKFB1	PPAN-P2RY11	PTGES2
GPSM1	HMGCS2	IQGAP3	KLHL12	LINC02347	MAP4K5	MRPL15	NEMP2	OLFML1	PFN3	PPBP	PTGIR
GPT	HMGN1	IQSEC2	KLHL15	LINC02370	MAPK10	MRPL19	NEO1	OLIG2	PGAP3	PPEF1	PTGS2
GPX3	HMGN4	IRF1	KLHL20	LINC02444	MAPK4	MRPL22	NEPRO	OPHN1	PGBD1	PPFIBP1	PTPN1
GRAP	HMHB1	IRF8	KLHL21	LINC02583	MAPK9	MRPL23	NEUROD2	OPN1LW	PGBD4	PPIC	PTPRC
GRASP	HMX1	IRGC	KLHL24	LINC02687	MARCH4	MRPS16	NEUROD6	OPRM1	PGBD5	PPIG	PTPRN
GRB10	HNRNPCL3	IRGM	KLHL28	LINGO4	MARCH6	MRPS18A	NEXN	ORM1	PGLS	PPIL3	PTPRN2
GREM1	HOMER1	ISL2	KLHL4	LIPM	MARCH9	MRPS18B	NFAM1	OSBP2	PGM2L1	PPIP5K1	PTPRZ1
GRID2	HOXA11	ISX	KLHL42	LIPN	MARF1	MRPS25	NFASC	OSBPL6	PGM5	PPL	PUS3
GRIFIN	HOXB7	ISYNA1	KMT2A	LMAN2L	MARK1	MRPS33	NFATC2	OSBPL7	PHAX	PPM1D	PVRIG
GRIN2A	HOXB9	ITFG1	KMT2C	LMBRD2	MAS1L	MRPS36	NFIC	OSGEPL1	PHEX	PPM1F	PWWP3A
GRIN2B	HOXD10	ITGA7	KMT2E	LMF1	MAST4	MS4A3	NFKB2	OTOR	PHF14	PPM1H	PWWP3B
GRIN3B	HOXD12	ITGA8	KMT5B	LMO7	MATN4	MSH3	NFKBIA	OTUD3	PHLDB2	PPM1K	PXK
GRIPAP1	HOXD4	ITGAL	KNOP1	LMOD2	MB	MSI2	NGEF	OTUD5	PHLPP1	PPOX	PYCARD-AS1
GRK1	HOXD9	ITGB3	KNSTRN	LNP1	MBD3L1	MSL3	NGF	OVGP1	PHOSPHO1	PPP1CA	PYCR1
GRK7	HPCA	ITGB5	KPNA4	LOC100130880	MBL2	MTA1	NHLRC2	OXSR1	PHYHIP	PPP1CB	PYCR3
GRM1	HPGD	ITGB6	KPNA7	LOC100131496	MBLAC1	MTA3	NHLRC3	P2RX1	PI4K2A	PPP1R12A	PYDC1
GRM6	HPR	ITPKC	KRBOX4	LOC100133315	MCAM	MTF1	NIBAN2	P2RX2	PI4KA	PPP1R16B	PYGB
GRPEL2	HPRT1	ITPRIP	KRI1	LOC100288966	MCF2L2	MTFMT	NID1	P2RX3	PI4KAP2	PPP1R2	PYGL
GRXCR2	HS1BP3	ITPRIPL1	KRT10	LOC100419583	MCM10	MTG2	NIPA2	P2RX5	PIAS2	PPP1R27	PYHIN1
GSC2	HS2ST1	IZUMO3	KRT18	LOC100421561	MCM3	MTHFSD	NIPAL1	P2RY14	PIGA	PPP1R36	PYROXD2
GSG1	HS3ST1	IZUMO4	KRT19	LOC100506124	MCM3AP	MTMR11	NIPSNAP1	P2RY8	PIGB	PPP1R3B	PYY
GSN	HS3ST3B1	JADE1	KRT33A	LOC101927572	MCM6	MTMR14	NKAIN2	P3H2	PIGC	PPP1R7	QTRT1
GSTA3	HS3ST5	JADE2	KRT34	LOC101928882	MCM9	MTMR6	NKAIN3	PA2G4	PIGG	PPP2R2B	R3HCC1L
GSTM4	HS6ST2	JAG1	KRT5	LOC102723701	MCMDC2	MTMR8	NKAIN4	PABPC1L2A	PIGL	PPP2R2C	R3HDM2
GSTO1	HSBP1L1	JAGN1	KRT6C	LOC102724957	MCOLN2	MTNR1B	NKAPL	PABPC1L2B	PIGN	PPP2R5A	RAB11FIP2
GSTT2	HSD11B1L	JAK3	KRT73	LOC339166	MDC1	MTO1	NKD1	PABPC4	PIGR	PPP3CC	RAB12
GTDC1	HSDL2	JMJD6	KRT80	LOC403312	MDN1	MTREX	NKG7	PACSIN3	PIGW	PPP6R1	RAB17
GTF2A1	HSF5	JMJD7	KRT81	LOC442028	ME1	MUC16	NKRF	PADI1	PIH1D1	PPP6R3	RAB19
GTF2A1L	HSPA4	JMJD8	KRT83	LOC646938	MED19	MUC17	NKTR	PAGE1	PIM1	PPY	RAB23
GTF2A2	HSPA6	JMY	KRT85	LOC728554	MED21	MUC2	NKX1-1	PAGE2B	PIM2	PQBP1	RAB24
GTF2H1	HSPBAP1	JPH4	KRTAP1-1	LOC730668	MED23	MVD	NKX6-1	PAK1	PIN1	PQLC1	RAB33A
GTF2H5	HTN1	JPT2	KRTAP1-4	LOX	MED28	MX1	NLK	PAK3	PIP4K2B	PRAMEF14	RAB33B
GTF2IRD2B	HTR4	JRK	KRTAP10-3	LOXL1	MED29	MXRA5	NLRP11	PALB2	PIP4P1	PRAMEF18	RAB34
GTF3C3	HTR5A-AS1	JUN	KRTAP13-2	LPA	MEF2C	MYCBPAP	NLRP3	PAN3	PISD	PRAMEF33	RAB3GAP2
GTPBP2	HTRA3	JUND	KRTAP13-3	LRFN4	MEFV	MYH1	NME4	PANK2	PITHD1	PRCP	RAB40A
GTPBP8	HVCN1	JUP	KRTAP16-1	LRG1	MEGF11	MYH13	NMI	PANK4	PITPNA	PRDM10	RAB42
GUCA2B	ICA1L	KANK4	KRTAP19-7	LRIG1	MEIS1	MYH2	NMNAT2	PAPSS1	PITX1	PRDM12	RAB6C
GYPE	ICAM4	KARS	KRTAP2-3	LRIT2	MEMO1	MYL7	NMRAL1	PAPSS2	PKIB	PRDM15	RAC3
H1F0	ICE2	KAT6A	KRTAP20-3	LRIT3	MEN1	MYLK	NNAT	PAQR6	PKP3	PRDM2	RACGAP1
H1FNT	IDH3G	KAT6B	KRTAP4-11	LRP1	MEPE	MYLPF	NOD1	PAQR7	PLA2G2F	PRDM6	RAD21L1
H2AFX	IFNA1	KAZN	KRTAP4-3	LRP10	METTL11B	MYO1B	NOL4L	PARD6A	PLA2G3	PRDM9	RAD51B
HADH	IFNA21	KCNA1	KRTAP5-3	LRP11	METTL2B	MYO1C	NOL8	PARN	PLAA	PREP	RAET1G
HAL	IFNAR1	KCNA7	KRTAP5-8	LRP1B	METTL5	MYO5C	NOP2	PARP11	PLAC8	PREX2	RAI2
HAND2-AS1	IFNK	KCNAB3	KRTAP5-9	LRP2	MFAP1	MYO6	NOTCH2	PARP14	PLAC8L1	PRG2	RALA
HAO2	IFNW1	KCNB1	KRTAP7-1	LRP2BP	MFF	MYOD1	NOX1	PARP4	PLAC9	PRH1	RALBP1
HAPLN4	IFRD2	KCNE1	KRTAP9-3	LRP4	MFN2	MYOF	NOX3	PARVG	PLAU	PRICKLE3	RALY
HAUS4	IFT74	KCNG3	KRTAP9-4	LRRC15	MFSD10	MYOZ1	NOXA1	PASD1	PLAUR	PRKAA1	RAMAC
HBM	IFT80	KCNH4	KRTAP9-7	LRRC17	MFSD13A	MYOZ2	NOXO1	PATJ	PLCB1	PRKAA2	RAN
HBP1	IFT88	KCNH5	LACRT	LRRC30	MFSD14C	MYPN	NPEPPS	PAX3	PLCD4	PRKAB1	RANBP17
HBZ	IGF1R	KCNIP1	LAG3	LRRC36	MFSD2A	MYPOP	NPFFR1	PAX4	PLCG1	PRKAG2	RANBP3
HCG27	IGF2-AS	KCNIP3	LAGE3	LRRC38	MGAM2	MYT1	NPHP3-ACAD11	PAX8	PLCL1	PRKCH	RASAL2
HCRTR1	IGFBPL1	KCNIP4	LAMA2	LRRC39	MGAT4B	MZT1	NPIPA1	PCDH11X	PLCXD1	PRKCZ	RASD1
HDAC2	IGFL3	KCNJ10	LAMB3	LRRC40	MGMT	MZT2B	NPIPA3	PCDH11Y	PLD2	PRKDC	RASGEF1A
HDAC4	IGLON5	KCNJ13	LAMP5	LRRC43	MIA	N4BP1	NPIPA5	PCDH12	PLEKHA4	PRKG1	RASGEF1B
HDAC5	IGSF10	KCNJ14	LARP1	LRRC45	MIB1	NAA11	NPIPB3	PCDH8	PLEKHG1	PRMT3	RASGEF1C
HDGF	IHH	KCNK13	LARP4	LRRC4B	MICOS10-NBL1	NAA16	NPM1	PCDHB1	PLEKHM1	PRMT9	RASGRF1
HDHD2	IKBKB	KCNK18	LARP6	LRRC75B	MICOS13	NAA80	NPTX2	PCDHB14	PLK5	PRODH2	RASGRF2
HDHD5	IKBKG	KCNK3	LAX1	LRRC8A	MIEN1	NAALAD2	NPY5R	PCDHB5	PLP2	PROKR1	RASL11B
HEATR5A	IKZF1	KCNQ1	LBP	LRRFIP1	MIER3	NACA	NR0B1	PCGF1	PLPP1	PROKR2	RASSF5
HEATR5B	IKZF5	KCNQ3	LCE2C	LRRIQ3	MIGA1	NACAD	NR1H2	PCGF2	PLPP4	PROP1	RASSF6
HEG1	IL10RB	KCNV1	LCN1	LRRIQ4	MIIP	NADK	NR2E3	PCGF3	PLPP5	PROSER1	RASSF7
HELT	IL11RA	KCTD12	LCN15	LRRN2	MINAR1	NAF1	NRARP	PCGF6	PLPPR4	PRPF3	RAVER2
HEMK1	IL13RA2	KCTD17	LDAH	LRRN3	MINDY2	NAIP	NRCAM	PCMTD1	PLSCR5	PRPF4	RBAK
HERC1	IL16	KCTD19	LDB1	LRRN4	MIR1-1HG-AS1	NANOS3	NREP	PCSK5	PLXNB3	PRR14	RBBP6
HERC2P2	IL17B	KCTD6	LDLR	LRRTM1	MIS12	NAP1L3	NRIP1	PCSK6	PM20D2	PRR19	RBIS
HERC3	IL17F	KDM1B	LDLRAD3	LRWD1	MITD1	NAP1L6	NRP2	PCTP	PMAIP1	PRR26	RBKS
HERC6	IL1A	KDM2A	LENG1	LSMEM1	MITF	NAPEPLD	NRROS	PCYOX1	PMCH	PRR7	RBM14-RBM4
HES7	IL1F10	KDM2B	LENG9	LSR	MKRN2	NAPRT	NRSN1	PCYT1B	PMEPA1	PRRG1	RBM18
HEXD	IL1RN	KDM4B	LEPROTL1	LURAP1L	MLH1	NAT8	NRSN2-AS1	PCYT2	PMPCA	PRRT3	RBM22
HEY2	IL32	KDM8	LETM1	LY6H	MLST8	NAT9	NRTN	PDC	PMPCB	PRRX1	RBM28
HFM1	IL34	KEAP1	LGALS4	LY75-CD302	MLXIP	NATD1	NSF	PDCL3	PNMA3	PRRX2	RBM34
HGF	IL36RN	KHDC1	LGALS7	LY9	MLYCD	NAXD	NSG1	PDE12	PNMA8A	PRSS41	RBM39
HGH1	IL3RA	KHDC3L	LGALS8	LY96	MMAA	NBL1	NSG2	PDE3A	PNOC	PRSS54	RBM46
HGS	IL5RA	KHDRBS2	LGR6	LYG1	MME	NBPF4	NSMAF	PDE3B	PNP	PRSS55	RBM4B
HHAT	ILVBL	KIAA0040	LGSN	LYPD1	MMP15	NCAM1	NSMCE1	PDE4B	PNPLA2	PRXL2A	RBMX2
HIP1R	IMMP1L	KIAA0319L	LHX6	LYPD3	MMP19	NCAPD2	NSUN5	PDE4D	PNPLA3	PSD2	RBMXL3
HIPK1	IMPDH1	KIAA0753	LILRB3	LYRM9	MMP8	NCAPH	NT5C1A	PDE6A	PNPLA7	PSD3	RBX1
HIPK2	IMPDH2	KIAA1109	LIMA1	LYZL4	MMS19	NCAPH2	NT5C2	PDE6H	POLA1	PSEN2	RC3H1
HIST1H1C	IMPG1	KIAA1191	LIMD1	MAB21L4	MMS22L	NCBP2	NT5C3B	PDE7A	POLR2D	PSENEN	RCC1L
HIST1H2AC	INAFM1	KIAA1328	LIMS4	MACROD1	MNDA	NCBP3	NT5M	PDE8A	POLR2G	PSKH2	RCN3
HIST1H2AG	INAFM2	KIAA1549	LIN28A	MAEA	MOAP1	NCEH1	NTMT1	PDF	POLR2H	PSMB8-AS1	RCOR1
HIST1H2BB	ING2	KIAA1549L	LIN7C	MAFA	MOB3A	NCKAP5	NTSR1	PDGFD	POLR2J4	PSMC1	RDH10-AS1
HIST1H2BK	ING5	KIF18A	LINC00243	MAGEA2	MOB3B	NCOA4	NUDCD1	PDGFRA	POLR2K	PSMD13	RDH11
HIST1H2BO	INHBA	KIF20A	LINC00311	MAGEB10	MOCOS	NCSTN	NUDCD2	PDHA1	POLR3F	PSMD6	RDH8
HIST1H3I	INHBC	KIF21B	LINC00337	MAGEB16	MOGAT1	NDE1	NUDT10	PDHB	POLR3GL	PSME1	REEP2
HIST1H4F	INKA2	KIF22	LINC00482	MAGEB6	MORN5	NDFIP2	NUDT17	PDK3	POLR3K	PSME4	REEP3

Supplementary Table 2 (3/9). Upregulated genes in response to metabolic stress ($Log_2FC>0.265$) in BRAF^{V600E} mutant cells.

Upregulated in BRAF^{V600E} mutant cells									
REEP4	S100G	SIX1	SMG5	STC1	TFPI2	TOR3A	UBXN6	WIF1	ZNF394
RELL2	SAFB2	SKIDA1	SMG7	STEAP2	TGFBR1	TP53BP2	UCP2	WIPF2	ZNF410
REP15	SAGE1	SKIL	SMIM14	STEAP3	TGFBR3L	TP53I13	UFD1	WLS	ZNF418
REPIN1	SAMD8	SKOR1	SMIM15	STH	TGIF2LY	TP53TG3B	UFM1	WNT10A	ZNF429
RERE	SARDH	SLA2	SMNDC1	STIL	TGM4	TP53TG3C	UGCG	WNT2	ZNF43
RERG	SBF2	SLAMF1	SMO	STIM1	TGM5	TP63	UGT2B11	WNT2B	ZNF443
RERGL	SBK3	SLAMF9	SMOC2	STK11	TH	TPD52L1	UGT2B15	WTAP	ZNF446
RESF1	SCAMP2	SLC10A5	SNAI3	STK26	THBS1	TPH2	UHRF1	WWC3	ZNF469
REV1	SCAMP3	SLC12A1	SNAP29	STK38L	THBS3	TPM1	ULBP1	WWP2	ZNF487
REV3L	SCAND1	SLC12A6	SNAPC5	STMND1	THEM5	TPP2	ULBP3	XAGE1B	ZNF503-AS2
REXO4	SCAPER	SLC12A8	SNF8	STN1	THOC1	TPPP2	ULK4	XAGE2	ZNF512B
RFK	SCARA3	SLC12A9	SNORD89	STON2	THOC3	TPRG1L	UMODL1-AS1	XDH	ZNF514
RFLNB	SCCPDH	SLC15A1	SNRNP200	STPG3	THOC5	TPRKB	UNC5A	XIRP2	ZNF543
RFNG	SCD	SLC15A2	SNRNP35	STRC	THRB	TPSD1	UNC5C	XK	ZNF550
RFPL3S	SCEL	SLC16A11	SNX19	STX11	THSD1	TPST1	UNCX	XKR3	ZNF555
RFPL4AL1	SCG3	SLC16A13	SNX25	STX18	THSD7B	TPX2	UPF3B	XKR8	ZNF556
RGPD4	SCG5	SLC16A14	SNX29	STX2	THUMPD3	TRA2B	UPK1A	XKRX	ZNF560
RGPD5	SCGB2A1	SLC16A7	SNX29P2	STXBP4	TICAM1	TRABD2B	UQCC1	XKRY2	ZNF575
RGPD6	SCGB2A2	SLC16A9	SNX6	SUCO	TIGD3	TRAF3IP1	UQCR10	XPO5	ZNF582-AS1
RGPD8	SCIN	SLC17A4	SNX8	SUGCT	TIGD5	TRAK1	UQCRQ	XYLB	ZNF583
RGS10	SCMH1	SLC17A6	SOAT1	SULT2B1	TIGD7	TRAM2	UROD	YARS2	ZNF584
RGS17	SCN1A	SLC18A2	SOBP	SUN2	TIMD4	TRAPPC12	USE1	YBEY	ZNF600
RGS18	SCN9A	SLC18A3	SOCS2	SUPT20H	TIMM17B	TRDN	USF3	YIPF1	ZNF605
RGS22	SCP2D1	SLC19A1	SOD3	SUPT7L	TIMM29	TREM2	USH1G	YIPF5	ZNF609
RGS9	SCRIB	SLC19A2	SOGA3	SUPV3L1	TJP3	TRHDE-AS1	USP12	YPEL2	ZNF614
RHBDF1	SCRN2	SLC1A2	SORL1	SUSD3	TK1	TRIB1	USP13	YPEL3	ZNF618
RHBDL1	SCUBE3	SLC1A5	SOS1	SUSD5	TLE5	TRIM16L	USP17L11	YWHAB	ZNF623
RHCE	SCYL3	SLC22A14	SOS2	SV2A	TLE6	TRIM2	USP17L12	YWHAG	ZNF628
RHD	SDF2L1	SLC22A16	SOWAHA	SVIL	TLL1	TRIM22	USP17L2	ZAN	ZNF630
RHOC	SDHD	SLC22A17	SOX12	SWI5	TLR1	TRIM23	USP17L20	ZBED1	ZNF638
RHOH	SEBOX	SLC22A18	SOX21	SYCE1	TLR3	TRIM33	USP17L21	ZBED4	ZNF660
RHOT1	SEC13	SLC22A20P	SOX6	SYCP3	TLX3	TRIM35	USP20	ZBTB10	ZNF664-RFLNA
RICTOR	SEC14L3	SLC25A15	SP100	SYDE2	TM6SF1	TRIM38	USP30	ZBTB2	ZNF669
RIDA	SEC14L6	SLC25A16	SP7	SYNGR4	TM9SF2	TRIM39	USP32P2	ZBTB3	ZNF674
RIN1	SEC16A	SLC25A22	SP8	SYNM	TMC3	TRIM49	USP36	ZBTB44	ZNF675
RLN3	SEC22C	SLC25A24	SPA17	SYNPO	TMCC3	TRIM59	USP45	ZBTB45	ZNF682
RMI1	SEC23B	SLC25A29	SPACA4	SYPL1	TMED4	TRIM62	USP47	ZBTB47	ZNF705D
RMND5B	SEC24C	SLC25A32	SPAG6	SYVN1	TMED5	TRIM64C	USP50	ZBTB9	ZNF705G
RNASE6	SEC62	SLC25A39	SPANXA1	TAF11	TMED8	TRIM71	USP54	ZC3H10	ZNF71
RNF103	SELENBP1	SLC25A44	SPANXD	TAF1L	TMEM101	TRIM72	UTF1	ZC3H12C	ZNF711
RNF113B	SEMA3A	SLC25A52	SPANXN3	TAF2	TMEM104	TRIM77	UTP20	ZC3H4	ZNF714
RNF115	SEMA4A	SLC27A2	SPARCL1	TAF3	TMEM105	TRIML2	UTP4	ZC3H7A	ZNF74
RNF13	SEMA4B	SLC29A1	SPATA16	TAF8	TMEM106B	TRIP4	UVRAG	ZCCHC14	ZNF740
RNF141	SEMA5A	SLC29A2	SPATA21	TANGO6	TMEM120A	TRIP6	UVSSA	ZCCHC17	ZNF75D
RNF144B	SEMA6C	SLC2A10	SPATA31A1	TARSL2	TMEM120B	TRMO	UXS1	ZCCHC24	ZNF783
RNF157	SEMG1	SLC2A13	SPATA31A3	TAS1R1	TMEM121B	TRMT44	UXT-AS1	ZDBF2	ZNF787
RNF170	SENP7	SLC2A2	SPATA31A5	TAS2R1	TMEM135	TRPC4AP	VAC14	ZDHHC14	ZNF792
RNF2	SEPTIN10	SLC2A6	SPATA31C2	TAS2R13	TMEM147	TRPM4	VANGL2	ZDHHC18	ZNF793
RNF212	SEPTIN12	SLC2A7	SPATA46	TAS2R20	TMEM160	TRPV3	VASH2	ZDHHC21	ZNF8
RNF216	SEPTIN14	SLC2A8	SPATA48	TAS2R30	TMEM161A	TRPV6	VAT1	ZDHHC23	ZNF804B
RNF26	SEPTIN3	SLC2A9	SPATA5	TAS2R41	TMEM168	TRUB1	VAV2	ZDHHC4	ZNF812P
RNF4	SERAC1	SLC30A4	SPATA9	TAS2R60	TMEM169	TSACC	VAV3	ZER1	ZNF814
RNF41	SERPINA13P	SLC30A8	SPATC1L	TAT	TMEM176A	TSHZ2	VAX1	ZFAND2B	ZNF837
RNF44	SERPINA4	SLC31A1	SPATS1	TBATA	TMEM184B	TSHZ3	VCAM1	ZFAND3	ZNF852
RNF6	SERPINB13	SLC35A3	SPCS1	TBC1D1	TMEM184C	TSKS	VCX	ZFAND4	ZNF860
RNF7	SERPINE2	SLC35B2	SPDYE1	TBC1D10B	TMEM186	TSKU	VCX3B	ZFAT	ZNF878
RNMT	SERTAD2	SLC35B3	SPDYE3	TBC1D12	TMEM200B	TSPAN11	VCY	ZFHX2	ZNF93
RNPC3	SESN1	SLC35D1	SPIN2A	TBC1D13	TMEM201	TSPAN14	VDAC2	ZFP28	ZNHIT6
RO60	SETD4	SLC35E1	SPIN2B	TBC1D15	TMEM210	TSPAN17	VDR	ZFP3	ZNRF4
ROCK1	SETD7	SLC35E2A	SPINK13	TBC1D22A-AS1	TMEM219	TSPAN3	VGF	ZFP30	ZP3
ROCK2	SETX	SLC35E2B	SPINK14	TBC1D22B	TMEM223	TSPOAP1	VGLL1	ZFP42	ZRANB1
ROPN1	SF3B3	SLC35F1	SPINK2	TBC1D23	TMEM229A	TSPYL4	VGLL4	ZFP57	ZSCAN22
ROPN1B	SFMBT1	SLC38A1	SPINK7	TBC1D26	TMEM237	TSR2	VHL	ZFP69B	ZSCAN26
ROR1-AS1	SFT2D3	SLC38A5	SPOCD1	TBC1D29P	TMEM238	TSSK2	VIL1	ZFP82	ZSCAN32
RP9	SGMS2	SLC39A14	SPOCK1	TBC1D3B	TMEM255B	TTC23	VIP	ZFP92	ZZZ3
RPGRIP1	SGO1	SLC39A9	SPPL2A	TBCC	TMEM259	TTC27	VKORC1L1	ZFPM2	
RPL10L	SGPP1	SLC43A1	SPPL2C	TBR1	TMEM268	TTC29	VPREB3	ZFR2	
RPL22L1	SGSM1	SLC4A2	SPR	TBRG1	TMEM270	TTC32	VPS13D	ZFY	
RPL39	SGSM3	SLC52A2	SPRED3	TBX10	TMEM272	TTC38	VPS18	ZFYVE27	
RPS10-NUDT3	SGTA	SLC5A2	SPRR1A	TBX21	TMEM31	TTF1	VPS53	ZHX2	
RPS19BP1	SH2D3A	SLC5A6	SPRR2E	TBX22	TMEM50A	TTN	VRK1	ZKSCAN2	
RPS27L	SH2D3C	SLC6A15	SPRR2G	TBX4	TMEM59	TUBA3D	VRK2	ZMYND19	
RPS6KA4	SH2D6	SLC6A20	SPRY4	TBXAS1	TMEM74B	TUBA4B	VRK3	ZNF133	
RPTOR	SH3D19	SLC6A6	SPTBN2	TCEA3	TMEM79	TUBAL3	VSTM2A	ZNF135	
RRAGA	SH3GL2	SLC6A7	SPTLC3	TCEAL1	TMEM87B	TUBGCP2	VSTM5	ZNF18	
RRP12	SH3RF1	SLC7A11	SPTSSA	TCEAL7	TMEM88B	TUFM	VTCN1	ZNF180	
RRP36	SH3RF3	SLC7A7	SPX	TCF3	TMEM8A	TULP1	VTI1A	ZNF195	
RRP8	SHANK1	SLC8A1	SRARP	TCF7L1	TMEM91	TUSC1	VWA2	ZNF215	
RSBN1	SHF	SLC8A2	SRM	TCF7L2	TMEM92	TUSC3	VWA5B1	ZNF226	
RSBN1L	SHISA6	SLC9A1	SRPK3	TCHHL1	TMEM94	TWSG1	WAPL	ZNF227	
RSPO1	SHISA7	SLC9A2	SRRM2	TCN2	TMPRSS11B	TXLNG	WARS2	ZNF236	
RSPO3	SHISAL1	SLC9A3R2	SRXN1	TCP1	TMPRSS11E	TXNDC2	WASHC2A	ZNF239	
RSPO4	SHLD1	SLC9A6	SRY	TDP1	TMPRSS13	TXNL1	WASL	ZNF25	
RTCA	SHLD2	SLC9A7	SS18L2	TDRD3	TMSB15B	TYMP	WDHD1	ZNF252P-AS1	
RTL1	SHMT1	SLCO1A2	SSH1	TDRD5	TMX3	TYRO3	WDR26	ZNF28	
RTL6	SHROOM4	SLCO4A1-AS1	SSRP1	TDRD6	TNFAIP2	TYROBP	WDR38	ZNF280B	
RTL8B	SI	SLCO5A1	SSX4B	TEAD3	TNFRSF11B	TYW5	WDR4	ZNF280C	
RTN4RL2	SIDT2	SLFN11	ST20-AS1	TEK	TNFSF10	U2AF1	WDR45B	ZNF282	
RTP3	SIGLEC9	SLFN14	ST3GAL2	TENT2	TNFSF12-TNFSF13	UBASH3B	WDR49	ZNF317	
RTTN	SIGMAR1	SLFNL1	ST3GAL3	TENT5B	TNFSF15	UBE2C	WDR54	ZNF32-AS3	
RUNX1	SIK3	SLIT2	ST6GAL2	TES	TNIK	UBE2F	WDR59	ZNF324	
RUNX2	SIKE1	SLITRK1	ST6GALNAC1	TEX19	TNKS1BP1	UBE2W	WDR5B	ZNF335	
RUSC1-AS1	SIL1	SLN	ST6GALNAC5	TEX264	TNNC1	UBE3C	WDR66	ZNF33B	
RUSC2	SIM2	SLX1A-SULT1A3	ST7L	TEX33	TNNC2	UBE3D	WDR78	ZNF354C	
RUVBL1	SIN3B	SLX4	ST8SIA4	TEX35	TNNI3	UBE4B	WDR81	ZNF358	
RWDD2A	SIPA1L2	SMAD2	STAG3L4	TEX50	TNNI3K	UBN2	WDR83OS	ZNF362	
RXRG	SIPA1L3	SMAGP	STARD3	TFB1M	TOMM22	UBOX5	WDYHV1	ZNF37A	
S100A1	SIRPB1	SMAP1	STAT5A	TFB2M	TOMM5	UBP1	WEE1	ZNF383	
S100A3	SIRT4	SMARCA2	STAU1	TFDP1	TOPBP1	UBR2	WFDC11	ZNF384	
S100A7A	SIRT7	SMC6	STAU2	TFG	TOPORS	UBR7	WHRN	ZNF385D	

Supplementary Table 2 (4/9). Upregulated genes in response to metabolic stress ($Log_2FC>0.265$) in BRAF^{V600E} mutant cells.

Downregulated in NRAS^{Q61R} mutant cells										
AGO2	BASP1	CREBBP	FOXK1	INPPL1	MCM3AP-AS1	PAGE2	RCOR1	SPRED3	TULP4	ZNF586
AGO3	BAZ2B	CRP	FOXK2	INSIG2	MDFIC	PAK2	RDH13	SPTAN1	UBE2J2	ZNF587
AAK1	BCL11B	CRYBG2	FOXO1	INTS5	MECP2	PAK3	RELCH	SPTB	UBN1	ZNF592
AAMDC	BCOR	CRYBG3	FUT11	IQCE	MED22	PAQR7	RELT	SPTLC2	UBQLN2	ZNF605
AARS2	BCORL1	CRYGS	FZD4	IQCJ	MED23	PARD6A	RERE	SRC	ULK1	ZNF609
AASS	BDP1	CSKMT	GAL3ST3	ITIH6	MEPCE	PARD6B	RETREG2	SREBF1	UMODL1-AS1	ZNF611
ABCB6	BIRC3	CTAGE9	GALNT2	ITM2A	METTL25	PARG	RGS19	SRGAP1	UNC80	ZNF625
ABCD2	BIRC7	CYP20A1	GCNA	ITPKA	METTL27	PARP14	RHBDL1	SS18L1	UPF1	ZNF625-ZNF20
ABHD13	BIVM-ERCC5	CYP2R1	GCNT4	IVL	MFAP1	PASK	RHOBTB1	STAC3	UPK1A	ZNF654
ABHD15	BMPR2	CYP4Z1	GDPD5	JAKMIP2-AS1	MFSD9	PCDHB2	RHPN2	STARD13	URB1	ZNF660
ABHD16B	BPTF	CYTH1	GEMIN8	JAM2	MGAT4B	PCF11	RIPOR1	STARD8	URB2	ZNF671
ACAD10	BRAF	CYTH3	GFOD1	JARID2	MGC27345	PCNX1	RIT1	STK35	URGCP	ZNF682
ACAP2	BRD3	DENND4C	GH1	JRK	MIB1	PCNX3	RLF	STK4	USP49	ZNF684
ACSF3	BRPF1	DENND6B	GHR	KALRN	MICAL3	PDCD7	RNF111	STK40	UVSSA	ZNF691
ACTL7B	BRPF3	DGKH	GIGYF1	KANK1	MIDN	PDE5A	RNF149	STRA6	VAV2	ZNF713
ACTR3B	BRWD3	DGKQ	GIPC1	KAT6B	MINDY1	PDIK1L	RNF213	STRN3	VCPIP1	ZNF714
ACVR1B	BTBD9	DHRS2	GJC1	KBTBD6	MINDY2	PDK3	RNF34	STX11	VEGFA	ZNF720
ACVRL1	BTG2	DIDO1	GK	KBTBD7	MIOX	PDPK1	RO60	STX12	VHL	ZNF727
ADAMTS4	BTK	DIO2	GLDC	KCNA2	MIR1915HG	PDZD2	ROCK2	STX16	VKORC1L1	ZNF736
ADAMTS9	BUD13	DIP2C	GLYR1	KCNH8	MLXIP	PER2	ROPN1B	STX1B	VPS13B	ZNF772
ADAMTSL4	C10orf105	DLEC1	GOLGA3	KCNQ3	MMP17	PFKFB4	RPL39L	STXBP4	VPS39	ZNF776
ADCY7	C12orf60	DLGAP2	GPCPD1	KCP	MOB1B	PHACTR4	RPP25	SUCO	VPS50	ZNF778
ADGRA2	C12orf77	DLX2	GPD1	KCTD7	MOCS3	PHF12	RRBP1	SULT1A1	VPS54	ZNF789
ADGRG6	C14orf28	DMXL2	GPR21	KDM2A	MOV10	PHF23	RSC1A1	SURF6	WAPL	ZNF791
ADGRL1	C16orf91	DNAAF3	GPRIN1	KDM3A	MPRIP	PHLPP2	RTEL1	SUSD2	WDHD1	ZNF793
ADGRL3	C19orf57	DNAJC21	GPSM2	KDM4B	MROH7	PHTF1	RTL6	SUV39H2	WDR17	ZNF800
ADGRV1	C1orf21	DNAJC6	GRAPL	KIAA1109	MRPS18C	PIGBOS1	RUBCN	SVIL	WDR26	ZNF805
ADNP	C1orf226	DNASE1L2	GRB10	KIAA1549L	MRTFB	PIK3C2B	RUNX3	SYCE2	WDR91	ZNF81
ADNP2	C1QTNF6	DNM1	GRIN2B	KIAA1841	MSANTD3-TMEFF1	PKD2	RUSC2	SYNGR4	WDR93	ZNF816-ZNF321P
ADPRH	C2orf49	DNM3	GRK5	KIF13A	MTMR10	PLAG1	RXFP1	SYNJ2	WFDC11	ZNF827
AFDN	C3orf62	DOCK1	GSK3B	KIF14	MTUS1	PLAGL2	S100A7A	SYTL3	WNK1	ZNF836
AFF4	C6orf222	DOCK5	GSTZ1	KIF15	MUC5B	PLCB4	SACS	TACC1	XIAP	ZNF841
AGAP1	C8orf48	DOP1B	GTF2A1	KIF26B	MX1	PLCE1	SAMD13	TANC2	YLPM1	ZNF85
AGAP4	C9orf50	DPY19L1	GTPBP2	KIF7	MYH11	PLEC	SAV1	TANGO6	YY1	ZNF850
AGL	CAPN6	DPY19L2	GUCD1	KIN	MYLK2	PLEKHG2	SBF1	TAOK1	ZBTB10	ZNFX1
AHDC1	CARD6	DRAM1	HAGHL	KLHL11	MYRF	PLEKHG4B	SCAF11	TAOK3	ZBTB17	ZNRF1
AHI1	CASTOR3	DST	HAND1	KLHL36	NABP1	PLEKHG5	SCAI	TAS2R14	ZBTB43	ZNRF3
AHSA2P	CBR4	DSTYK	HAO1	KLHL42	NACC2	PLEKHH1	SCARB2	TASOR	ZBTB47	ZSCAN21
AK8	CCDC103	DUS2	HAUS1	KLKB1	NAIP	PLEKHH3	SCN10A	TATDN2	ZBTB5	ZSCAN31
AKAP13	CCDC12	DYNAP	HCLS1	KMT2A	NAPB	PLGLB1	SCN8A	TBC1D24	ZBTB7A	ZSWIM3
AKIRIN2	CCDC122	DZIP1	HDAC4	KMT2B	NAV1	PLXNB1	SCT	TBC1D3B	ZBTB9	ZSWIM6
AKNAD1	CCDC144A	DZIP1L	HEATR5A	KMT2C	NAV2	PM20D2	SDHAF1	TBPL2	ZC2HC1C	ZZEF1
ALB	CCDC167	EDEM1	HECTD1	KMT2D	NBPF1	PMEPA1	SEC61A2	TCF20	ZC3H12C	
ALG6	CCDC186	EDN2	HELB	KMT2E	NBPF6	PNPLA3	SEPSECS	TCF3	ZC3HAV1	
ALMS1	CCDC71	EFCAB14	HIC2	KMT5C	NBPF9	POLD1	SESN1	TCP11L1	ZCCHC14	
ALPL	CCDC74B	EFCAB7	HIP1	KRIT1	NCKAP5	POLG	SESTD1	TEAD3	ZCCHC2	
AMDHD1	CCDC84	EFHB	HIPK1	KRT14	NCKAP5L	POLQ	SETD5	TENT4A	ZFC3H1	
AMMECR1L	CCDC92	EFNA4	HIPK2	KRT15	NDP	POM121C	SGTB	TET3	ZFP30	
AMN	CCL1	EHHADH	HIST1H1C	KRT24	NEK11	POMK	SH3PXD2A	THAP6	ZFP36L2	
AMOT	CCL11	ELMOD2	HIST1H1D	KRTAP10-3	NEK9	PPM1F	SH3RF2	THRA	ZFP69B	
AMPD3	CCND2	ELMSAN1	HIST1H2AB	L2HGDH	NELFB	PPM1J	SHPK	TIAM1	ZFP90	
ANK3	CCNF	ENKD1	HIST1H2AE	LARP1	NF1	PPP1R16B	SHROOM2	TICRR	ZFX	
ANKEF1	CCNYL1	ENPP4	HIST1H2AI	LARP4B	NFAT5	PPP1R26	SIGLEC16	TIGD5	ZFYVE27	
ANKRD16	CCP110	EP300	HIST1H2AJ	LCOR	NFXL1	PPP1R3B	SIK2	TLN1	ZKSCAN1	
ANKRD18B	CD6	EPHA7	HIST1H2AK	LDHC	NGB	PPP1R9B	SIK3	TMCC1	ZKSCAN4	
ANKRD27	CDC42BPB	EPOP	HIST1H2BB	LENG9	NHSL1	PPP2CB	SIPA1L2	TMEFF1	ZKSCAN5	
ANKRD33B	CDC42EP4	ERC1	HIST1H2BD	LGALS9C	NIPAL1	PPP4R3A	SIX4	TMEM105	ZMYND12	
ANKRD36C	CDH19	ERCC6L2	HIST1H2BG	LIMD1	NKD2	PPP6R1	SKI	TMEM129	ZNF124	
ANKRD50	CDH6	ESAM	HIST1H2BJ	LINC00550	NKX6-1	PRAG1	SKIV2L	TMEM131L	ZNF133	
ANKRD52	CDK19	ETV3	HIST1H2BL	LINC00649	NLGN2	PRDM2	SLAIN1	TMEM141	ZNF14	
ANKRD54	CDK6	ETV3L	HIST1H3D	LINC01126	NLRX1	PRELID3A	SLC16A5	TMEM170A	ZNF141	
ANKRD63	CELSR1	EVA1A	HIST1H3H	LINC01561	NMRK1	PRKAA2	SLC16A9	TMEM260	ZNF2	
AP1S3	CENPO	EVC	HIST1H4A	LINC01711	NOD1	PRKCD	SLC17A4	TMEM265	ZNF200	
APC	CENPS-CORT	EVI5L	HIST1H4I	LINC02591	NOL3	PRKCE	SLC23A2	TMEM81	ZNF205	
API5	CEP135	EXPH5	HIST2H2AA3	LIPT2	NOTCH2	PRKDC	SLC25A2	TMIGD2	ZNF222	
APPL2	CEP164	F11-AS1	HIST2H2AA4	LMNTD2	NOX4	PRR12	SLC25A29	TMPRSS13	ZNF223	
ARFGEF1	CEP170	FAAP100	HIST2H2AB	LNPEP	NPAS3	PRR18	SLC2A11	TNC	ZNF229	
ARFGEF3	CEP170B	FAM102A	HIST2H2BE	LOC100506639	NPAS4	PRR34	SLC2A4RG	TNFAIP6	ZNF233	
ARHGAP31	CEP72	FAM122B	HIST2H3D	LOC101928168	NPIPA1	PRRC2A	SLC35F5	TNFRSF10D	ZNF250	
ARHGAP35	CERS1	FAM167A	HIST2H4A	LOC101928841	NPIPA3	PRRC2C	SLC36A4	TNKS	ZNF254	
ARHGAP45	CES3	FAM172A	HIST2H4B	LOC389834	NPIPA5	PRRG4	SLC7A1	TNP2	ZNF260	
ARHGEF12	CFAP46	FAM182B	HIST3H2A	LOC646938	NPIPA7	PRRT1	SLC9A1	TNRC18	ZNF284	
ARHGEF17	CFH	FAM20C	HIVEP2	LPCAT1	NPIPB11	PRTG	SLCO5A1	TNRC6A	ZNF285	
ARHGEF4	CFI	FAM214A	HOOK3	LRCH2	NPIPB13	PRY	SLITRK2	TNRC6B	ZNF287	
ARID1A	CGAS	FAM222A	HOXA-AS3	LRIG1	NPIPB3	PSME4	SLURP1	TOB2	ZNF319	
ARID2	CHCHD6	FAM243A	HOXA2	LRRC10B	NPIPB4	PTGFR	SLX4	TOP2B	ZNF322	
ARID4A	CHD4	FAM76B	HOXA6	LRRC23	NPIPB5	PTPDC1	SLX4IP	TP53I13	ZNF37A	
ARMC4	CHFR	FAM78A	HOXB5	LRRC37A2	NPLOC4	PTPN14	SMCHD1	TP53TG5	ZNF394	
ARNT2	CHRFAM7A	FAM83B	HOXB6	LRRC57	NPPA	PTPN21	SMO	TPH1	ZNF404	
ARR3	CHRNG	FAM83F	HPDL	LRRC58	NR1H2	PTPRD	SMURF1	TPRG1L	ZNF407	
ARRDC2	CHST3	FAM83G	HSPA12A	LTBP4	NR2F1	PTPRG	SNPH	TPRN	ZNF415	
ARRDC4	CHST6	FAN1	HSPG2	LYNX1	NRSN2-AS1	PURB	SNX25	TPST1	ZNF416	
ARSG	CHST9	FASTKD3	ICA1L	LZTS1	NSD1	PUS3	SNX33	TPTE	ZNF417	
ARTN	CHSY1	FBLN7	ICAM4	MACROD1	NSUN5P1	PVRIG	SOCS2	TRAF3	ZNF420	
ASAP1	CIT	FBXL19	IFFO1	MAFK	NT5C1B	PWP2	SOGA1	TRAF3IP1	ZNF432	
ASAP2	CLLU1OS	FBXL20	IFT74	MAGEA12	NT5DC3	QSOX2	SOGA3	TRAF5	ZNF445	
ASH1L	CLN8	FBXO25	IFT88	MAGI1	NT5M	QTRT2	SON	TRAK1	ZNF460	
ASMTL	CMC1	FBXW7	IGFN1	MAN1A1	NUAK1	R3HCC1L	SOS1	TRAPPC8	ZNF468	
ASPM	CNST	FCRL4	IKBKG	MAN1C1	OR11L1	RAB12	SOS2	TRERF1	ZNF470	
ATAD2B	CNTF	FDXACB1	IL10RB	MAN2C1	OR2T27	RAB20	SOX11	TRIB2	ZNF483	
ATG10	CNTLN	FEM1A	IL15	MAP2K7	OR4F15	RAB40C	SOX5	TRIM27	ZNF490	
ATG2B	COA5	FGF1	IL16	MAP3K1	OR51B2	RAD54L2	SP4	TRIM56	ZNF493	
ATP11A	COL12A1	FHDC1	IL17RC	MAP3K4	OR51I1	RALGAPA2	SPANXN3	TRIM6	ZNF507	
ATP11C	COL27A1	FMN1	IL36RN	MAPK7	OR52B2	RANBP3L	SPATA31A3	TRPS1	ZNF512B	
ATP6V1E2	COL5A1	FMNL1	IL6R	MARCH4	OR52D1	RAPGEF1	SPATA46	TRPV1	ZNF517	
ATP9A	COL6A6	FN1	INAFM1	MAST2	OR5M9	RAPH1	SPEN	TRPV4	ZNF518A	
ATR	CPEB2	FNBP1	INAFM2	MAST4	OSBPL5	RASA1	SPG11	TSHZ1	ZNF526	
AZI2	CPOX	FNIP1	INKA2	MBD3	OTUD3	RASA2	SPICE1	TTF2	ZNF549	
B4GAT1	CRAMP1	FOXD1	INO80D	MBD5	OTUD4	RBIS	SPIN3	TTL	ZNF565	
BAG1	CREB3L4	FOXD4L3	INPP4A	MCM10	OXGR1	RBMS1	SPINT1	TTPA	ZNF570	

Supplementary Table 2 (5/9). Downregulated genes in response to metabolic stress ($Log_2FC<-0.265$) in NRAS^{Q61R} mutant cells.

Downregulated in NRAS^{Q61R} and BRAF^{V600E} mutant cells		
ABL2	ITPKB	TRIM41
ADAM23	ITPRID2	TRIM65
ADAMTS16	JMJD4	TRIM66
ADARB1	KIAA2013	TRIO
ADCYAP1R1	KLHL25	TRRAP
AFF1-AS1	KLHL33	TXNIP
ALG12	LMNB2	UBAP1L
AMDHD2	LPO	UBE2O
AMER1	LRIF1	UGGT2
ANGPT4	LTBP2	USP31
ANKRD17	LZTS2	USP40
ANKRD20A3	MAB21L2	USP53
ANKRD36B	MAGEL2	VPS13C
ARAP1	MAPK8IP3	VPS37D
ARHGAP11B	MARC2	WWC1
ARHGAP17	MEX3C	ZBTB18
ARHGAP32	MKI67	ZBTB24
ARHGAP40	MMEL1	ZBTB39
ARHGEF1	MRPL33	ZFHX3
ARHGEF26	MSL1	ZFP69
ATRX	MTLN	ZNF107
AUTS2	MZF1	ZNF142
BBS9	NAA40	ZNF175
BORCS5	NACC1	ZNF275
BTBD7	NANOG	ZNF283
C1QTNF3-AMACR	NBPF10	ZNF292
C22orf46	NBPF14	ZNF304
C2orf81	NBPF8	ZNF316
C8orf58	NCOA6	ZNF318
CAPN10	NEK10	ZNF35
CAPN3	NES	ZNF462
CCL25	NEURL4	ZNF574
CD8B	NLRP1	ZNF624
CDAN1	NPIPB6	ZNF646
CDC42BPA	NPIPB8	ZNF652
CDKL1	NPIPB9	ZNF730
CDKN1B	NPL	ZNF774
CEP97	NR2C2	ZNF775
CERK	OGA	ZNF777
CHGA	OPRL1	
CHRM4	PCDHB9	
CMTM4	PGAP1	
CNKSR3	PGBD2	
CNPY1	PHOSPHO2-KLHL23	
CRB1	PI4KB	
CSF1R	PIF1	
CUX1	PIK3R4	
DCST1	PLD5	
DDHD1	PLEKHM3	
DDR1	PNLIPRP2	
DEFB113	PRDM11	
DIAPH1	PROSER2	
DLEU2	PRR14L	
DMPK	PRRG2	
DMRTA1	PRSS53	
DOCK4	PSG5	
DOP1A	PTPRJ	
DUSP19	PTPRU	
DUSP7	PUS7L	
DVL1	PYM1	
DYNC2LI1	PZP	
E2F8	RBP3	
EDRF1	RC3H2	
EFNA1	RDH5	
EFNB1	REL	
EFNB2	RNASEL	
ELFN1	RNF145	
ELP1	RNF180	
FAM156B	ROPN1L	
FAM160B1	RPS6KC1	
FAM200A	SARM1	
FANCF	SCG2	
FBXO30	SCUBE2	
FGD4	SEMA3B	
FLVCR1	SERPINA11	
FUT2	SERTAD3	
FUT3	SETD1B	
GATA5	SFMBT2	
GATAD1	SLC25A35	
GK5	SLC29A4	
GOLGA8H	SLC4A5	
GPR135	SMCR8	
GRIP1	SNX15	
GSC	SNX27	
HABP4	SNX9	
HARBI1	SPATA13	
HAUS5	SPATA2	
HCP5	SPATA2L	
HERC2P3	STAG3L1	
HIST1H1B	SYNGAP1	
HIST1H2BM	TAB2	
HIST1H3A	TAF1A	
HIVEP3	TBC1D3	
HMGXB3	TBC1D3L	
HRCT1	TBX15	
HTT	TCAF2	
IFFO2	TMEM200A	
IL18BP	TMEM273	
INPP5J	TOB1	
IRF2BPL	TRAF1	

Supplementary Table 2 (6/9). Downregulated genes in response to metabolic stress ($Log_2FC<-0.265$) in NRAS^{Q61R} and BRAF^{V600E} mutant cells.

Downregulated in BRAF^{V600E} mutant cells											
A2ML1	AK7	ASH1L-AS1	C11orf53	CATSPER2	CES5A	CRBN	DICER1	EME2	FCAMR	GJB1	HIPK4
AACSP1	AK9	ASNA1	C12orf10	CATSPERG	CFAP206	CREB3L1	DIMT1	EMILIN2	FCGR3B	GJB7	HIST1H1A
AANAT	AKAP11	ASPRV1	C12orf49	CAV3	CFAP43	CREB5	DIO3	EML1	FCRL3	GJC2	HIST1H2AM
AASDH	AKAP6	ASXL2	C12orf57	CBFA2T2	CFAP45	CREBL2	DIPK1B	EML4	FCRLA	GJD2	HIST1H4C
ABCB1	AKAP7	ATAD2	C12orf71	CBWD1	CFAP61	CRLF3	DIPK2B	ENDOV	FDPS	GLCE	HIST1H4E
ABCB11	AKIP1	ATE1	C12orf73	CBWD5	CFAP73	CRTAP	DIRAS2	ENGASE	FEM1C	GLI2	HIST1H4G
ABCC10	AKR1B1	ATF2	C12orf76	CC2D2A	CFD	CRTC3	DIRC1	ENKUR	FEN1	GLIPR1L2	HIST3H3
ABCC2	AKR1C2	ATF6	C15orf32	CCDC116	CFHR5	CRYGB	DISP2	ENO1	FERMT3	GLIPR2	HIST4H4
ABCC8	AKR7A2	ATG13	C15orf39	CCDC120	CFL1	CRYL1	DKC1	ENPP5	FEZ1	GLMN	HJURP
ABCE1	AKT1	ATG4A	C15orf41	CCDC126	CH25H	CSAG3	DKFZp779M0652	ENTPD1	FEZF1	GLP1R	HK3
ABCF2	AKT3	ATL3	C15orf56	CCDC127	CHAF1B	CSDE1	DKK1	ENTPD5	FGD1	GMFB	HKDC1
ABCG2	ALDH1A2	ATMIN	C15orf61	CCDC13	CHAMP1	CSF2RB	DLAT	ENTPD6	FGF13	GMFG	HLA-A
ABHD14A	ALDH1L1	ATN1	C16orf54	CCDC136	CHCHD10	CSK	DLC1	EPHA5	FGF16	GML	HLA-C
ABHD17C	ALDH3A1	ATOX1	C16orf92	CCDC14	CHCHD4	CSMD2	DLL3	EPHB4	FGF23	GMNN	HLA-DMB
ABHD18	ALDH3B1	ATP11AUN	C17orf102	CCDC146	CHD6	CSN3	DLX6	EPHX4	FGF4	GMPPB	HLA-DOA
ABITRAM	ALDH7A1	ATP11B	C17orf58	CCDC151	CHD8	CSPG5	DMAP1	EPPIN	FGF5	GMPR	HLA-DQB1
ABLIM2	ALG1	ATP1A1	C17orf82	CCDC154	CHI3L2	CSRNP3	DMBT1	EPS8L3	FGFR3	GMPR2	HLTF
ABLIM3	ALG10	ATP2B1	C19orf24	CCDC160	CHIT1	CST3	DMRTA2	EREG	FGL2	GMPS	HMG20B
ABO	ALG13	ATP5F1A	C19orf73	CCDC162P	CHKB	CST6	DNAH12	ERI2	FIG4	GNB1	HMGA2-AS1
ABT1	ALG14	ATP5IF1	C1GALT1C1	CCDC166	CHKB-CPT1B	CST8	DNAH3	ERICH4	FILIP1	GNB3	HMGCS1
ACAA1	ALG1L2	ATP5MC1	C1orf109	CCDC178	CHMP4C	CST9L	DNAH5	ERICH6	FKBP1A	GNL1	HMGN2
ACAA2	ALG8	ATP5MD	C1orf131	CCDC179	CHORDC1	CSTB	DNAI1	ERLIN2	FKBP1A-SDCBP2	GNLY	HMGN3
ACACB	ALG9	ATP5MGL	C1orf158	CCDC18	CHPF2	CSTF2	DNAJB8	ERMN	FKBP2	GNPDA2	HMX3
ACBD4	ALKBH3	ATP5PD	C1orf185	CCDC190	CHRD	CSTL1	DNAJC12	ERMP1	FKBP6	GNPNAT1	HNF1A
ACE	ALOX12B	ATP5PF	C1orf229	CCDC25	CHRNA3	CT47A10	DNAJC15	ERP27	FKBP8	GNRH2	HNF4A
ACHE	ALPK2	ATP6AP1	C1orf74	CCDC28B	CHST7	CT47A12	DNAJC16	ESCO1	FLJ30679	GOLGA6L9	HNMT
ACIN1	ALX4	ATP6V0A4	C1orf87	CCDC34	CHTF8	CT47A3	DNAJC2	ESF1	FLRT1	GOLGA8A	HNRNPA1L2
ACKR4	AMBN	ATP6V0E1	C1QBP	CCDC36	CINP	CT47A6	DNAJC27	ESYT3	FLT3	GOLGA8B	HNRNPD
ACLY	AMBP	ATP6V1B2	C1QTNF8	CCDC39	CIR1	CT47A7	DNAJC28	EVX1	FLT4	GOLGA8F	HNRNPLL
ACOT1	AMD1	ATP6V1E1	C20orf197	CCDC58	CITED1	CT47A9	DNAJC9	EXOC3-AS1	FLYWCH1	GP1BA	HOMEZ
ACOT12	AMH	ATP8B1	C20orf202	CCDC85B	CITED4	CT62	DNAL1	EXOC4	FMNL2	GPATCH2	HORMAD1
ACOT4	AMN1	ATP8B3	C20orf203	CCDC88B	CKAP2L	CTAG1B	DND1	EXOC6	FMO2	GPATCH3	HOXA4
ACOT6	ANAPC15	ATPAF2	C22orf31	CCDC90B	CKLF	CTAGE15	DNMBP	EXOSC1	FOSL1	GPHB5	HOXA7
ACOT7	ANKRD11	ATRAID	C2CD2L	CCDC91	CKMT1B	CTBS	DNTTIP1	EXOSC10	FOXB2	GPIHBP1	HOXB-AS3
ACSBG2	ANKRD18A	AUNIP	C2CD4B	CCK	CKS2	CTDSP1	DOCK8	EXOSC2	FOXD4	GPN1	HOXB13
ACSL1	ANKRD20A4	AURKB	C2orf16	CCKBR	CLC	CTSB	DOCK8-AS1	EXOSC4	FOXI3	GPN3	HOXB3
ACSL3	ANKRD22	AURKC	C2orf42	CCL16	CLCA2	CTSL	DOK3	EYA2	FOXJ1	GPNMB	HOXC12
ACSL6	ANKRD30A	AVEN	C2orf68	CCL27	CLCF1	CTSS	DOK5	EYS	FOXN3	GPR143	HPS1
ACSM1	ANKRD61	AVIL	C3orf18	CCL7	CLCN1	CUL4A	DOLPP1	EZHIP	FOXN4	GPR148	HPS5
ACSM4	ANKS1A	AVP	C3orf20	CCNB1IP1	CLCNKA	CUL4B	DOT1L	EZR	FOXO3	GPR156	HRH1
ACSM5	ANLN	AXDND1	C3orf22	CCND1	CLCNKB	CWH43	DPAGT1	F10	FOXP1	GPR158-AS1	HRH4
ACTG1	ANP32B	AXIN2	C3orf70	CCNE2	CLDN12	CXCL1	DPEP2NB	F12	FOXR1	GPR173	HS3ST3A1
ACTL10	ANXA5	B2M	C3orf80	CCNL2	CLDN15	CXCL17	DPH1	F2	FOXRED2	GPR176	HS3ST6
ACTL6B	ANXA7	B3GNT3	C3orf85	CCNQ	CLIC1	CXorf49B	DPH2	F7	FPGS	GPR179	HSBP1
ACTN3	AOAH	B3GNT9	C4BPB	CCR4	CLIC3	CXorf51A	DPH3	FAAH	FRAS1	GPR50	HSD17B1
ACVR2A	AOX1	B4GALNT1	C4orf47	CCR9	CLIC5	CXXC4	DPH5	FADD	FRAT1	GPRIN2	HSD17B10
ACY3	AP2B1	B4GALT2	C5AR1	CCSER1	CLIC6	CYB561A3	DRAM2	FAF2	FRG2	GPRIN3	HSD17B13
ACYP1	AP3M1	BAALC	C5orf15	CCT2	CLIP4	CYB561D1	DRC7	FAHD2B	FRMD4A	GPS1	HSD17B6
ADAM2	AP5Z1	BABAM2	C5orf22	CCT5	CLLU1	CYB561D2	DRG1	FAIM2	FRMPD2	GPX8	HSD3B1
ADAM21	APELA	BAG3	C5orf38	CCT6A	CLMN	CYB5A	DRICH1	FAM110C	FRMPD3	GRAMD2B	HSD3B2
ADAM30	APLP2	BAG5	C5orf63	CCT7	CLP1	CYB5R1	DSCAML1	FAM118B	FRRS1L	GREB1	HSDL1
ADAMTS1	APOA5	BAIAP2L2	C6orf136	CCZ1	CLPB	CYBA	DSE	FAM120AOS	FSD1	GRHPR	HSF4
ADAMTS12	APOBEC3D	BCAP31	C6orf141	CD163L1	CLPSL2	CYC1	DSG1	FAM136A	FSIP2	GRID2IP	HSPA13
ADAMTS13	APOE	BCAR3	C6orf223	CD24	CLSTN2	CYP26A1	DSN1	FAM13C	FTCDNL1	GRIK1-AS2	HSPA1L
ADAMTS17	APOLD1	BCAS1	C6orf226	CD300LD	CLUL1	CYP27C1	DSPP	FAM151B	FTL	GRIN3A	HSPA4L
ADAMTS19	AQR	BCDIN3D	C6orf99	CD33	CMAS	CYP2A13	DTD1	FAM153CP	FTSJ1	GRM5	HSPA8
ADAMTSL2	ARAP2	BCL2L1	C7	CD3D	CMKLR1	CYP2B6	DTWD1	FAM162A	FUNDC2	GRSF1	HSPA9
ADAMTSL3	ARC	BCL2L11	C7orf61	CD3E	CMTM1	CYP2C18	DTX2	FAM168B	FUT10	GSDMC	HSPB6
ADAP2	ARCN1	BCL2L13	C7orf66	CD3EAP	CNGB1	CYP2C8	DUOX2	FAM171A1	FUT4	GSPT2	HSPD1
ADAT1	ARF1	BCS1L	C8A	CD47	CNIH4	CYP3A5	DUS4L	FAM171B	FXR1	GSTM1	HSPE1
ADCK1	ARF4	BDKRB2	C8orf74	CD5	CNKSR1	CYP7A1	DUSP11	FAM174B	FZD1	GSTO2	HTATIP2
ADCK5	ARFGAP3	BEAN1-AS1	C9orf131	CD55	CNN2	CYTL1	DUSP13	FAM185A	FZD10	GTF2E1	HTR1D
ADCY1	ARFGEF2	BEST1	C9orf135-DT	CD63	CNOT7	DAAM2	DUSP15	FAM186B	G3BP1	GTF2E2	HTR3B
ADCY3	ARHGAP1	BET1	C9orf152	CD79A	CNP	DAZ2	DUSP21	FAM189A2	G6PC3	GTF2IRD1	HTR3D
ADGRA1	ARHGAP21	BEX4	C9orf64	CD8A	CNTN3	DBH	DUT	FAM205A	GAB4	GTF2IRD2	HTR5A
ADGRF5	ARHGAP22	BHLHE40	C9orf78	CD99L2	CNTN6	DBR1	DUX4	FAM207A	GABBR1	GTF3A	HYDIN
ADGRG1	ARHGAP30	BIN3-IT1	CA12	CDC42EP5	CNTNAP1	DCAF11	DVL3	FAM215A	GABRQ	GTF3C6	IAPP
ADGRG5	ARHGAP4	BLACE	CA7	CDCA3	COA3	DCAF15	DYNLL1	FAM216A	GABRR1	GUCY1A2	ICMT
ADGRL4	ARHGEF10	BLOC1S5-TXNDC5	CA9	CDCA8	COA7	DCST2	DYNLL2	FAM219B	GADD45B	GUCY1B1	ICOSLG
ADH1C	ARHGEF2	BLOC1S6	CABP1	CDH17	COBL	DCT	DYRK4	FAM222B	GAK	GUSBP2	ID1
ADH6	ARHGEF35	BMP2K	CABS1	CDH24	COG3	DCTD	E2F2	FAM229A	GALNT12	GVQW3	ID2
ADIPOR2	ARHGEF37	BMP5	CACNA1D	CDH5	COL13A1	DDT	EBLN2	FAM24B	GALNT6	GYG1	IDH1
ADM2	ARHGEF40	BMP8A	CACNA1E	CDHR1	COL15A1	DDX17	EBP	FAM25G	GANAB	GYS1	IDI1
ADM5	ARHGEF5	BMPER	CACNA1G	CDK10	COL26A1	DDX23	ECHDC1	FAM30A	GANC	GZMM	IDNK
ADORA3	ARHGEF7	BMPR1A	CACNA2D3	CDK14	COL4A3BP	DDX31	EDARADD	FAM47A	GAPDH	H1FX	IDUA
ADPGK	ARHGEF9	BNC1	CACNG4	CDK2	COL4A4	DDX49	EDC3	FAM50A	GAS6	H2AFB1	IER2
ADPRHL1	ARID1B	BNC2	CACNG5	CDK2AP1	COL5A2	DDX53	EDN1	FAM53C	GATB	H2AFJ	IER3
ADPRHL2	ARID4B	BOC	CALCB	CDK5RAP1	COL8A1	DECR1	EEF1E1	FAM71F2	GBA	H2AFZ	IFI35
ADRA1A	ARL2-SNX15	BOLA2	CALCOCO1	CDK7	COMMD5	DEF6	EEF1G	FAM76A	GBP3	H3F3B	IFI6
ADRA2A	ARL3	BORA	CALHM1	CDK8	COPS8	DEFA1	EFCAB2	FAM83A	GBP6	HAAO	IFITM2
ADRB1	ARL4C	BORCS6	CALHM5	CDKN2A	COQ4	DEFA1B	EFNA5	FAM86B2	GCC2	HABP2	IFITM3
AEBP2	ARL5B	BPIFB2	CALR	CDKN2AIP	COQ7	DEFA3	EGLN1	FAM86C1	GCK	HACD3	IFITM5
AEN	ARL6	BRD9	CAMK2A	CDKN2C	COQ8B	DEFA4	EGR4	FAM91A1	GCLM	HAS1	IFNA13
AFG1L	ARMH1	BRDT	CAMK2G	CDNF	COTL1	DEFB124	EI24	FAM98A	GCNT3	HAS2	IFNA2
AGAP9	ARNT	BRIP1	CAMK4	CDR1	COX4I2	DEFB125	EID1	FANCD2OS	GCSAML	HAUS2	IFNL1
AGBL4	ARPC2	BRIX1	CAMLG	CDT1	COX6C	DEFB128	EID2B	FANCG	GDAP1L1	HAX1	IFT46
AGER	ARPC4	BROX	CAMTA2	CDYL	COX7C	DEFB4B	EIF1AY	FAR1	GDAP2	HBE1	IFT57
AGGF1	ARRDC3	BSG	CANX	CEACAM19	COX8A	DEK	EIF2B3	FAR2	GDF11	HBQ1	IGF1
AGPAT1	ARRDC5	BSN	CAP1	CEACAM21	CPA5	DENND1C	EIF3H	FASTKD2	GDF15	HBS1L	IGF2BP2
AGPAT2	ARSF	BTBD19	CAPN12	CEACAM8	CPLANE1	DENND2D	EIF4A2	FAT3	GDPD3	HCFC1R1	IGF2R
AGPAT5	ARV1	BTBD6	CAPN2	CEBPB	CPNE3	DENND3	EIF4EBP1	FBH1	GEMIN6	HCG22	IGFL4
AGTRAP	ASAP3	BTG3	CAPNS2	CEBPG	CPNE4	DENND5B	EIF4G3	FBLL1	GFI1B	HEATR6	IGIP
AGXT	ASB15	BTLA	CAPS2	CELF4	CPNE6	DEPTOR	ELL	FBN3	GFPT1	HECW1	IGLL5
AGXT2	ASB5	BTN2A2	CAPZA1	CENPK	CPPED1	DGAT2L6	ELL2	FBXL12	GFRA1	HELQ	IKZF2
AHCYL1	ASB6	BTN3A3	CARD19	CENPU	CPQ	DGKB	ELMO3	FBXL17	GGN	HES1	IL12RB2
AHRR	ASB7	BUB1	CARD9	CEP104	CPSF6	DGKI	ELN	FBXL18	GGT1	HEXIM2	IL17RA
AHSA1	ASCC1	BUD31	CASC4	CEP19	CPT1B	DGUOK	ELOC	FBXL7	GGT6	HEY1	IL17RD
AIFM2	ASF1B	BZW2	CASP4	CEP85	CPXM2	DHFR	EMC4	FBXO11	GHITM	HIGD1C	IL17REL
AIG1	ASGR1	C11orf24	CASP6	CERS4	CRACR2B	DHX29	EMC6	FBXO34	GIT1	HINT1	IL19
AK1	ASGR2	C11orf44	CASQ1	CERS5	CRB2	DHX37	EMC9	FBXO44	GIT2	HIPK3	IL20RB

Supplementary Table 2 (7/9). Downregulated genes in response to metabolic stress ($Log_2FC<-0.265$) in BRAF^{V600E} mutant cells.

Downregulated in BRAF^{V600E} mutant cells											
IL21	KLRG2	LOC100506403	ME2	MRVI1	NEU1	OSTN	PJA1	PRELP	RAPGEF5	RPL35	SFTA2
IL22RA1	KPNA6	LOC100506422	MEAF6	MS4A2	NEURL1B	OTOG	PKD1	PRIMPOL	RASAL1	RPL36A	SFXN2
IL27	KPNB1	LOC101927178	MEAK7	MS4A7	NEUROD1	OTOP2	PKDCC	PRKCG	RASD2	RPL36AL	SFXN5
IL27RA	KRAS	LOC101927322	MECR	MSANTD3	NF2	OTOP3	PKDREJ	PRKCQ	RASL11A	RPL37	SGCB
IL2RG	KRT16	LOC101927844	MED1	MSANTD4	NFKBID	OTUB2	PKIG	PRLHR	RAVER1	RPL38	SGCD
IL31RA	KRT222	LOC101928436	MED10	MST1	NFKBIE	OTUD7B	PKLR	PRM3	RBBP8	RPL41	SGK1
ILDR1	KRT33B	LOC145783	MED15	MSTO1	NFYB	OTX2	PKNOX1	PRNT	RBCK1	RPL5	SGMS1
ILF3	KRT40	LOC149373	MED16	MT1B	NGFR	OXA1L	PLA2G12A	PROS1	RBFA	RPL7	SH2B3
IMMP2L	KRT75	LOC339803	MED17	MT1F	NHLH2	P3H3	PLA2G2D	PROX1	RBFOX1	RPL8	SH2D1B
IMPA1	KRT77	LOC389199	MED18	MT1H	NIBAN3	P3H4	PLA2G4E	PROZ	RBM11	RPLP0	SH2D2A
INHA	KRT84	LOC389895	MED20	MTCH2	NID2	P4HA2	PLA2R1	PRPS1	RBM12	RPLP2	SH3D21
INO80	KRTAP1-5	LOC441155	MED30	MTERF1	NIPBL	P4HA3	PLCD1	PRPS1L1	RBM20	RPRD1B	SHANK2-AS3
INO80C	KRTAP12-1	LOC728743	MED7	MTHFD2	NIT1	P4HTM	PLEK	PRPSAP1	RBM27	RPS13	SHC3
INPP5A	KRTAP19-4	LOC730183	MEF2D	MTMR2	NKX2-8	PABPC1L	PLEKHA1	PRPSAP2	RBM45	RPS15	SHCBP1
INPP5E	KRTAP21-1	LOC79999	MEGF6	MTRF1	NKX3-1	PABPN1L	PLEKHA3	PRR11	RBM5	RPS15A	SHD
INSC	KRTAP21-3	LOXL4	MEIOB	MTRNR2L7	NLRC5	PADI3	PLEKHG6	PRR13	RBM7	RPS16	SHFL
INSL4	KRTAP23-1	LPAR2	MELTF	MTRNR2L8	NLRP4	PAH	PLEKHH2	PRR15L	RBMS3	RPS23	SHH
INSL5	KRTAP24-1	LPAR3	MEOX1	MTRNR2L9	NLRP5	PAK4	PLEKHM2	PRR23A	RBMY1D	RPS26	SHISA5
INSYN1	KRTAP25-1	LPAR4	MEP1A	MTRR	NLRP9	PALLD	PLEKHO1	PRR30	RBMY1F	RPS28	SHKBP1
INTS9	KRTAP26-1	LPAR6	MESP1	MTTP	NMB	PALM2	PLIN1	PRR5L	RBP2	RPS4X	SHOC1
IPP	KRTAP4-1	LRAT	MET	MTX3	NME1	PAM	PLK2	PRRG3	RBP7	RPS6KB2	SHPRH
IPPK	KRTAP4-12	LRGUK	METAP1D	MUC19	NNMT	PANO1	PLK3	PRSS12	RCAN1	RRAGD	SHQ1
IQCC	KRTAP4-2	LRMDA	METTL21A	MUC3A	NOBOX	PANX1	PLPP6	PRSS16	RCAN2	RREB1	SIAE
IRAK4	KRTAP4-4	LRMP	METTL21C	MUCL1	NODAL	PANX2	PLS1	PRSS21	RCCD1	RRM2B	SIAH1
IREB2	KRTAP9-2	LRP5L	METTL2A	MVB12A	NOL11	PANX3	PLSCR2	PRSS22	RCHY1	RRN3	SIGLEC10
IRF2	KRTAP9-8	LRRC18	METTL7A	MYBL2	NOP10	PAQR4	PLXDC1	PRSS27	RCN1	RRP15	SIGLEC6
IRF2BP2	KY	LRRC2	METTL9	MYBPH	NOP56	PAQR8	PLXDC2	PRSS3	RCN2	RRP9	SIK1
IRF7	KYAT1	LRRC26	MEX3D	MYBPHL	NOP58	PARD3B	PLXNA2	PRSS56	RCOR2	RRS1	SIMC1
IRX1	KYAT3	LRRC27	MFAP3L	MYC	NOXRED1	PARL	PMEL	PRUNE2	RDM1	RSF1	SIPA1
ISCA1	L3MBTL4	LRRC3	MFAP5	MYCL	NPBWR1	PARP10	PMFBP1	PSCA	REC8	RSL24D1	SIRPD
ISCU	LALBA	LRRC32	MFGE8	MYDGF	NPC2	PARS2	PNISR	PSG11	RECQL	RSPH9	SIRT5
ISG20L2	LAMA3	LRRC37B	MFSD12	MYEF2	NPDC1	PARVB	PNLIPRP3	PSMA1	RECQL5	RSRC1	SIRT6
ISL1	LAMC3	LRRC46	MFSD14A	MYEOV	NPFFR2	PATE4	PNMA6A	PSMA4	REEP1	RSRP1	SKAP2
ISM2	LAMTOR1	LRRC47	MGAT4D	MYF5	NPHP1	PAX1	PNMT	PSMB1	REN	RTL8A	SLAIN2
ISOC1	LAMTOR3	LRRC6	MGAT5	MYH9	NPHS2	PAX5	PNRC2	PSMB10	REPS1	RTL8C	SLBP
ITGAD	LAMTOR5	LRRC8C	MGAT5B	MYL10	NPIPB15	PAX9	POC1B	PSMB4	REXO1L2P	RTL9	SLC10A3
ITGB7	LANCL1	LRRTM3	MGST1	MYL12A	NPM2	PAXBP1	PODNL1	PSMC5	RFC1	RTN3	SLC10A6
ITK	LAPTM4B	LRRTM4	MICAL1	MYL12B	NPM3	PAXX	PODXL	PSMD10	RFC4	RTN4RL1	SLC12A2
ITLN1	LARP7	LSM6	MICAL2	MYL3	NPPB	PCDHB12	POGK	PSMD11	RFFL	RWDD4	SLC14A1
ITLN2	LARS	LSM8	MICALCL	MYL6B	NPR1	PCDHB15	POGZ	PSMD12	RFT1	S100A11	SLC15A4
ITM2B	LARS2	LTA	MICB	MYL9	NPR2	PCDHB4	POLD3	PSMD2	RFX1	S100A12	SLC15A5
IWS1	LAT	LTB4R	MICU1	MYLIP	NPRL3	PCDHB6	POLE2	PSMD5	RFX6	S100A14	SLC16A6
IZUMO1	LAYN	LTBP3	MID1	MYLK3	NPSR1	PCMTD2	POLR1A	PSTPIP1	RGMB	S100A2	SLC19A3
IZUMO2	LBX2	LTF	MIEF1	MYO15A	NPTX1	PCOLCE-AS1	POLR2C	PTBP1	RGR	S100A7L2	SLC1A1
JADE3	LCA5	LTV1	MILR1	MYO1E	NPY	PCP4	POLR2I	PTCD1	RGS3	S100A8	SLC1A6
JAZF1	LCE2D	LUC7L	MINDY3	MYO3B	NPY4R	PCSK9	POLR3E	PTCHD3	RGS5	S100A9	SLC22A1
JDP2	LCE3E	LUM	MIP	MYO5A	NQO1	PDAP1	POLR3H	PTGDR2	RGS8	S100PBP	SLC22A6
JKAMP	LCN9	LURAP1	MIPOL1	MYO7A	NR0B2	PDCD5	POM121L12	PTGDS	RHBDL3	S1PR4	SLC22A9
KANK3	LCP2	LY6G6C	MIR1247	MYO9B	NR1D2	PDE1A	PON2	PTGFRN	RHBG	SAMD11	SLC23A3
KANSL1L	LDHB	LY6K	MIR17HG	MYOC	NR2C2AP	PDE1B	PON3	PTGR1	RHEB	SAMD9	SLC25A11
KANSL3	LDHD	LYN	MIR22HG	MYOCD	NR3C2	PDE6G	POP1	PTH1R	RHOB	SAP30BP	SLC25A12
KATNAL1	LDOC1	LYSMD4	MIR7162	NAA20	NR4A1	PDE8B	POU1F1	PTN	RHOJ	SAPCD2	SLC25A25
KBTBD12	LEF1	LZTFL1	MIR99AHG	NAA35	NRAS	PDGFB	POU2F1	PTPN2	RHOU	SASH3	SLC25A28
KBTBD3	LEMD1	MAD2L1BP	MLANA	NAA38	NRK	PDHX	POU3F1	PTPN20	RIBC2	SASS6	SLC25A3
KBTBD4	LEMD3	MAF	MLF2	NAAA	NRSN2	PDIA3	POU4F1	PTPN3	RIIAD1	SBDS	SLC25A30
KCNA3	LENEP	MAFB	MLLT10	NADSYN1	NSMCE4A	PDIA6	POU5F1	PTPN7	RIMBP3C	SBK1	SLC25A31
KCNAB1	LENG8	MAGEA10-MAGEA5	MLN	NAGS	NSRP1	PDRG1	POU5F1B	PTPRT	RIMS1	SBK2	SLC25A34
KCNAB2	LEPR	MAGEB1	MMD	NAMPT	NSUN7	PDS5B	POU6F1	PTRH1	RIOK1	SCAF1	SLC25A40
KCNC3	LEXM	MAGEB18	MMP1	NANOS1	NTF4	PDZD7	PP2D1	PTRHD1	RIPK1	SCAF4	SLC25A45
KCND1	LFNG	MAGEB2	MMP10	NANS	NTN4	PDZRN3	PPA1	PTTG1	RIPK2	SCARF1	SLC25A46
KCNF1	LGALS1	MAGED1	MMP11	NAP1L2	NTNG2	PEA15	PPARGC1B	PTTG1IP	RIPPLY2	SCARF2	SLC25A6
KCNG2	LGI1	MALSU1	MMP20	NAT10	NTPCR	PEPD	PPFIA3	PTX3	RIT2	SCGB1C1	SLC26A10
KCNIP2	LGI2	MAMDC2	MMP3	NAT16	NTRK1	PEX11B	PPIAL4A	PUF60	RLIM	SCGB3A2	SLC26A11
KCNJ1	LGI4	MAMSTR	MNT	NAXE	NTS	PEX2	PPIAL4C	PUM1	RLN1	SCGN	SLC26A5
KCNJ3	LGR5	MAN1B1-DT	MOGS	NBEAL1	NUAK2	PEX3	PPIAL4E	PUM3	RMDN1	SCLY	SLC26A9
KCNJ5	LHFPL3	MAN2A2	MORC2	NBEAL2	NUBP1	PFAS	PPIAL4F	PURG	RMDN2	SCML1	SLC2A14
KCNJ8	LIF	MANEA	MORN2	NBN	NUBPL	PFN2	PPIB	PUS7	RMDN3	SCN11A	SLC30A3
KCNK6	LIG3	MAP11	MORN3	NBPF12	NUDT13	PGAM1	PPIE	PVALB	RMND1	SCN2B	SLC33A1
KCNMB2	LILRB1	MAP1A	MPC1	NBPF20	NUDT15	PGGHG	PPIL2	PWP1	RNASE3	SCN4A	SLC35E4
KCNN1	LIN37	MAP3K15	MPDZ	NBR1	NUDT4B	PGGT1B	PPIP5K2	PWWP2A	RNASEH2A	SCNN1D	SLC35F2
KCTD11	LIN54	MAP4K3	MPHOSPH10	NCBP2AS2	NUDT5	PGLYRP4	PPM1M	PYGO2	RNASEK	SCRN3	SLC35F3
KCTD13	LIN9	MAP7	MPP1	NCCRP1	NUDT9	PGM1	PPME1	QPCTL	RNF114	SCYL1	SLC35G4
KCTD20	LINC00222	MAP9	MPP2	NCK1	NUMB	PGPEP1	PPP1R15B	QRICH1	RNF122	SDC1	SLC36A2
KCTD21-AS1	LINC00273	MAPK15	MPP3	NCKAP1	NUP205	PHACTR1	PPP1R18	R3HCC1	RNF123	SDC3	SLC38A4
KCTD5	LINC00494	MAPKBP1	MPP5	NCKAP1L	NUP35	PHACTR2	PPP1R32	RAB11B	RNF165	SDCBP	SLC38A9
KDELR3	LINC00504	MAPRE1	MPST	NCLN	NUP50	PHACTR3	PPP1R3E	RAB13	RNF185	SDHC	SLC39A10
KDM5D	LINC00518	MAPRE3	MPV17	NCOA3	NUP62CL	PHC3	PPP1R3F	RAB27A	RNF186	SDK1	SLC39A6
KHSRP	LINC00525	MARCKS	MPV17L2	NCOA5	NUP85	PHETA1	PPP1R8	RAB27B	RNF222	SDR16C5	SLC39A7
KIAA1257	LINC00552	MARCKSL1	MRFAP1L1	NDN	NUP88	PHF10	PPP2R3B	RAB31	RNF224	SEC22B	SLC3A1
KIAA1586	LINC00598	MARK3	MRM2	NDST2	NVL	PHF11	PPP2R5B	RAB38	RNF43	SEC24B	SLC41A1
KIAA2026	LINC00656	MARS2	MRNIP	NDST4	NXF5	PHF5A	PPP5D1	RAB3C	RNFT2	SELP	SLC44A2
KIF16B	LINC01089	MATN2	MROH5	NDUFA10	NXNL1	PHLDA1	PPTC7	RAB3IL1	RNPEP	SEMA5B	SLC45A3
KIF17	LINC01521	MATN3	MROH6	NDUFA6	NYAP1	PHLDB1	PQLC2L	RAB9A	ROBO3	SENP3	SLC45A4
KIF1C	LINC01537	MBD2	MRPL13	NDUFA8	OAS1	PHRF1	PQLC3	RABEP1	ROGDI	SENP6	SLC47A2
KIF24	LINC02210-CRHR1	MBNL2	MRPL14	NDUFAF1	OAS3	PI4K2B	PRAC2	RABEPK	ROMO1	SEPHS1	SLC4A1AP
KIFC3	LIPF	MBNL3	MRPL24	NDUFB2	OASL	PI4KAP1	PRAMEF1	RABL2B	ROR1	SEPTIN2	SLC4A9
KIR2DS5	LITAF	MBTD1	MRPL40	NDUFB8	OAT	PIANP	PRAMEF4	RAD51AP2	RPAP2	SEPTIN7	SLC5A10
KLF1	LLCFC1	MC2R	MRPL46	NDUFS6	OBP2A	PIDD1	PRAMEF5	RAD51C	RPAP3	SEPTIN9	SLC5A3
KLF17	LLGL1	MCEE	MRPL47	NECTIN1	OCSTAMP	PIGO	PRAMEF6	RAD52	RPARP-AS1	SERINC2	SLC6A12
KLHDC7A	LLPH	MCEMP1	MRPL49	NECTIN4	ODAPH	PIH1D2	PRAMEF9	RADIL	RPEL1	SERPINA2	SLC6A14
KLHDC7B	LMAN2	MCF2L	MRPL58	NEDD1	ODF3L2	PIK3CD	PRB1	RAI1	RPGR	SERPINA7	SLC6A17
KLHL14	LMBRD1	MCFD2	MRPL9	NEDD4L	ODR4	PIK3R6	PRB2	RALGPS1	RPH3AL	SERPINA9	SLC7A6
KLHL22	LMNA	MCHR1	MRPS10	NEFL	OLA1	PIKFYVE	PRB3	RAMP1	RPL10A	SERPINB11	SLC7A8
KLHL31	LMO1	MCTP1	MRPS11	NEK6	OLFM1	PILRB	PRDM14	RAMP3	RPL13A	SERPINB8	SLC9A3R1
KLHL5	LMO2	MCTS1	MRPS12	NEK7	OPN3	PIP	PRDM16-DT	RANBP10	RPL14	SERPINC1	SLCO1B3
KLK12	LMO7DN	MDGA1	MRPS14	NEK8	ORC2	PIP4K2C	PRDM5	RANGRF	RPL18	SERTM1	SLITRK5
KLK14	LOC100130370	MDH1	MRPS21	NELFE	ORMDL3	PIPOX	PRDM8	RAP1A	RPL18A	SF3A1	SLK
KLK4	LOC100287036	MDH2	MRPS22	NELL1	OSBPL11	PITPNM2	PRDX1	RAP2B	RPL22	SFI1	SMARCA4
KLK5	LOC100505549	MDM4	MRPS28	NEMF	OSGIN2	PITRM1	PRDX5	RAPGEF2	RPL23A	SFRP1	SMARCA5
KLK8	LOC100506388	MDP1	MRPS30	NETO2	OSM	PIWIL4	PRDX6	RAPGEF3	RPL26	SFT2D2	SMARCB1

Supplementary Table 2 (8/9). Downregulated genes in response to metabolic stress ($Log_2FC<-0.265$) in BRAF^{V600E} mutant cells.

Downregulated in BRAF^{V600E} mutant cells						
SMC2	STYX	TIMM10	TPO	UBTFL1	YIPF4	ZNF589
SMC3	STYXL1	TIMM10B	TPPP3	UBXN1	YKT6	ZNF599
SMG6	SUCLA2	TIMM21	TPRXL	UBXN2A	YME1L1	ZNF606
SMIM10	SUGT1	TIMP1	TPTEP2	UCK2	YTHDF1	ZNF607
SMIM10L2A	SULT1E1	TIMP4	TRAK2	UCKL1	ZACN	ZNF621
SMIM10L2B-AS1	SUN5	TINAG	TRAM1L1	UCN	ZADH2	ZNF622
SMIM11A	SUPT16H	TIPRL	TRAPPC13	UCP1	ZAP70	ZNF641
SMIM2	SUPT3H	TK2	TRAPPC2	UEVLD	ZBED2	ZNF658B
SMIM25	SURF1	TKTL2	TRAPPC5	UFSP2	ZBED3	ZNF667
SMIM26	SURF2	TLDC2	TRAPPC6B	UGGT1	ZBED6CL	ZNF680
SMIM29	SURF4	TLE1	TREH	UGT2B28	ZBED8	ZNF681
SMIM4	SVEP1	TLK1	TRHR	UGT2B7	ZBTB32	ZNF683
SMIM6	SWSAP1	TLK2	TRIL	UGT3A1	ZBTB33	ZNF687
SMN1	SWT1	TLL2	TRIM13	UNC119B	ZBTB40	ZNF688
SMPD1	SYCE1L	TLNRD1	TRIM17	UNC13C	ZBTB41	ZNF692
SMYD3	SYK	TLR2	TRIM26	UNC93A	ZBTB42	ZNF697
SNAP25	SYNPO2L	TM2D2	TRIM28	UQCR11	ZBTB49	ZNF70
SNAP47	SYT15	TM4SF1-AS1	TRIM31	UQCRH	ZBTB8OS	ZNF701
SND1	SYT9	TM4SF18	TRIM39-RPP21	UQCRHL	ZC3H12A	ZNF705B
SNHG32	SZRD1	TM4SF19-TCTEX1D2	TRIM40	URAD	ZC3H18	ZNF708
SNRNP40	TAF7	TM4SF20	TRIM54	URM1	ZC3H6	ZNF709
SNRNP48	TAF7L	TM7SF2	TRIM6-TRIM34	USF1	ZC3H7B	ZNF718
SNRPA1	TAFA4	TM9SF3	TRIM60	USP10	ZCCHC18	ZNF724
SNRPD2	TANC1	TMCO1	TRIM9	USP15	ZCCHC7	ZNF746
SNRPD3	TANGO2	TMEM114	TRIML1	USP16	ZCRB1	ZNF761
SNRPE	TANK	TMEM132D	TRMT13	USP17L24	ZDHHC1	ZNF764
SNRPN	TARP	TMEM138	TRPA1	USP17L25	ZDHHC11	ZNF765
SNTB2	TARS2	TMEM159	TRPC5	USP17L28	ZDHHC12	ZNF768
SNUPN	TAS2R4	TMEM161B	TRPM8	USP17L7	ZDHHC17	ZNF77
SNX1	TAS2R42	TMEM167A	TSEN34	USP21	ZDHHC19	ZNF773
SNX10	TASP1	TMEM173	TSN	USP27X	ZDHHC3	ZNF780A
SNX11	TATDN3	TMEM178A	TSNARE1	USP34	ZDHHC7	ZNF785
SNX14	TBC1D16	TMEM178B	TSNAX	USP37	ZFP36	ZNF788P
SNX2	TBC1D2	TMEM181	TSNAX-DISC1	USP39	ZFP37	ZNF790
SNX7	TBC1D20	TMEM184A	TSNAXIP1	USP43	ZFP91	ZNF816
SOAT2	TBC1D22A	TMEM187	TSPAN33	USP6NL	ZFP91-CNTF	ZNF829
SOCS3	TBC1D31	TMEM189-UBE2V1	TSPY3	USP8	ZG16	ZNF839
SOD1	TBC1D3C	TMEM191B	TSPY8	USP9X	ZGRF1	ZNF862
SOD2	TBC1D3H	TMEM191C	TSPYL1	VAMP3	ZIC1	ZNF865
SOHLH2	TBC1D3P5	TMEM192	TSPYL5	VANGL1	ZKSCAN7	ZNF879
SORD	TBC1D5	TMEM198	TSSC4	VAPA	ZMAT4	ZNF880
SOST	TBC1D7	TMEM199	TST	VARS	ZMYND8	ZNF90
SOWAHB	TBCD	TMEM200C	TSTD2	VBP1	ZNF10	ZNF91
SOX1	TBL1XR1	TMEM205	TTBK1	VCL	ZNF101	ZNF92
SOX14	TBL3	TMEM206	TTC1	VCP	ZNF131	ZNF98
SOX30	TBP	TMEM209	TTC14	VCPKMT	ZNF157	ZNF99
SPAG5	TBX18	TMEM211	TTC19	VENTX	ZNF174	ZNRF2
SPANXB1	TBXT	TMEM214	TTC21B	VEZT	ZNF182	ZP2
SPATA25	TCEAL4	TMEM220	TTC36	VGLL2	ZNF185	ZPBP2
SPATA3	TCEAL5	TMEM225B	TTC37	VIPR1	ZNF189	ZRANB2
SPATA31A7	TCEANC2	TMEM231	TTC39A	VKORC1	ZNF197	ZSWIM4
SPATA45	TCERG1	TMEM240	TTC8	VMP1	ZNF208	ZSWIM5
SPATA7	TCFL5	TMEM243	TTC9	VN1R2	ZNF211	ZSWIM7
SPC25	TCIM	TMEM244	TTC9B	VN1R5	ZNF217	ZUP1
SPCS2	TCP10L2	TMEM25	TTC9C	VOPP1	ZNF224	ZW10
SPDYE6	TCTA	TMEM267	TTI1	VPREB1	ZNF225	
SPECC1L	TCTE1	TMEM30A	TTI2	VPS13A	ZNF251	
SPG21	TCTEX1D2	TMEM30B	TTK	VPS16	ZNF257	
SPINK4	TDGF1	TMEM35B	TTLL10	VPS4B	ZNF263	
SPIRE1	TDO2	TMEM37	TTLL3	VSIG10L	ZNF264	
SPOPL	TDRD1	TMEM39B	TTLL4	VSIG2	ZNF266	
SPOUT1	TECRL	TMEM41A	TUB	VSTM1	ZNF267	
SPRR2D	TEDDM1	TMEM42	TUBA3C	VTN	ZNF268	
SPRR4	TEKT1	TMEM45A	TUBB	VWA3B	ZNF273	
SPRTN	TEKT2	TMEM52B	TUT1	VWA7	ZNF274	
SPTBN5	TEKT4	TMEM54	TVP23A	WASF2	ZNF276	
SPTLC1	TERF1	TMEM61	TVP23B	WASHC1	ZNF280D	
SPTSSB	TERF2IP	TMEM62	TWF2	WASHC2C	ZNF302	
SRD5A3	TESPA1	TMEM65	TWIST2	WASHC4	ZNF324B	
SRFBP1	TEX26	TMEM69	TXLNB	WDFY1	ZNF329	
SRP14	TEX28	TMEM74	TXN	WDR19	ZNF331	
SRP19	TEX30	TMEM86B	TXN2	WDR35	ZNF337	
SRRM3	TEX46	TMEM97	TXNDC15	WDR41	ZNF33A	
SRRM5	TFAM	TMPRSS11A	TXNDC5	WDR47	ZNF354A	
SSB	TFAP2E	TMPRSS6	TXNDC9	WDR62	ZNF391	
SSBP2	TFCP2	TMSB15A	TYMS	WDR7	ZNF431	
SSC4D	TFCP2L1	TMTC2	TYR	WDR74	ZNF436	
SSH2	TFDP3	TMX1	TYRP1	WDR89	ZNF438	
SSR4	TFEC	TNFRSF13C	TYSND1	WDR92	ZNF440	
SSTR2	TFPT	TNFSF13B	UAP1L1	WDSUB1	ZNF442	
SSTR3	TGFA	TNIP3	UBA52	WFDC10B	ZNF45	
SSX2	TGFB2	TNP1	UBA6	WIPI1	ZNF474	
SSX2B	TGFB3	TNS2	UBAC1	WNK2	ZNF479	
SSX6P	TGIF2	TNXB	UBD	WNK3	ZNF491	
ST13	TGM1	TOGARAM2	UBE2D3-AS1	WNT10B	ZNF492	
ST3GAL4	TGM2	TOMM20	UBE2E1	WNT16	ZNF510	
ST8SIA6	THAP2	TOMM20L	UBE2E3	WSB1	ZNF525	
STAG3L3	THAP7-AS1	TOMM34	UBE2G1	XIRP1	ZNF529	
STAM2	THAP8	TOMM7	UBE2H	XPA	ZNF529-AS1	
STARD5	THBS4	TOMM70	UBE2NL	XPNPEP1	ZNF534	
STARD6	THEG	TOP3A	UBE2Q2L	XPO6	ZNF544	
STATH	THEG5	TOP3B	UBE2S	XPOT	ZNF547	
STK10	THEGL	TOPAZ1	UBE2U	XRCC5	ZNF548	
STK31	THEM6	TOR1A	UBL3	XRCC6	ZNF552	
STK33	THEMIS2	TOR2A	UBL4B	YAE1	ZNF57	
STK36	THNSL1	TOX3	UBL5	YAF2	ZNF572	
STOM	THOC6	TP53INP1	UBLCP1	YARS	ZNF576	
STX17	THSD4	TP53TG3D	UBQLN3	YDJC	ZNF582	
STXBP2	TIAM2	TP73-AS1	UBQLN4	YEATS2	ZNF585A	
STYK1	TIGD2	TPBG	UBR5	YIF1B	ZNF587B	

Supplementary Table 2 (9/9). Downregulated genes in response to metabolic stress ($Log_2FC<-0.265$) in BRAF^{V600E} mutant cells.

		SKMel103				*UACC903*			
Protein	**Description**	**High Gluc.**	**w/o Gluc.**	**High Gluc. + SF**	**w/o Gluc. + SF**	**High Gluc.**	**w/o Gluc.**	**High Gluc. + SF**	**w/o Gluc. + SF**
ACTB	Actin, cytoplasmic 1	0	21	4	11	3	4	3	5
AHNAK	Neuroblast differentiation-associated protein AHNAK	0	0	0	0	5	7	12	6
AKAP2	A-kinase anchor protein 2	17	8	11	5	0	0	2	0
ALB	Serum albumin	8	0	4	14	15	2	5	7
ANXA2	Annexin A2	0	12	1	6	0	0	0	0
ATXN2	Ataxin-2	1	13	3	9	6	6	6	5
ATXN2L	Ataxin-2-like protein	26	31	25	27	49	44	52	38
BAG3	BAG family molecular chaperone regulator 3	115	55	102	80	114	111	121	117
BCLAF1	Bcl-2-associated transcription factor 1	40	28	42	12	36	36	29	21
BRD4	Bromodomain-containing protein 4	19	16	19	21	17	17	18	14
C20orf27	UPF0687 protein C20orf27	10	16	8	11	4	7	5	6
CALM1	Calmodulin-1	20	14	21	21	17	19	17	19
CALU	Calumenin	4	0	6	2	8	9	10	10
CAMSAP2	Calmodulin-regulated spectrin-associated protein 2	1	11	1	9	0	0	0	0
CASC3	Protein CASC3	15	10	15	11	12	11	15	14
CCAR2	Cell cycle and apoptosis regulator protein 2	8	29	7	0	5	6	4	4
CCDC50	Coiled-coil domain-containing protein 50	53	29	53	47	47	46	55	53
CCDC6	Coiled-coil domain-containing protein 6	24	22	30	34	7	9	12	22
CCDC9	Coiled-coil domain-containing protein 9	18	8	19	14	16	14	14	20
CCDC97	Coiled-coil domain-containing protein 97	6	6	11	5	6	7	7	6
CCT2	T-complex protein 1 subunit beta	0	12	0	3	0	0	0	0
CDC37	Hsp90 co-chaperone Cdc37	10	7	10	10	6	7	9	8
CDK11B	Cyclin-dependent kinase 11B	0	16	3	16	0	0	2	0
CDK12	Cyclin-dependent kinase 12	2	17	3	0	5	5	5	4
CEP170	Centrosomal protein of 170 kDa	14	27	16	7	45	45	38	42
CEP55	Centrosomal protein of 55 kDa	8	5	11	6	9	11	16	15
CKAP4	Cytoskeleton-associated protein 4	32	35	32	37	30	32	32	33
CKS2	Cyclin-dependent kinases regulatory subunit 2	11	11	12	8	9	6	7	6
CLPB	Caseinolytic peptidase B protein homolog	0	10	0	2	0	0	0	0
CNN2	Calponin-2	7	2	7	2	11	5	9	3
CORO1C	Coronin-1C	1	14	2	8	0	0	0	0
CPSF6	Cleavage and polyadenylation specificity factor subunit 6	18	24	18	15	16	18	18	15
CPSF7	Cleavage and polyadenylation specificity factor subunit 7	12	18	11	13	13	14	10	11
CSRP2	Cysteine and glycine-rich protein 2	12	11	13	9	2	4	2	6
CSTF2	Cleavage stimulation factor subunit 2	11	6	13	9	7	5	10	6
CTTN	Src substrate cortactin	69	65	78	69	83	75	82	75
CWC22	Pre-mRNA-splicing factor CWC22 homolog	4	12	3	16	4	4	2	2
CYR61	Protein CYR61	45	31	36	30	15	11	13	18
DAP	Death-associated protein 1	19	8	17	11	2	5	5	10
DBR1	Lariat debranching enzyme	6	15	5	12	4	3	3	4
DDX1	OS=Homo sapiens OX=9606 GN=DDX1 PE=1 SV=2	0	16	0	6	2	3	1	1
DDX18	ATP-dependent RNA helicase DDX18	0	13	0	5	0	0	0	0
DDX3X	ATP-dependent RNA helicase DDX3X	0	32	0	16	0	1	0	0
DDX42	ATP-dependent RNA helicase DDX42	21	46	19	44	24	24	22	22
DDX47	Probable ATP-dependent RNA helicase DDX47	1	15	1	6	0	0	0	0
DDX6	Probable ATP-dependent RNA helicase DDX6	3	24	1	7	1	2	1	1
DHX15	Pre-mRNA-splicing factor ATP-dependent RNA helicase DHX15	6	50	5	20	2	2	2	3
DHX30	ATP-dependent RNA helicase DHX30	0	15	0	1	0	0	0	0
DHX36	ATP-dependent DNA/RNA helicase DHX36	1	20	0	5	1	2	0	1
DHX38	Pre-mRNA-splicing factor ATP-dependent RNA helicase PRP16	0	21	0	12	0	2	0	1
DNAJA1	DnaJ homolog subfamily A member 1	16	10	14	13	14	17	17	24
DNAJB11	DnaJ homolog subfamily B member 11	6	7	4	3	8	13	10	10
ECM1	Extracellular matrix protein 1	18	6	16	11	44	41	49	48
EEF1A1	Elongation factor 1-alpha 1	17	24	19	25	21	16	17	13
ELAVL1	ELAV-like protein 1	3	12	1	7	0	1	1	1
ELOA	Elongin-A	6	11	7	6	11	11	13	11
FAU	40S ribosomal protein S30	6	6	7	6	10	9	11	11
FIP1L1	Pre-mRNA 3'-end-processing factor FIP1	21	13	21	8	30	33	29	18
FUBP1	Far upstream element-binding protein 1	9	3	13	7	4	5	5	4
GAPDH	Glyceraldehyde-3-phosphate dehydrogenase	7	12	8	5	8	9	6	5
GPATCH4	G patch domain-containing protein 4	11	7	6	3	21	22	20	10
GPNMB	Transmembrane glycoprotein NMB	0	0	0	0	11	12	8	9
GRN	Granulins	26	18	21	19	31	30	33	29
HEXIM1	Protein HEXIM1	16	12	12	16	32	22	27	32
HEXIM2	Protein HEXIM2	4	0	4	2	10	12	15	12
HLA-DRB1	HLA class II histocompatibility antigen, DRB1-1 beta chain	0	2	0	0	10	10	9	8
HMGB1	High mobility group protein B1	13	4	13	9	6	5	11	8
HMGB2	High mobility group protein B2	8	2	10	7	0	0	3	0
HMMR	Hyaluronan mediated motility receptor	25	12	22	17	20	17	19	17
HNRNPH1	Heterogeneous nuclear ribonucleoprotein H	4	19	3	13	6	8	4	4
HNRNPL	Heterogeneous nuclear ribonucleoprotein L	8	33	13	26	10	13	13	6
HNRNPLL	Heterogeneous nuclear ribonucleoprotein L-like	2	13	3	9	0	2	2	3
HNRNPU	Heterogeneous nuclear ribonucleoprotein U	25	51	30	47	15	24	19	21
HOMER3	Homer protein homolog 3	11	8	6	5	6	5	4	4
HOXC4	Homeobox protein Hox-C4	16	7	18	9	14	12	12	14
HSP90AA1	Heat shock protein HSP 90-alpha	13	19	22	21	6	11	12	12
HSP90AB1	Heat shock protein HSP 90-beta	14	17	19	18	13	17	21	19
HSPA1A	Heat shock 70 kDa protein 1A	0	13	0	13	9	11	0	4
HSPA2	Heat shock-related 70 kDa protein 2	0	0	0	0	0	11	0	0
HSPA5	Endoplasmic reticulum chaperone BiP	26	31	30	20	42	44	34	40
HSPA8	Heat shock cognate 71 kDa protein	24	50	28	40	31	35	27	23
IGF2BP2	Insulin-like growth factor 2 mRNA-binding protein 2	2	15	4	9	4	5	2	1
ILF3	Interleukin enhancer-binding factor 3	2	16	3	9	0	0	0	0
IMPDH2	Inosine-5'-monophosphate dehydrogenase 2	0	18	0	22	1	0	0	2
KAZN	Kazrin	0	0	0	0	11	8	11	9
KIF5B	Kinesin-1 heavy chain	3	19	1	16	1	1	1	1
KNOP1	Lysine-rich nucleolar protein 1	8	6	6	9	12	10	8	6
KRT1	Keratin, type II cytoskeletal 1	33	15	23	40	16	7	27	39
KRT10	Keratin, type I cytoskeletal 10	20	8	15	21	14	12	18	28
KRT13	Keratin, type I cytoskeletal 13	0	0	0	0	0	0	0	14
KRT14	Keratin, type I cytoskeletal 14	24	0	0	7	0	0	0	8
KRT16	Keratin, type I cytoskeletal 16	34	0	0	8	0	0	0	8
KRT17	Keratin, type I cytoskeletal 17	13	0	0	0	0	0	0	0
KRT2	Keratin, type II cytoskeletal 2 epidermal	9	4	5	24	6	3	9	27
KRT4	Keratin, type II cytoskeletal 4	0	0	0	0	0	0	0	14
KRT5	Keratin, type II cytoskeletal 5	10	0	0	4	0	0	0	9
KRT6B	Keratin, type II cytoskeletal 6B	23	0	0	7	0	0	0	10
KRT6C	Keratin, type II cytoskeletal 6C	23	0	0	0	0	0	0	0
KRT9	Keratin, type I cytoskeletal 9	21	4	8	35	6	3	20	12
LANCL2	LanC-like protein 2	2	11	1	7	0	1	1	2

Supplementary Table 3 (1/3). LC-MS/MS obtained peptide counts. Gluc.=Glucose, SF=Sorafenib

		SKMel103				*UACC903*			
Protein	**Description**	**High Gluc.**	**w/o Gluc.**	**High Gluc. + SF**	**w/o Gluc. + SF**	**High Gluc.**	**w/o Gluc.**	**High Gluc. + SF**	**w/o Gluc. + SF**
LEF1	Lymphoid enhancer-binding factor 1	9	4	9	9	17	22	20	16
LMNA	Prelamin-A/C	126	100	115	86	268	256	242	203
LRPAP1	Alpha-2-macroglobulin receptor-associated protein	43	34	43	37	42	40	45	45
LUC7L	Putative RNA-binding protein Luc7-like 1	19	12	18	6	12	12	14	14
LUC7L2	Putative RNA-binding protein Luc7-like 2	40	34	42	20	36	42	38	39
LUZP1	Leucine zipper protein 1	6	11	6	5	17	17	14	11
LYAR	Cell growth-regulating nucleolar protein	15	21	15	17	5	10	2	4
MAP2	Microtubule-associated protein 2	1	0	2	0	5	8	7	14
MAPK1	Mitogen-activated protein kinase 1	0	17	0	11	0	0	0	2
MATR3	Matrin-3	0	17	1	3	3	3	1	2
MAX	Protein max	16	9	18	16	17	16	17	18
MCM3	DNA replication licensing factor MCM3	15	44	13	36	23	22	22	18
MCM5	DNA replication licensing factor MCM5	0	30	0	22	2	4	1	3
MCRIP1	Mapk-regulated corepressor-interacting protein 1	34	17	33	28	15	20	18	15
MFAP1	Microfibrillar-associated protein 1	17	13	18	23	12	12	13	13
MFGE8	Lactadherin	2	11	2	5	0	0	0	0
MID1	E3 ubiquitin-protein ligase Midline-1	0	16	0	8	0	0	0	0
MTHFD1L	Monofunctional C1-tetrahydrofolate synthase, mitochondrial	0	10	0	2	0	0	0	0
MYCBP	c-Myc-binding protein	9	9	11	11	9	10	12	10
MYL6	Myosin light polypeptide 6	15	11	13	11	13	13	12	13
NCL	Nucleolin	7	2	11	7	8	11	9	10
NDE1	Nuclear distribution protein nudE homolog 1	7	1	7	5	9	9	10	7
NHP2	H/ACA ribonucleoprotein complex subunit 2	8	8	10	5	6	7	7	6
NOB1	RNA-binding protein NOB1	3	14	3	11	4	5	3	0
NONO	Non-POU domain-containing octamer-binding protein	79	84	62	73	58	66	57	42
NOTCH2	Neurogenic locus notch homolog protein 2	6	5	6	2	8	14	16	9
NPM1	Nucleophosmin	7	8	11	10	7	10	8	8
NRP1	Neuropilin-1	1	10	1	9	0	1	0	1
NSRP1	Nuclear speckle splicing regulatory protein 1	29	14	34	26	29	24	28	28
NUCB1	Nucleobindin-1	59	50	64	80	35	43	34	63
NUCB2	Nucleobindin-2	3	3	4	4	5	16	15	32
NUDT21	Cleavage and polyadenylation specificity factor subunit 5	10	21	13	13	8	14	6	9
NUFIP2	Nuclear fragile X mental retardation-interacting protein 2	7	6	6	7	19	21	26	20
NUSAP1	Nucleolar and spindle-associated protein 1	11	8	9	10	4	2	6	2
OGFR	Opioid growth factor receptor	15	7	14	7	13	8	10	9
PABPC1	Polyadenylate-binding protein 1	1	15	1	14	0	1	1	0
PALLD	Palladin	14	11	11	10	23	20	15	17
PBXIP1	Pre-B-cell leukemia transcription factor-interacting protein 1	9	10	10	8	8	9	9	10
PDLIM4	PDZ and LIM domain protein 4	35	35	37	33	29	29	29	29
PELO	Protein pelota homolog	4	15	6	10	4	1	1	1
PFKFB2	6-phosphofructo-2-kinase/fructose-2,6-bisphosphatase 2	47	135	43	93	53	58	51	47
PFKFB3	6-phosphofructo-2-kinase/fructose-2,6-bisphosphatase 3	0	13	0	10	0	0	0	0
PHF6	PHD finger protein 6	13	20	13	15	5	10	5	3
PIP4K2C	Phosphatidylinositol 5-phosphate 4-kinase type-2 gamma	2	10	1	4	1	1	2	3
PITHD1	PITH domain-containing protein 1	2	10	3	6	2	6	4	3
POLDIP2	Polymerase delta-interacting protein 2	0	10	0	2	0	1	0	1
PPIL4	Peptidyl-prolyl cis-trans isomerase-like 4	12	22	11	12	10	16	11	12
PPP1R10	Serine/threonine-protein phosphatase 1 regulatory subunit 10	11	12	6	9	15	12	15	10
PQBP1	Polyglutamine-binding protein 1	21	19	19	22	21	20	18	21
PRDX1	Peroxiredoxin-1	6	12	6	8	5	5	4	7
PRKAA1	5'-AMP-activated protein kinase catalytic subunit alpha-1	0	11	2	6	0	0	0	1
PRPF38B	Pre-mRNA-splicing factor 38B	3	10	4	3	2	2	2	2
PRPF40A	Pre-mRNA-processing factor 40 homolog A	9	16	12	18	10	12	8	3
PRRC2C	Protein PRRC2C	3	1	0	5	6	7	8	19
PSAP	Prosaposin	12	4	14	9	10	7	10	15
PSMD9	26S proteasome non-ATPase regulatory subunit 9	10	6	9	4	9	9	7	12
PSPC1	Paraspeckle component 1	28	29	28	26	28	28	27	25
RAI1	Retinoic acid-induced protein 1	0	0	1	1	13	7	10	7
RAVER1	Ribonucleoprotein PTB-binding 1	3	16	2	7	2	4	0	2
RBM25	RNA-binding protein 25	25	29	25	32	19	21	21	14
RBM27	RNA-binding protein 27	15	13	13	13	20	15	18	19
RBM33	RNA-binding protein 33	6	5	5	5	12	9	16	6
RCN1	Reticulocalbin-1	16	12	17	13	9	16	11	12
RNF20	E3 ubiquitin-protein ligase BRE1A	2	11	3	6	0	2	1	1
RNF40	E3 ubiquitin-protein ligase BRE1B	0	12	0	7	0	1	0	0
RPL23A	60S ribosomal protein L23a	9	11	11	11	12	12	14	8
RPL31	60S ribosomal protein L31	10	9	8	9	10	8	7	12
RPL9	60S ribosomal protein L9	1	10	1	4	2	1	0	3
RPLP2	60S acidic ribosomal protein P2	14	11	16	11	11	11	14	15
RPS10	40S ribosomal protein S10	16	17	13	13	7	11	9	16
RPS11	40S ribosomal protein S11	1	10	2	6	5	4	1	3
RPS14	40S ribosomal protein S14	12	14	10	12	12	12	9	11
RPS15A	40S ribosomal protein S15a	6	16	6	9	6	7	5	7
RPS17	40S ribosomal protein S17	15	21	9	14	11	17	10	10
RPS19	40S ribosomal protein S19	32	20	21	21	22	20	20	24
RPS2	40S ribosomal protein S2	2	19	2	13	3	4	1	3
RPS20	40S ribosomal protein S20	9	11	8	8	7	8	9	8
RPS21	40S ribosomal protein S21	9	10	11	10	8	10	8	11
RPS3	40S ribosomal protein S3	22	43	22	40	21	19	18	21
RPS3A	40S ribosomal protein S3a	13	36	14	26	17	20	14	16
RPS4X	40S ribosomal protein S4, X isoform	6	36	9	31	6	10	8	11
RPS5	40S ribosomal protein S5	15	17	18	14	11	16	13	10
RSRC2	Arginine/serine-rich coiled-coil protein 2	17	8	14	14	13	13	13	17
RTCB	tRNA-splicing ligase RtcB homolog	0	15	0	9	2	4	0	2
RTRAF	RNA transcription, translation and transport factor protein	26	19	31	24	29	32	31	30
RUVBL1	RuvB-like 1	2	16	6	6	4	3	0	1
RUVBL2	RuvB-like 2	5	17	3	12	1	1	0	0
SAFB	Scaffold attachment factor B1	14	9	14	13	13	12	10	6
SAFB2	Scaffold attachment factor B2	14	8	14	14	12	12	9	7
SAP30BP	SAP30-binding protein	9	9	10	7	7	7	8	6
SART1	U4/U6.U5 tri-snRNP-associated protein 1	60	55	57	42	53	54	53	42
SASH1	SAM and SH3 domain-containing protein 1	1	0	0	0	12	15	14	13
SCAF8	Protein SCAF8	3	3	7	5	11	12	12	9
SEC16A	Protein transport protein Sec16A	16	6	12	5	25	25	26	16
SEC31A	Protein transport protein Sec31A	0	16	0	9	0	0	0	0
SERBP1	Plasminogen activator inhibitor 1 RNA-binding protein	112	92	110	121	79	97	92	106
SERPINH1	Serpin H1	17	47	19	20	26	40	22	30
SF1	Splicing factor 1	84	62	82	69	80	73	77	76
SF3A1	Splicing factor 3A subunit 1	71	60	69	66	54	70	60	60
SF3A2	Splicing factor 3A subunit 2	16	13	13	9	10	12	9	8

Supplementary Table 3 (2/3). LC-MS/MS obtained peptide counts. Gluc.=Glucose, SF=Sorafenib

		SKMel103				*UACC903*			
Protein	**Description**	**High Gluc.**	**w/o Gluc.**	**High Gluc. + SF**	**w/o Gluc. + SF**	**High Gluc.**	**w/o Gluc.**	**High Gluc. + SF**	**w/o Gluc. + SF**
SF3A3	Splicing factor 3A subunit 3	25	26	19	26	18	18	15	17
SF3B1	Splicing factor 3B subunit 1	7	53	1	39	2	2	3	5
SF3B2	Splicing factor 3B subunit 2	55	50	56	59	40	61	42	40
SF3B3	Splicing factor 3B subunit 3	10	48	8	33	3	5	0	4
SF3B4	Splicing factor 3B subunit 4	19	21	17	10	18	16	11	11
SF3B5	Splicing factor 3B subunit 5	10	9	8	9	7	7	6	10
SFPQ	Splicing factor, proline- and glutamine-rich	90	95	88	103	102	105	89	89
SKP1	S-phase kinase-associated protein 1	12	4	9	9	5	6	7	8
SLC9A3R2	Na(+)/H(+) exchange regulatory cofactor NHE-RF2	26	17	28	26	29	27	29	29
SMAP	Small acidic protein	19	14	19	16	9	10	8	16
SMARCC1	SWI/SNF complex subunit SMARCC1	1	10	0	9	0	3	0	0
SMARCE1	SWI/SNF matrix-assoc actin-dependent regulator of chromatin E1	12	10	11	9	13	14	12	10
SNRPA1	U2 small nuclear ribonucleoprotein A'	3	6	3	10	4	4	4	7
SNW1	SNW domain-containing protein 1	15	15	12	25	11	16	15	22
SORBS2	Sorbin and SH3 domain-containing protein 2	6	5	5	3	17	13	11	13
SOX10	Transcription factor SOX-10	17	15	18	14	20	24	26	19
SOX5	Transcription factor SOX-5	0	0	0	0	8	8	7	6
SPATS2L	SPATS2-like protein	6	15	7	6	8	10	11	12
SPTY2D1	Protein SPT2 homolog	11	3	9	5	7	6	10	8
SRPK1	SRSF protein kinase 1	12	22	13	17	4	6	6	7
SRPK2	SRSF protein kinase 2	0	10	0	8	4	3	4	7
SRRM1	Serine/arginine repetitive matrix protein 1	6	2	8	25	5	7	6	14
SRRT	Serrate RNA effector molecule homolog	8	23	7	19	4	12	5	8
SYNJ2	Synaptojanin-2	0	10	0	3	0	0	0	0
SYNM	Synemin	0	0	0	0	11	8	6	4
TAOK1	Serine/threonine-protein kinase TAO1	0	14	3	7	2	0	2	2
TCF20	Transcription factor 20	0	0	0	0	12	7	7	4
THRAP3	Thyroid hormone receptor-associated protein 3	23	23	32	7	33	36	24	20
TJAP1	Tight junction-associated protein 1	17	9	16	15	20	21	19	19
TJP1	Tight junction protein ZO-1	11	27	15	16	6	6	6	2
TJP2	Tight junction protein ZO-2	22	34	29	31	2	4	2	2
TMA16	Translation machinery-associated protein 16	17	14	17	17	26	21	23	23
TMSB4X	Thymosin beta-4	8	5	10	10	5	5	8	7
TNIP1	TNFAIP3-interacting protein 1	14	5	14	7	10	10	10	9
TOP1	DNA topoisomerase 1	17	41	14	33	7	18	8	9
TPM1	Tropomyosin alpha-1 chain	8	0	10	0	8	9	8	8
TPM3	Tropomyosin alpha-3 chain	16	8	17	14	12	14	15	16
TPM4	Tropomyosin alpha-4 chain	20	13	26	18	14	17	11	17
TPX2	Targeting protein for Xklp2	33	15	25	23	17	21	22	18
TRA2B	Transformer-2 protein homolog beta	17	7	15	9	14	13	10	8
TRIM28	Transcription intermediary factor 1-beta	2	12	4	4	0	3	1	1
TSR1	Pre-rRNA-processing protein TSR1 homolog	5	28	6	21	3	6	3	2
TUBA1B	Tubulin alpha-1B chain	0	30	13	23	11	15	0	16
TUBA1C	Tubulin alpha-1C chain	11	32	13	24	0	13	0	0
TUBB	Tubulin beta chain	23	48	20	38	17	18	14	15
TUBB2A	Tubulin beta-2A chain	0	32	0	0	0	0	0	0
TUBB4B	Tubulin beta-4B chain	21	42	20	38	15	16	12	13
TUBB6	Tubulin beta-6 chain	0	13	0	10	0	0	0	0
TUFM	Elongation factor Tu, mitochondrial	14	35	12	27	12	18	13	18
U2AF2	Splicing factor U2AF 65 kDa subunit	10	20	9	16	8	11	7	10
U2SURP	U2 snRNP-associated SURP motif-containing protein	4	20	6	20	5	5	5	1
UBAP2	Ubiquitin-associated protein 2	5	12	7	9	12	13	10	8
UBAP2L	Ubiquitin-associated protein 2-like	40	28	36	30	33	28	32	25
USP7	Ubiquitin carboxyl-terminal hydrolase 7	0	27	0	10	1	2	1	2
VGLL4	Transcription cofactor vestigial-like protein 4	16	8	14	15	20	22	20	22
VIM	Vimentin	73	90	76	21	75	71	54	32
WBP11	WW domain-binding protein 11	18	12	15	23	12	18	12	29
WDR33	pre-mRNA 3' end processing protein WDR33	6	5	12	10	19	16	14	8
WDR82	WD repeat-containing protein 82	0	11	0	6	0	0	0	0
WTAP	Pre-mRNA-splicing regulator WTAP	15	9	18	11	19	15	16	13
WWTR1	WW domain-containing transcription regulator protein 1	27	16	32	19	20	17	20	21
YBX1	Nuclease-sensitive element-binding protein 1	28	14	21	16	18	14	24	17
YY1	Transcriptional repressor protein YY1	14	11	15	8	12	11	10	12
ZC3H4	Zinc finger CCCH domain-containing protein 4	18	23	33	32	20	28	23	17
ZFP91	E3 ubiquitin-protein ligase ZFP91	7	6	6	6	5	5	4	3
ZNF593	Zinc finger protein 593	9	5	11	7	9	10	10	7
ZNF787	Zinc finger protein 787	11	7	8	8	7	6	4	6

Supplementary Table 3 (3/3). LC-MS/MS obtained peptide counts. Gluc.=Glucose, SF=Sorafenib

	Score	Mr calc.	Delta	Sequence	Site Analysis
S466	53.7	1502.6766	-0.0001	NSFTPLSSSNTIR	**Phospho S2 99.12%**
	33.1	1502.6766	-0.0001	NSFTPLSSSNTIR	**Phospho T4 0.86%**
	16.1	1502.6766	-0.0001	NSFTPLSSSNTIR	**Phospho S7 0.02%**
	14.2	1502.6643	0.0122	ASLRAKTSPEGAR	
	11.9	1502.6766	-0.0001	GSEGTPDSLHKAPK	
	10	1502.6766	-0.0001	NSFTPLSSSNTIR	**Phospho S8 0.00%**
	8.8	1501.6674	1.009	ASTHDSLAHGASLR	
	6.1	1502.6701	0.0064	YPIRSGMVSSGNR	
	5.4	1502.6766	-0.0001	NSFTPLSSSNTIR	**Phospho S9 0.00%**
	5	1502.6766	-0.0001	KSSINEQFVDTR	
T468	26.7	1658.7777	-0.0013	RNSFTPLSSSNTIR	**Phospho T5 49.85%**
	26.6	1658.7777	-0.0013	RNSFTPLSSSNTIR	**Phospho S3 49.05%**
	12.1	1658.7681	0.0082	IKSTNPGISIGDVAK	
	7.1	1658.7777	-0.0013	RNSFTPLSSSNTIR	**Phospho S9 0.55%**
	5.8	1658.7699	0.0065	RLGSDLTSAQKEMK	
	5.8	1658.7699	0.0065	RLGSDLTSAQKEMK	
	4.8	1657.7865	0.9899	GGPLDFSSIPSRAFK	
	3.3	1657.76	1.1064	ADIIASSDIEEFLR	
	2.9	1657.76	1.1064	ADIIASSDIEEFLR	
	2.9	1658.7777	-0.0013	RNSFTPLSSSNTIR	**Phospho S8 0.21%**
S483	34.7	1862.9767	0.0011	NYSVGSRPLKPLSPLR	**Phospho S3 95.97%**
	20.9	1862.9767	0.0011	NYSVGSRPLKPLSPLR	**Phospho S6 3.99%**
	10.7	1862.9615	0.0163	SHLSLVGTASGLGSNKKK	
	6	1861.9646	1.0132	IDDGQGQVSAILGHSLPR	
	3.7	1862.9924	-0.0146	QEYETKLKGLMPASLR	
	3.5	1861.9597	1.0181	RMHTAVKLNEVIVTR	
	3.1	1862.9615	0.0163	SHLSLVGTASGLGSNKKK	
	3.1	1861.9777	1.0001	ISSISKIFPVLMLYR	
	1.9	1862.9615	0.0164	AQLEKLQAEISQAARK	
	1.6	1862.9625	0.0153	LKNAYEEALDQLETVK	
S486	20.4	1862.9767	0.0007	NYSVGSRPLKPLSPLR	
	20.3	1862.9767	0.0007	NYSVGSRPLKPLSPLR	
	8.9	1862.9924	-0.0149	QEYETKLKGLMPASLR	
	7.2	1861.9646	1.0128	IDDGQGQVSAILGHSLPR	
	5.4	1862.9615	0.0159	SHLSLVGTASGLGSNKKK	
	5.1	1862.9746	0.0028	EVQIMKMLDHPHIIK	
	3.7	1862.9615	0.0159	KKSHLSLVGTASGLGSNK	
	3.1	1861.9568	1.0207	SLSSSLQAPVVSTVGMQR	
	2.6	1862.9729	0.0045	AFHLLQKLLTMDPIK	
	1.7	1862.9811	-0.0037	AQMKEDPELAKSFIK	
S493	27.3	1862.9767	0.0029	NYSVGSRPLKPLSPLR	**Phospho S13 99.53%**
	2.4	1862.9767	0.0029	NYSVGSRPLKPLSPLR	**Phospho S6 0.32%**
	1.2	1861.9591	1.0206	TVQFGGTVTEVLLKYK	
	0.1	1862.9823	-0.0027	ARGAAAGSGVPAAPGPSGRTR	
S483+ S493	27.6	1942.9431	0.0017	NYSVGSRPLKPLSPLR	**Phospho S3, S13 88.19%**
	17.3	1942.9431	0.0017	NYSVGSRPLKPLSPLR	**Phospho S3, S6 8.29%**
	13.6	1942.9431	0.0017	NYSVGSRPLKPLSPLR	**Phospho S6. S13 3.52%**
	6.4	1942.9497	-0.0049	HGAGAEISTVNPEQYSKR	
	5.2	1942.9352	0.0096	AEALVLMGTKANLVTPR	
	1.8	1942.9278	0.017	ASLIGTPSRASLIGTPSR	
	1.5	1942.9278	0.017	ASLIGTPSRASLIGTPSR	
	1.2	1942.9587	-0.0139	QEYETKLKGLMPASLR	
	1.2	1942.9278	0.017	ALRLGDAILSVNGTDLR	
	1	1942.9634	-0.0186	ASIMRLTISYLRMHR	

Supplementary Table 4. Phosphorylation of PFKFB2 peptides identified by mass spectrometry. Monoisotopic mass of neutral peptide (Mr calc.) values are represented along with the observed deviation of the measured values from the theoretical mass of the peptides (delta) and sequence. Score indicates how well the observed spectrum matches to the stated peptide. Large score differences will strongly favor one arrangement over the other (site analysis).

Cell line	Organism	Tissue	NRAS/BRAF mutational status	Culture media
SKMel103	*H. sapiens*	*Skin*	$NRAS^{Q61R}$	DMEM 10% FBS
SKMel147	*H. sapiens*	*Skin*	$NRAS^{Q61R}$	DMEM 10% FBS
SKMel28	*H. sapiens*	*Skin*	$BRAF^{V600E}$	EMEM 10% FBS
UACC903	*H. sapiens*	*Skin*	$BRAF^{V600E}$	RPMI 10% FBS
A375	*H. sapiens*	*Skin*	$BRAF^{V600E}$	DMEM 10% FBS
G361	*H. sapiens*	*Skin*	$BRAF^{V600E}$	DMEM 10% FBS
NHEM	*H. sapiens*	*Skin*	-	M2 media
HEK-293-T	*H. sapiens*	*Kidney*	-	DMEM 10% FBS
Mmln1	*H. sapiens*	*Skin*	-	DMEM 20% FBS
Mmgp3	*H. sapiens*	*Skin*	-	DMEM 20% FBS
Mmsk8	*H. sapiens*	*Skin*	-	DMEM 20% FBS
Mmln9	*H. sapiens*	*Skin*	$NRAS^{Q61}$	DMEM 20% FBS
Mmln10	*H. sapiens*	*Skin*	$NRAS^{Q61}$	DMEM 20% FBS
Mmln14	*H. sapiens*	*Skin*	-	DMEM 20% FBS
Mmln16	*H. sapiens*	*Skin*	$NRAS^{Q61}$	DMEM 20% FBS
Mmsk22	*H. sapiens*	*Skin*	-	DMEM 20% FBS
Mmln23	*H. sapiens*	*Skin*	-	DMEM 20% FBS
Mmln24	*H. sapiens*	*Skin*	-	DMEM 20% FBS
Mmsk29	*H. sapiens*	*Skin*	-	DMEM 20% FBS
Mmln30	*H. sapiens*	*Skin*	-	DMEM 20% FBS
Mmln31	*H. sapiens*	*Skin*	-	DMEM 20% FBS

Supplementary Table 5. Cell lines information. Compilation of cell lines information including organism and tissue of origin; mutational status for *BRAF* and *NRAS;* and cell culture media.

BIBLIOGRAPHY

1. Bray, F. *et al.* Global cancer statistics 2018: GLOBOCAN estimates of incidence and mortality worldwide for 36 cancers in 185 countries. *CA. Cancer J. Clin.* 68, 394–424 (2018).
2. Nehal, K. S. & Bichakjian, C. K. Update on keratinocyte carcinomas. *N. Engl. J. Med.* 379, 363–374 (2018).
3. American Cancer Society. http://cancerstatisticscenter.cancer.org.
4. The Skin Cancer Foundation. http://skincancer.org.
5. Lo, J. A. & Fisher, D. E. The melanoma revolution: From UV carcinogenesis to a new era in therapeutics. *Science (80-.).* 346, 945–949 (2014).
6. Miller, Arlo J.; Mihm, M. C. Melanoma. *N. Engl. J. Med.* 355, 51–65 (2006).
7. Whiteman, D. C., Whiteman, C. A. & Green, A. C. Childhood sun exposure as a risk factor for melanoma: A systematic review of epidemiologic studies. *Cancer Causes Control* 12, 69–82 (2001).
8. Alexandrov, L. B. *et al.* Signatures of mutational processes in human cancer. *Nature* 500, 415–421 (2013).
9. Hayward, N. K. *et al.* Whole-genome landscapes of major melanoma subtypes. *Nature* 545, 175–180 (2017).
10. Clark, W. H. *et al.* A study of tumor progression: The precursor lesions of superficial spreading and nodular melanoma. *Hum. Pathol.* 15, 1147–1165 (1984).
11. Gray-Schopfer, V., Wellbrock, C. & Marais, R. Melanoma biology and new targeted therapy. *Nature* 445, 851–857 (2007).
12. Ward, William H.; Lambreton, Fernando; Goel, Neha;Yu, Jian Q.; Farma, J. M. Clinical Presentation and Staging of Melanoma. *Round Table Ser. - R. Soc. Med.* 39–47 (1987) doi:10.1007/978-3-642-96258-5_8.
13. Seuradge, J. & Wong, E. www.pathophys.org/melanoma/. www.pathophys.org/melanoma/.
14. Pollock, P. M. *et al.* High frequency of BRAF mutations in nevi. *Nat. Genet.* 33, 19–20 (2003).
15. Michaloglou, C. *et al.* BRAFE600-associated senescence-like cell cycle arrest of human naevi. *Nature* 436, 720–724 (2005).
16. Marks, R., Dorevitch, A. B. E. P. & Mason, G. DO ALL MELANOMAS COME FROM " MOLES "? A STUDY OF THE HISTOLOGICAL ASSOCIATION BETWEEN MELANOCYTIC NAEVI AND MELANOMA. 77–80 (1990).
17. Bevona, C., Goggins, W., Quinn, T., Fullerton, J. & Tsao, H. Cutaneous Melanomas Associated With Nevi. 139, (2016).
18. Gershenwald, J. E. *et al.* Melanoma staging: Evidence-based changes in the American Joint Committee on Cancer eighth edition cancer staging manual. *CA. Cancer J. Clin.* 67, 472–492 (2017).
19. Davies, H. *et al.* Mutations of the BRAF gene in human cancer. *Nature* 417, 949–954 (2002).
20. Curtin, J. A., Busam, K., Pinkel, D. & Bastian, B. C. Somatic activation of KIT in distinct subtypes of melanoma. *J. Clin. Oncol.* 24, 4340–4346 (2006).
21. Furge, K. A. *et al.* Suppression of Ras-mediated tumorigenicity and metastasis through inhibition of the Met receptor tyrosine kinase. *Proc. Natl. Acad. Sci. U. S. A.* 98, 10722–10727 (2001).
22. Gille, J. *et al.* Simultaneous blockade of VEGFR-1 and VEGFR-2 activation is necessary to efficiently inhibit experimental melanoma growth and metastasis formation. *Int. J. Cancer* 120, 1899–1908 (2007).
23. Van Raamsdonk, C. D. *et al.* Frequent somatic mutations of GNAQ in uveal melanoma and blue naevi. *Nature* 457, 599–602 (2009).
24. Stahl, J. M. *et al.* Deregulated Akt3 activity promotes development of malignant melanoma. *Cancer Res.* 64, 7002–7010 (2004).
25. Stark, M. & Hayward, N. Genome-wide loss of heterozygosity and copy number analysis in melanoma using high-density single-nucleotide polymorphism arrays. *Cancer Res.* 67, 2632–2642 (2007).
26. McKay, M. M. & Morrison, D. K. Integrating signals from RTKs to ERK/MAPK. *Oncogene* 26, 3113–3121 (2007).
27. McGrath, J. P. *et al.* Structure and organization of the human Ki-ras proto-oncogene and a related processed pseudogene. *Nature* 304, 501–506 (1983).
28. Malumbres, M. & Barbacid, M. RAS oncogenes: The first 30 years. *Nat. Rev. Cancer* 3, 459–465 (2003).
29. Durrant, D. E. & Morrison, D. K. Targeting the Raf kinases in human cancer: The Raf dimer dilemma. *Br. J. Cancer* 118, 3–8 (2018).

30. Lavoie, H. & Therrien, M. Regulation of RAF protein kinases in ERK signalling. *Nat. Rev. Mol. Cell Biol.* 16, 281–298 (2015).
31. Dougherty, M. K. *et al.* Regulation of Raf-1 by direct feedback phosphorylation. *Mol. Cell* 17, 215–224 (2005).
32. Ascierto, P. A. *et al.* The role of BRAF V600 mutation in melanoma. *J. Transl. Med.* 10, 1–9 (2012).
33. Lowy, D. R. & Willumsen, B. M. Function and regulation of Ras. *Annu. Rev. Biochem.* 62, 851–891 (1993).
34. Fedorenko, I. V., Gibney, G. T. & Smalley, K. S. M. NRAS mutant melanoma: Biological behavior and future strategies for therapeutic management. *Oncogene* 32, 3009–3018 (2013).
35. Buday, L. & Downward, J. Epidermal growth factor regulates p21ras through the formation of a complex of receptor, Grb2 adapter protein, and Sos nucleotide exchange factor. *Cell* 73, 611–620 (1993).
36. Hobbs, G. A., Der, C. J. & Rossman, K. L. RAS isoforms and mutations in cancer at a glance. *J. Cell Sci.* 129, 1287–1292 (2016).
37. Castellano, E. & Santos, E. Functional specificity of Ras isoforms: So similar but so different. *Genes and Cancer* 2, 216–231 (2011).
38. Muñoz-Maldonado, C., Zimmer, Y. & Medová, M. A comparative analysis of individual ras mutations in cancer biology. *Front. Oncol.* 9, 1–22 (2019).
39. Whitwam, T. *et al.* Differential oncogenic potential of activated RAS isoforms in melanocytes. *Oncogene* 26, 4563–4570 (2007).
40. Muñoz-Couselo, E., Adelantado, E. Z., Ortiz, C., García, J. S. & Perez-Garcia, J. NRAS-mutant melanoma: Current challenges and future prospect. *Onco. Targets. Ther.* 10, 3941–3947 (2017).
41. Drosten, M. *et al.* Genetic analysis of Ras signalling pathways in cell proliferation, migration and survival. *EMBO J.* 29, 1091–1104 (2010).
42. Dumaz, N. *et al.* In melanoma, RAS mutations are accompanied by switching signaling from BRAF to CRAF and disrupted cyclic AMP signaling. *Cancer Res.* 66, 9483–9491 (2006).
43. Ritt, D. A., Monson, D. M., Specht, S. I. & Morrison, D. K. Impact of Feedback Phosphorylation and Raf Heterodimerization on Normal and Mutant B-Raf Signaling. *Mol. Cell. Biol.* 30, 806–819 (2010).
44. Devitt, B. *et al.* Clinical outcome and pathological features associated with NRAS mutation in cutaneous melanoma. *Pigment Cell Melanoma Res.* 24, 666–672 (2011).
45. Colebatch, A. J. *et al.* Molecular Genomic Profiling of Melanocytic Nevi. *J. Invest. Dermatol.* 139, 1762–1768 (2019).
46. Maldonado, J. L. *et al.* Determinants of BRAF mutations in primary melanomas. *J. Natl. Cancer Inst.* 95, 1878–1880 (2003).
47. Thumar, J., Shahbazian, D., Aziz, S. A., Jilaveanu, L. B. & Kluger, H. M. MEK targeting in N-RAS mutated metastatic melanoma. *Mol. Cancer* 13, 1–10 (2014).
48. Goel, V. K., Lazar, A. J. F., Warneke, C. L., Redston, M. S. & Haluska, F. G. Examination of mutations in BRAF, NRAS, and PTEN in primary cutaneous melanoma. *J. Invest. Dermatol.* 126, 154–160 (2006).
49. Castellano, E. & Downward, J. Ras interaction with PI3K: More than just another effector pathway. *Genes and Cancer* 2, 261–274 (2011).
50. Jakob, J. A. *et al.* NRAS mutation status is an independent prognostic factor in metastatic melanoma. *Cancer* 118, 4014–4023 (2012).
51. Edlundh-Rose, E. *et al.* NRAS and BRAF mutations in melanoma tumours in relation to clinical characteristics: A study based on mutation screening by pyrosequencing. *Melanoma Res.* 16, 471–478 (2006).
52. Ferretta, A. *et al.* New insight into the role of metabolic reprogramming in melanoma cells harboring BRAF mutations. *Biochim. Biophys. Acta - Mol. Cell Res.* 1863, 2710–2718 (2016).
53. Ratnikov, B. I., Scott, D. A., Osterman, A. L., Smith, J. W. & Ronai, Z. A. Metabolic rewiring in melanoma. *Oncogene* 36, 147–157 (2017).
54. Fischer, G. M. *et al.* Metabolic strategies of melanoma cells: Mechanisms, interactions with the tumor microenvironment, and therapeutic implications. *Pigment Cell Melanoma Res.* 31, 11–30 (2018).
55. Smith, L. K., Rao, A. D. & McArthur, G. A. Targeting metabolic reprogramming as a potential therapeutic strategy in melanoma. *Pharmacol. Res.* 107, 42–47 (2016).

56. Ruocco, M. R. *et al.* Metabolic flexibility in melanoma: A potential therapeutic target. *Semin. Cancer Biol.* (2019) doi:10.1016/j.semcancer.2019.07.016.
57. Haq, R. *et al.* Oncogenic BRAF regulates oxidative metabolism via PGC1α and MITF. *Cancer Cell* 23, 302–315 (2013).
58. Luke, J. J. & Schwartz, G. K. Chemotherapy in the management of advanced cutaneous malignant melanoma. *Clin. Dermatol.* 31, 290–297 (2013).
59. Ambrosi, L., Khan, S., Carvajal, R. D. & Yang, J. Novel Targets for the Treatment of Melanoma. *Curr. Oncol. Rep.* 21, 1–16 (2019).
60. Hauschild, A. *et al.* Dabrafenib in BRAF-mutated metastatic melanoma: A multicentre, open-label, phase 3 randomised controlled trial. *Lancet* 380, 358–365 (2012).
61. Chapman, P. B. *et al.* Improved survival with vemurafenib in melanoma with BRAF V600E mutation. *N. Engl. J. Med.* 364, 2507–2516 (2011).
62. Sullivan, R. J. & Flaherty, K. T. Resistance to BRAF-targeted therapy in melanoma. *Eur. J. Cancer* 49, 1297–1304 (2013).
63. Su, F. *et al.* RAS mutations in cutaneous squamous-cell carcinomas in patients treated with BRAF inhibitors. *N. Engl. J. Med.* 366, 207–215 (2012).
64. Mattei, P. L. *et al.* Cutaneous effects of BRAF inhibitor therapy: A case series. *Ann. Oncol.* 24, 530–537 (2013).
65. Johnson, D. B. *et al.* Acquired BRAF inhibitor resistance: A multicenter meta-analysis of the spectrum and frequencies, clinical behaviour, and phenotypic associations of resistance mechanisms. *Eur. J. Cancer* 51, 2792–2799 (2015).
66. Villanueva, J. *et al.* Acquired Resistance to BRAF Inhibitors Mediated by a RAF Kinase Switch in Melanoma Can Be Overcome by Cotargeting MEK and IGF-1R/PI3K. *Cancer Cell* 18, 683–695 (2010).
67. Paraiso, K. H. T. *et al.* PTEN loss confers BRAF inhibitor resistance to melanoma cells through the suppression of BIM expression. *Cancer Res.* 71, 2750–2760 (2011).
68. Haq, R. *et al.* BCL2A1 is a lineage-specific antiapoptotic melanoma oncogene that confers resistance to BRAF inhibition. *Proc. Natl. Acad. Sci. U. S. A.* 110, 4321–4326 (2013).
69. Smalley, K. S. M. *et al.* Increased cyclin D1 expression can mediate BRAF inhibitor resistance in BRAF V600E-mutated melanomas. *Mol. Cancer Ther.* 7, 2876–2883 (2008).
70. Nazarian, R. *et al.* Melanomas acquire resistance to B-RAF(V600E) inhibition by RTK or N-RAS upregulation. *Nature* 468, 973–977 (2010).
71. Wagle, N. *et al.* Dissecting therapeutic resistance to RAF inhibition in melanoma by tumor genomic profiling. *J. Clin. Oncol.* 29, 3085–3096 (2011).
72. Hernandez-Davies, J. E. *et al.* Vemurafenib resistance reprograms melanoma cells towards glutamine dependence. *J. Transl. Med.* 13, 1–11 (2015).
73. Ross, K. C., Andrews, A. J., Marion, C. D., Yen, T. J. & Bhattacharjee, V. Identification of the serine biosynthesis pathway as a critical component of BRAF inhibitor resistance of melanoma, pancreatic, and non–small cell lung cancer cells. *Mol. Cancer Ther.* 16, 1596–1609 (2017).
74. Poulikakos, P. I., Zhang, C., Bollag, G., Shokat, K. M. & Rosen, N. RAF inhibitors transactivate RAF dimers and ERK signalling in cells with wild-type BRAF. *Nature* 464, 427–430 (2010).
75. Heidorn, S. J. *et al.* Kinase-Dead BRAF and Oncogenic RAS Cooperate to Drive Tumor Progression through CRAF. *Cell* 140, 209–221 (2010).
76. Cope, N. *et al.* Mechanism of BRAF Activation through Biochemical Characterization of the Recombinant Full-Length Protein. *ChemBioChem* 19, 1988–1997 (2018).
77. Flaherty, K. T. *et al.* Combined BRAF and MEK inhibition in melanoma with BRAF V600 mutations. *N. Engl. J. Med.* 367, 1694–1703 (2012).
78. Robert, C. *et al.* Improved overall survival in melanoma with combined dabrafenib and trametinib. *N. Engl. J. Med.* 372, 30–39 (2015).
79. Long, G. V. *et al.* Dabrafenib and trametinib versus dabrafenib and placebo for Val600 BRAF-mutant melanoma: A multicentre, double-blind, phase 3 randomised controlled trial. *Lancet* 386, 444–451 (2015).
80. Basso, A. D., Kirschmeier, P. & Bishop, W. R. Farnesyl transferase inhibitors. *J. Lipid Res.* 47, 15–31 (2006).
81. Ryan, M. B. & Corcoran, R. B. Therapeutic strategies to target RAS-mutant cancers. *Nat. Rev. Clin. Oncol.* 15, 709–720 (2018).
82. Konstantinopoulos, P. A., Karamouzis, M. V. & Papavassiliou, A. G. Post-translational modifications and regulation of the RAS superfamily of GTPases as anticancer targets. *Nat.*

Rev. Drug Discov. 6, 541–555 (2007).
83. Kim, K. B. *et al.* Phase II trial of imatinib mesylate in patients with metastatic melanoma. *Br. J. Cancer* 99, 734–740 (2008).
84. Wyman, K. *et al.* Multicenter phase II trial of high-dose imatinib mesylate in metastatic melanoma: Significant toxicity with no clinical efficacy. *Cancer* 106, 2005–2011 (2006).
85. Carvajal, R. D. *et al.* Phase II study of nilotinib in melanoma harboring KIT alterations following progression to prior KIT inhibition. *Clin. Cancer Res.* 21, 2289–2296 (2015).
86. Atkins, M. B. *et al.* High-dose recombinant interleukin 2 therapy for patients with metastatic melanoma: Analysis of 270 patients treated between 1985 and 1993. *J. Clin. Oncol.* 17, 2105–2116 (1999).
87. Topalian, S. L. *et al.* Safety, activity, and immune correlates of anti-PD-1 antibody in cancer. *N. Engl. J. Med.* 366, 2443–2454 (2012).
88. Hamid, O. *et al.* Safety and tumor responses with lambrolizumab (anti-PD-1) in melanoma. *N. Engl. J. Med.* 369, 134–144 (2013).
89. Hodi, F. S. *et al.* Improved survival with ipilimumab in patients with metastatic melanoma. *N. Engl. J. Med.* 363, 711–723 (2010).
90. Amaria, R. N. *et al.* Neoadjuvant immune checkpoint blockade in high-risk resectable melanoma. *Nat. Med.* 24, 1649–1654 (2018).
91. Wolchok, J. D. *et al.* Overall Survival with Combined Nivolumab and Ipilimumab in Advanced Melanoma. *N. Engl. J. Med.* 377, 1345–1356 (2017).
92. Luke, J. J., Flaherty, K. T., Ribas, A. & Long, G. V. Targeted agents and immunotherapies: Optimizing outcomes in melanoma. *Nat. Rev. Clin. Oncol.* 14, 463–482 (2017).
93. Leonardi, G. C., Candido, S., Falzone, L., Spandidos, D. A. & Libra, M. Cutaneous melanoma and the immunotherapy revolution. *Int. J. Oncol.* 57, 609–618 (2020).
94. Skoulidis, F. *et al.* STK11/LKB1 mutations and PD-1 inhibitor resistance in KRAS-mutant lung adenocarcinoma. *Cancer Discov.* 8, 822–835 (2018).
95. Falchook, G. S. *et al.* Activity of the oral MEK inhibitor trametinib in patients with advanced melanoma: A phase 1 dose-escalation trial. *Lancet Oncol.* 13, 782–789 (2012).
96. Yeh, T. C. *et al.* Biological characterization of ARRY-142886 (AZD6244), a potent, highly selective mitogen-activated protein kinase kinase 1/2 inhibitor. *Clin. Cancer Res.* 13, 1576–1583 (2007).
97. Adjei, A. A. *et al.* Phase I pharmacokinetic and pharmacodynamic study of the oral, small-molecule mitogen-activated protein kinase kinase 1/2 inhibitor AZD6244 (ARRY-142886) in patients with advanced cancers. *J. Clin. Oncol.* 26, 2139–2146 (2008).
98. Rinehart, J. *et al.* Multicenter phase II study of the oral MEK inhibitor, CI-1040, in patients with advanced non-small-cell lung, breast, colon, and pancreatic cancer. *J. Clin. Oncol.* 22, 4456–4462 (2004).
99. Lebb, C. *et al.* Pimasertib Versus Dacarbazine in Patients With with Crossover. 1–11 (2020).
100. Dummer, R. *et al.* Binimetinib versus dacarbazine in patients with advanced NRAS-mutant melanoma (NEMO): a multicentre, open-label, randomised, phase 3 trial. *Lancet Oncol.* 18, 435–445 (2017).
101. Warburg, O., Wind, F. & Negelein, E. The Metabolism of Tumors in the Body. *J. Gen. Physiol.* 8, 519–530 (1927).
102. Hsu, P. P. & Sabatini, D. M. Cancer cell metabolism: Warburg and beyond. *Cell* 134, 703–707 (2008).
103. Hay, N. Reprogramming glucose metabolism in cancer: Can it be exploited for cancer therapy? *Nat. Rev. Cancer* 16, 635–649 (2016).
104. Dang, C. V., Le, A. & Gao, P. MYC-induced Cancer Cell Energy Metabolism and Therapeutic Opportunities. *Clin. Cancer Res.* 15, 6479–6483 (2009).
105. Semenza, G. L. Hypoxia-inducible factors: coupling glucose metabolism and redox regulation with induction of the breast cancer stem cell phenotype. *EMBO J.* 36, 252–259 (2017).
106. DeBerardinis, R. J., Lum, J. J., Hatzivassiliou, G. & Thompson, C. B. The Biology of Cancer: Metabolic Reprogramming Fuels Cell Growth and Proliferation. *Cell Metab.* 7, 11–20 (2008).
107. Esteve-Puig, R., Canals, F., Colomé, N., Merlino, G. & Recio, J. Á. Uncoupling of the LKB1-AMPKα energy sensor pathway by growth factors and oncogenic BRAFV600E. *PLoS One* 4, (2009).
108. Olenchock, B. A. & Vander Heiden, M. G. XPyruvate as a pivot point for oncogene-induced senescence. *Cell* 153, 1429 (2013).
109. Kaplon, J. *et al.* A key role for mitochondrial gatekeeper pyruvate dehydrogenase in

oncogene-induced senescence. *Nature* 498, 109–112 (2013).
110. Patel, M. S. & Korotchkina, L. G. Regulation of the pyruvate dehydrogenase complex. *Biochem. Soc. Trans.* 34, 217–222 (2006).
111. Michelakis, E. D., Webster, L. & Mackey, J. R. Dichloroacetate (DCA) as a potential metabolic-targeting therapy for cancer. *Br. J. Cancer* 99, 989–994 (2008).
112. Kang, H. B. *et al.* Metabolic Rewiring by Oncogenic BRAF V600E Links Ketogenesis Pathway to BRAF-MEK1 Signaling. *Mol. Cell* 59, 345–358 (2015).
113. Yuan, P. *et al.* Phenformin enhances the therapeutic benefit of BRAFV600E inhibition in melanoma. *Proc. Natl. Acad. Sci. U. S. A.* 110, 18226–18231 (2013).
114. Niehr, F. *et al.* Combination therapy with vemurafenib (PLX4032/RG7204) and metformin in melanoma cell lines with distinct driver mutations. *J. Transl. Med.* 9, 1–13 (2011).
115. Janzer, A. *et al.* Metformin and phenformin deplete tricarboxylic acid cycle and glycolytic intermediates during cell transformation and NTPs in cancer stem cells. *Proc. Natl. Acad. Sci. U. S. A.* 111, 10574–10579 (2014).
116. Baenke, F. *et al.* Resistance to BRAF inhibitors induces glutamine dependency in melanoma cells. *Mol. Oncol.* 10, 73–84 (2016).
117. Yun, J. *et al.* Glucose deprivation contributes to the development of KRAS pathway mutations in tumor cells. *Science (80-.).* 325, 1555–1559 (2009).
118. Szablewski, L. Expression of glucose transporters in cancers. *Biochim. Biophys. Acta - Rev. Cancer* 1835, 164–169 (2013).
119. Patra, K. C. *et al.* Hexokinase 2 is required for tumor initiation and maintenance and its systemic deletion is therapeutic in mouse models of cancer. *Cancer Cell* 24, 213–228 (2013).
120. Yi, W. *et al.* Phosphofructokinase 1 glycosylation regulates cell growth and metabolism. *Science (80-.).* 337, 975–980 (2012).
121. Anastasiou, D. *et al.* Inhibition of Pyruvate Kinase M2 by Reactive Oxygen Species Contributes to Cellular Antioxidant Responses. *Science (80-.).* 334, 1278–1283 (2011).
122. Israelsen, W. J. & Vander Heiden, M. G. Pyruvate kinase: Function, regulation and role in cancer. *Semin. Cell Dev. Biol.* 43, 43–51 (2015).
123. Vander Heiden, M. G. *et al.* Evidence for an alternative glycolytic pathway in rapidly proliferating cells. *Science (80-.).* 329, 1492–1499 (2010).
124. Bartrons, R. *et al.* Fructose 2 , 6-Bisphosphate in Cancer Cell Metabolism. 8, (2018).
125. Atsumi, T. *et al.* High Expression of Inducible 6-Phosphofructo-2-Kinase / Fructose-2 , 6-Bisphosphatase. *Cancer Res.* 62, 5881–5887 (2002).
126. Von Der Crone, S. *et al.* Glucose deprivation induces Akt-dependent synthesis and incorporation of GLUT1, but not of GLUT4, into the plasma membrane of 3T3-L1 adipocytes. *Eur. J. Cell Biol.* 79, 943–949 (2000).
127. Bensaad, K. *et al.* TIGAR, a p53-Inducible Regulator of Glycolysis and Apoptosis. *Cell* 126, 107–120 (2006).
128. Cheung, E. C., Ludwig, R. L. & Vousden, K. H. Mitochondrial localization of TIGAR under hypoxia stimulates HK2 and lowers ROS and cell death. *Proc. Natl. Acad. Sci. U. S. A.* 109, 20491–20496 (2012).
129. Ros, S. & Schulze, A. Balancing glycolytic flux: the role of 6-phosphofructo-2-kinase/fructose 2,6-bisphosphatases in cancer metabolism. *Cancer Metab.* 1, 1–10 (2013).
130. Semenza, G. L. HIF-1 mediates metabolic responses to intratumoral hypoxia and oncogenic mutations Find the latest version : Review series HIF-1 mediates metabolic responses to intratumoral hypoxia and oncogenic mutations. *J. Clin. Invest.* 123, 3664–3671 (2013).
131. Feng, Y. *et al.* Lactate dehydrogenase A: A key player in carcinogenesis and potential target in cancer therapy. *Cancer Med.* 7, 6124–6136 (2018).
132. Costa Leite, T., Da Silva, D., Guimarães Coelho, R., Zancan, P. & Sola-Penna, M. Lactate favours the dissociation of skeletal muscle 6-phosphofructo-1- kinase tetramers down-regulating the enzyme and muscle glycolysis. *Biochem. J.* 408, 123–130 (2007).
133. Gatenby, R. A., Gawlinski, E. T., Gmitro, A. F., Kaylor, B. & Gillies, R. J. Acid-mediated tumor invasion: A multidisciplinary study. *Cancer Res.* 66, 5216–5223 (2006).
134. Feron, O. Pyruvate into lactate and back: From the Warburg effect to symbiotic energy fuel exchange in cancer cells. *Radiother. Oncol.* 92, 329–333 (2009).
135. Stine, Z. E., Walton, Z. E., Altman, B. J., Hsieh, A. L. & Dang, C. V. MYC, metabolism, and cancer. *Cancer Discov.* 5, 1024–1039 (2015).
136. Seidler, N. W. *GAPDH: Biological Properties and Diversity*. *Advances in experimental medicine and biology* vol. 985 (2013).

137. Ganapathy-kanniappan, S. & Geschwind, J. H. Tumor Glycolysis as a Target for Cancer Therapy: Progress and Prospects. *Mol. Cancer* 12, 152 (2013).
138. Liberti, M. V. & Locasale, J. W. The Warburg Effect: How Does it Benefit Cancer Cells? *Trends Biochem. Sci.* 41, 211–218 (2016).
139. Kostakoglu, L., Agress, H. & Goldsmith, S. J. Clinical Role of FDG PET in Evaluation of Cancer Patients. *Radiographics* 23, 315–340 (2003).
140. Jeon, S. M., Chandel, N. S. & Hay, N. AMPK regulates NADPH homeostasis to promote tumour cell survival during energy stress. *Nature* 485, 661–665 (2012).
141. Dunaway, G. A., Kasten, T. P., Sebo, T. & Trapp, R. Analysis of the phosphofructokinase subunits and isoenzymes in human tissues. *Biochem. J.* 251, 677–683 (1988).
142. Semenza, G. L., Roth, P. H., Fang, H. M. & Wang, G. L. Transcriptional regulation of genes encoding glycolytic enzymes by hypoxia-inducible factor 1. *J. Biol. Chem.* 269, 23757–23763 (1994).
143. Kole, H. K., Resnick, R. J., Van Doren, M. & Racker, E. Regulation of 6-phosphofructo-1-kinase activity in ras-transformed rat-1 fibroblasts. *Arch. Biochem. Biophys.* 286, 586–590 (1991).
144. Kim, N. H. *et al.* Snail reprograms glucose metabolism by repressing phosphofructokinase PFKP allowing cancer cell survival under metabolic stress. *Nat. Commun.* 8, 1–12 (2017).
145. Staal, G. E. J., Kalff, A., Heesbeen, E. C., Van Veelen, C. W. M. & Rijksen, G. Subunit Composition, Regulatory Properties, and Phosphorylation of Phosphofructokinase From Human Gliomas. *Cancer Res.* 47, 5047–5051 (1987).
146. Foe, L. G. & Kemp, R. G. lsozyme Composition and Phosphorylation of Brain Phosphofructokinase. 228, 503–511 (1984).
147. Lee, J. H. *et al.* Stabilization of phosphofructokinase 1 platelet isoform by AKT promotes tumorigenesis. *Nat. Commun.* 8, 1–14 (2017).
148. Sola-Penna, M., Da Silva, D., Coelho, W. S., Marinho-Carvalho, M. M. & Zancan, P. Regulation of mammalian muscle type 6-phosphofructo-1-kinase and its implication for the control of the metabolism. *IUBMB Life* 62, 791–796 (2010).
149. Clem, B. F. *et al.* Targeting 6-phosphofructo-2-kinase (PFKFB3) as a therapeutic strategy against cancer. *Mol. Cancer Ther.* 12, 1461–1470 (2013).
150. Rider, M. H. *et al.* 6-Phosphofructo-2-kinase/fructose-2,6-bisphosphatase: Head-to-head with a bifunctional enzyme that controls glycolysis. *Biochem. J.* 381, 561–579 (2004).
151. Minchenko, O., Opentanova, I. & Caro, J. Hypoxic regulation of the 6-phosphofructo-2-kinase/fructose-2,6- bisphosphatase gene family (PFKFB-1-4) expression in vivo. *FEBS Lett.* 554, 264–270 (2003).
152. Okar, D. A. *et al.* PFK-2/FBPase-2: Maker and breaker of the essential biofactor fructose-2,6-bisphosphate. *Trends Biochem. Sci.* 26, 30–35 (2001).
153. Zhao, S. J. *et al.* SLIT2/ROBO1 axis contributes to the Warburg effect in osteosarcoma through activation of SRC/ERK/c-MYC/PFKFB2 pathway. *Cell Death Dis.* 9, (2018).
154. He, Z., You, C. & Zhao, D. Long non-coding RNA UCA1/miR-182/PFKFB2 axis modulates glioblastoma-associated stromal cells-mediated glycolysis and invasion of glioma cells. *Biochem. Biophys. Res. Commun.* 500, 569–576 (2018).
155. Zhao, L. *et al.* Long noncoding RNA LINC00092 acts in cancer-associated fibroblasts to drive glycolysis and progression of ovarian cancer. *Cancer Res.* 77, 1369–1382 (2017).
156. Chesney, J. *et al.* An inducible gene product for 6-phosphofructo-2-kinase with an AU-rich instability element: Role in tumor cell glycolysis and the Warburg effect. *Proc. Natl. Acad. Sci. U. S. A.* 96, 3047–3052 (1999).
157. Imbert-Fernandez, Y. *et al.* Estradiol stimulates glucose metabolism via 6-phosphofructo-2-kinase (PFKFB3). *J. Biol. Chem.* 289, 9440–9448 (2014).
158. Novellasdemunt, L. *et al.* PFKFB3 activation in cancer cells by the p38/MK2 pathway in response to stress stimuli. *Biochem. J.* 452, 531–543 (2013).
159. Seo, M. & Lee, Y. H. PFKFB3 regulates oxidative stress homeostasis via its S-glutathionylation in cancer. *J. Mol. Biol.* 426, 830–842 (2014).
160. Calvo, M. N. *et al.* PFKFB3 gene silencing decreases glycolysis, induces cell-cycle delay and inhibits anchorage-independent growth in HeLa cells. *FEBS Lett.* 580, 3308–3314 (2006).
161. Mondal, S. *et al.* Therapeutic targeting of PFKFB3 with a novel glycolytic inhibitor PFK158 promotes lipophagy and chemosensitivity in gynecologic cancers. *Int. J. Cancer* 144, 178–189 (2019).
162. Maik-Rachline, G., Hacohen-Lev-Ran, A. & Seger, R. Nuclear erk: Mechanism of translocation, substrates, and role in cancer. *Int. J. Mol. Sci.* 20, 1–18 (2019).

163. Peeters, K. *et al.* Fructose-1,6-bisphosphate couples glycolytic flux to activation of Ras. *Nat. Commun.* 8, (2017).
164. Zhou, F. F., Xue, Y., Chen, G. L. & Yao, X. GPS: A novel group-based phosphorylation predicting and scoring method. *Biochem. Biophys. Res. Commun.* 325, 1443–1448 (2004).
165. Wang, C. *et al.* GPS 5.0: An Update on the Prediction of Kinase-specific Phosphorylation Sites in Proteins. *Genomics, Proteomics Bioinforma.* 18, 72–80 (2020).
166. Pajak, B. *et al.* 2-Deoxy-D-Glucose and its analogs: From diagnostic to therapeutic agents. *Int. J. Mol. Sci.* 21, (2020).
167. Esteve-Puig, R. Nuevo mecanismo de evasión a estrés energético en melanoma. (2011).
168. Groenendijk, F. H. *et al.* Sorafenib synergizes with metformin in NSCLC through AMPK pathway activation. *Int. J. Cancer* 136, 1434–1444 (2015).
169. Ajenjo, N. *et al.* Subcellular localization determines the protective effects of activated ERK2 against distinct apoptogenic stimuli in myeloid leukemia cells. *J. Biol. Chem.* 279, 32813–32823 (2004).
170. Rosseland, C. M. *et al.* Cytoplasmic retention of peroxide-activated ERK provides survival in primary cultures of rat hepatocytes. *Hepatology* 42, 200–207 (2005).
171. Zhao, Z. & Bourne, P. E. Overview of Current Type I/II Kinase Inhibitors. *Next Gener. Kinase Inhib.* 13–28 (2020) doi:10.1007/978-3-030-48283-1_2.
172. Verlande, A. *et al.* Metabolic stress regulates ERK activity by controlling KSR-RAF heterodimerization. *EMBO Rep.* 19, 320–336 (2018).
173. Eisen, T. *et al.* Sorafenib in advanced melanoma: A Phase II randomised discontinuation trial analysis. *Br. J. Cancer* 95, 581–586 (2006).
174. Corazao-Rozas, P. *et al.* Mitochondrial oxidative stress is the achille's heel of melanoma cells resistant to Braf-mutant inhibitor. *Oncotarget* 4, 1986–1998 (2013).
175. Wu, L. W., Zhang, G. & Herlyn, M. Mitochondrial biogenesis meets chemoresistance in BRAF-mutant melanoma. *Mol. Cell. Oncol.* 3, 1–2 (2016).
176. Ferraz, L. S. *et al.* Targeting mitochondria in melanoma: Interplay between MAPK signaling pathway and mitochondrial dynamics. *Biochem. Pharmacol.* 178, 114104 (2020).
177. Prabhu, A. *et al.* Ras-mediated modulation of pyruvate dehydrogenase activity regulates mitochondrial reserve capacity and contributes to glioblastoma tumorigenesis. *Neuro. Oncol.* 17, 1220–1230 (2015).
178. Humpton, T. J. *et al.* Oncogenic KRAS induces NIX-mediated mitophagy to promote pancreatic cancer. *Cancer Discov.* 9, 1268–1287 (2019).
179. Lock, R. *et al.* Autophagy facilitates glycolysis during Ras-mediated oncogenic transformation. *Mol. Biol. Cell* 22, 165–178 (2011).
180. Ying, H. *et al.* Oncogenic kras maintains pancreatic tumors through regulation of anabolic glucose metabolism. *Cell* 149, 656–670 (2012).
181. Josiah, E. H. *et al.* Oncogenic KRAS and BRAF drive metabolic reprogramming in colorectal cancer. *Mol. Cell. Proteomics* 15, 2924–2938 (2016).
182. Houles, T. *et al.* RSK regulates PFK-2 activity to promote metabolic rewiring in melanoma. *Cancer Res.* 78, 2191–2204 (2018).
183. Tesori, V. *et al.* The multikinase inhibitor Sorafenib enhances glycolysis and synergizes with glycolysis blockade for cancer cell killing. *Sci. Rep.* 5, 1–9 (2015).
184. Tomizawa, M. *et al.* 2-Deoxyglucose and sorafenib synergistically suppress the proliferation and motility of hepatocellular carcinoma cells. *Oncol. Lett.* 13, 800–804 (2017).
185. Reyes, R., Wani, N. A., Ghoshal, K., Jacob, S. T. & Motiwala, T. Sorafenib and 2-deoxyglucose synergistically inhibit proliferation of both sorafenib-sensitive and -resistant HCC cells by inhibiting ATP production. *Gene Expr.* 17, 129–140 (2017).
186. Wang, L., Yang, Q., Peng, S. & Liu, X. The combination of the glycolysis inhibitor 2-DG and sorafenib can be effective against sorafenib-tolerant persister cancer cells. *Onco. Targets. Ther.* 12, 5359–5373 (2019).
187. Wang, S. Y. *et al.* 2-Deoxy-D-glucose can complement doxorubicin and sorafenib to suppress the growth of papillary thyroid carcinoma cells. *PLoS One* 10, 1–15 (2015).
188. Castello, A. *et al.* Metabolic Switch in Hepatocellular Carcinoma Patients Treated with Sorafenib: a Proof-of-Concept Trial. *Mol. Imaging Biol.* 22, 1446–1454 (2020).
189. Stein, M. *et al.* Targeting tumor metabolism with 2-deoxyglucose in patients with castrate-resistant prostate cancer and advanced malignancies. *Prostate* 70, 1388–1394 (2010).
190. Raez, L. E. *et al.* A phase i dose-escalation trial of 2-deoxy-d-glucose alone or combined with docetaxel in patients with advanced solid tumors. *Cancer Chemother. Pharmacol.* 71, 523–

530 (2013).
191. Llovet, J. M. *et al.* Sorafenib in Advanced Hepatocellular Carcinoma. *N. Engl. J. Med.* 359, 378–390 (2008).
192. Ratain, M. J. *et al.* Phase II placebo-controlled randomized discontinuation trial of sorafenib in patients with metastatic renal cell carcinoma. *J. Clin. Oncol.* 24, 2505–2512 (2006).
193. Wang, Y., Qu, C., Liu, T. & Wang, C. PFKFB3 inhibitors as potential anticancer agents: Mechanisms of action, current developments, and structure-activity relationships. *Eur. J. Med. Chem.* 203, 112612 (2020).
194. Wan, P. T. C. *et al.* Mechanism of activation of the RAF-ERK signaling pathway by oncogenic mutations of B-RAF. *Cell* 116, 855–867 (2004).
195. Zhou, Y. *et al.* Metascape provides a biologist-oriented resource for the analysis of systems-level datasets. *Nat. Commun.* 10, (2019).
196. Babicki, S. *et al.* Heatmapper: web-enabled heat mapping for all. *Nucleic Acids Res.* 44, W147–W153 (2016).
197. Thingholm, T. E., Jørgensen, T. J. D., Jensen, O. N. & Larsen, M. R. Highly selective enrichment of phosphorylated peptides using titanium dioxide. *Nat. Protoc.* 1, 1929–1935 (2006).